PROTON INDUCED REACTIONS ON ^{14}N AND ^{16}O AND THE CREATION OF ELEMENTS LITHIUM, BERYLLIUM AND BORON

by

Helmut Wolfram Laumer

Cyclotron Laboratory, Michigan State University
East Lansing, Michigan 48823

October 1971

ABSTRACT

PROTON INDUCED REACTIONS ON ^{14}N AND ^{16}O AND THE CREATION OF ELEMENTS LITHIUM, BERYLLIUM AND BORON

by

Helmut Wolfram Laumer

Measurements of cross-sections for production of masses 6 to 11 by proton spallation of ^{14}N and ^{16}O have been carried out. The proton energy range covered was 17 MeV to 42 MeV.

These cross-sections are indispensable in attacking an unsolved astrophysical problem, the origin of the light elements Li, Be and B. A number of theories have been proposed, and proton spallation of C, N and O is found to play a dominant role in several of them.

Two methods were employed in the cross-section measurements. For the main body of data collected particle identification was accomplished with a time-of-flight technique based on the narrow proton burst width of the M.S.U. Cyclotron. The particle energy measured with a silicon surface barrier detector and the particle flight time from target to detector yielded mass identification of spallation products. Angular distributions were collected and an integration over angle determined total cross-sections. For these measurements gas targets were used, contained in a specially designed gas cell with an exit beam window areal density in the range

50 $\mu g/cm^2$ to 130 $\mu g/cm^2$. As a check on the time-of-flight technique we measured ^{7}Be and ^{11}C cross-sections for proton spallation of ^{14}N at 21.7 MeV using radioactivation followed by γ-ray detection. Gas targets in a gas cell designed for γ-ray counting with the Ge(Li) detector were used. Good agreement was obtained for the cross-sections measured by the two methods.

A specific model for Li, Be, B production, proton spallation in the surfaces of stars, based on a theory by Bernas, is tested using the newly acquired cross-sections. A proton spectrum of the form $E^{-\gamma}$, based on solar flares, is considered. It is found that ^{14}N proton spallation is a large contributor to light element production in spite of the low ^{14}N abundance compared to ^{12}C and ^{16}O. To produce the ratio $^{11}B/^{10}B = 4$ as observed in the earth and in meteorites a value of γ low compared to that of proton spectra measured for solar flares is required. The ratio $^7Li/^6Li = 12.5$ as observed for earth and meteorites, on the other hand, can be produced only by proton spectra with improbably high values of γ. A depletion mechanism for ^{6}Li or alternate production mechanisms for ^{7}Li are the more likely explanations for this ratio.

PROTON INDUCED REACTIONS ON ^{14}N AND ^{16}O AND THE CREATION OF ELEMENTS LITHIUM, BERYLLIUM AND BORON

by

Helmut Wolfram Laumer

A THESIS

Submitted to
Michigan State University
in partial fulfillment of the requirements
for the degree of

DOCTOR OF PHILOSOPHY

Department of Physics

1971

TABLE OF CONTENTS

LIST OF TABLES

Table Page

LIST OF FIGURES

Figure Page

1. INTRODUCTION

1.1 Nucleosynthesis in Stars

One of the more spectacular successes of nuclear astrophysics is the explanation (CL68) of many of the features of the natural abundance curve of the elements. The correlation of nuclear properties of heavier elements with the observed abundances is so striking that the mechanisms for their production are quite well established. Figure 1 shows a relative abundance curve with regions labeled by their dominant production mechanisms in stars. During the lifetime of a star the fusion reactions in its interior fuse nuclei in an ascending sequence of mass. Hydrogen-burning converts hydrogen into ^{4}He, and if ^{12}C and ^{16}O are present these are converted largely to ^{14}N if the star's mass is large enough. Once the hydrogen fuel is exhausted the star contracts until the temperature at the center is high enough to overcome the coulomb barrier of ^{4}He + ^{4}He, and the helium burning process begins. The major products are ^{12}C and ^{16}O, with ^{20}Ne and ^{24}Mg also perhaps possible (IB 66, TU 71). Once ^{4}He is also exhausted ^{12}C + ^{12}C and later ^{16}O + ^{16}O are expected to react, to form nuclei up to ^{32}S. The temperature necessary to burn the next most likely fuel, ^{24}Mg, is so high that (γ,p), (γ,n) and (γ,α) reactions become dominant before it is ever reached. These reactions convert the products

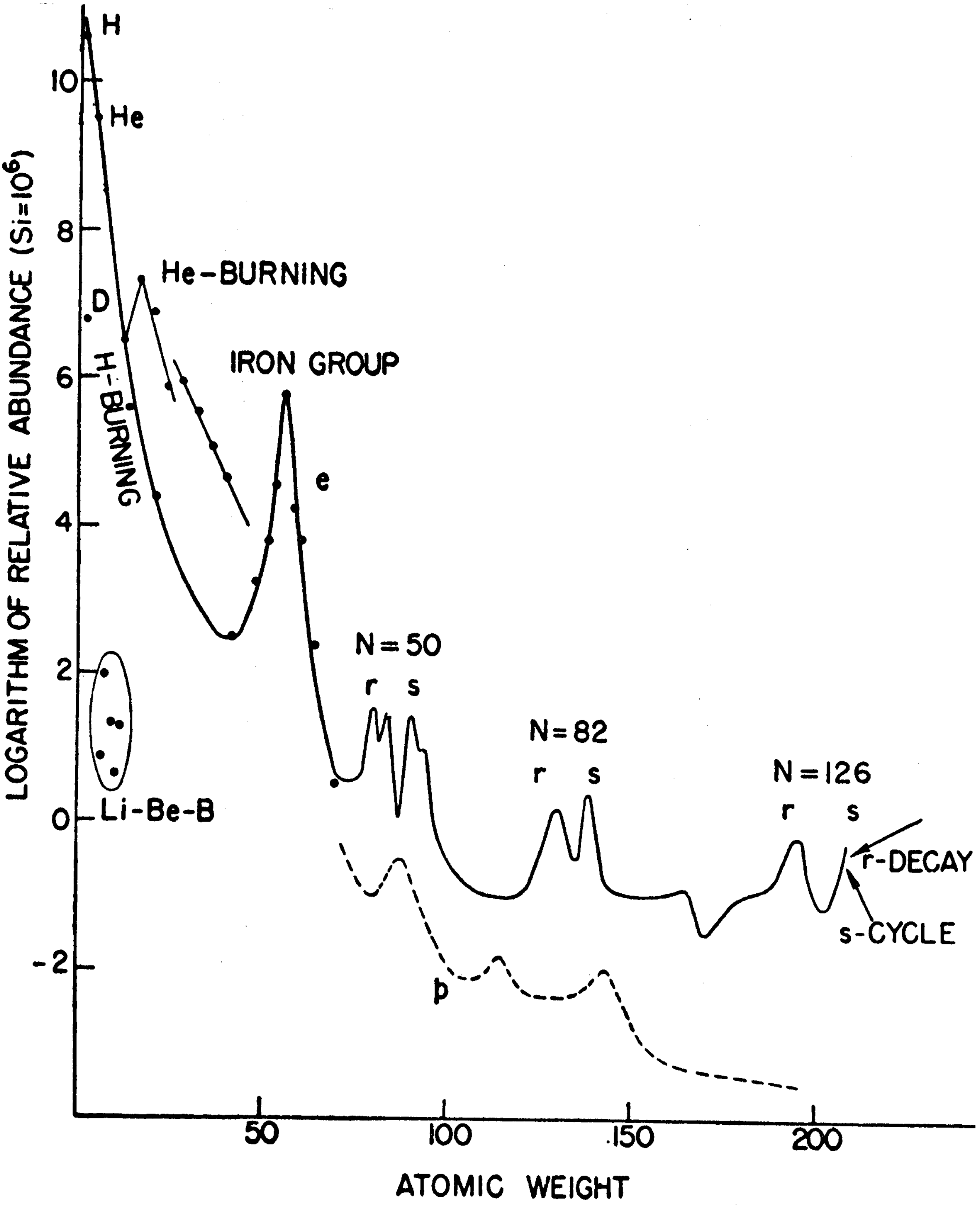

Figure 1. Curve of Relative Abundances From (BBFH 57) Based on Suess and Urey.

from the last burning stage, A near 28, to the more stable nuclei with A near 56. This last process is called silicon burning or photodisintegration rearrangement. Recent calculations (AC 70) show that explosive carbon, oxygen and silicon burning can give good agreement with observed abundances in the range $20\leq A\leq 62$. At temperatures higher than necessary for silicon burning, the photodisintegration and net production of iron group nuclei becomes balanced. This is called the equilibrium or e process. The elements heavier than those of the iron peak are more abundant than expected from these processes. The mechanism for their production is neutron capture. Two processes, r (rapid) and s (slow), are postulated. In the s process there is time for β decay after (n,γ) reactions have produced a β^- unstable nucleus; a neutron capture chain climbing the valley of stability of the nucleidic chart is the result. In the r process fast neutron captures produce a highly β^- unstable, neutron rich nucleus near the neutron drip line. Subsequent β^- decay then leads to the resulting stable nucleus. There are some proton rich heavy isotopes which cannot conceivably be produced by the r or s process. Their abundances are considerably lower than those of isotopes accessible by the r or s process. Presumably (p,γ) and (γ,n) reactions on nuclei synthesized by the r or s process can account for the abundances. In Figure 1 the abundance of Li, Be, and B is seen to be anomalously low compared to their neighbors. In the nuclear burning processes in stars described above, they are largely bypassed. They are also very fragile so if present or produced during hydrogen burning, (p,α) reactions quickly destroy them (BGRS 67). For example ^{7}Li can be produced in hydrogen burning by the reaction chain:

$$^1H + {}^1H \rightarrow {}^2H + e^+ + \nu$$
$$^2H + {}^1H \rightarrow {}^3He + \gamma$$
$$^3He + {}^3He \rightarrow {}^4He + {}^1H + {}^1H$$
$$^3He + {}^4He \rightarrow {}^7Be + \gamma$$
$$^7Be + e^- \rightarrow {}^7Li + \nu$$

only to be destroyed by $^7Li + {}^1H \rightarrow {}^4He + {}^4He$. As a result even the low abundance of Li, Be and B becomes difficult to explain. Spallation reactions on the more plentiful nuclei are the suggested (FBB 55) mechanisms for their production. In the case of ^{7}Li cosmological production is also a possibility (WFH 67).

1.2 Need for Cross Section Measurements

Since ^{12}C, ^{14}N, and ^{16}O are the most abundant of the nuclei heavier than Li, proton induced spallation of these targets is the process most likely involved in forming the light elements Li, Be and B (FBB 55). The reaction cross-sections for these targets are thus of great interest. While data for ^{12}C exist at most energies (DLA 70, AER 67), only a few cross-section measurements for ^{16}O above 100 MeV proton energy are available, and there was little data on

^{14}N until the recent ^{11}C and ^{7}Be cross-section measurements by M. Epherre and C. Seide (ES 71). The threshold region for light element production cross-sections is of special interest for several reasons. Theoretical calculations are most unreliable for this region, hence predictions valid at higher energies are of marginal value here. Proton spectra encountered in nature (FW 63) usually vary as a negative power of the energy, hence there are considerably more protons available for reactions at lower energies where in addition the cross-sections are also often larger than at high energies. Due to differences in threshold energies for their production, the formation ratios of isotopes vary most drastically in the threshold region; in view of the proton spectrum cited above, relative abundance calculations will be sensitive to these cross-sections.

1.3 Difficulty of Measurements

The sparse cross-section data for Li, Be, and B production is not due to lack of interest on the part of experimenters, but is the result of extreme experimental difficulty encountered. The most straightforward technique used in the past is radioactivation analysis. This is limited to radioactive products however and thus cannot yield all the cross-sections of interest. Mass spectrometry has also been employed in some measurements, but this technique is beset by difficulties such as sample contamination and variable sensitivity to isotopes; hence, it is very time consuming (see for example (YI 68)). Attempts have also been made (JU 70) to use emulsions; but contributions to cross-sections from break up which leads to more than one free neutron could not be measured. The data collected also suffered from poor statistics.

1.4 Time of Flight Technique

The method used in my measurements is the time-of-flight technique reported in (DLA 70), as modified for application to gas cells. A collimation system limits the volume from which particles may reach an energy sensitive particle detector. By choosing a flight path which is long compared to the dimensions of this gas volume, particles can be assigned a flight time which in conjunction with the energy measurement determines the particle mass:

E = particle energy

t = flight time

D = path length

$$E = mv^2/2 = m\,(\frac{D}{t})^2/2$$

hence $m = \dfrac{2Et^2}{D^2}$.

Angular distributions are obtained by integrating spectra over energy for each particular mass. An integration of a distribution over angle then yields the total cross-section for the mass.

It may seem that particle mass identification is insufficient since ^{11}B and ^{11}C, for example, cannot be distinguished. For the astrophysical application however the information is quite complete since only one isobar per mass number is stable in the region $6 \leq A \leq 11$. All other isobars of the same A detected in our experiment decay to it on astrophysical time scales with two minor exceptions. The ^{9}C production threshold from ^{14}N is at a proton energy of 39 MeV. Since $^{9}C(\beta^{+})\ ^{9}B \rightarrow p(2\alpha)$ this does not lead to ^{9}Be. The production threshold of ^{9}C from ^{16}O is at 50 MeV proton energy, hence it cannot be produced in our accessible energy range. Although ^{10}Be does decay to ^{10}B, its half-life is 2.7×10^{6} years; fortunately ^{10}Be production is low at least at the high proton energies measured (YBDFGB 68, 0.3±0.2 mb for 135 MeV protons on ^{16}O). The threshold for its production from ^{14}N is 34 MeV, from ^{16}O it is 36 MeV. The time of flight technique does have the weakness that it fails for very low energy products. Since at 22 MeV proton energy ^{7}Be and ^{11}C are the only isotopes of A=7 and A=11 produced from spallation of ^{14}N, I performed a cross-section measurement based on their radioactive decay to check the time of flight technique; this is presented in chapter 5.

The MSU Cyclotron is particularly suited to make measurements with proton energies from 22 MeV to above 40 MeV. In this range the beam intensity needed (≃500 n amp), and narrow pulse width (0.2 n sec has been achieved) of beam bursts essential for the success of the time of flight technique can be routinely obtained. This energy range is also important for relevant theories of nucleosynthesis of LiBeB as pointed out above.

The experimental equipment used in the time of flight measurements is discussed in chapter 2. Chapters 3 and 4 treat data acquisition and reduction respectively. Chapter 5 contains the radioactivation-decay measurements and chapter 6 presents the major developments in astrophysical theories on the production of LiBeB. Conclusions and calculations based on the newly acquired cross-sections and pertinent to these theories are presented in chapter 7.

2. EXPERIMENTAL EQUIPMENT AND TECHNIQUES FOR TIME-OF-FLIGHT MEASUREMENTS

2.1 The M.S.U. Cyclotron Facility

The proton beam of the MSU cyclotron was used for all experiments. The time-of-flight technique depends most of all on the narrow beam burst width that can be achieved with this cyclotron. Widths as low as 0.2 nsec FWHM have been measured. The widths during our experiment have usually varied from 0.3 nsec to 0.5 nsec. The spacing between beam bursts depends on the frequency of the cyclotron RF and is therefore beam energy dependent. This spacing is 53 nsec at 42 MeV and 72 nsec at 22 MeV. As explained below (Appendix F) this spacing limits particle detection at low particle energy.

A schematic drawing of the beam transport and analyzing system is shown in Figure 2. The time-of-flight measurements were done in the large scattering chamber shown. Lately this is a 40 in. diameter chamber; in the early parts of the experiment a 35 in. diameter chamber was in its place. The irradiations for γ-ray counting were done in the small scattering chamber associated with the Enge split-pole-spectrograph because it allows faster access.

On-target-beam-spots were 0.030" to 0.050" wide by less than 0.1" high and beam currects from 300 to 800 namp were routinely obtained. Usually 3 to 4 μamps were extracted with 100% efficiency from the cyclotron under these conditions

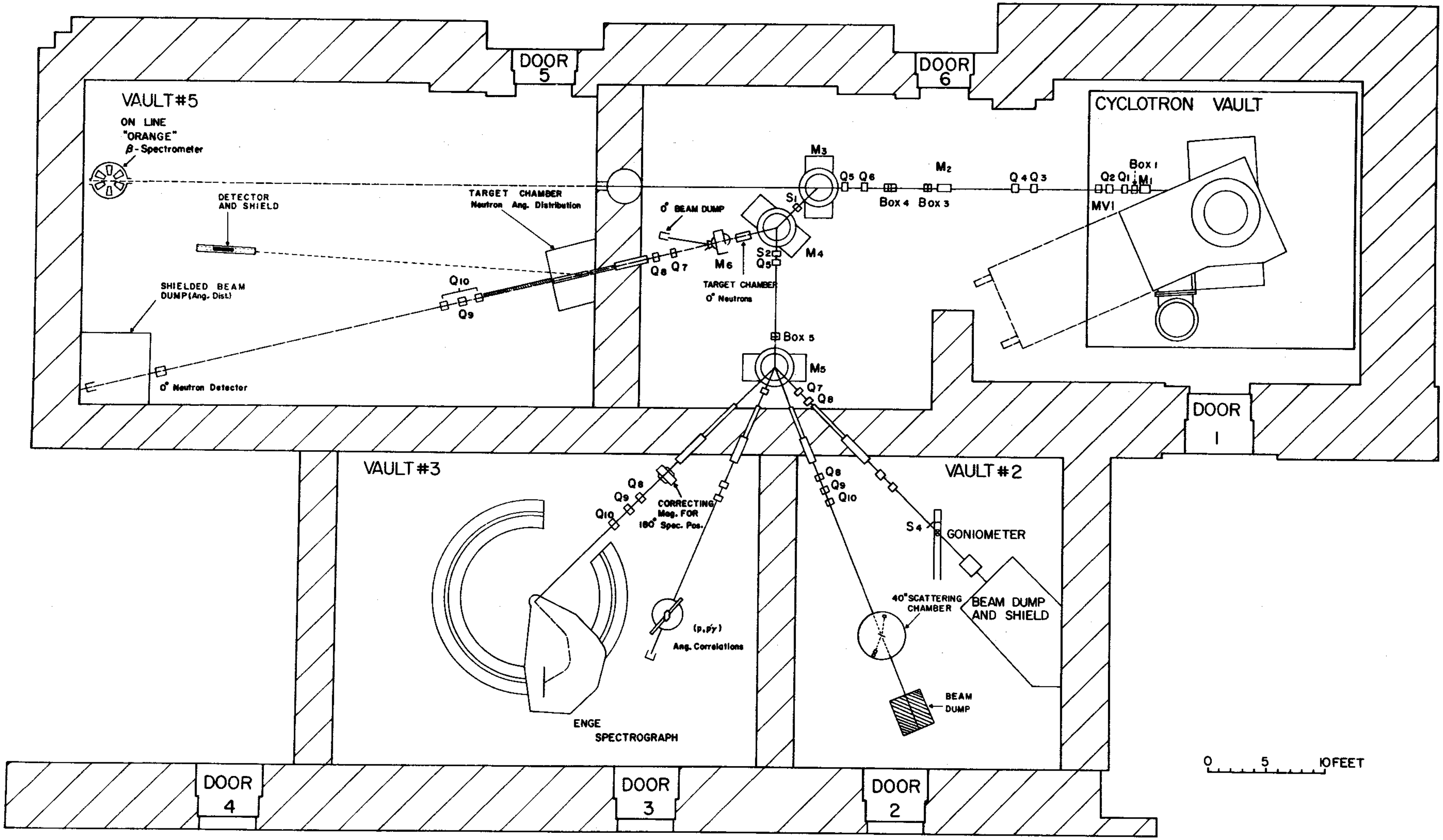

Figure 2. Schematic Drawing of the Beam Transport and Analyzing System.

with beam loss occurring at the various slits in the analysis system.

2.2 Target Choice

At room temperature N and O are gases, so if a solid target is wanted one must select some compound which contains the desired target elements as a constituent. The contribution to the observed yield due to the other elements in the compound must be determined however. The use of gas targets appears advantageous in this respect. They are also desirable for other reasons. Target thickness measurements for solid targets in the 100 $\mu g/cm^2$ range are not easily performed to an accuracy of better than 10%. For gas targets a pressure measurement need only be made. Here 1% accuracy can be easily achieved in the range 0.1 to 1 atmospheres. Target stability under bombardment is also no problem for N and O gas. There are also some disadvantages encountered in using gas targets. The gas cell design described below minimizes them so the experiment could be carried out successfully.

2.3 Gas Cell Design

2.3.1 Introduction

All gas cells must have a thin foil or "window" which confines the gas and through which the beam enters and reaction products leave to be detected outside the cell. The foil is hence chosen as thin as possible subject to the limitation that it must withstand the required gas pressure and stand up to the irradiating beam. A common foil used for gas cells is Kapton[1] available in 0.00025", 0.0005", or 0.001" thicknesses. For the relatively heavy, low energy reaction products which are to be detected in spallation of ^{14}N and ^{16}O, this still implies a large and unacceptable energy loss (see Appendix A). While a specially thin window must be used for these products, in our case it is a 30 μg/cm^2 formvar film, Kapton is quite acceptable as proton beam window; the energy loss for a 22.0 MeV proton traversing a 1/2 mil foil is only 0.040 MeV.

2.3.2 Slit System Design

When measuring yields with solid (foil) targets, the volume from which reaction products originate is usually well defined. One need only use one aperture in front of the detector to fix the solid angle for particle acceptance. In gas cells reaction products can originate anywhere along the line segment joining the point of entrance and the point of exit of the bombarding beam. Since the nuclear debris from the gas cell wall is not what one wants to measure, an additional slit is needed to limit the volume from which particles may reach the detector.

For the time-of-flight technique the slit system must be carefully designed. In Figure 3 the acceptance angle determined by slits 1 and 2 is shown. The beam intersects the rays of angle β at points A1 and A2. Reaction products falling on the detector may originate from any point on

---

[1] Available from E.I. Du Pont de Nemours, Wilmington, Delaware.

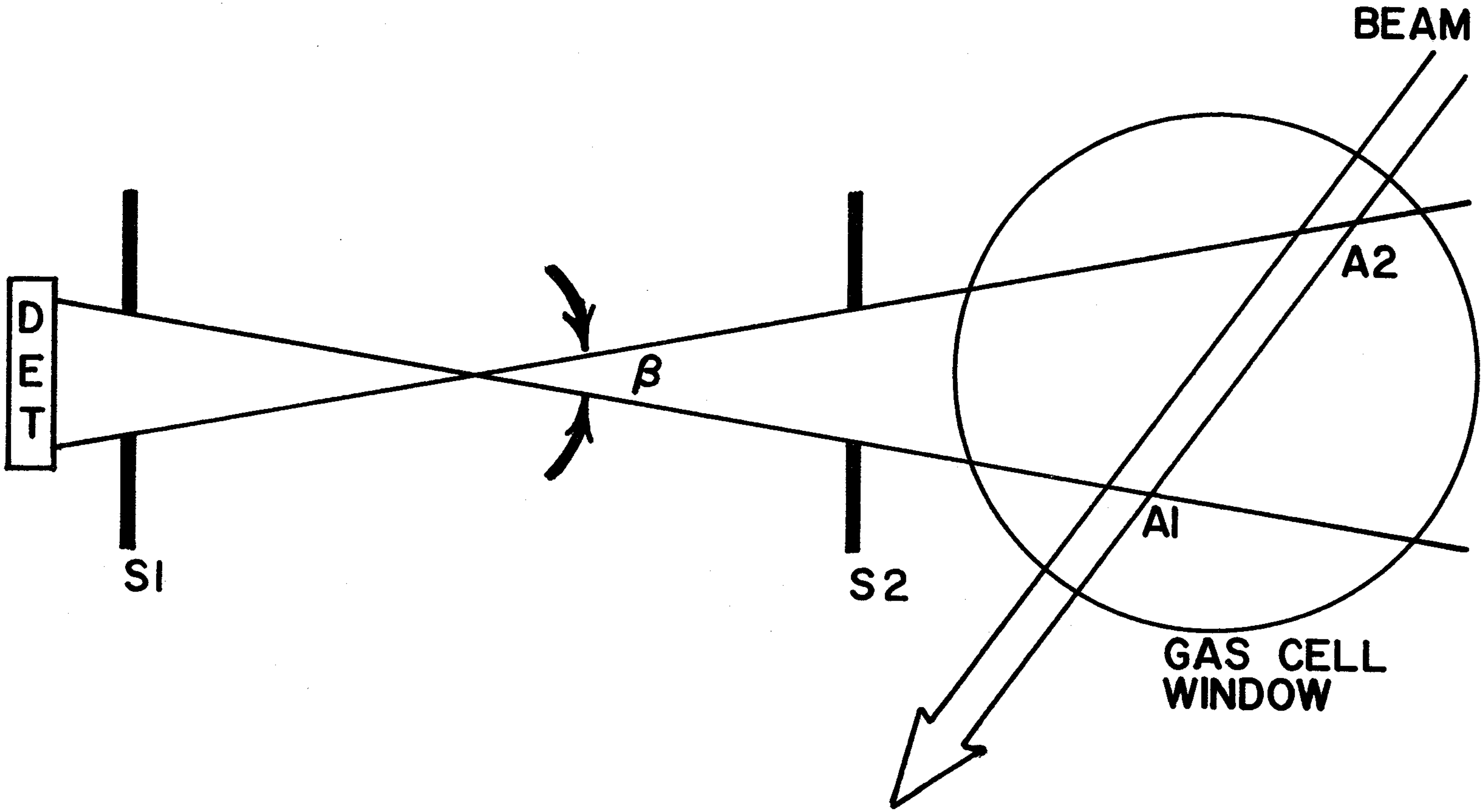

Figure 3. Schematic Drawing of a Gas Cell and its Slit System.

the line segment A1A2. This means that there is a range of flight distances. This manifests itself in terms of an uncertainty in the flight time of reaction products. In Appendix B the calculations relating the slit geometry to counting rate and flight time resolution are presented. The conclusions one can draw are that S2 should be as close to the origin of reaction products as possible. The width of S2 and the width of the beam are then equally critical as far as flight time resolution is concerned. Making S2 smaller than the width of the beam would gain little for flight time resolution but would lower the yield, an obvious disadvantage. The size of S1 is not as critical and is mainly determined by the active area of the detector. S1 represents the horizontal extent of the aperture in front of the detector. The vertical dimension of this aperture has even less effect on differences in flight path length. The dimensions of the aperture used were .125" wide x .25" high.

2.3.3 The Shell, Collimation Slit and Formvar Window Support

The above considerations led to the gas cell design shown in Figure 4. The important element is a cylindrical shell sliding in a keyway in the cell. The end of the shell closest to the beam acts as defining slit S2. It also supports a formvar film which acts as the cell exit window for the spallation products. Since S2 must be fixed with respect to the detector, and since S2 is rigidly secured to the gas cell, the slit, cell, and detector must rotate together when the detection angle is to be changed.

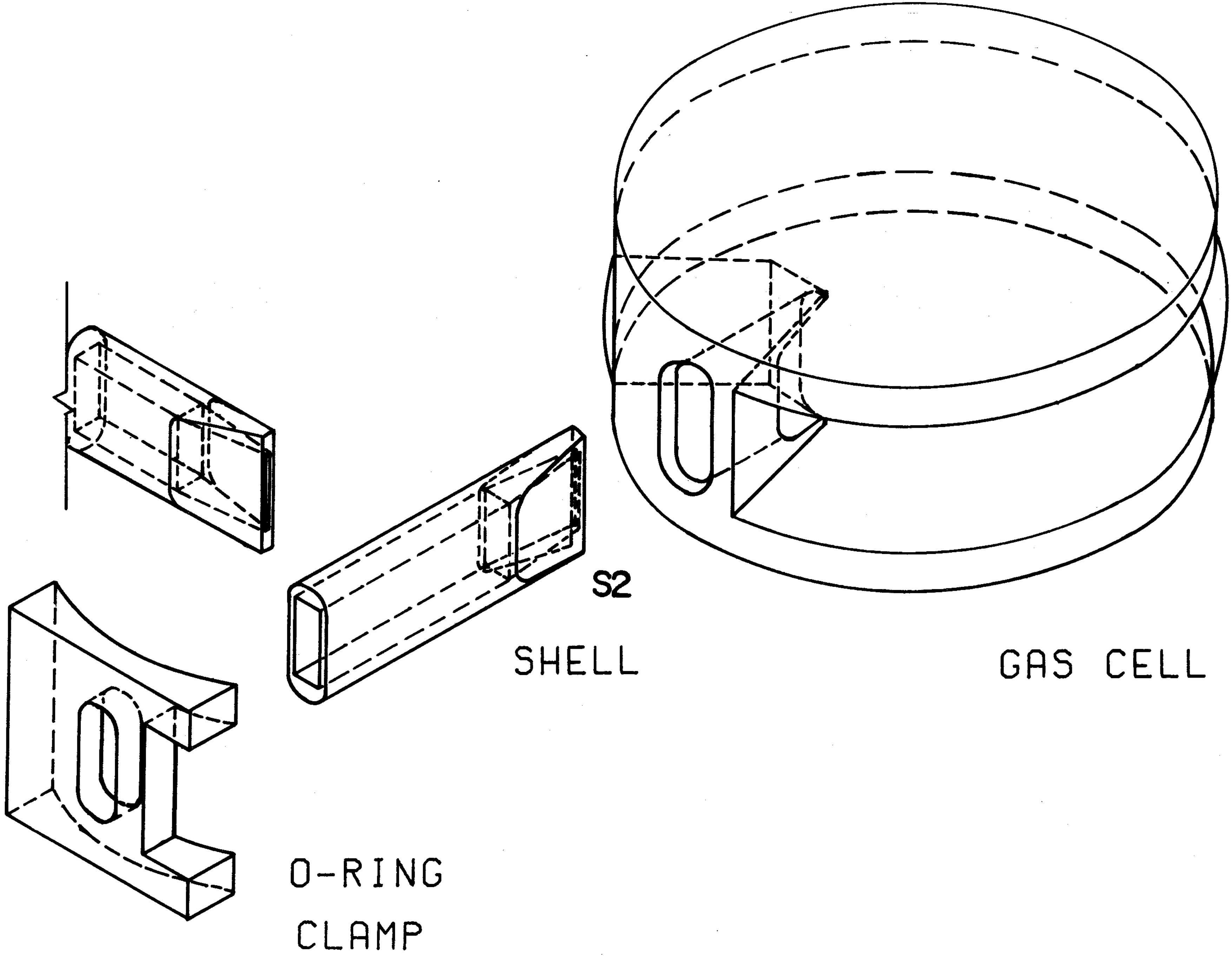

Figure 4. Gas Cell Design

The shell is milled in two parts which are then sweat-soldered together. The curved surfaces are milled last, after which the shell is polished. The lips at S2 are rounded by buffing. This ensures that the stresses causing rupture of the formvar window under pressure are better distributed. The slit end of the shell is also tapered so it can be moved as close to the beam as possible.

Reaction products lose energy not only in the formvar window but also in the gas they must traverse. Depending on the detection angle the shell is positioned to minimize this distance. At 1/10 atmosphere the density of N_2 is 125 $\mu g/cm^3$. It would seem desirable to work with low gas pressures to minimize energy loss; however the yield and hence the time needed to perform the experiment is directly proportional to the gas pressure. Also background events are largely independent of gas pressure; this implies a minimum pressure for a successful experiment. For a nitrogen pressure of 25 torr and a 30 $\mu g/cm^2$ formvar exit window we can obtain an average total exit areal density of 50 $\mu g/cm^2$ at 90° and 130 $\mu g/cm^2$ at 15° detection angle.

In order to avoid repeated mechanical adjustments of the shell, but to still minimize energy loss in the gas , we simply mounted the gas cell and slit system slightly off center on the scattering chamber table. As shown in Figure 5 table rotations between 15° (or 165°) and 90° can be carried out with one shell setting. The distance between the beam and the closest point of the shell is

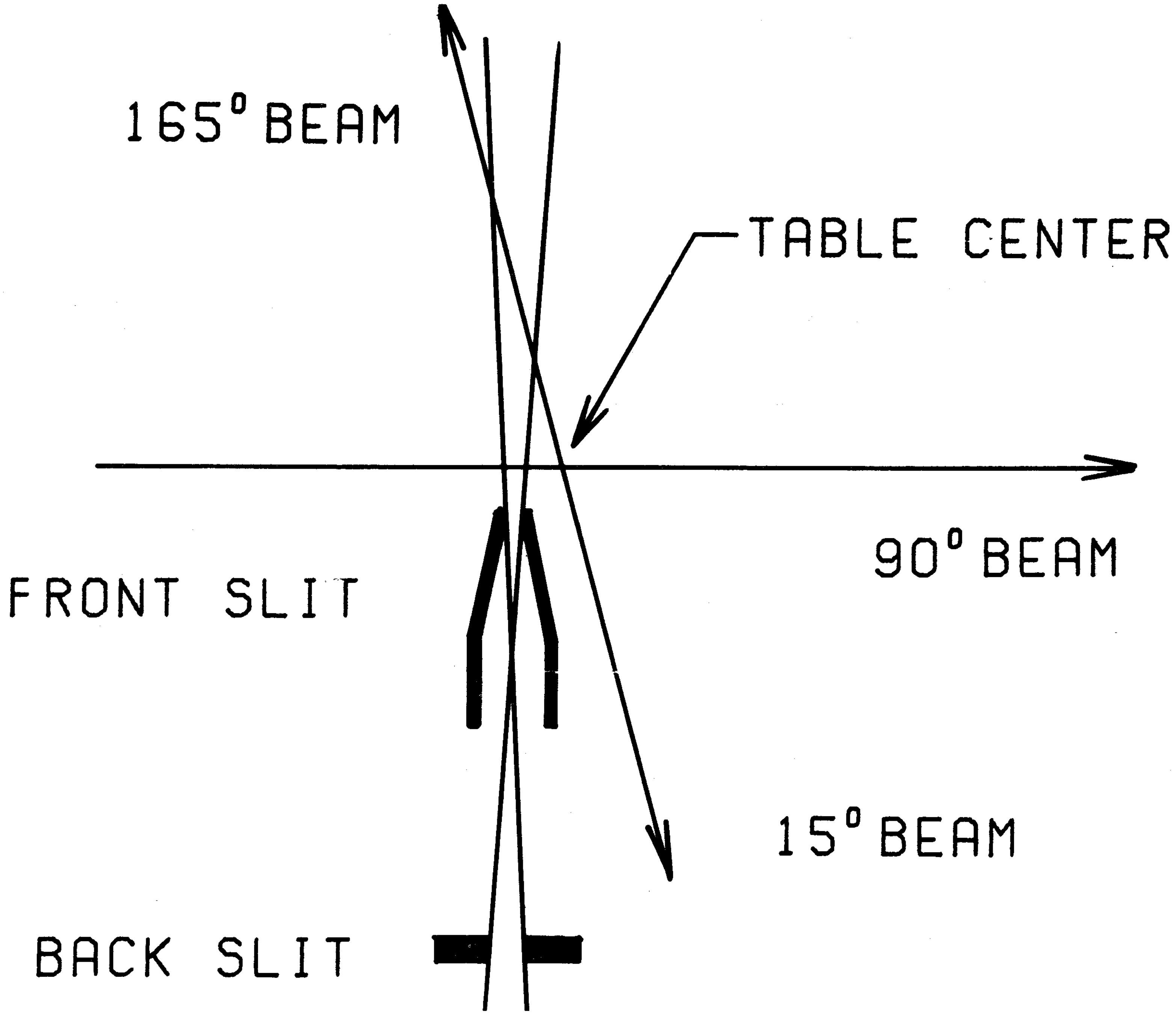

Figure 5. Schematic Drawing Showing Slit System - Table Center Geometry.

about constant and as a result practically minimum in-gas flight distance is achieved at all angles in this range.

The vertical extension of S2 is 0.750". Since the detector aperture is 0.250" high and the beam was always less than 0.1" high, this represents a big margin of safety for vertical alignment. The variation of the beam height with respect to the cell center was always less then ±3/32" as seen by beam spot burns on the Kapton window.

The horizontal dimension of the shell was chosen to be 7/16" so S2 widths up to 1/4" could be accommodated.

2.3.4 Gas Cell Construction

The gas cell structure is made of brass. Two 5" disks were silver soldered to a spacer which had been milled with a keyway for receiving the shell. The spacer subtends 60° from the center of the cell. After silver soldering, the cell diameter was turned down to 4.75". A chamfer was then milled at the mouth of the keyway. This forms one surface of an O-ring vacuum seal; the other is the side of the sliding shell. The pressure needed for the seal is exerted with a clamp screwed to the body of the cell.

The geometry of the shell and the vacuum seal determine the minimum detection angle. This is the reason for the non-circular design of the shell. A tube of 1.125" diameter in a gas cell of the same diameter would allow a minimum detection angle near 20°, while for the actual design it is 10°.

A 0.25" Imperial Eastman vacuum fitting soldered into the top disk of the cell serves the double function of evacuation outlet and gas inlet. Kapton foil 0.0005" thick was bonded to the gas cell using the epoxy Ciba Araldite 502. The brass surface was prepared by light sanding or filing just prior to the epoxy application. At pressures up to 50 torr and beam currents up to 800 nano-amps the Kapton held up indefinitely.

2.4 Formvar Windows

Formvar $(H_{16}O_8C_4)$[1] is available in powder form. To cast formvar film a 2% solution by weight of formvar in 1, 2 Dichloroethane is prepared. A 6" diameter glass beaker is filled with distilled water (care must be taken that no soap residue is in the beaker, since the surface tension of the water would be reduced). A 14 B.S. gauge wire is dipped into the formvar solution and a line is drawn with the wire tip across the water surface. A thin layer of solution spreads on the water and within a few seconds the 1, 2 Dichloroethane evaporates, leaving a formvar film.

This film is lifted from the water with a square wire loop. The plane of the loop is held perpendicular to the water surface during the lifting process. A double layer of formvar clings to the loop and is transferred immediately to the slit end of the shell by passing the shell through

---

[1] Available from Shawinigan Resins Corporation, Springfield 1, Mass.

the wire loop. This process is repeated until a formvar window of the desired thickness has been built up. Air drying for a few hours cures the formvar film. The drying may be speeded up by using an infrared heat lamp. Very thin wrinkle free formvar films are produced by the technique just described. To measure the average thickness of formvar film produced by the above technique, 44 double layers were cast and transferred to a 5/8" i.d. copper tubing. The energy loss of the 5.48 MeV alpha particles from an americium source was used to calculate the thickness. The electronics to process pulses suitable for a Nuclear Data 160 multichannel analyzer was the same as for the energy signals for particle identification described under data acquisition and shown in Figure 7. The electronics was checked for linearity with test pulses, making sure E=0 corresponded to channel 0 of the ND 160. The 5.48 MeV peak centered in channel 587 shifted by 9.5 channels when the built up formvar film was introduced between the source and the silicon surface barrier detector. The calculation in Appendix C shows this represents an average thickness of 2.4±0.2 $\frac{\mu g}{cm^2}$/ double layer.

A 30 $\mu g/cm^2$ formvar window over a 0.040" slit sustains a pressure of 25 torr for many hours. The films are weakened by the variable stress occurring during repeated pumping down to vacuum and letting up to air pressure.

2.5 Pressure Measurements

2.5.1 Equipment

The gas pressure was measured and monitored at first with a Wallace and Tierman Type FA 145PP12296 aneroid gauge, later with an oil manometer designed and constructed by Lolo Panggabean. It has a range of 135 cm of oil; each miniscus can be read to ±0.5mm, hence the net error is ≃ ±1 mm for a pressure measurement. The oil used is the pump fluid Octoil[1]. At 25°C its density is 0.983 g/cm^3; its vapor pressure is 2×10^{-7} mm Hg.

A manifold interconnects gas cell, scattering chamber, manometer and target gas source. During data taking one side of the manometer is held at scattering chamber pressure (vacuum) while the other side is connected to the gas cell. During pump down all components are held at the same pressure, evacuation proceeds through the scattering chamber pumps.

2.5.2 Beam Heating

To calculate the target gas density, besides knowing the pressure, one must know the gas temperature. Since the beam loses energy as it traverses Kapton and gas, it is not obvious what the temperature of the irradiated volume is.

To obtain a rough estimate of how much the gas in the beam trajectory might be heated, the naive model described in Appendix D is considered; for our average operating conditions it predicts a temperature rise of ≃ 25°C above

---

[1] Octoil is manufactured by Consolidated Vacuum Corporation.

ambient gas temperature.

To experimentally check the effect and compare it to values given by the model, the beam was focused to produce a beam spot 0.025" wide, 0.045" high on the Kapton window. A cesium-iodide crystal mounted on a phototube was used to monitor the proton spectrum for scattering of 35 MeV protons from ^{20}Ne. The proton counts from the ground and first excited state were used to monitor the product of beam current and ^{20}Ne density. A 500 nano amp beam and a 100 nano amp beam were compared, results are given in Table 1.

TABLE 1. Beam heating comparison data.

Beam Current (nano amps)	Monitor Counts	Pressure (cm oil)	Integrated charge (10^{-7} coulombs)
500	152,277	53.35±0.2	3375.4
100	4,494	53.10±0.1	100.1

These date imply $T_{500}/T_{100} = 1.00 \pm 0.015$. The model predicts $T_{500}/T_{100} = 1.06$; the discrepancy is most likely due to more efficient gas mixing than postulated. To first order any error in charge integration is the same for both cases so the error in the ratio due to the pressure readings and total charge collected is negligible compared to the statistical error of 1.5% for the 100 nano amp beam measurement. To make sure the beam spot was of the same dimensions in both cases, slits near a beam antinode were used to cut the beam from 500 n amps to 100 n amps; this should not have influenced beam spot size which is determined by the object slits.

2.6 Beam Integration

A 57" section of 4" diameter beam pipe served as Faraday cup for charge collection. The beam was dumped on an aluminum plug at the end of the pipe. The section was insulated from the scattering chamber by a 1.5" plastic ring. Charge integration was performed with an Elcor model A310B current indicator and integrator. Performance of the integrator was checked with a 1.35 volt mercury cell in series with a 1% 4.5 meg. ohm resistor. This test was performed both at the input to the integrator in the data room and at the Faraday cup. The maximum deviation between expected and observed total charge was 1.6%. The average deviation was less than 1%. Two successive 9 min calibrations were consistent to within 0.17%.

2.7 Particle Detectors

2.7.1 Spallation Product Detection

Particle energy was measured with silicon surface barrier detectors manufactured by Ortec. Thinner detectors have faster rise times, hence yield better timing pulses for low energy signals. For this reason thin detectors, 75μ and 85μ thick, were used for all proton beam energies below 40 MeV. At or above 40MeV a 150 μ detector was used for the ^{14}N target. Minimum detector thickness was set by the requirement that all spallation products heavier than mass 5 be stopped in the detector. A 250 μ detector placed behind the thin detector served as veto for particles not stopped in the first detector. This was done to minimize computer processing time for uninteresting events.

To achieve best possible energy resolution, the detector was cooled by pumping alcohol cooled to near dry ice temperature through a copper yoke which held the detector. It was also usually overbiased by 50% to insure short collection times and hence achieve optimum timing signals. The energy resolution, checked with the 5.48 MeV α peak of an americium source, was always better than 40 keV FWHM. The detector holder, solid angle defining aperture, and gas cell are all mounted rigidly on a rail held in a block of aluminum which is provided with pins that fit precisely into positioning holes of the rotary scattering chamber table. This system assures reproducibility of geometry.

2.7.2 Proton Elastic Peak Monitor

To calculate the cross-section corresponding to an experimental yield measurement, one has to know both the integrated charge of the proton beam and the density of the gas target. A gas leak during a bombardment would present a difficult pressure monitoring problem. It is a common technique to use a monitor cross-section to integrate the product of gas density and beam intensity during a bombardment. The proton detector is set at a fixed angle and the proton energy spectrum is recorded. The number of events in the elastic peak for each bombardment represents the integration. The pressure must then be accurately known only for a calibration point (see Chapter 2, section 2.5.1).

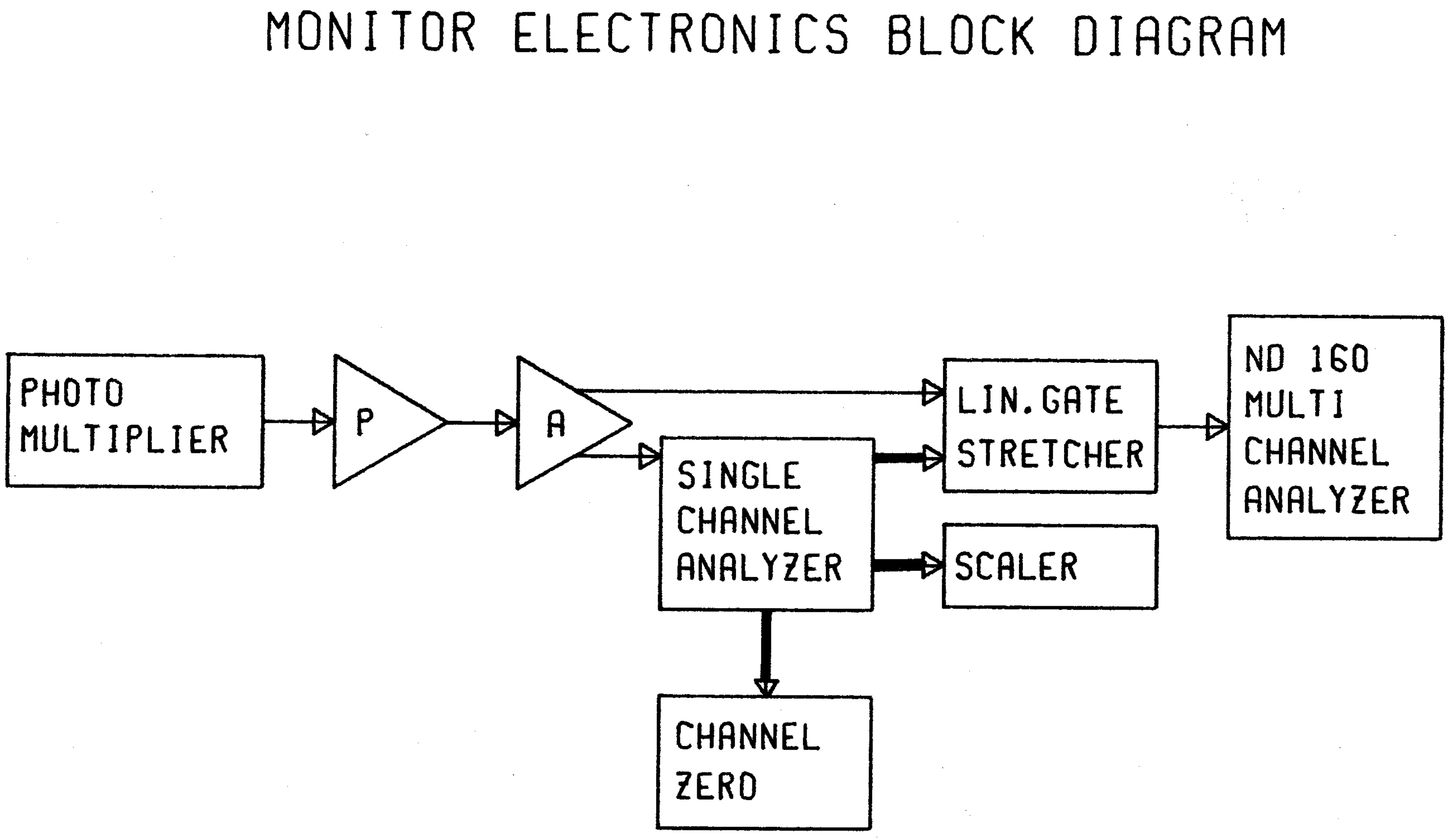

Figure 6. Monitor Electronics Block Diagram.

A cesium iodide crystal mounted on a phototube was used to monitor the proton spectrum. (This detector was designed and constructed by Larry Learn of the MSU Cyclotron Lab.) Figure 6 shows the electronics used to record the spectra. A single channel analyzer was set to accept only pulses from the elastically scattered proton peak. The proton spectrum was also collected in a Nuclear Data 160 multichannel analyzer so gain shifts in the photomultiplier could be detected and scaler counts could be corrected if necessary.

2.8 Time-of-flight Electronics

A schematic of the electronics configuration is shown in Figure 7. Table 2 identifies abbreviations, manufacturers, and model numbers.

Reaction products of interest are stopped in a silicon surface barrier detector, labeled E detector. It is connected by a 3ft, 22pfd/ft Microdot cable to a time-pickoff unit and then to a preamplifier. The time-pickoff in conjunction with a time-pickoff control derives a timing pulse from each energy pulse. This system employs leading edge timing. A time-to-amplitude converter (TAC) is started by this timing signal. The stop pulse is obtained from the cyclotron RF system.

To avoid the non-linear region of the TAC ($\simeq$15% of the 100 nsec range), it is desirable that the RF stop pulse occurs at least 25 nanoseconds after the start pulse. To

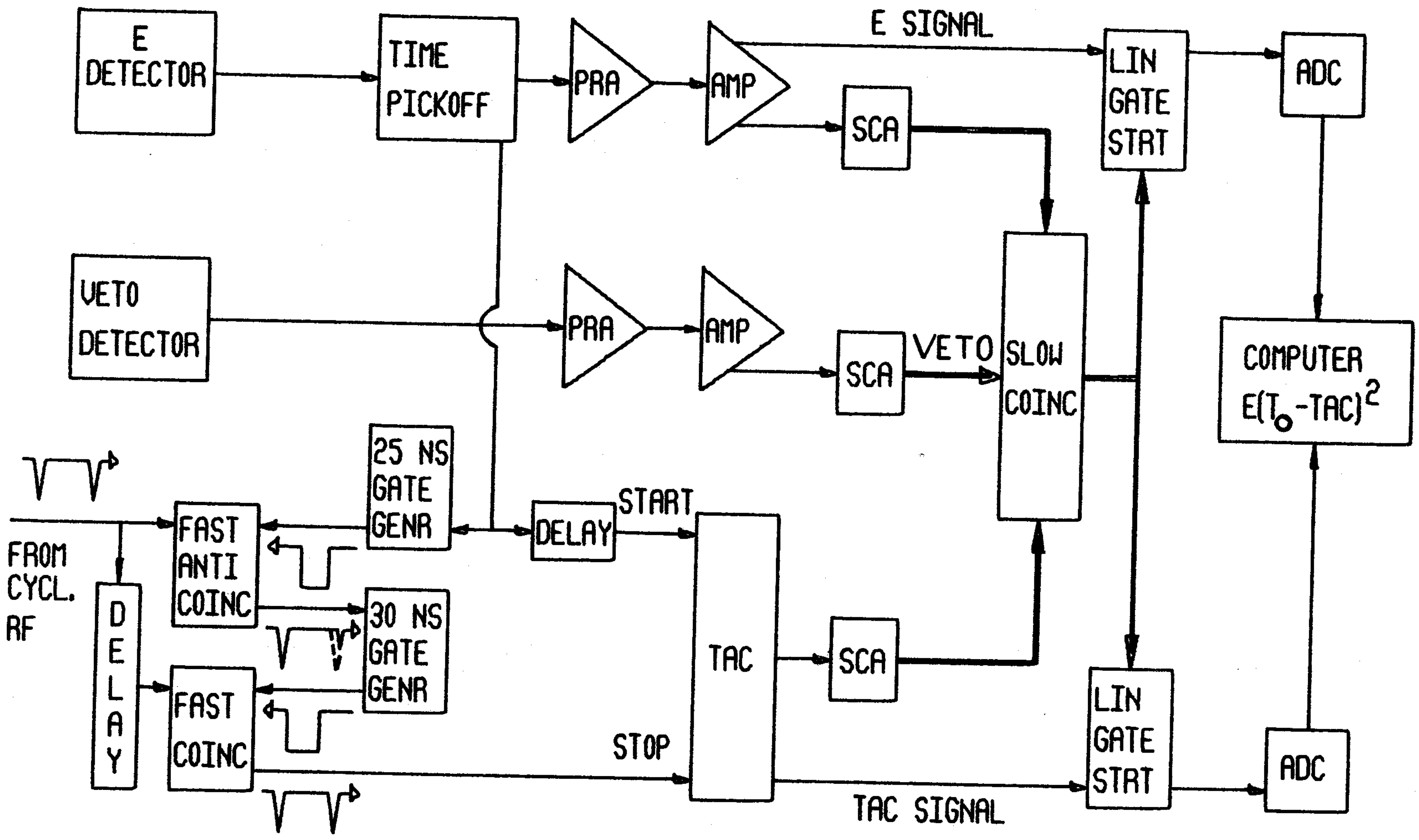

Figure 7. Electronics Block Diagram for Charged Particle Time-of-Flight.

Table 2. Electronics Equipment.

Unit		Model Number and Manufacturer
(ADC) Analog to digital converter		629 Northern Scientific
AMP amplifier		440 ORTEC
COMPUTER		SIGMA 7 XDS
Detector, E and Veto		Si surface barrier ORTEC
Fast anticoincidence Fast coincidence	one module	C102B/N EG+G
Gate generator, 25 and 30 NS, one module		121LRS
TAC time to amplitude converter		437 ORTEC
Time pickoff		260 ORTEC
Time pickoff control		403A ORTEC
SCA Single-channel analyzer		420A ORTEC
Slow coincidence		418 ORTEC
Linear gate stretcher		442 ORTEC
PRA preamplifier		109A ORTEC

do this in a fashion which also maintains the dynamic range of particle flight times, logic has to be done on the start and stop signals. The start signal triggers a discriminator which is set to give a 25 nsec long positive going pulse. This pulse and the RF pulse are presented to a fast coincidence operated in anticoincidence mode. Only RF pulses which come later than 25 nsec after the start pulse yield an output signal. Figure 8 represents three situations of the start and stop pulse relationship. Time increases from left to right. In each set of pulses the first line represents stop pulses, the second line is the 25 nsec gate pulse generated by the start pulse in line three. Line four schematically represents the height of the TAC pulse by the length of the rectangular pulse shown. The first set shows the stop pulse arriving later than 25 nsec after the start pulse; the second set is an example of the first stop pulse coming within 25 nsec of the start pulse and the third set illustrates the nonlinear effect for stop pulses arriving ≃25 nsec after the start pulse. To avoid the nonlinear effects for signals which are close to the edge of the 25 nsec pulse and hence are partially attenuated (see Figures 7,8), the second channel of the LRS model 121 is used to provide a negative going 30 nsec pulse for each accepted RF pulse. This negative pulse and the original RF pulse appropriately delayed are fed into the second channel of the fast coincidence module. A uniform RF stop pulse with the correct time relation to the start

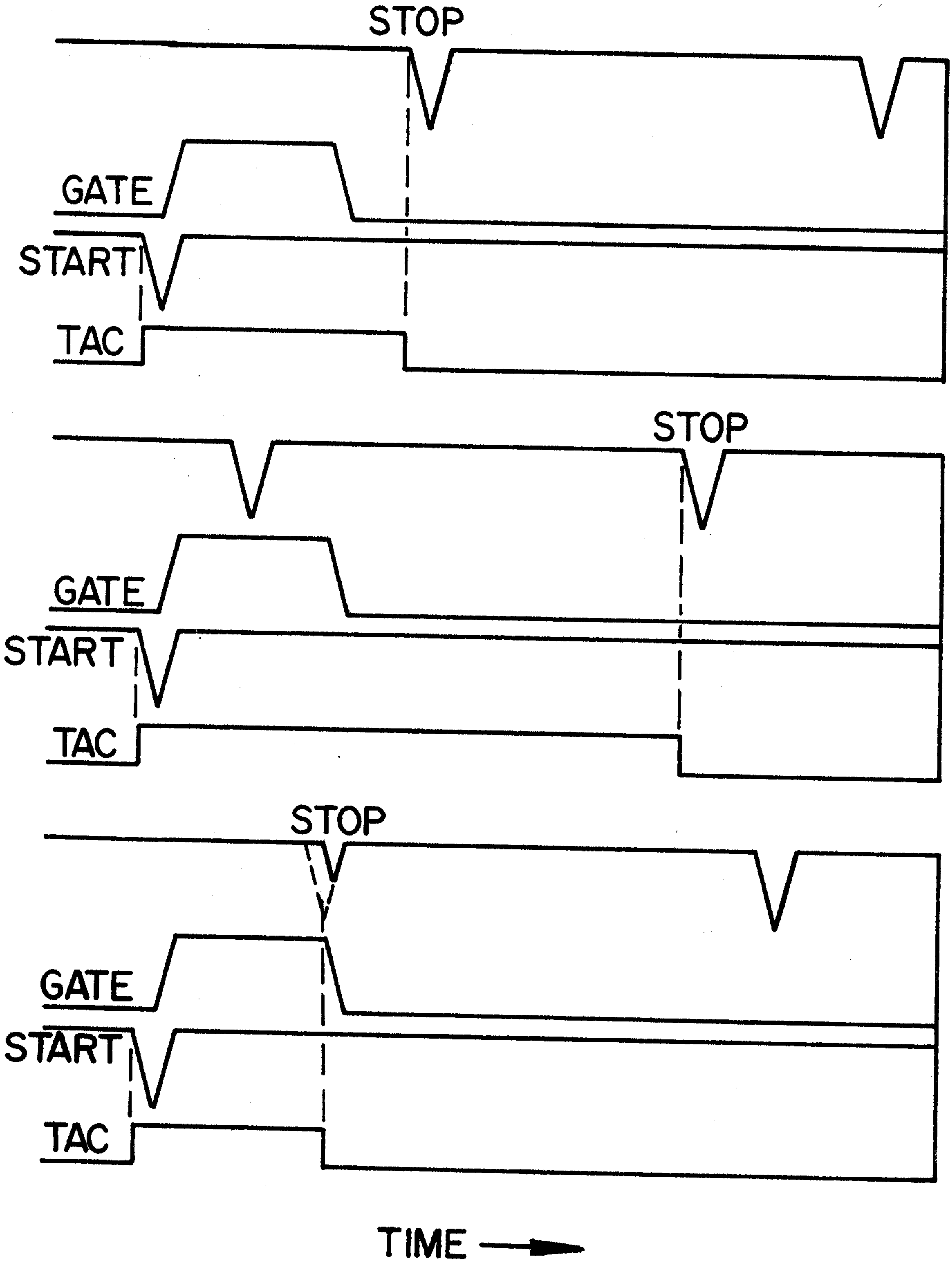

Figure 8. Start, Stop and TAC Pulses.

pulse is obtained by this means. Of course the start pulse presented to the TAC has to be delayed by the time needed to perform these logic operations. With the noted choice of start and stop pulses, fast particles, hence short flight times, are associated with large TAC pulses, while slow particles are associated with small TAC pulses. A pulser simulating events should produce a flat, continuous random time spectrum. The smallest TAC pulse should represent 25 nsec delay between start and stop, while the largest TAC pulse should represent (25 nsec + 1-RF-period) delay.

The energy pulse from the preamp is fed into an amplifier. A single-channel analyzer in the integral mode provides a logic pulse for each energy pulse above a set level. Similarly the TAC pulses are fed into a single channel analyzer for logic pulses. To be able to discriminate out particles passing through the front detector, a detector placed behind it provides veto pulses. The single channel analyzer pulses from the energy signal and TAC signal are fed into the coincidence input of a slow coincidence circuit while the veto pulses are fed into the anticoincidence input. Linear gate-stretchers for energy and TAC linear signals are gated by the coincidence logic output. These are presented to 8192 channel ADC's. The ADC's are then read by the XDS Sigma 7 Computer.

2.9 The 17 MeV Measurement

The lowest proton energy available with good timing characteristics and sufficient beam intensity is presently near 22 MeV. The cross-sections for masses 7, 10, 11 from proton spallation of ^{14}N are still large at this energy. It was thus very desirable to perform a cross-section measurement at a lower energy, lowering the beam energy by introducing a degrader. In Appendix E are calculations to choose degrader material and thickness. Aluminum is better than heavy elements such as lead in terms of energy spread caused by degrading the beam by a fixed energy differential. Aluminum is also advantageous since when irradiated by protons the radioactive products have comparatively short half-lifes and handling equipment after irradiation is less of a problem. The beam emerging from the degrader also has an increased angular spread. It is therefore important to position the degrader as close to the gas cell as possible. Since the resolution is still quite marginal for masses 10 and 11, it was desirable to have the display for the non-degraded beam as a guide. Therefore a mechanism for inserting and removing the degrader was devised. A solenoid was designed to lift the degrader in and out of the beam path at 0.25" from the Kapton gas cell window. The mechanism could be actuated in less than a second. This made it possible to compare instantaneous beam intensity ratios with the degrader in and out of the beam. Due to the angular spread not all of the degraded beam was collected in the Faraday cup. Spot checks were made throughout the experiment to determine the ratio. The total charge collected was scaled by the average of these rather constant ratios.

The beam degrader chosen was 0.085" thick 6061 aluminum alloy. For the proton beam energy of 21.65 MeV the degraded beam energy is calculated in Appendix E to be 16.8 MeV. Experimentally the degraded beam energy was determined to be 17.2 MeV ±0.2 MeV from the cesium iodide monitor spectra for degraded and direct beam.

3. DATA ACQUISITION

3.1 On Line Setting Up Procedure for Data Taking

3.1.1 Introduction

When the proton beam is first brought into the scattering chamber, the detector-gas cell assembly is removed. The beam is focused on a plastic scintillator at the center of the scattering chamber. The beam spot on the scintillator is viewed by remote TV. Once a satisfactory spot, appropriately centered on the scintillator, is obtained, the gas-cell-detector assembly is positioned in the scattering chamber. Manometer, gas cell and scattering chamber are evacuated. The gas cell is then filled with the gas target of interest to the pressure desired. The detector is replaced and the detection angle is set to 15° with respect to the beam which is again brought into the scattering chamber.

3.1.2 Software

Data taking is done under the all purpose code TOOTSIE, written by Douglas L. Bayer (BA 71). Data is displayed at run time on a Tektronix 611 storage scope. Data and display are manipulated and interacted with by both teletype and switch commands.

The EDE mode of TOOTSIE is used for choosing the correct delay for RF stop pulses. In this mode TOOTSIE plots two variables, x-axis=energy pulse, y-axis=TAC pulse as shown in Figure 9.

Starting with the first display, where the timing pulse of the fastest particle arrives sometime between RF stop

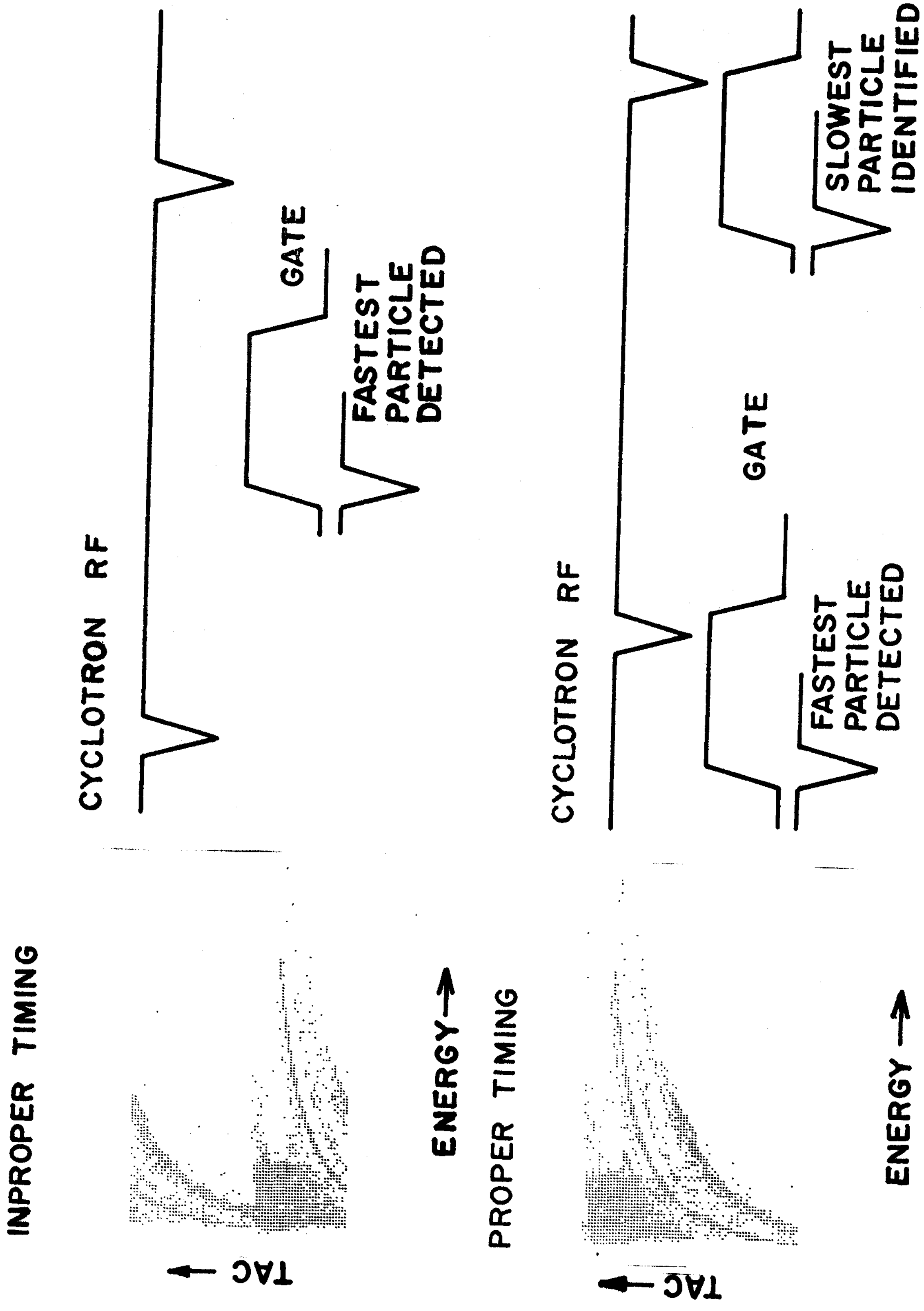

Figure 9. Stop Pulse Timing Adjustment.

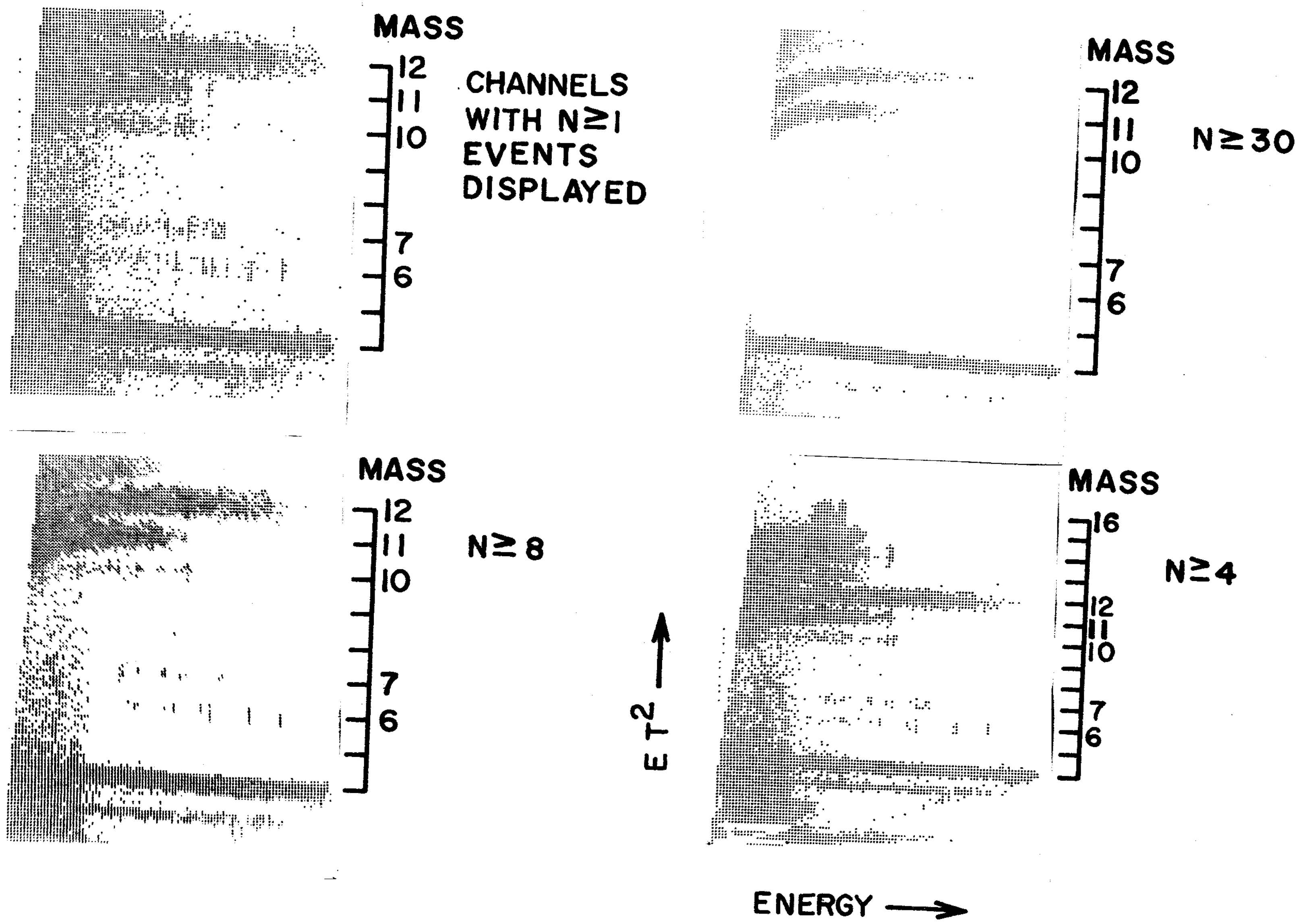

Figure 10. Mass Band Displays.

pulses, delay is added to (or subtracted from) the RF stop pulses until the second display, with the timing relation indicated, is obtained. Optimum delay is such that the fastest particle of interest has the longest TAC pulse (25 nsec+1 RF period). The slowest particle that can then be identified will come one RF period later and will have a TAC pulse equivalent to 25 nsec. Once the RF delay has been determined, the E*T**2 option of TOOTSIE is entered. In this mode the quantity [A+E*(TAC-TZERO)**2/NORM] is plotted against E on a two-dimensional analyzer. E is the energy signal and TAC is the time signal. The parameters A, TZERO, and NORM are selected at run time to display data in the most convenient form (see Figure 10).

3.2 Data Taking

Once the parameters are satisfactory, data is accumulated. Energy spectra of the various masses can be derived from the two-dimensional display. An option in TOOTSIE makes it possible to define upper and lower bounds of a mass band. This is done by choosing points with a cross which is moved from scope switches. Up to a ninth degree polynomial fit can be performed on these points. The resulting curve is then one of the mass band boundaries. Given upper and lower bounds, TOOTSIE generates energy spectra by summing all counts in the band identified by the same horizontal (energy) channel number. Since data is taken on a 128x128 array, the energy spectra are 128 channels long. Sample energy spectra are shown in Figure 11. The complete two-dimensional array as well as the energy spectra derived from it were punched on cards. The data, as read from the ADC's can also be stored on tape. The tape can later be read by TOOTSIE and the data can be reanalyzed. It is thus possible to use different parameters to display portions of the data for easier analysis. Figure 10 shows four oscilloscope displays for the data from ^{16}O for 37.9 MeV protons with the detector at 15° to the beam. One display shows all data up to mass 16; by using a different set of values for the parameters NORM and A, and by displaying only those channels which have N or more events, one obtains the other three displays (N=1, N=8, N=30). The valley between mass 11 and 12 can thus be seen on the (N=30) oscilloscope display. The nonlinearity (mass defect) of the mass bands toward low particle energy is due to incomplete charge collection by the detector.

Background events, presumably neutron induced reactions in the silicon detector,contaminate the spectrum at low particle energy as is evident in Figure 10. This data represents the most severe case. For lower energy proton beams the background is considerably less. Since ^{14}N spallation cross-sections are considerably larger, background is less of a problem even at high proton beam energy for that target. For the 41.9 and 37.9 MeV data, background runs were taken with no gas in the cell. Cross-section calculations in Table 8 and angular distributions for these runs are labeled "Vac". The cross-sections summarized in Table 9 are corrected for this contribution.

3.3 Dead Time Correction

Dead time of the analog to digital converters (ADC) is monitored using the option "channel zero" in the program TOOTSIE (BA 71). A logic pulse presented to channel 0 is counted only if the ADC's are free to accept an event. Thus the ratio of the number of counts in channel zero to the number of pulses presented is the fractional lifetime of the ADC's. The source of pulses for channel zero has to be chosen carefully. For example if the beam intensity fluctuates, then a random or fixed frequency pulser will indicate less deadtime than is actually the case. Suppose, for example, that the beam is off for 9 sec and on for 1 sec periodically; then even if the ADC's are completely dead during the 1 sec, the channel zero count will indicate only 10% deadtime while actually the deadtime is 100%. This shows the channel zero pulses should come from a source which is directly correlated with scattered particle intensity. The proton elastic peak monitor was used for this purpose.

3.4 Mass Band Resolution

For the correct choice of TZERO the quantity (TAC-TZERO) is proportional to the flight time t of the particle. Beam bursts have a finite duration; flight path length varies for different particles; and the energy resolution of the detector is not perfect; hence what is ideally a series of sharp lines representing the energy spectra of different masses, becomes a set of bands. As shown in Appendix G the width of a band is governed by the equation:

width of band = $\Delta(Et^2) = Et^2[(\Delta E/E)^2 + 4((\Delta x/x)^2+(\Delta t/t)^2)]^{\frac{1}{2}}$

E = energy,

X = flight distance,

t = flight time,

ΔE = energy resolution,

ΔX = uncertainty in the flight distance

Δt = width of the beam pulse.

Suppose the quantity Et^2 is given in mass units. To separate one mass band from the next, $\Delta(Et^2)$ should be less than one mass unit. From the equation for $\Delta(Et^2)$ it can be seen that the higher the mass, the more difficult it is to resolve it.

To resolve mass m the fraction $\Delta(Et^2)/Et^2$ must be less than 1/m. This represents 17% resolution for mass 6 and 9% resolution for mass 11. Table 3 summarizes individual contributions to the mass resolution as discussed in Appendix G. The observed band width can be accounted for by these contributions. Table 4 gives a specific example. It is fortunate that for low energy particles where energy resolution starts to become significant, the beam time-resolution is less limiting than for higher energy particles.

Table 3. Individual Contributions to $\Delta(Et^2)$ in Terms of Percentage of Et^2.

	Particle Energy ΔE
Source:	Detector resolution of 5.48 MeV α is $\approx$ 40 kev
Max:	8% (for a 0.5 MeV particle)
Min:	0.2% (for a 20 MeV particle)
	Time Resolution (Cyclotron) δt
Source:	Average width of cyclotron beam burst was 0.5 nsec (.3 to .7 nsec were measured)
Min:	1.2% (slowest particle, flight time $\approx$ 84 nsec)
Max:	8% (fastest particle, taken to be 20 MeV mass 6, flight time $\approx$ 12 nsec)
	Time Resolution due to Δd (flight path length uncertainty)
Source:	geometry; beam width 0.040", front slit S_2=0.040"
Min:	0.8% (detector at 90°, holds for all particles)
Max:	5% (detector at 15°, holds for all particles)

Table 4. Band Resolution of Spallation Data from ^{14}N by a 41.9 MeV Proton Beam.

Geometry: Detector angle 15°, beam width 0.040", front slit S_2 = 0.040".

Particle energy considered: 5.48 MeV.

Observed mass resolution: 6±1 channels FWHM for mass 11,
4±0.5 channels FWHM for mass 6.

One mass unit = 9.6±0.1 channels.

Theoretical Resolution Contributions to $\Delta(Et^2)$ in % of Et^2

	Mass 6	Mass 11
Due to ΔE=40 kev	.7	.7
Due to beam burst width δt	4.4	3.3
Due to flight path length uncertainty Δd	5.0	5.0
Contributions combined in quadrature	6.7	6.0
Observed band spread percentage of Et^2 (FWHM)	7.0±0.9	6.9±1.1

4. DATA REDUCTION

4.1 Energy spectra and low energy cutoff correction

Energy spectra were obtained directly from the data taking routine TOOTSIE as outlined in section 3.1.2. An alternate method was also employed based on the two dimensional array obtained in card form. A fortran program was written for converting the two dimensional data into a set of mass spectra by generating line-printer plots of the events stored in the set of channels in a line parallel to the (Et^2) axis. The mass band fitting could then be done off line. This was of advantage for two reasons; time did not have to be spent at run time to perform all band fits, and, as can be seen from Figure 9, mass separation for mass 11 is not always easily determined on the scope display. A second fortran program was written to generate 128 channel energy spectra from the two dimensional data, given the band fits determined from the printer plots.

A few energy spectra are shown in Figures 11 to 39. They are representative in the sense that the 37.9 MeV data is the lowest quality taken, while that at 25.6 MeV is among the better data sets. The energy spectra collected all have a low energy cutoff. This is usually due to the finite flight time available and the energy losses in gas and formvar window. The energy cutoff for particle detection due to detector and time pickoff sensitivity limitations is near 0.5 MeV; this represents the limiting factor for masses 6,7 for proton beam energies below 30 MeV (since then the

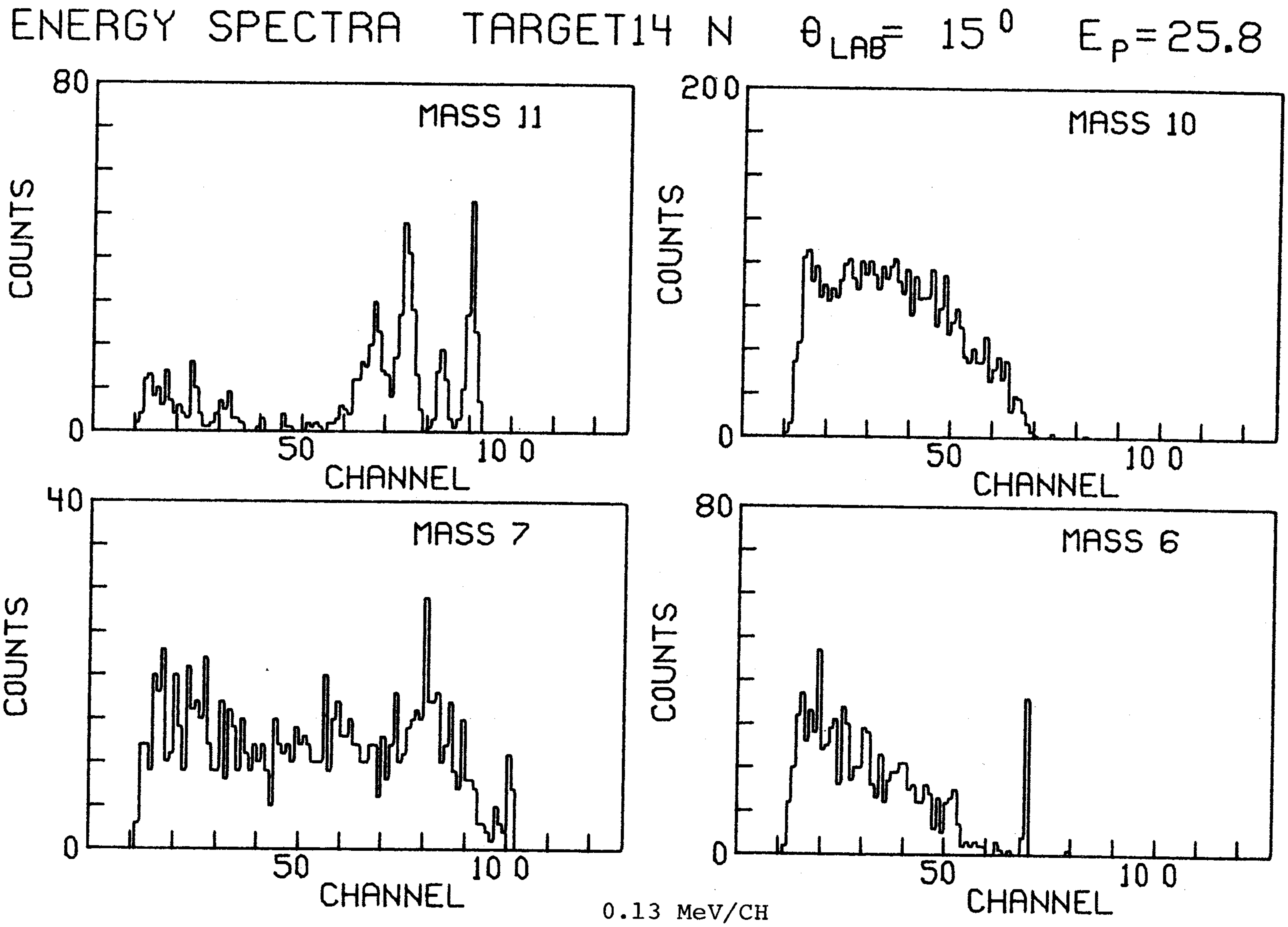

Figure 11. Selected Energy Spectra from Proton Spallation of ^{14}N and ^{16}O Targets.

Figure 11. (continued)

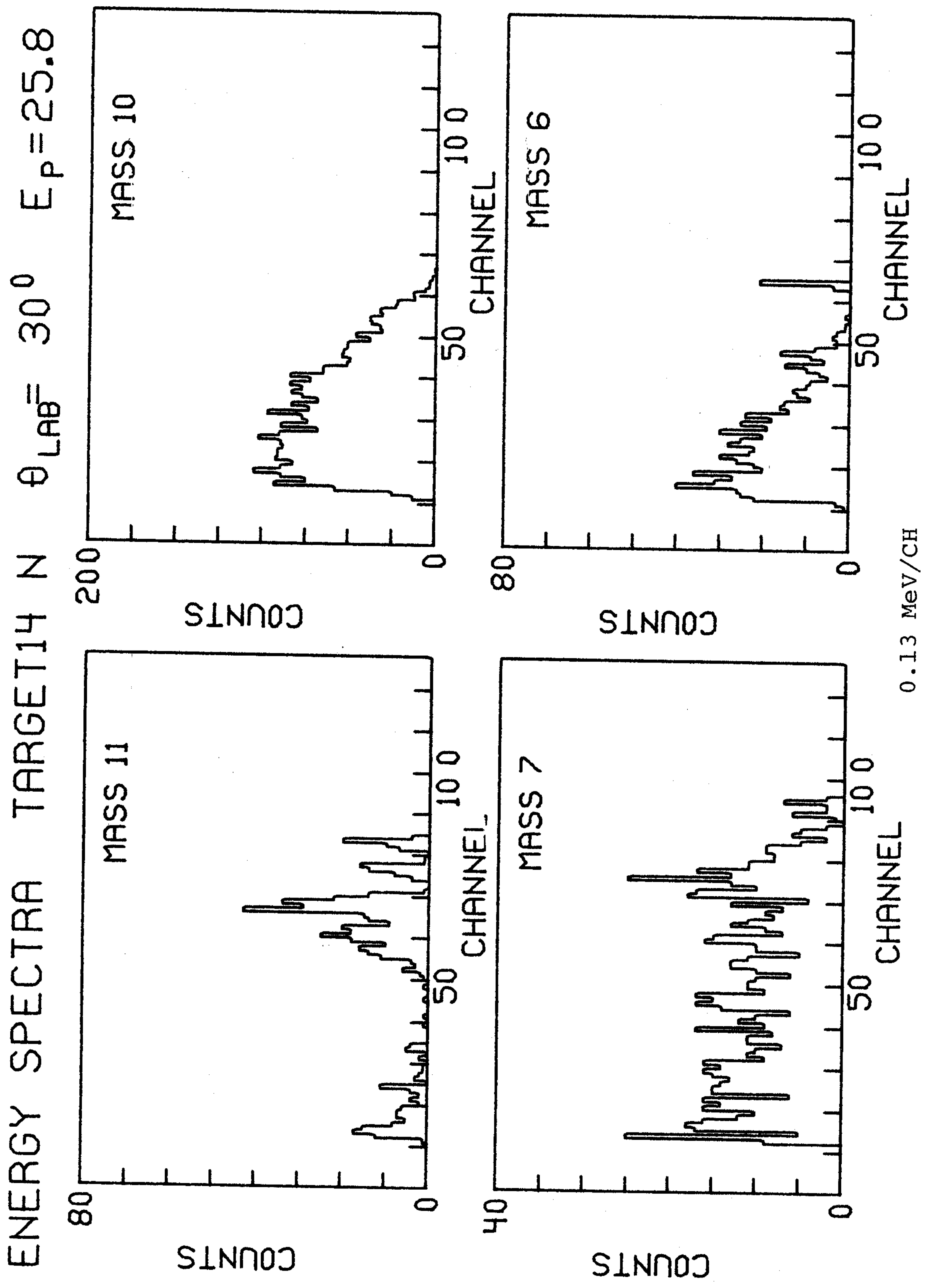

Figure 11. (continued)

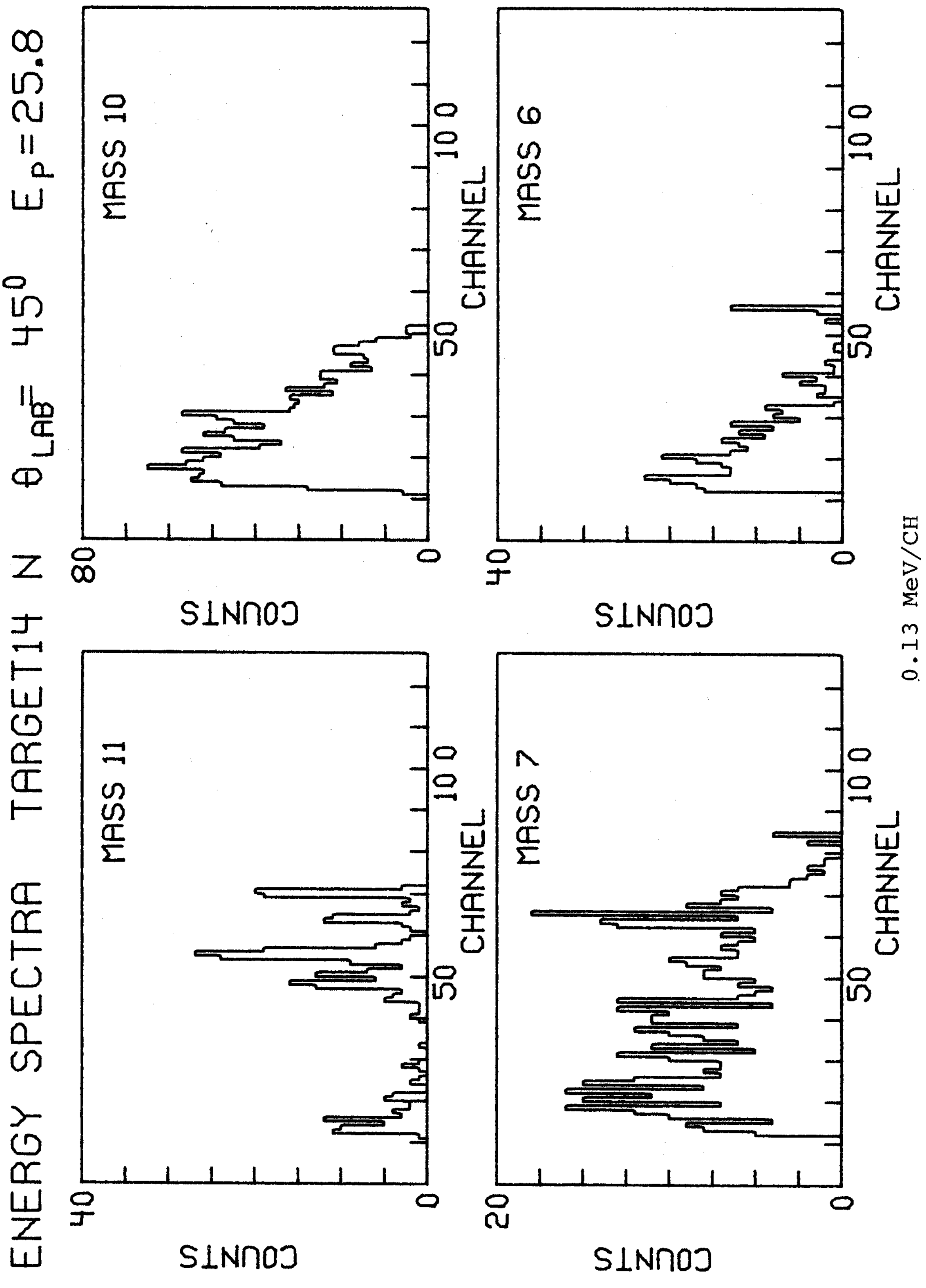

Figure 11. (continued)

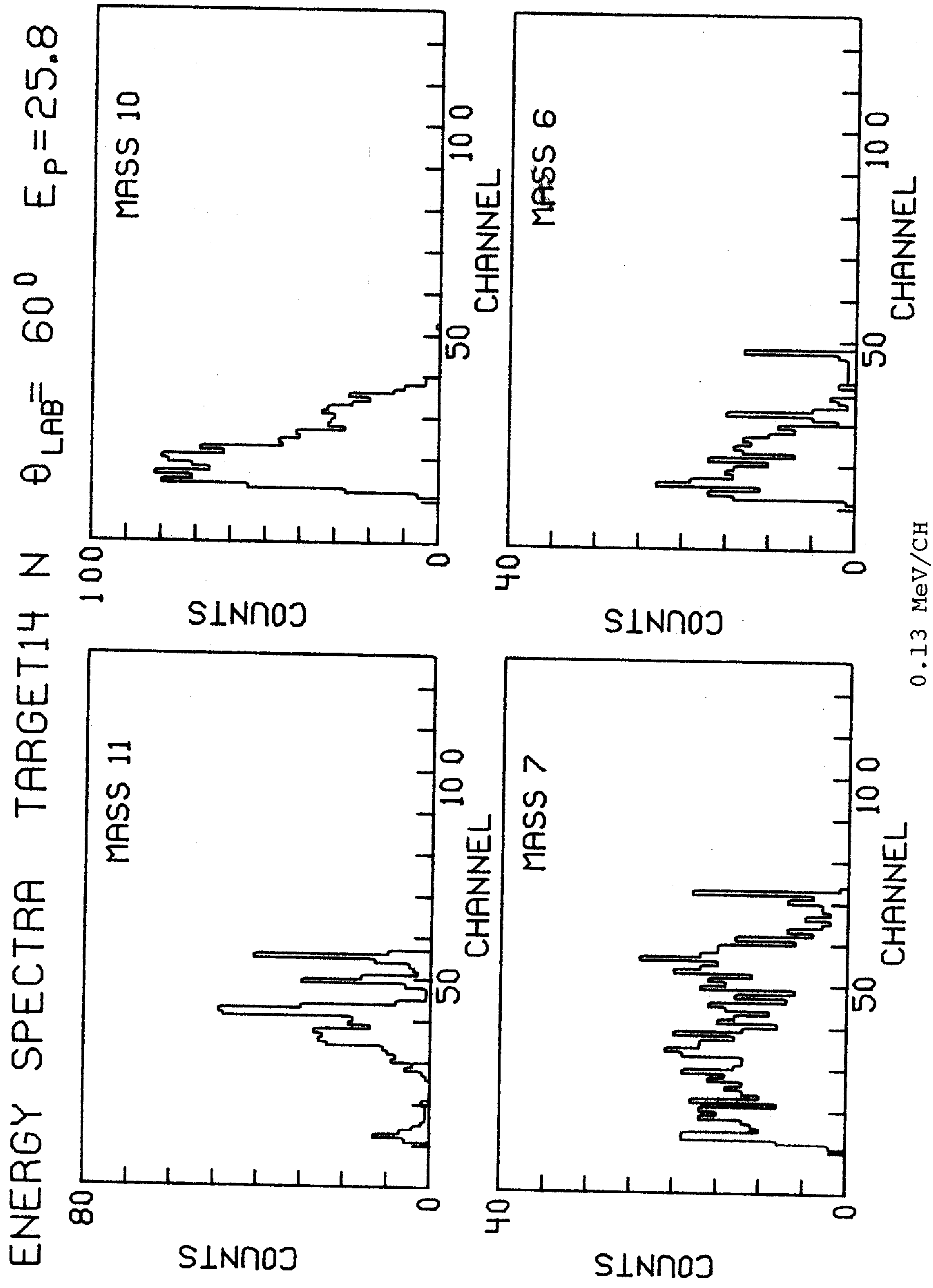

Figure 11. (continued)

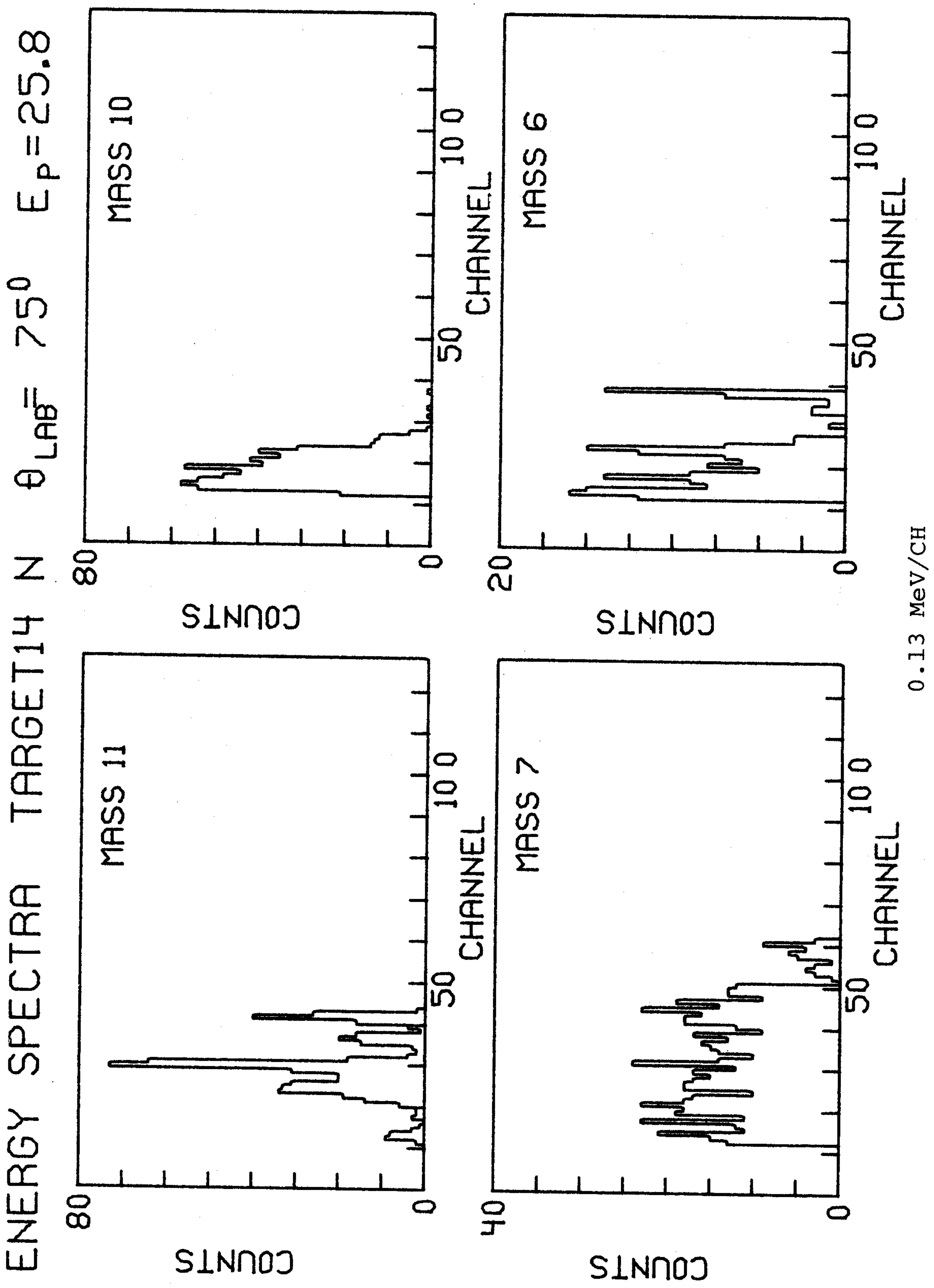

Figure 11. (continued)

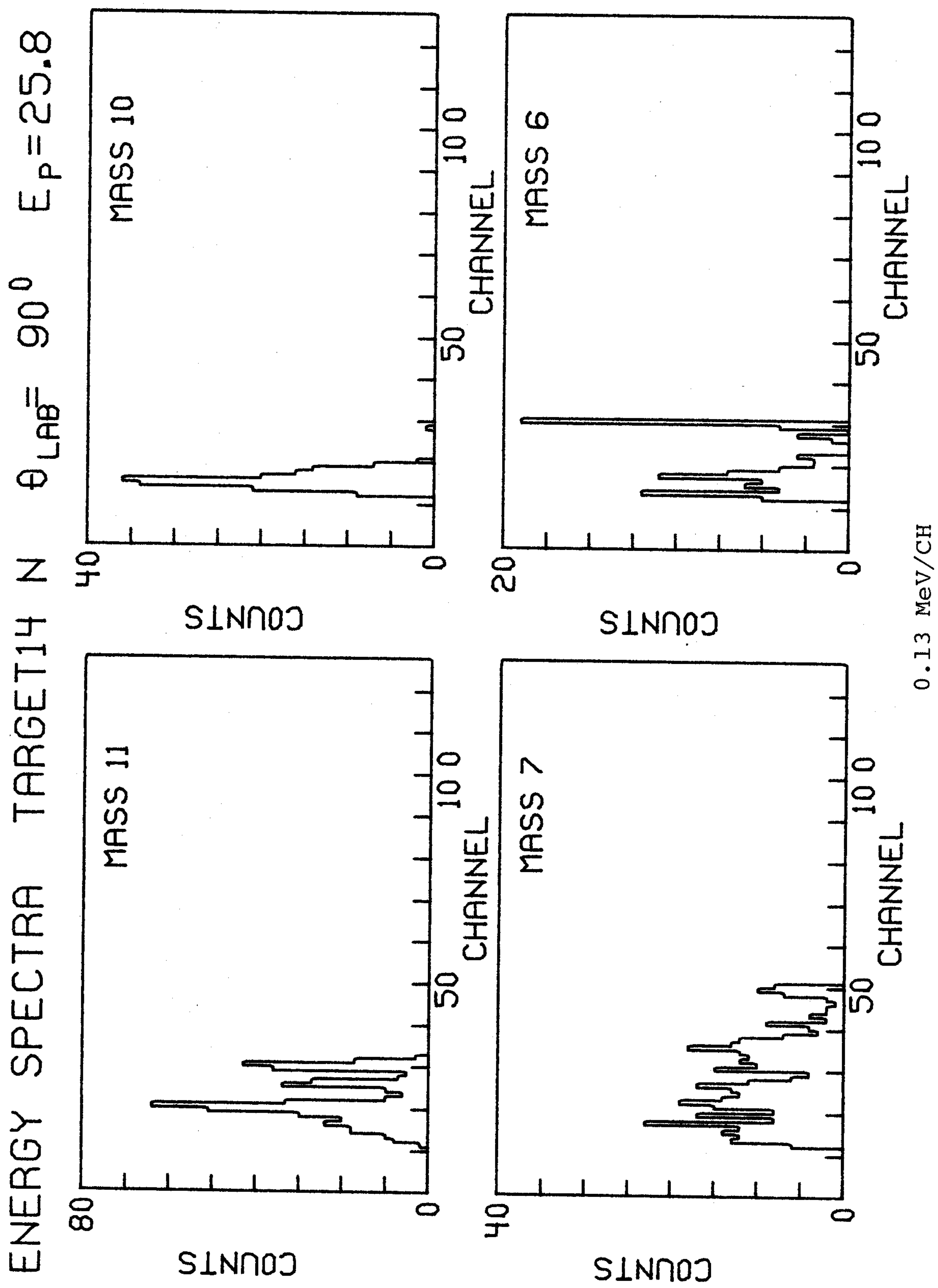

Figure 11. (continued)

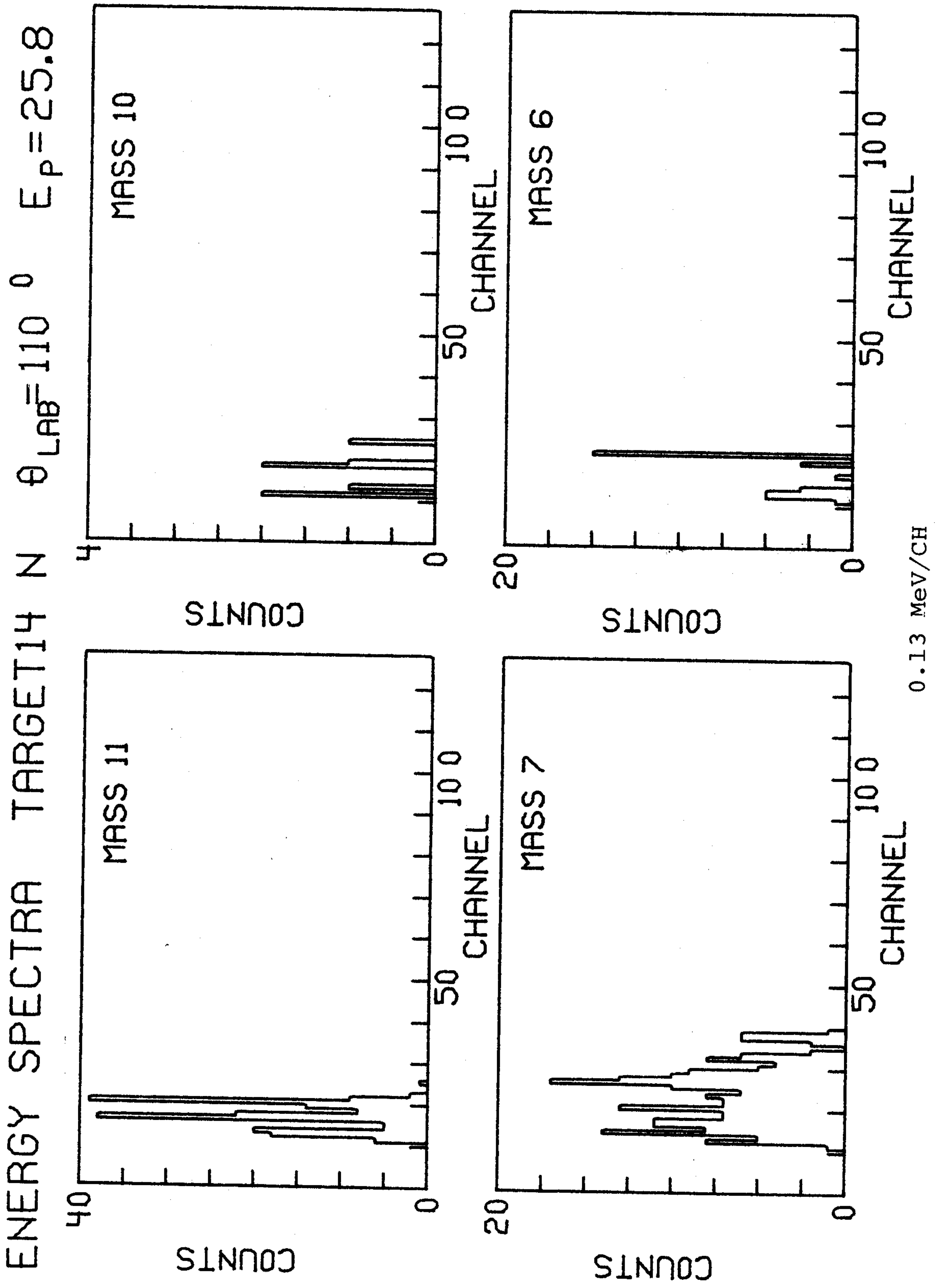

Figure 11. (continued)

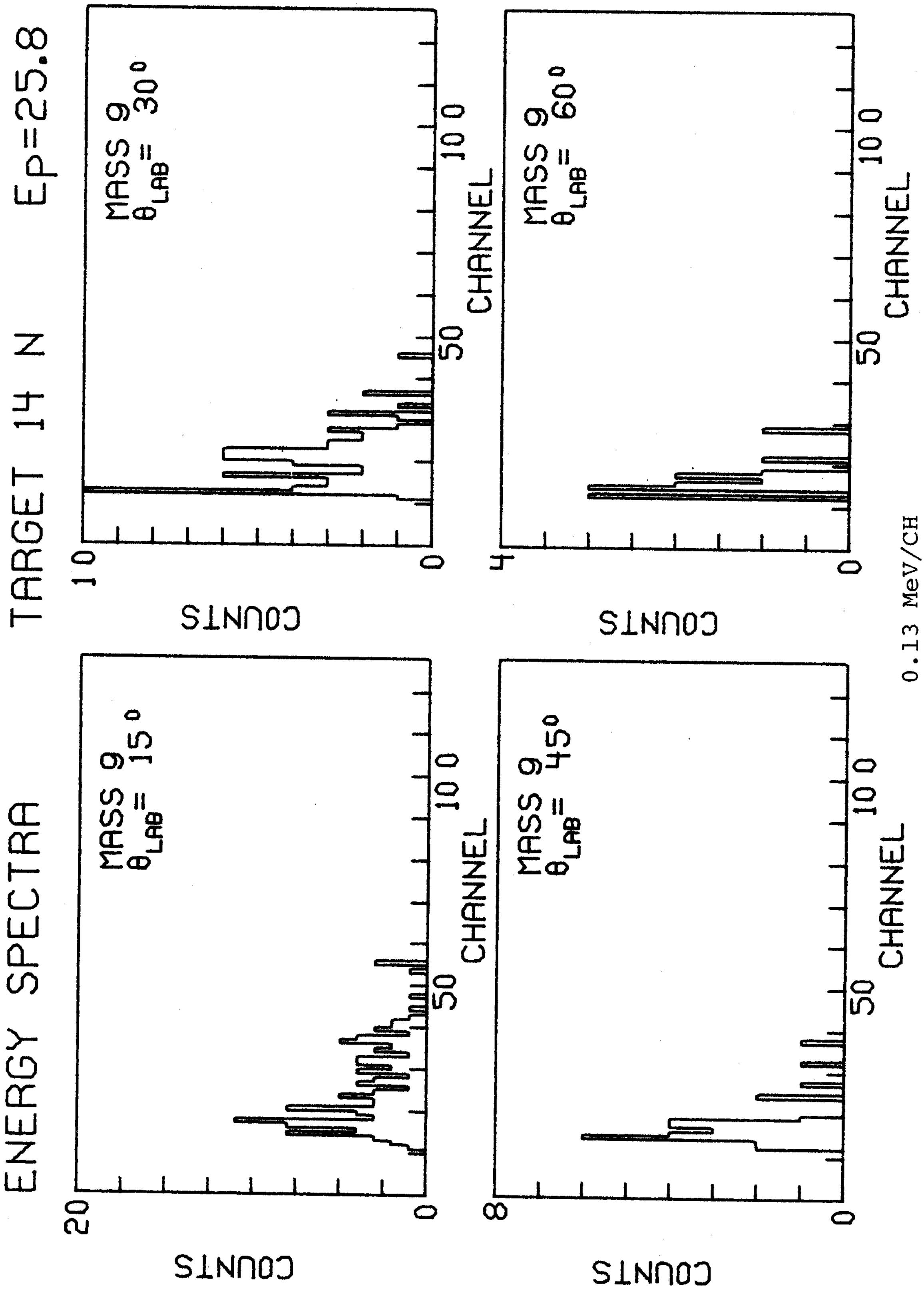

Figure 11. (continued)

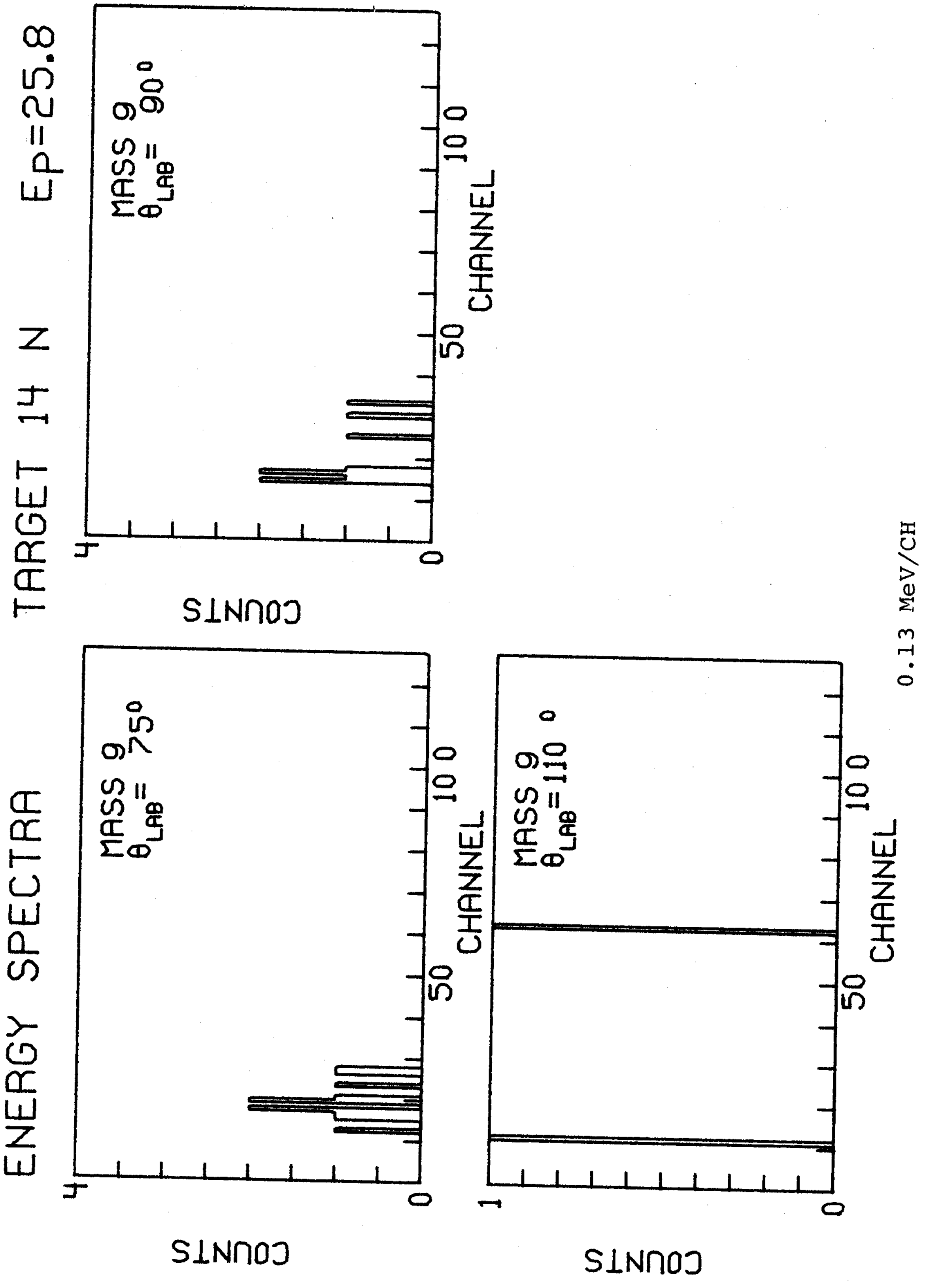

Figure 11. (continued)

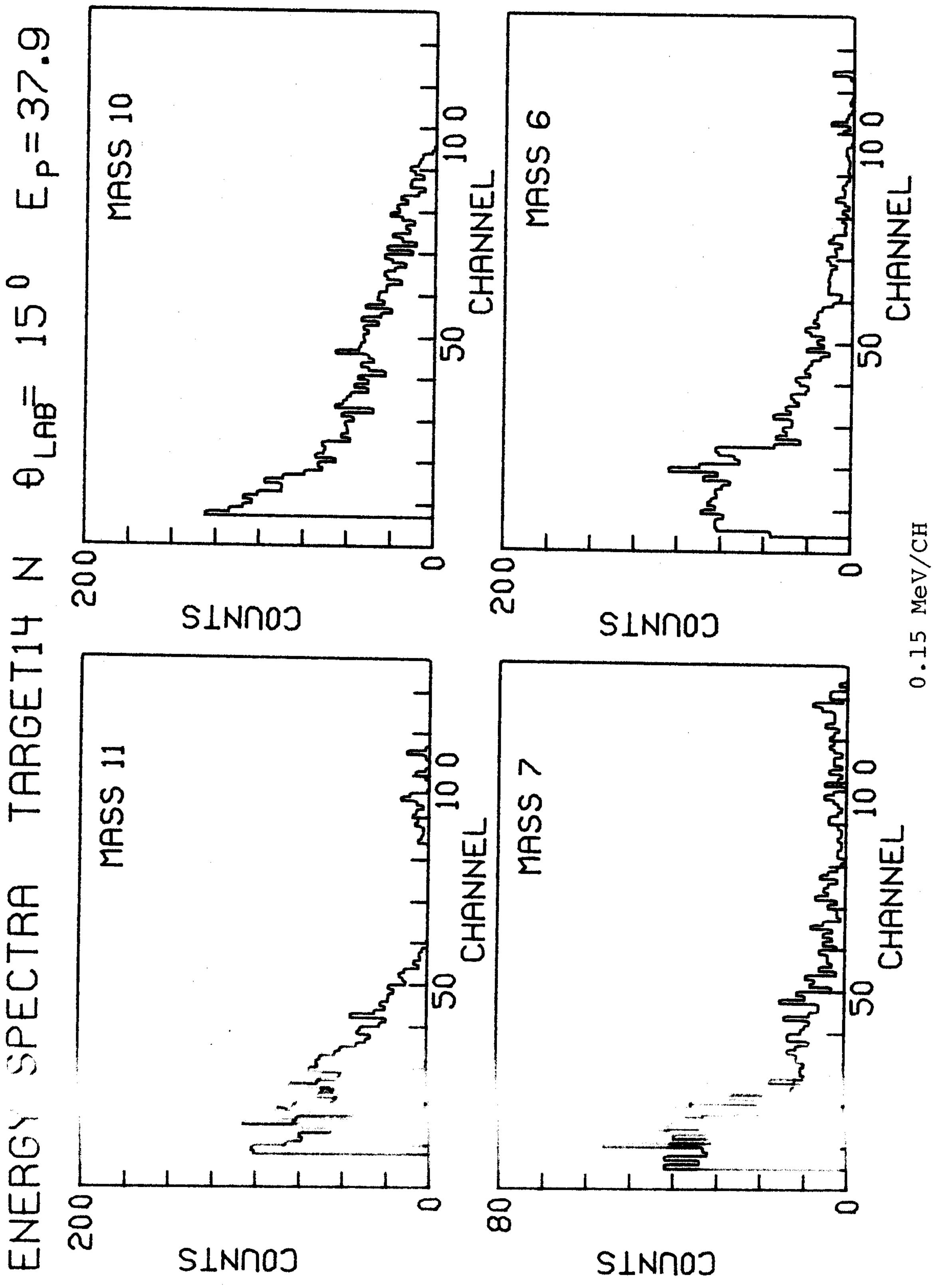

Figure 11. (continued)

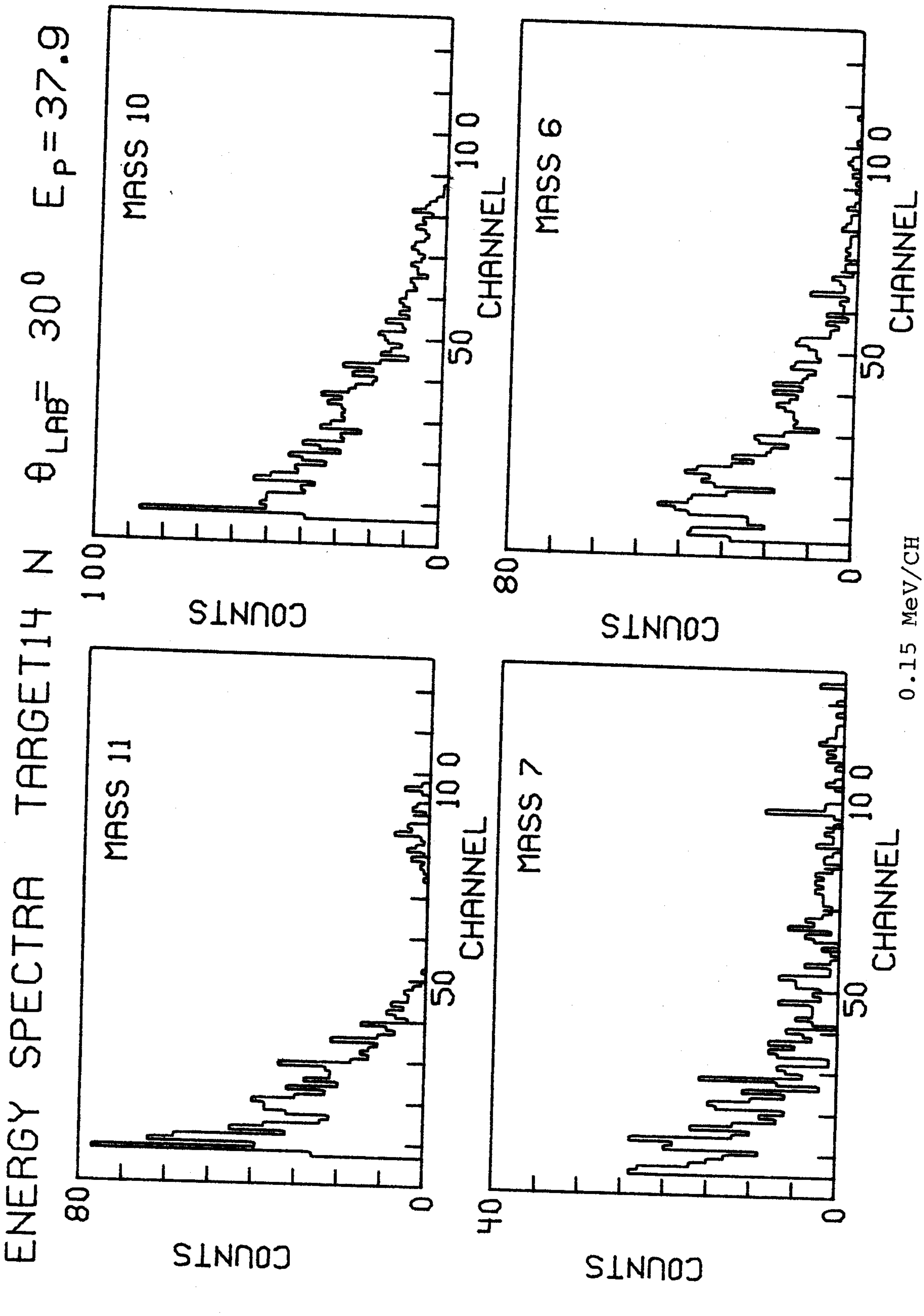

Figure 11. (Continued)

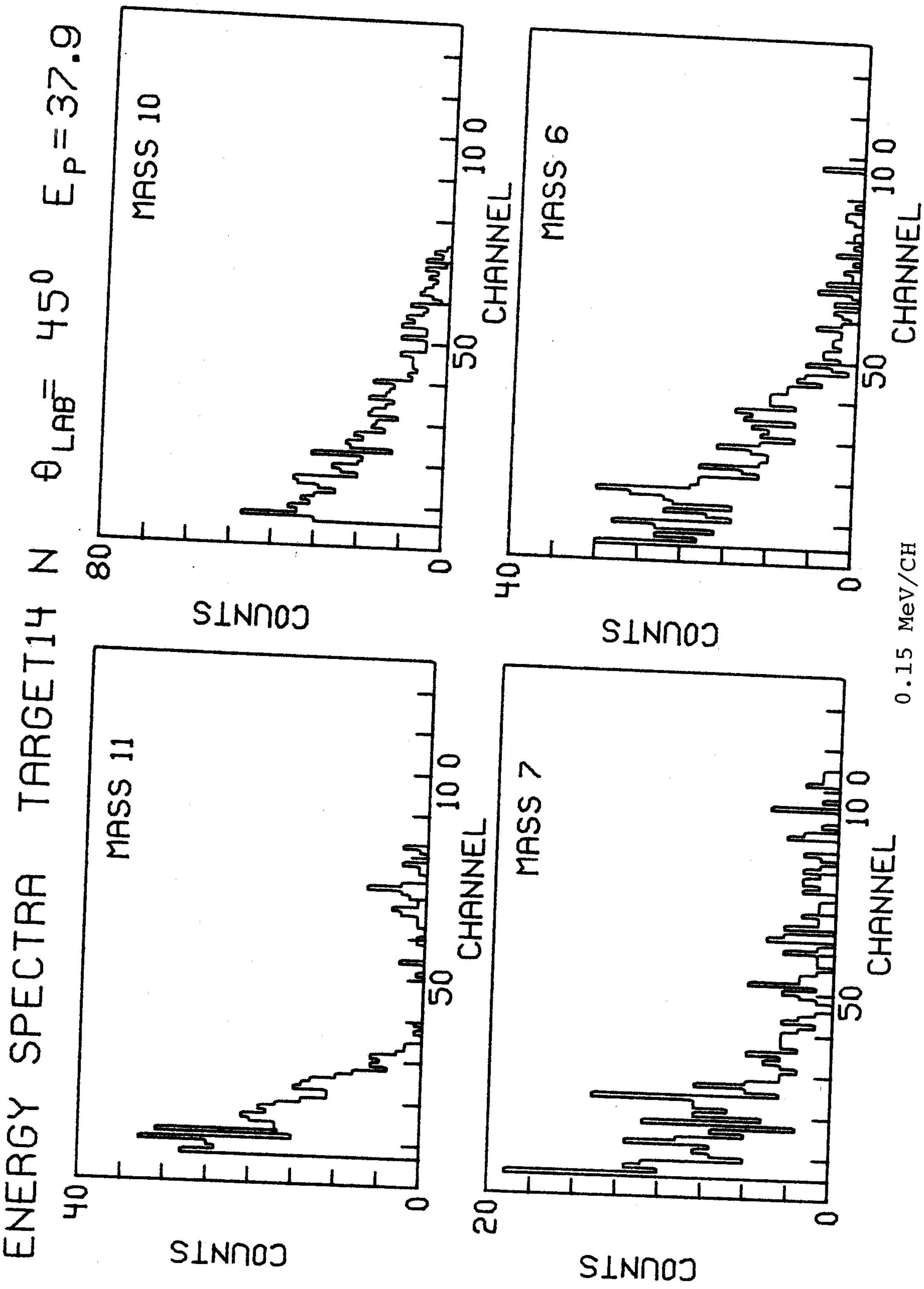

Figure 11. (continued)

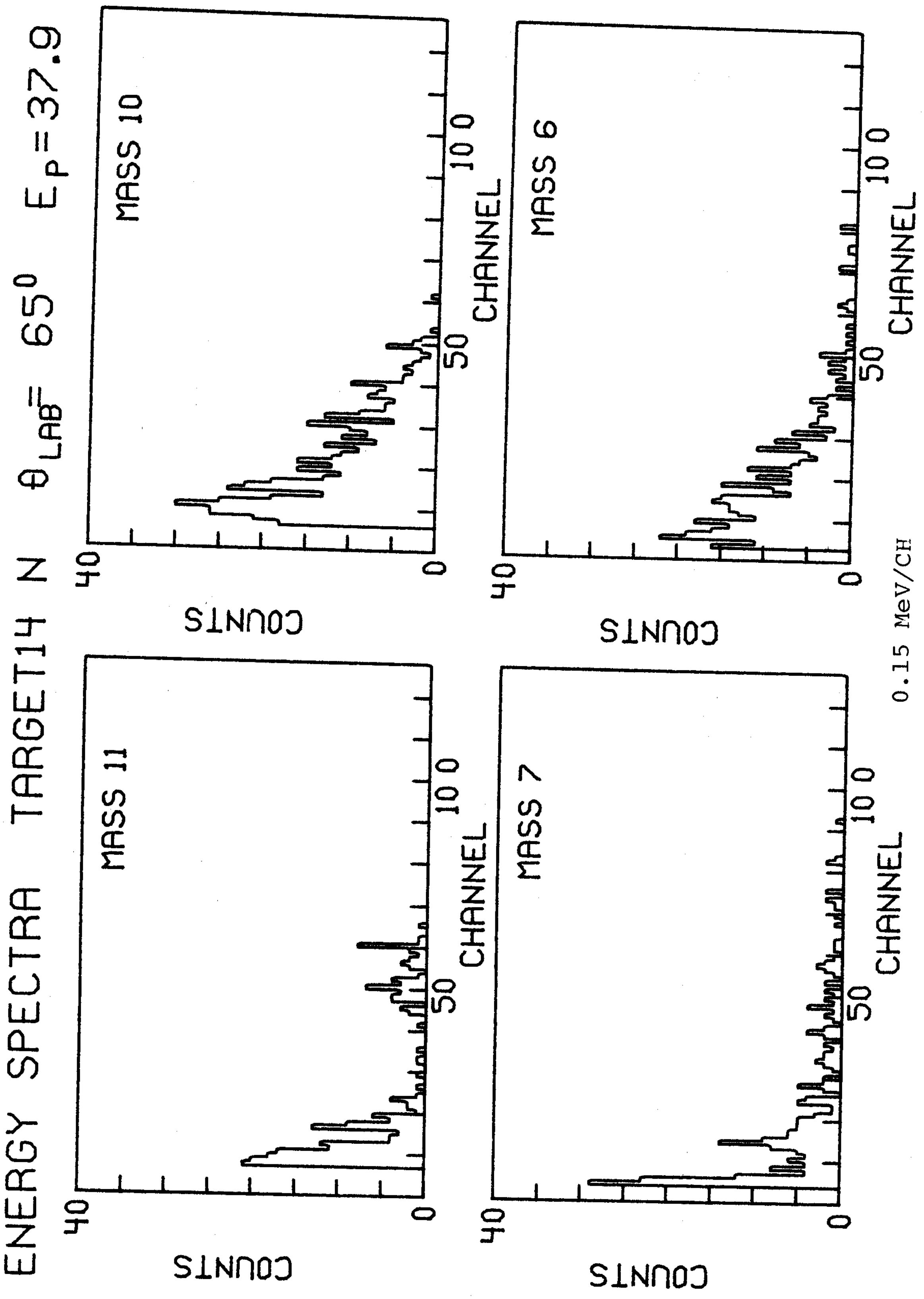

0.15 MeV/CH

Figure 11. (continued)

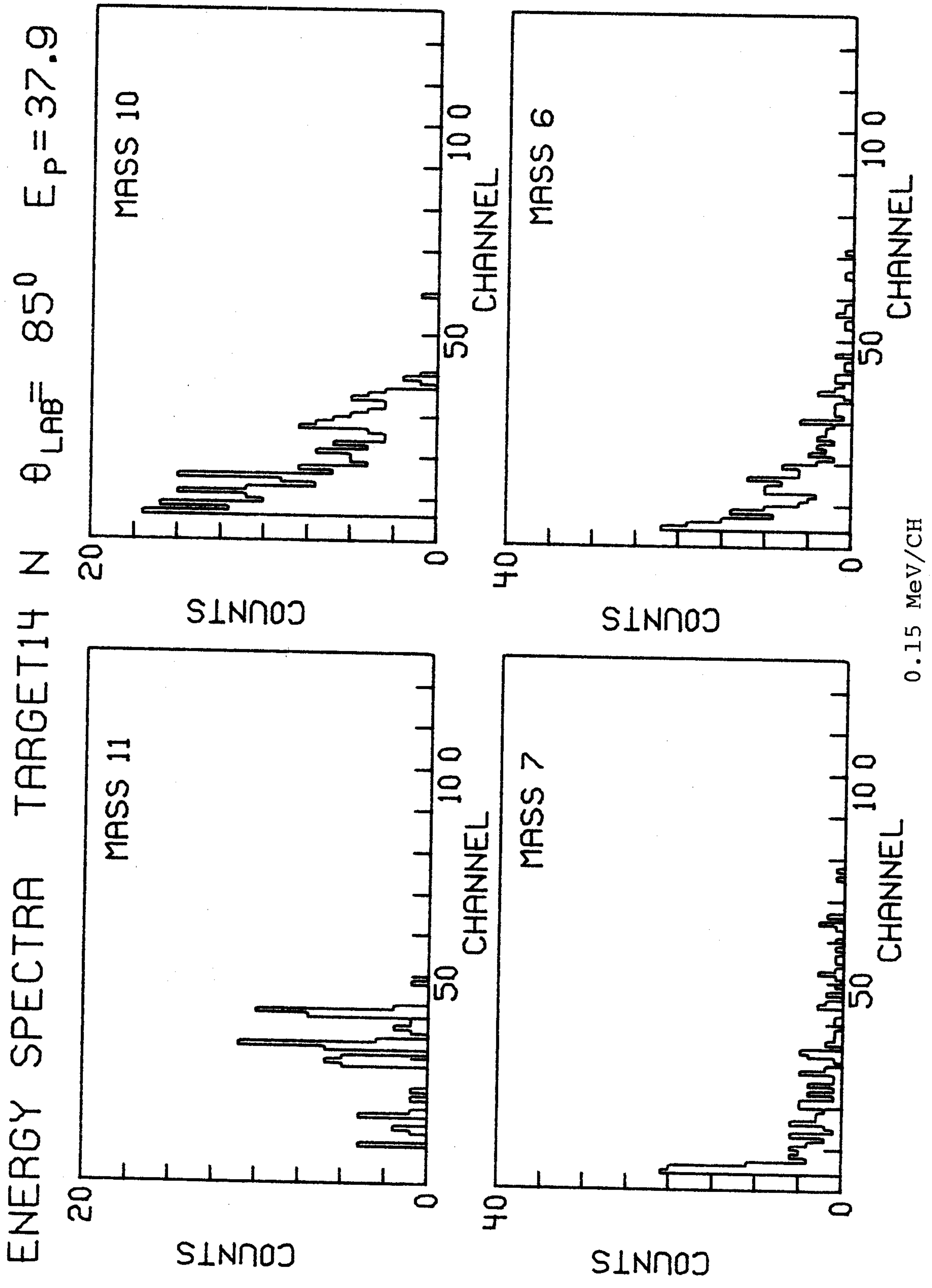

Figure 11. (continued)

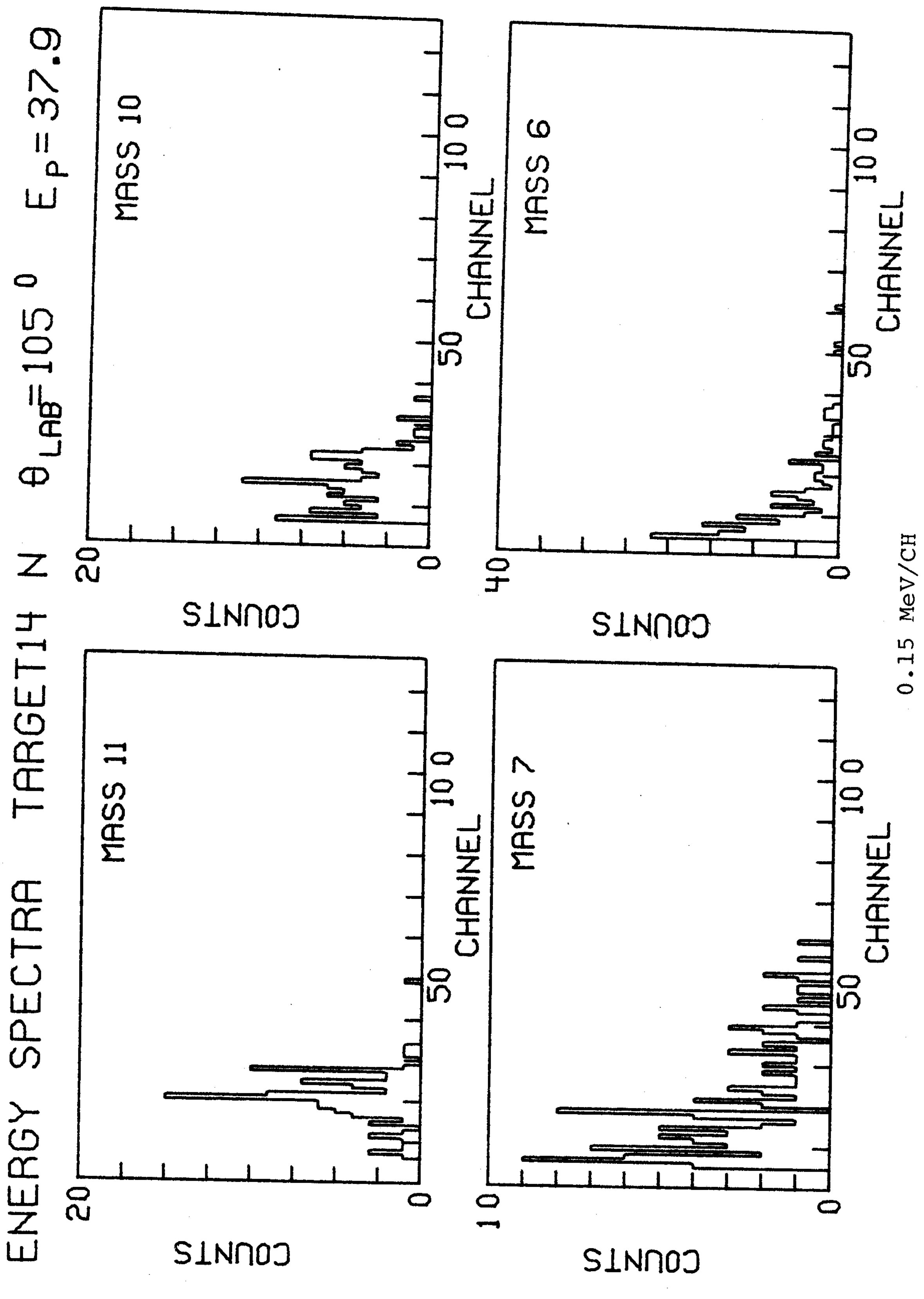

Figure 11. (continued)

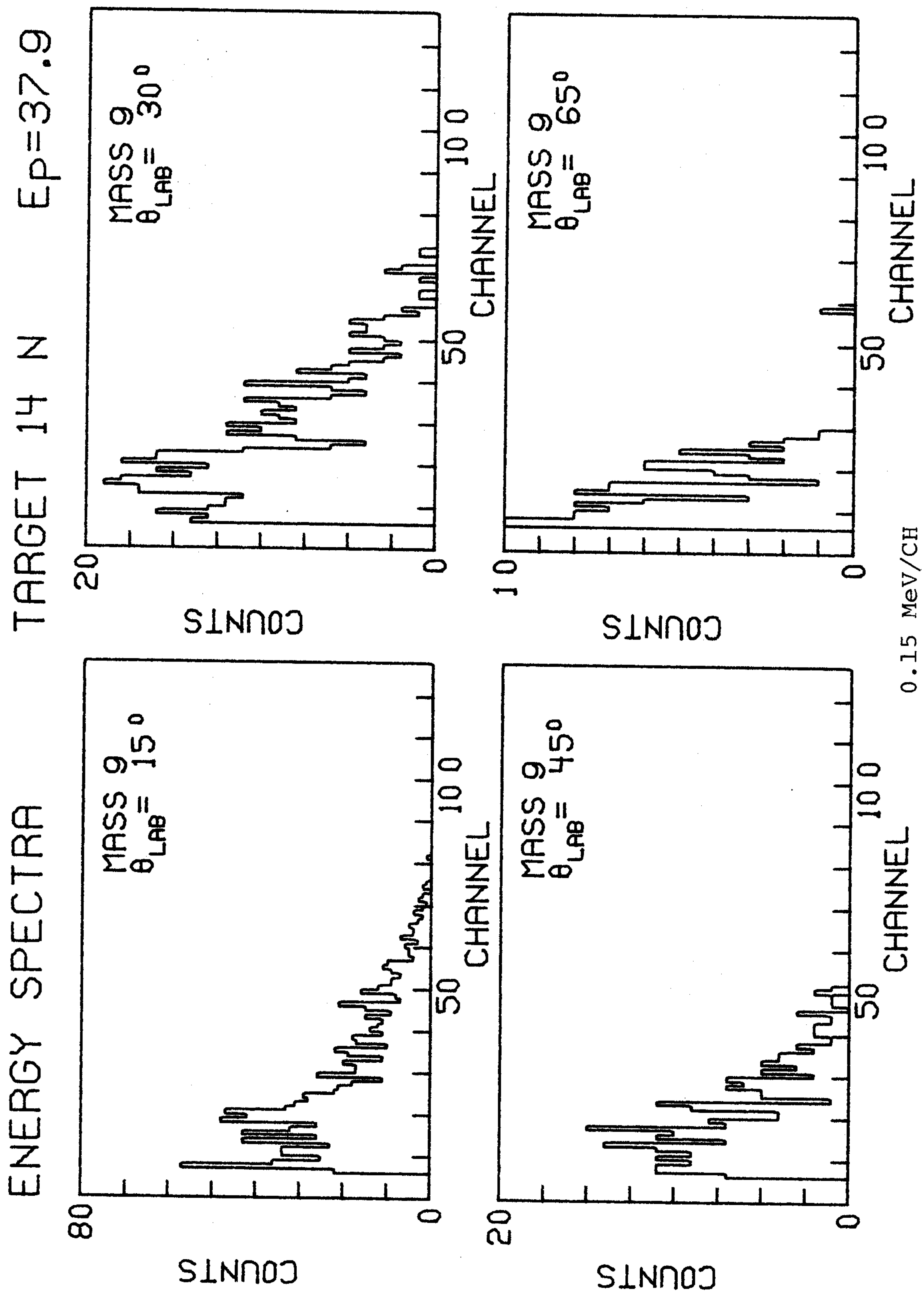

Figure 11. (continued)

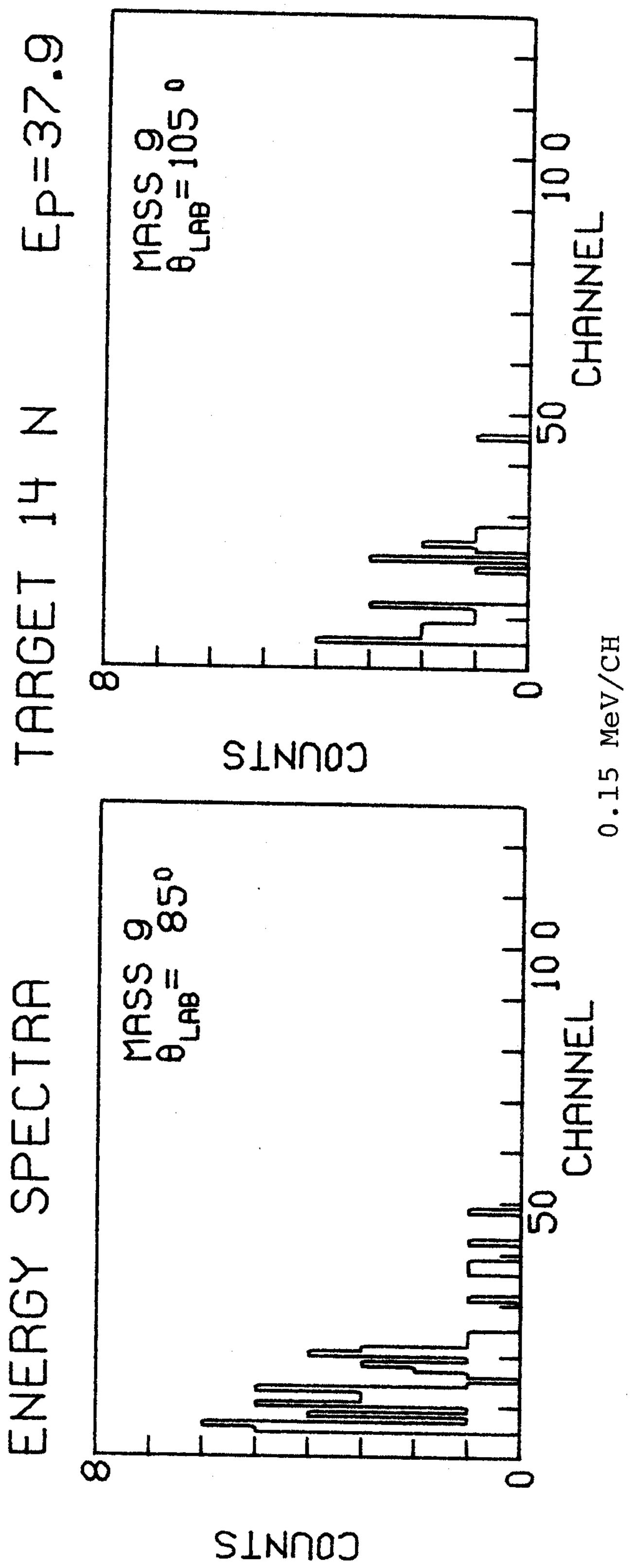

Figure 11. (continued)

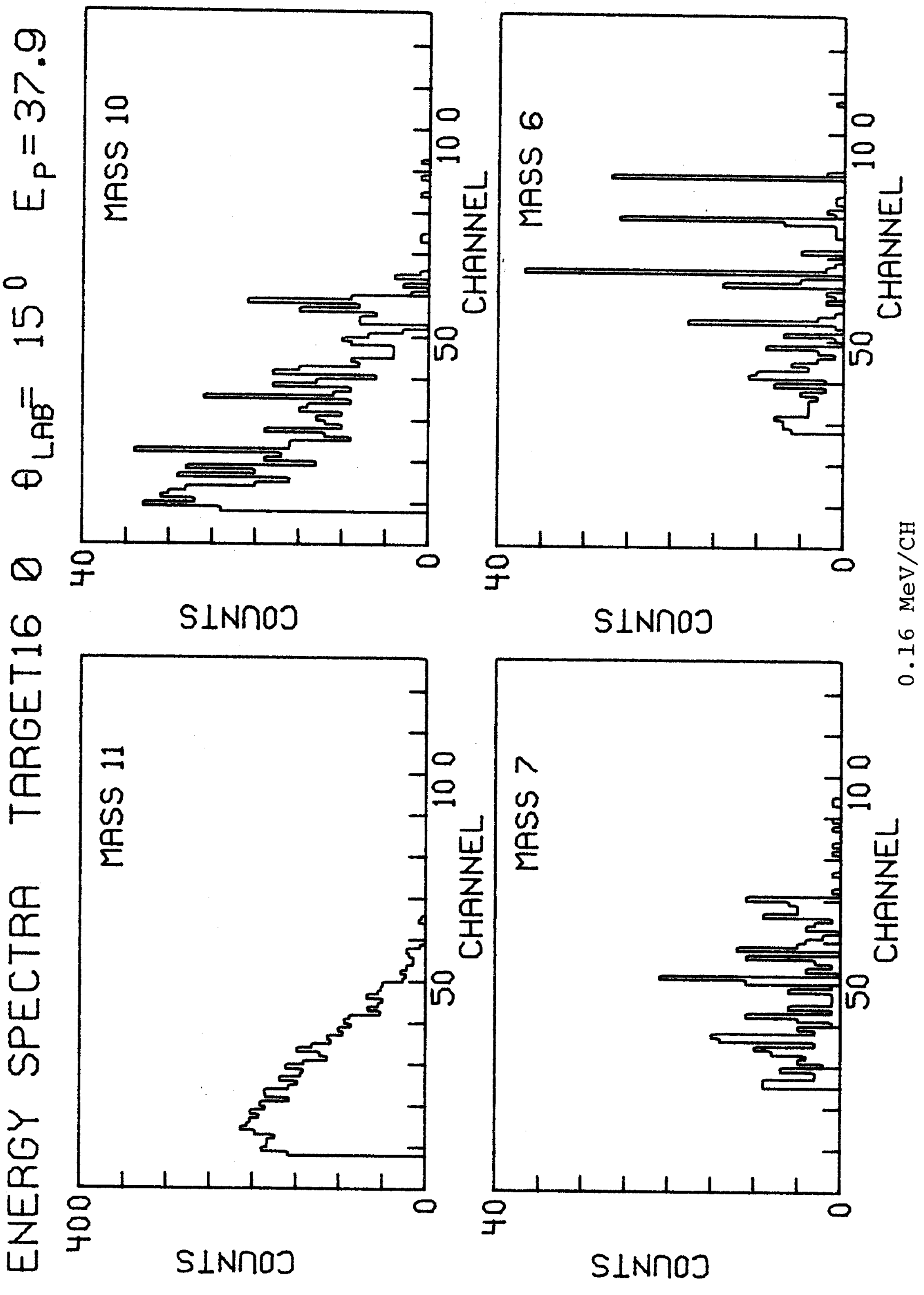

Figure 11. (continued)

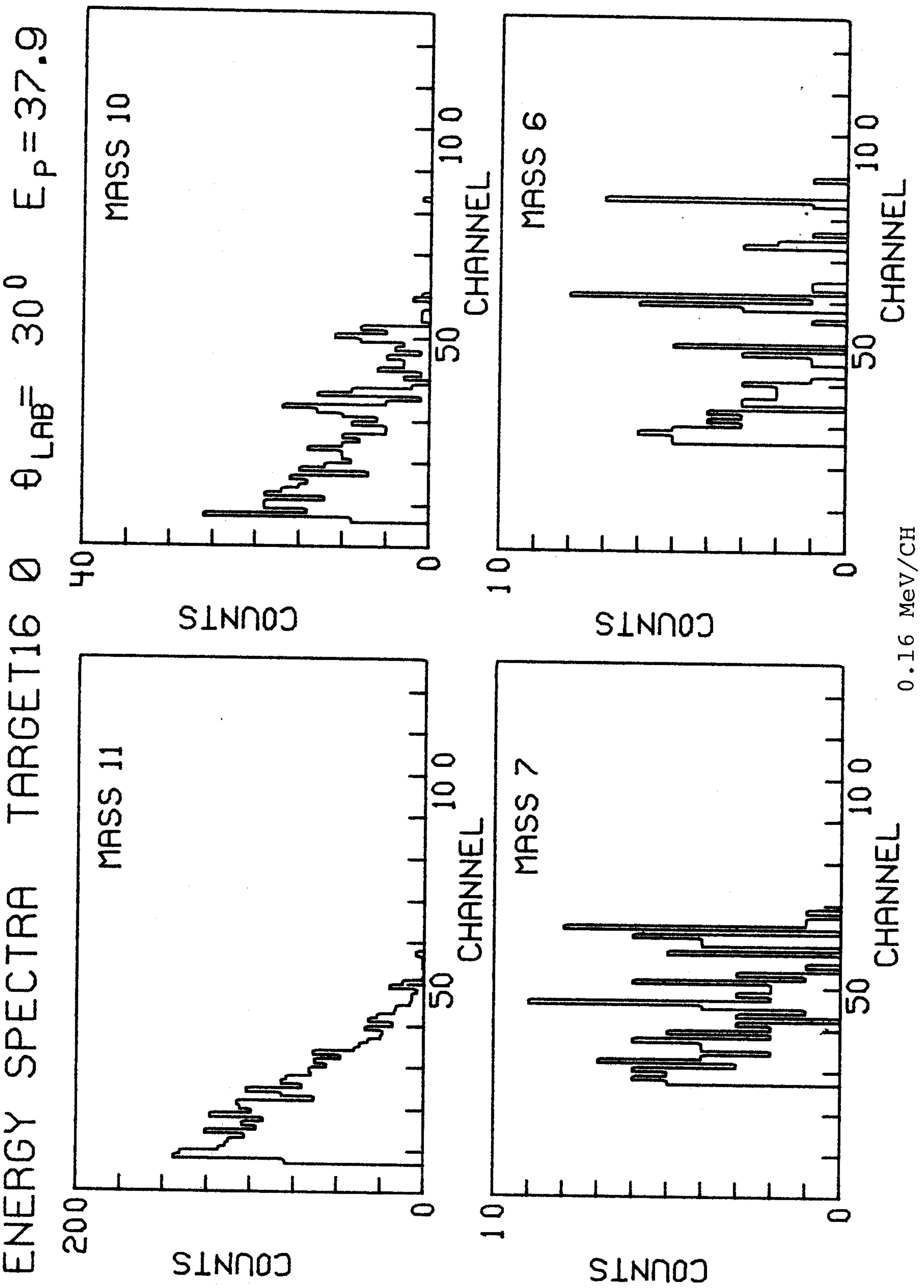

Figure 11. (continued)

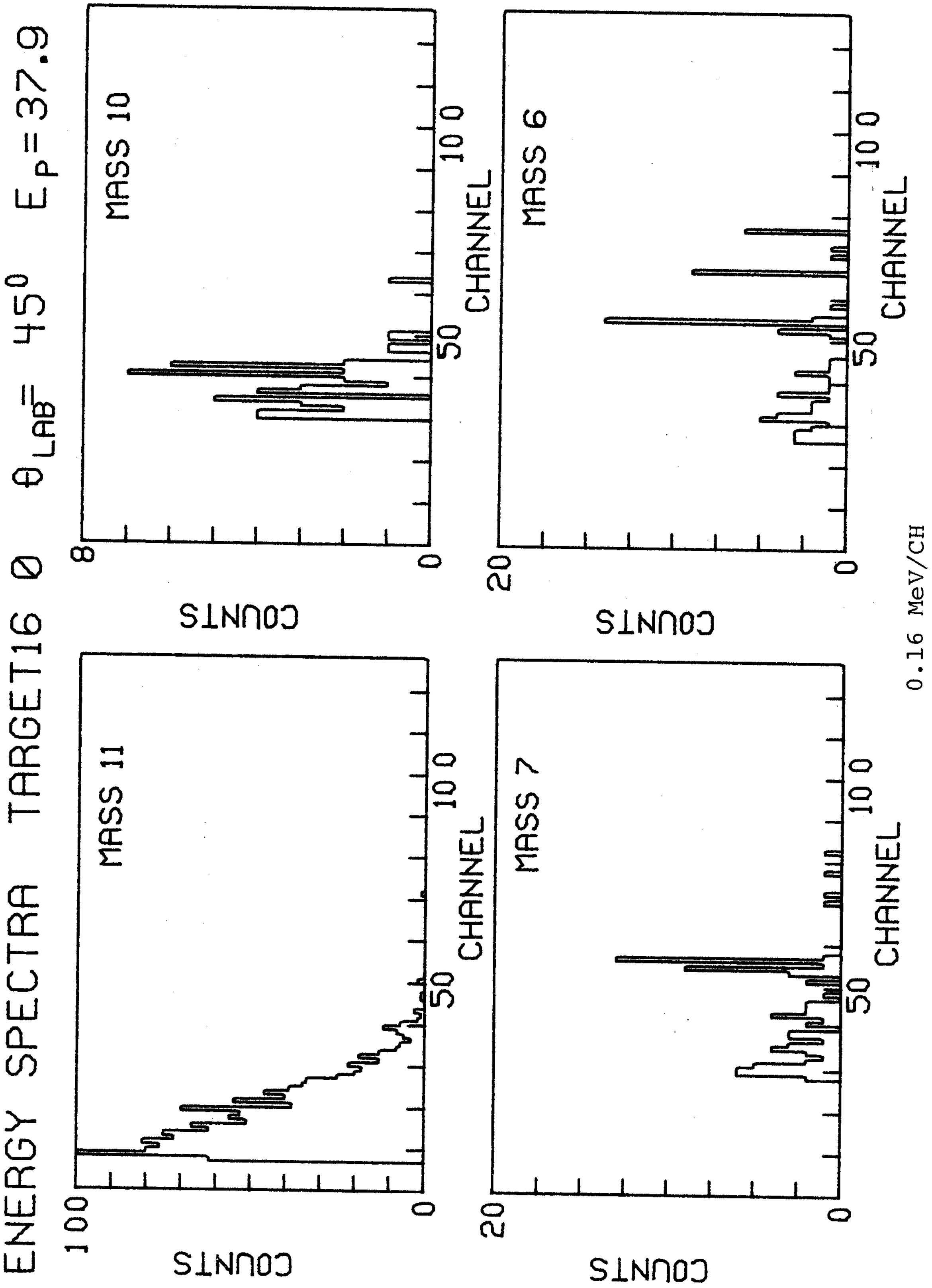

Figure 11. (continued)

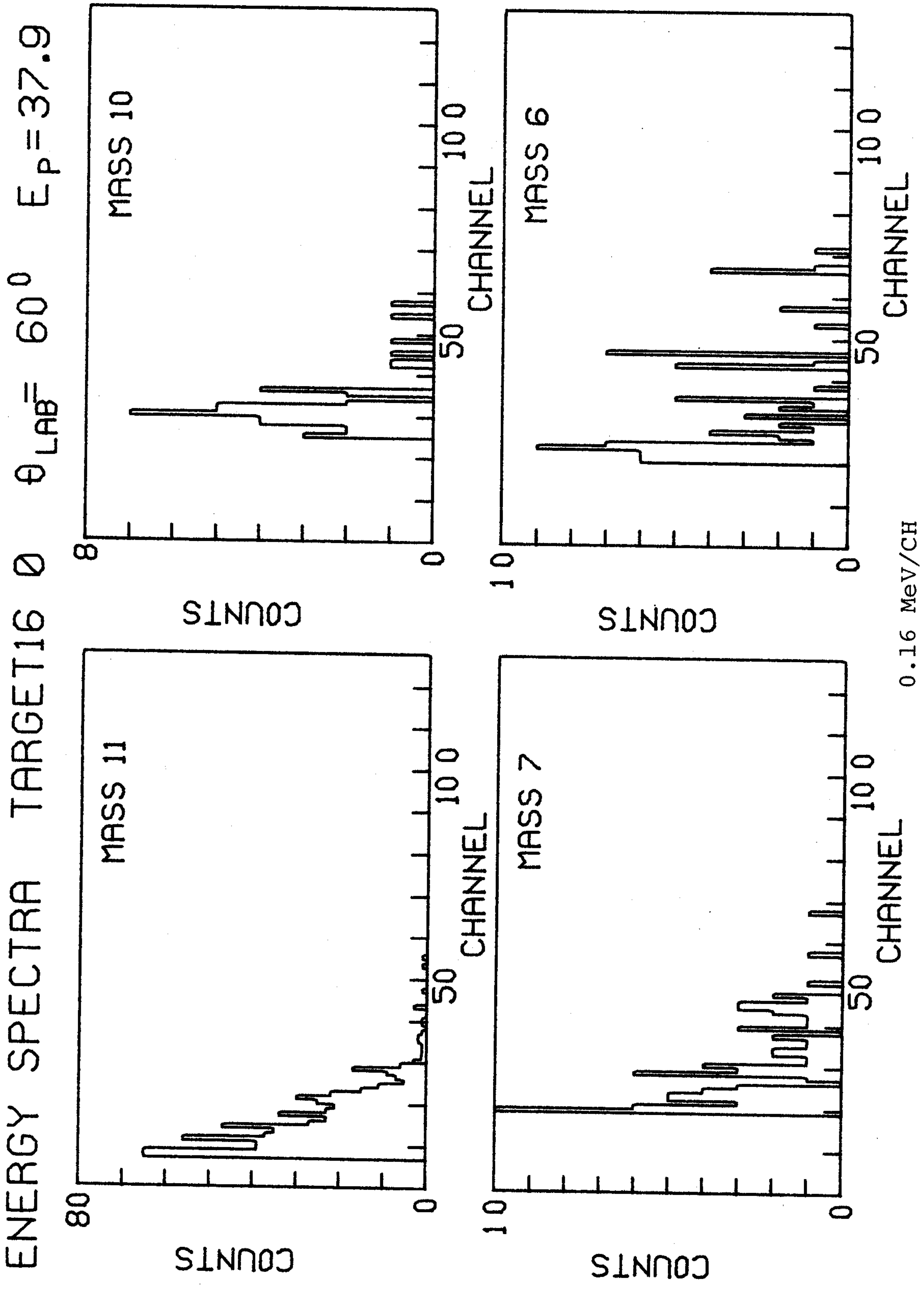

Figure 11. (continued)

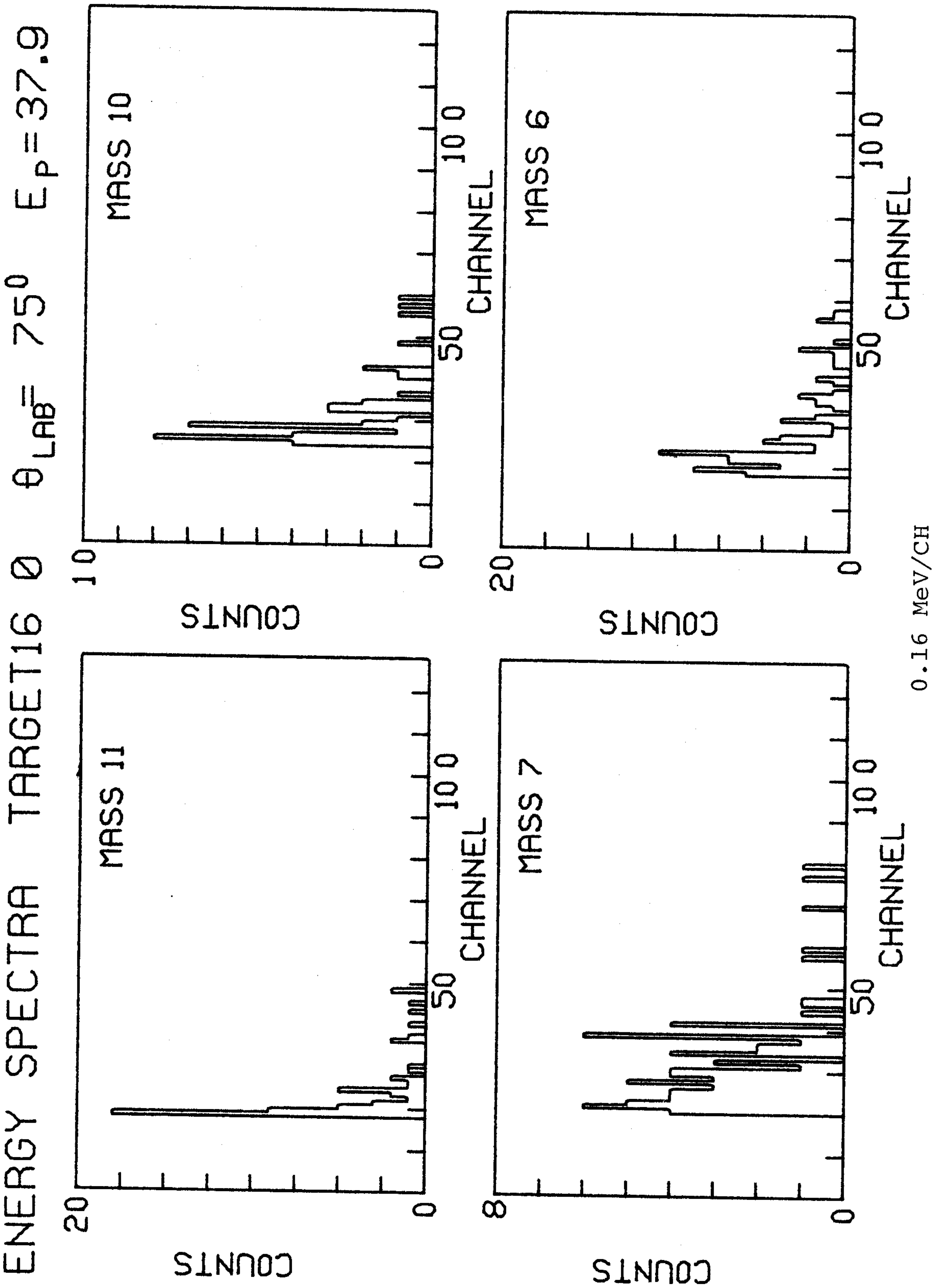

0.16 MeV/CH

Figure 11. (continued)

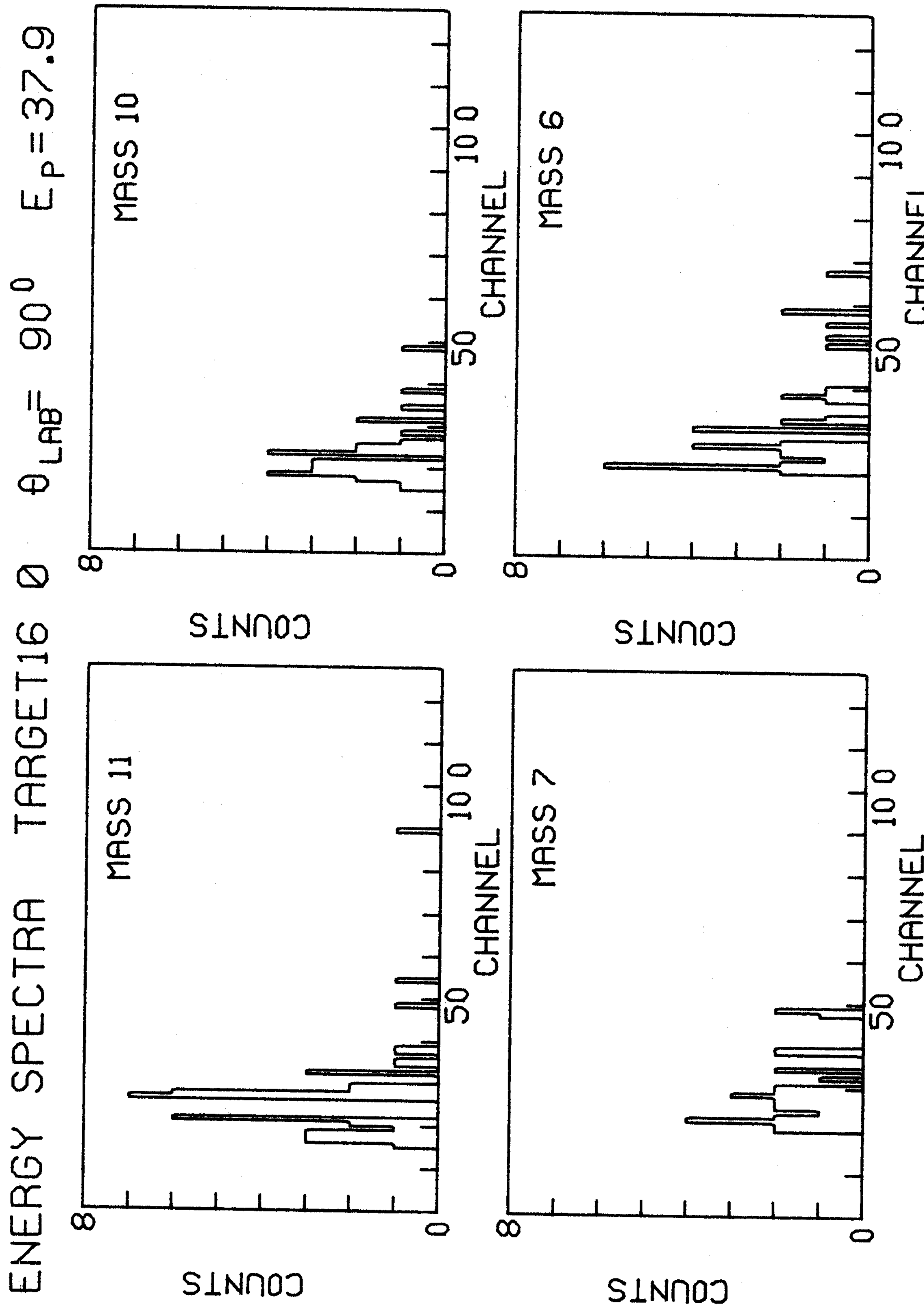

0.16 MeV/CH

Figure 11. (continued)

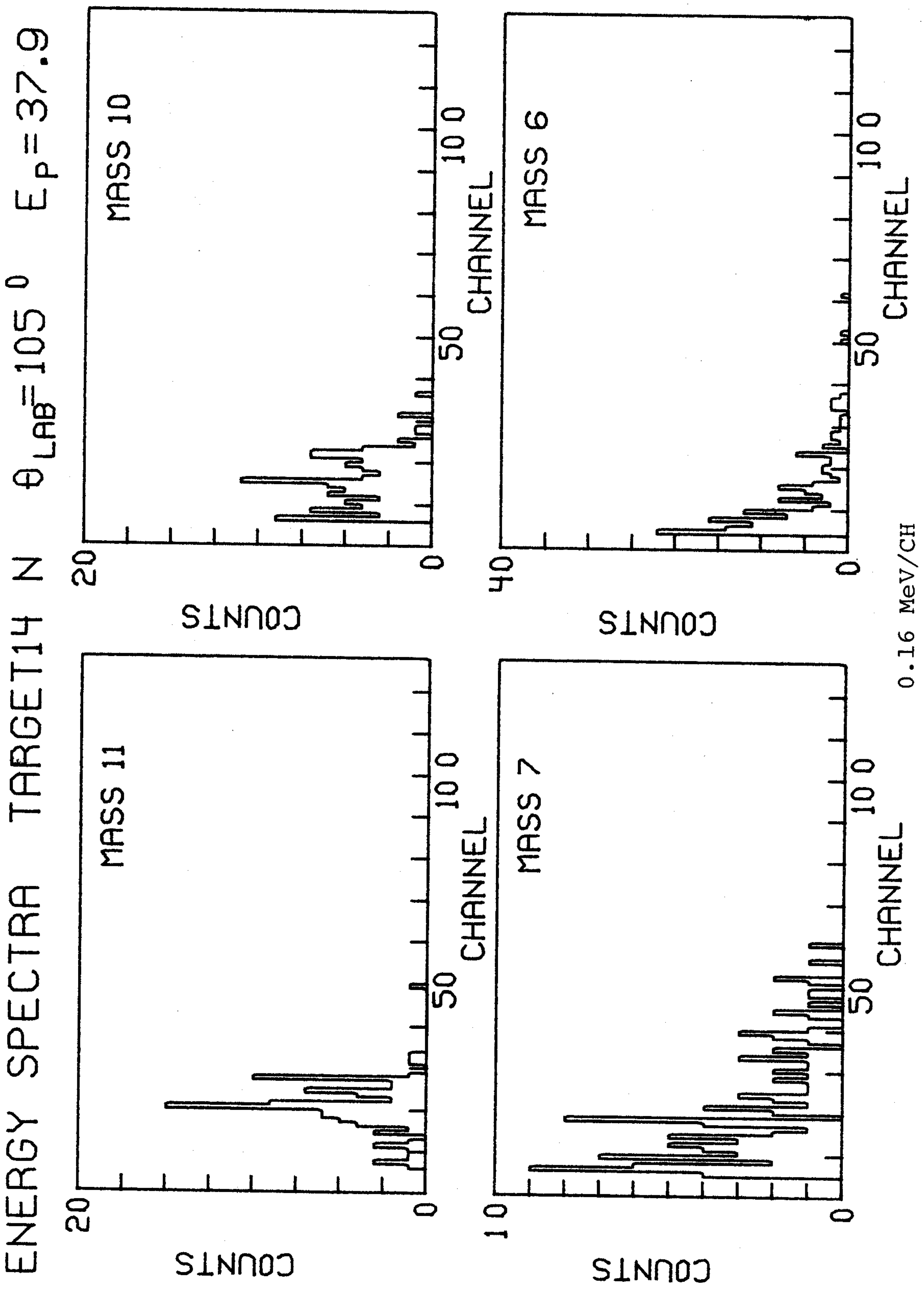

Figure 11. (continued)

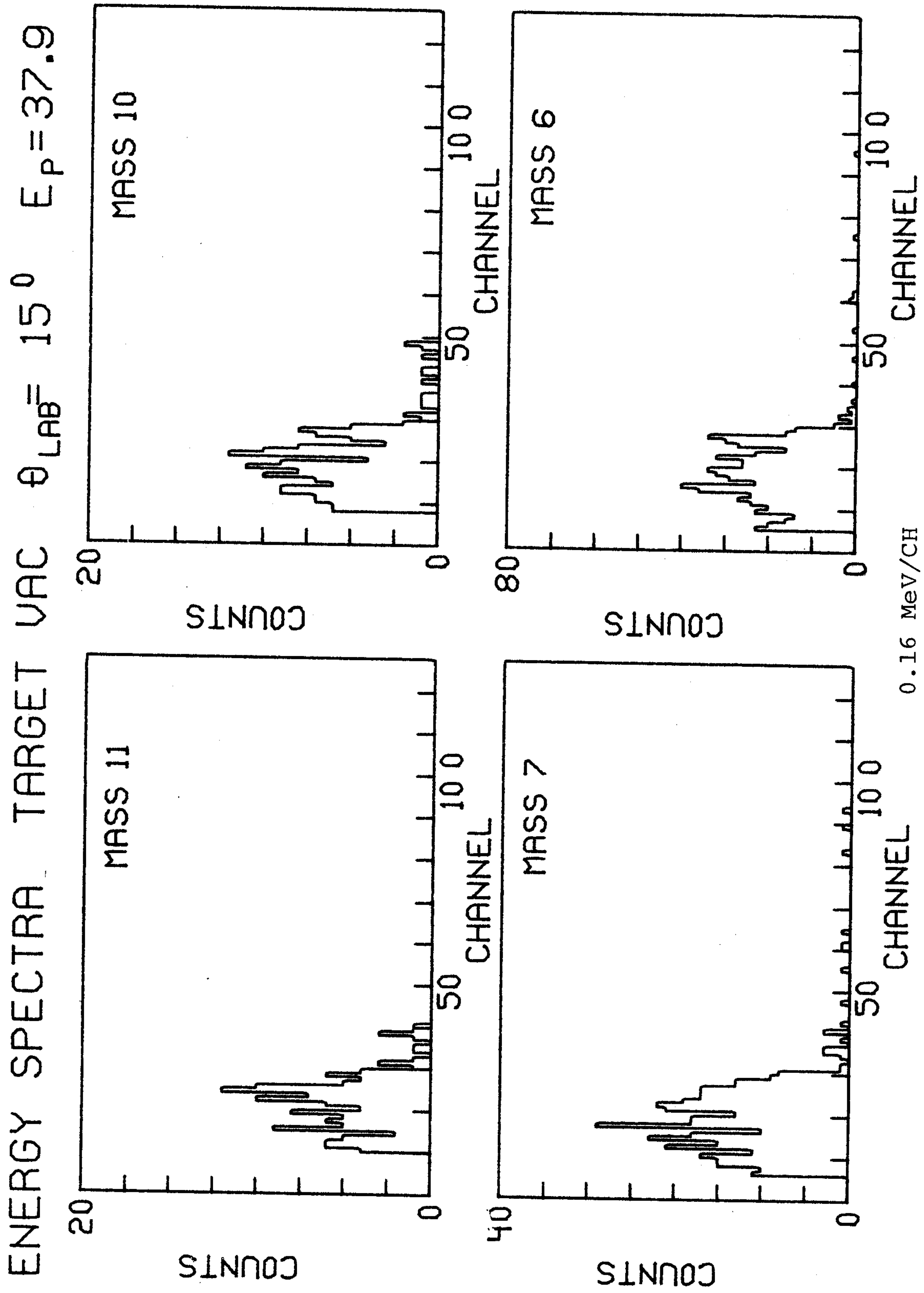

Figure 11. (continued)

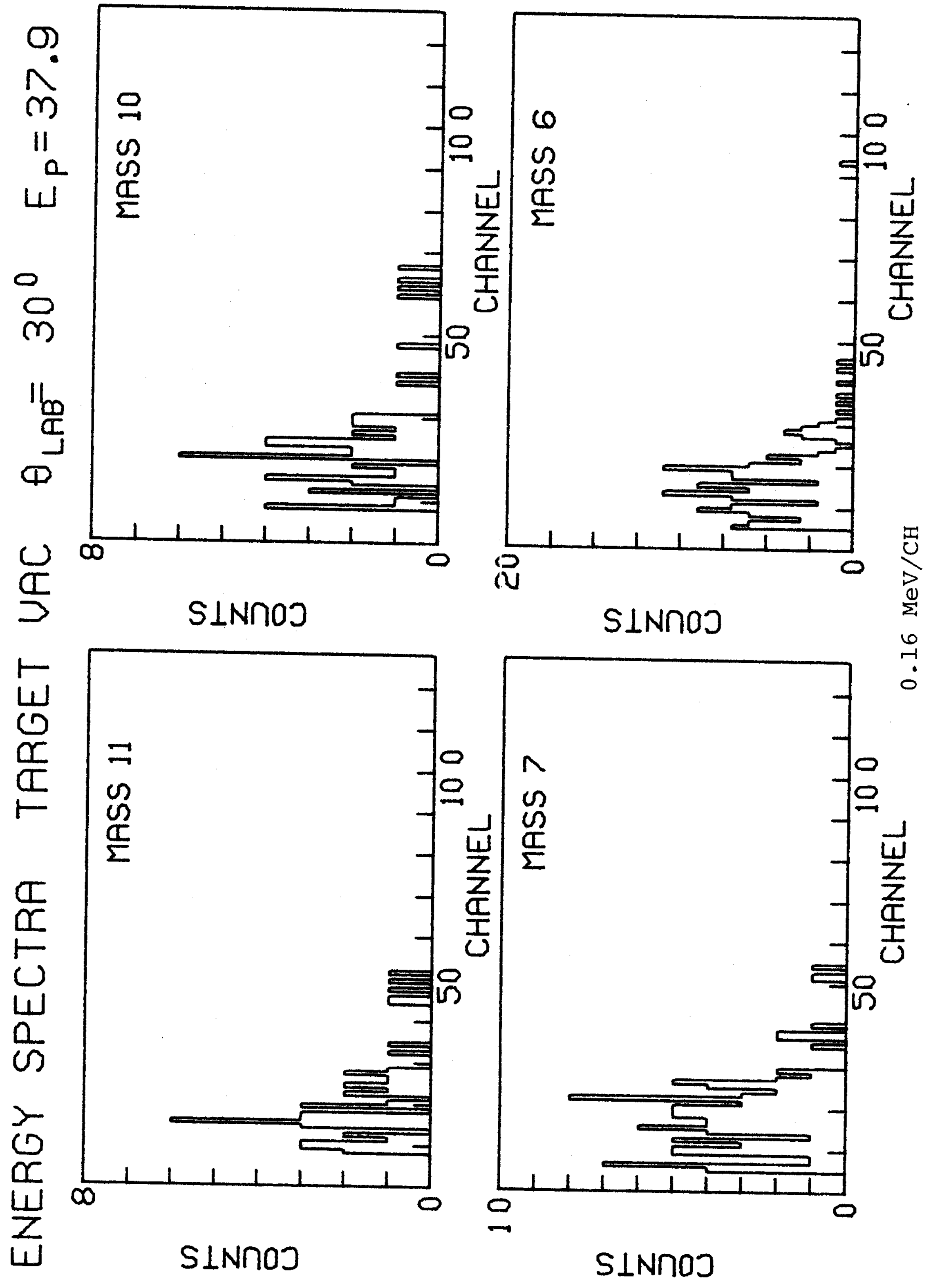

Figure 11. (continued)

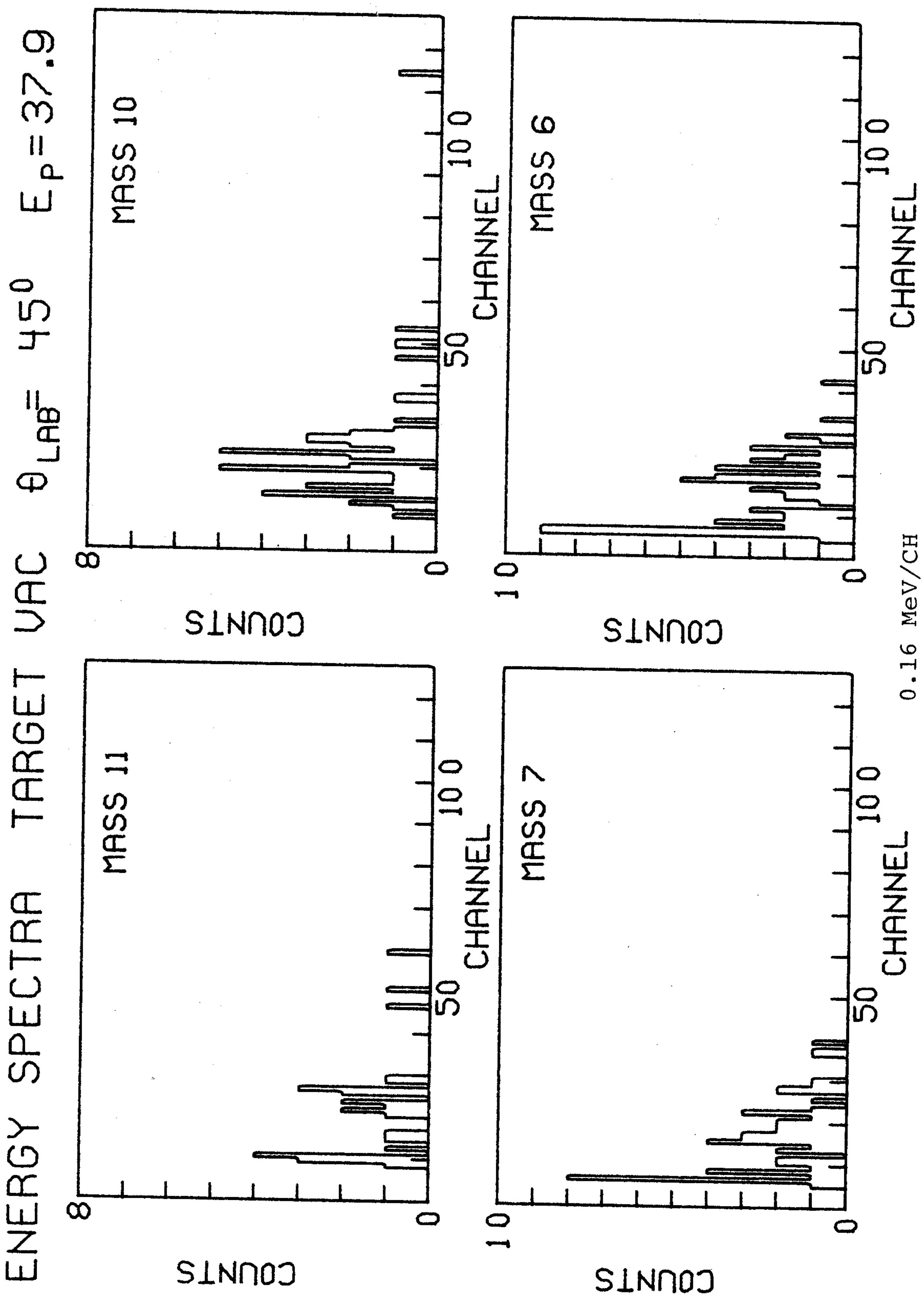

Figure 11. (continued)

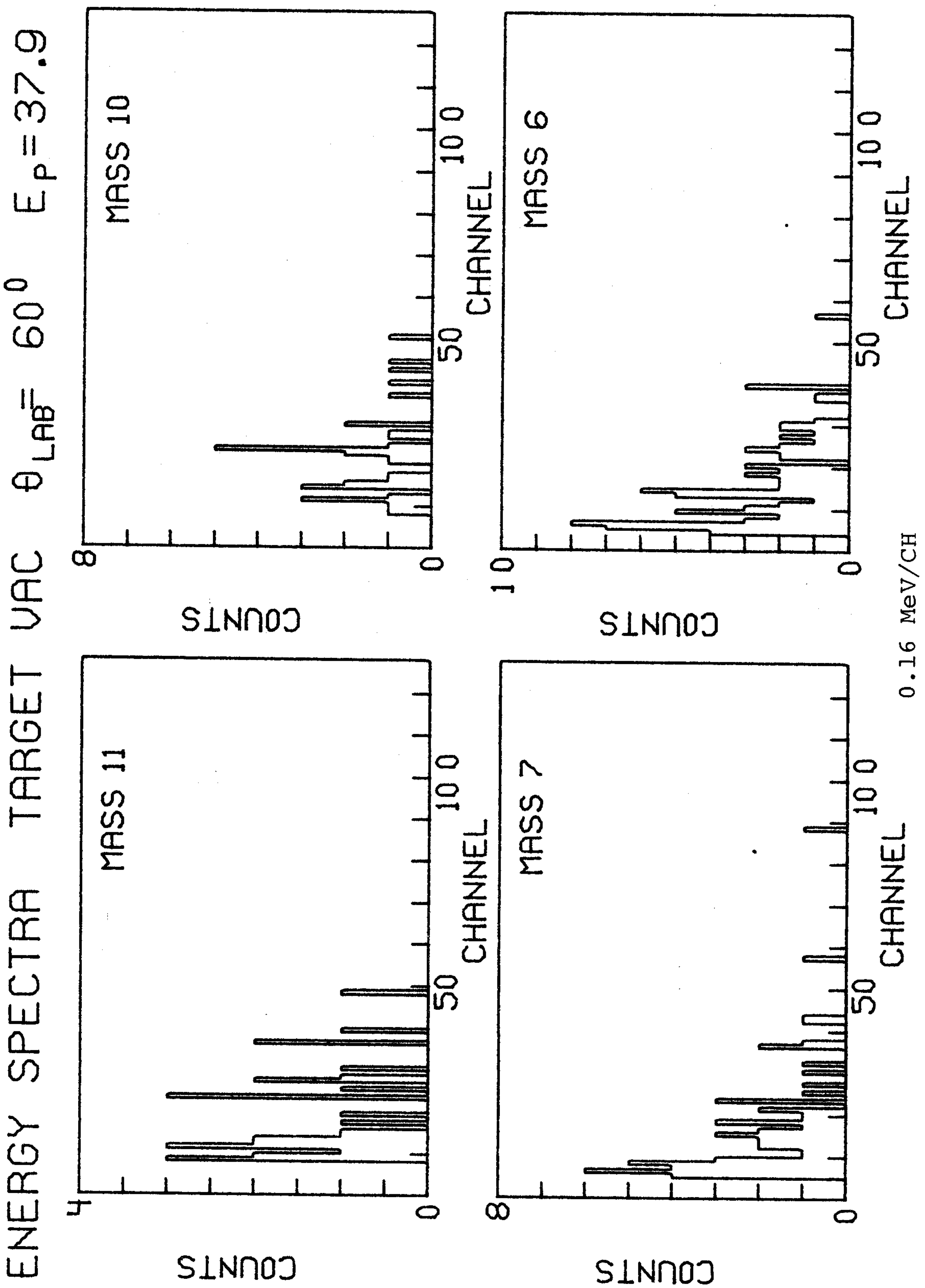

Figure 11. (continued)

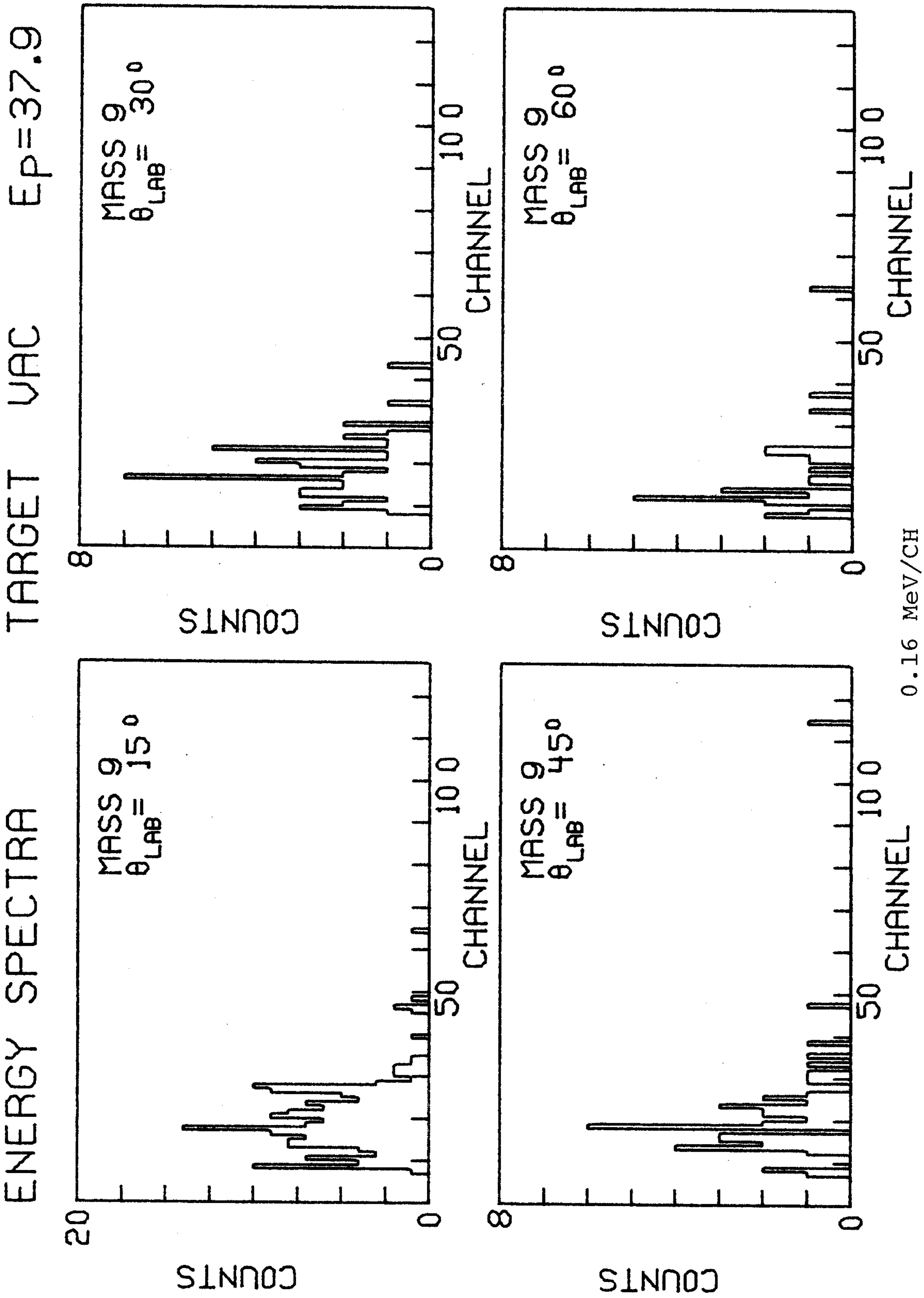

RF period is longer at low beam energy). To account for energy losses in gas and formvar window a formula for stopping power from (SE 68) modified from a theory by Lindhard _et_ _al_. (LS 61) is used:

$$(dE/dR)\,\mathrm{MeVcm}^2/\mathrm{g} = \frac{7.39 \times 10^4\, Z_1^{1.207} Z_2}{A_2 (Z_1^{2/3} + Z_2^{2/3})^{3/2}}\ \varepsilon^{\frac{1}{2}}$$

Z_1 = atomic number of projectile

Z_2 = atomic number of target

A_2 = atomic weight of target

ε = the specific energy of the projectile in MeV/nucleon

Experimental stopping power data of carbon on carbon (NO 63) is compared to the values obtained by this formula in Table 5.

Table 5. Validity of stopping power equation

Stopping power of Carbon on Carbon ($\mathrm{MeVcm}^2/\mathrm{g}$) ($Z_1$=6, Z_2=6, A_2=12)	ε = 0.01	ε = 0.1
Experimental	1870	5760
Calculated	1890	5980

In the calculations for projectile energy loss it is assumed that ε, the energy per nucleon, is 0.1. This is valid since the energy cutoff for mass 6 is near 0.5 MeV and for mass 11 it is near 1 MeV. As explained in section 2.3.3 reaction products traverse varying areal densities of gas depending on detection angle, hence the low energy cutoff also depends on angle. Table 6 summarizes the range of the cutoff effects. In Appendix G some more details of the calculations can be found.

The front surface electrode of the detector is a 40 μg/cm^2 gold layer; the energy loss it causes is negligible as shown in table 6, and since the time cutoff limit is usually above the detector sensitivity limit, it has no effect on particle detection.

Table 6. Energy cutoff limits

		Energy in MeV	
	Product ion:	^{6}Li	^{11}C
Minimum cutoff due to finite beam burst spacing	E_p=22MeV	0.3	0.6
	E_p=42MeV	0.5	0.9
energy loss in exit window	15° detection angle	0.4	0.7
	90° detection angle	0.2	0.3
energy loss in gold electrode of detector		0.02	0.03

The number of channels which the energy loss in the exit window represents is added to the number of channels for the low energy cutoff obtained from the energy spectra. The energy calibration curve necessary for determining the energy/channel ratio is determined from the two-body final state peaks appearing in the energy spectra. A low energy cutoff correction is performed by multiplying the number of cutoff-channels by a weighted average (60:30:10) of the number of events in the last three low energy channels of the energy spectrum. The resulting number is added to the total number of counts in the spectrum and this represents the yield Y. One-half of the low energy extrapolation contribution is assigned as error. The justification for the low energy extrapolation and error assignment is that phase space considerations (see Sternheimer (ST 63) for example) for multiparticle breakup assure that the energy spectra show zero yield at zero particle energy.

4.2 Time-of-Flight cross-section calculation

The equation relating differential cross-section and yield at a specific angle is:

$$d\sigma/d\Omega = Y/n_i n_t \Delta\Omega \; .$$

Y = yield in counts.

n_i = no. of beam particles.

n_t = no. of target atoms/cm^2 traversed by beam as seen from detector

$\Delta\Omega$ = solid angle subtended by aperture S1 in steradians

Y is found by summing the events recorded in the 128 channels of an energy spectrum and adding the energy cutoff extrapolation as outlined in 4.1.

$$n_i = Q/(1.6 \times 10^{-19})$$

Silverstein
↓

$$n_t' \Delta\Omega = \frac{S2 \times \ell}{H} \times \frac{A}{R^2} = \frac{S2 \times A}{H \times R} = G_{00}$$

Q(coul) is the integrated charge.

$$n_t = \frac{2\text{x}S2\text{x}R}{H \sin\theta} \times \frac{273.1}{T} \times P \times 2.687 \times 10^{19} \; .$$

This is an approximation, but for our geometry the maximum error introduced is less than 0.02% (shown by comparison with the program G-FACTOR based on (SI 59) and written by Dr. R. A. Paddock at the M.S.U. Cyclotron laboratory).

S2(cm) is the front slit width,

R(cm) is the average flight distance to S1,

H(cm) is the distance between S1 and S2,

θ(deg) is the angle between particle trajectory and proton beam axis,

T(°K) is the gas temperature,

P(atm) is the gas pressure.

The factor of 2 enters since N and O are diatomic gases.

$$\Delta\Omega = \frac{A}{R^2}$$

A(cm^2) is the area of aperture S1,

R(cm) as above.

Once $\frac{d\sigma}{d\Omega}$ is known at all angles, the total cross-section is obtained from

$$\sigma = 2\pi\int(d\sigma/d\Omega)\sin\theta d\theta$$

In the actual experiment performed $\frac{d\sigma}{d\Omega}$ is measured only at a few angles A_i. To perform the integration some arbitrary method must be chosen to fill in the missing points. Given $\frac{d\sigma}{d\Omega}(A_i)$, it was assumed $\frac{d\sigma}{d\Omega}(\theta) = \frac{d\sigma}{d\Omega}(A_i)$ for θ in the range

$$(A_i + A_{i-1})/2 < \theta < (A_{i+1} + A_i)/2 .$$

There was always a maximum angle, A_{max}, beyond which no data could be obtained because of the low energy cutoff.

Depending on the behavior of the angular distribution for $A_{max} < \theta \leq 180°$, $\frac{d\sigma}{d\Omega}(\theta)$ was either assumed to be equal to $\frac{d\sigma}{d\Omega}(A_{max})$ or it was assumed to go linearly to 0. Similarly for $0 < \theta < A_{min}$, $\frac{d\sigma}{d\Omega}(\theta) = \frac{d\sigma}{d\Omega}(A_{min})$ was assumed; no large error contribution is expected from this source except possibly for mass 11 at 26 MeV or below where the mass 11 yield is comprised largely or entirely of 2-body-final-state breakup. A modification of the $\frac{d\sigma}{d\Omega}(\theta) = \frac{d\sigma}{d\Omega}(A_{max})$ extrapolation, taking account of peaks falling below the low energy cutoff, was used for these cases.

All angular distributions used in calculating total cross-sections are shown in Figure 12, p. 115. A fortran program was written to carry out the total cross-section calculations. Basic equations in the program are shown in Appendix G. Table 8 presents individual cross-section calculations. Table 9 and Figure 13 summarize all cross-sections measured. Table 10 reproduces the cross-sections from ^{12}C published in (DLA 70).

The abbreviations in Table 8 stand for:

N = number of monitor counts for calibration run,

P = pressure for calibration run,

Q = integrated charge in coulombs x 10^{-4},

H = distance between S1 and S2,

R = distance from S1 to the center of the cell,

B = width of front slit S2.

<u>Lab angle</u>: angle at which data was taken (θ),

<u>Diff. Cross Sect</u>. gives the calculated differential cross section at the angle given in the same row (mb/sr),

<u>Contrib. to total cross sect</u>. gives the result of the integration step from $(A_{i-1}+A_i)/2 \leq \theta \leq (A_{i+1}+A_i)/2$ (mb),

<u>Assigned error</u>: error due to low energy cutoff and the statistical error combined in quadrature (mb),

<u>Yield</u> is obtained from E spectra as explained in section 4.2 (counts),

<u>Low E corr</u>.: the low energy cutoff correction as explained in section 4.1 (counts),

<u>Monitor counts</u>: the events in the elastic proton peak of the cesium iodide detector used to integrate beam current and particle density,

<u>Far</u>: yield from extrapolation of integration to $\theta=0°$ (mb),

<u>Back</u>: yield from extrapolation of integration to $\theta = 180°$ (mb),

<u>Total cross section</u>: the result of the angular distribution integration (mb).

The "total error" quoted in Table 8 is arrived at as follows: For each angle the statistical error of the yield and the low energy cutoff error are combined by their square. These are then added linearly, weighted by the contribution of the corresponding yield to the total cross-section. This conservative error estimate is used since all cutoff corrections may very well be in error in the same direction. The last value under the column "Assigned error" is the sum of these errors. One half of the back angle extrapolation and 0.2 of the extrapolation to $\theta=0$ are also added as error contributions. This final sum appears as the total error of the cross-sections in the tables. Table 7 summarizes other error sources entering into the cross-section calculation.

Table 7. Error contribution not associated with particle detection.

Error Source	Error in %	Measuring Apparatus
A = area of back aperture S1	0.39	Traveling Microscope
S2 front slit width	1.2 to 1.7	Feeler gauge
R the average particle flight distance to S1	1.0	Steel rule and micrometer (sensitive to beam centering)
H distance between S1 and S2	0.3	Steel rule and micrometer
T temperature	0.7	Thermometer
T temperature (beam heating)	1.5	
P gas pressure	.33	Oil manometer
P gas pressure	.7	Aneroid gauge
Q integrated charge	2.0	Elcor A310B current integrator

Added in quadrature these error contributions yield:

$$\sqrt{\Sigma E_r^2} = 3.3\%.$$

When folded in with the smallest "total error" appearing in Table 8, namely 8.0%, the probable error becomes 8.7%. Hence these error contributions are negligible compared to the low energy cutoff correction.

Table 8. Individual Cross-Section Calculations for ^{14}N and ^{16}O Targets.

```
  14 N   P SPALLATION  CROSS SECTION FOR MASS  7 ;    E=17.0 MEV
  ----------------------------------------------------------------

N=  15470  P=2.21CM HG  Q=.765E 00  H=23.1CM  R=24.7CM  B=.109CM

                          CONTRIB.
 LAB      DIFF.         TO TOTAL    ASSIGNED             LOW E   MONITOR
ANGLE  CROSS SECT.  CROSS SECT.      ERROR      YIELD   CORR.    COUNTS

 30.0   .682E 01      .739E 01     .132E 01     2018    1111      15470
 45.0   .622E 01      .722E 01     .162E 01     1380    1125      18905
 60.0   .398E 01      .565E 01     .135E 01      689     627      18875
 75.0   .290E 01      .460E 01     .125E 01      295     349      14011
  FOR                 .146E 01     .260E 00
 BACK                 .103E 02     .281E 01
                      --------     --------
                      .366E 02     .861E 01

TOTAL CROSS SECTION = 36.6 MB±14.1 MB (TOTAL ERROR=38 % )
```

```
  14 N   P SPALLATION  CROSS SECTION FOR MASS 10 ;    E=17.0 MEV
  ----------------------------------------------------------------

N=  15470  P=2.21CM HG  Q=.765E 00  H=23.1CM  R=24.7CM  B=.109CM

                          CONTRIB.
 LAB      DIFF.         TO TOTAL    ASSIGNED             LOW E   MONITOR
ANGLE  CROSS SECT.  CROSS SECT.      ERROR      YIELD   CORR.    COUNTS

 30.0   .133E 02      .144E 02     .554E 01     1418    4693      15470
 45.0   .372E 01      .431E 01     .172E 01      306    1190      18905
 60.0   .129E 01      .183E 01     .489E 00      201     226      18875
 75.0   .582E 00      .922E 00     .232E 00       66      63      14011
  FOR                 .285E 01     .109E 01
 BACK                 .207E 01     .521E 00
                      --------     --------
                      .264E 02     .959E 01

TOTAL CROSS SECTION = 26.4 MB±11.2 MB (TOTAL ERROR=42 % )
```

Table 8. (continued)

```
  14 N  P SPALLATION  CROSS SECTION FOR MASS 11 ;   E=17.0 MEV
  ------------------------------------------------------------

N=  15470  P=2.21CM HG  Q=.765E 00  H=23.1CM  R=24.7CM  B=.109CM

                          CONTRIB.
 LAB      DIFF.          TO TOTAL    ASSIGNED                LOW E   MONITOR
ANGLE  CROSS SECT.  CROSS SECT.      ERROR        YIELD   CORR.    COUNTS

 30.0    .110E 02      .120E 02     .168E 00      5039      27      15470
 45.0    .736E 01      .854E 01     .158E 00      2947      18      18905
 60.0    .720E 01      .102E 02     .208E 00      2371      12      18875
 75.0    .401E 01      .635E 01     .212E 00       875      13      14011
  FOR                  .236E 01     .332E-01
 BACK                  .284E 02     .952E 00
                       --------     --------
                       .679E 02     .173E 01

TOTAL CROSS SECTION = 67.9 MB±16.4 MB (TOTAL ERROR=24 % )
```

```
  14 N  P SPALLATION  CROSS SECTION FOR MASS  6 ;   E=21.7 MEV
  ------------------------------------------------------------

N= 431392  P=2.21CM HG  Q=.510E 01  H=23.1CM  R=24.7CM  B=.109CM

                          CONTRIB.
 LAB      DIFF.          TO TOTAL    ASSIGNED                LOW E   MONITOR
ANGLE  CROSS SECT.  CROSS SECT.      ERROR        YIELD   CORR.    COUNTS

 15.0    .130E 01      .553E 00     .124E 00       481     390      50768
 30.0    .108E 01      .883E 00     .211E 00       257     230      63776
 45.0    .419E 00      .486E 00     .876E-01        91      46      64291
 60.0    .232E 00      .330E 00     .574E-01        47      20      68914
 75.0    .196E 00      .310E 00     .537E-01        36      11      63497
 90.0    .162E 00      .265E 00     .519E-01        27      11      63962
105.0    .512E-01      .812E-01     .221E-01        11       0      56184
  FOR                  .700E-01     .158E-01
 BACK                  .993E-01     .271E-01
                       --------     --------
                       .308E 01     .651E 00

TOTAL CROSS SECTION =  3.1 MB±  .7 MB (TOTAL ERROR=23 % )
```

Table 8. (continued)

```
   14 N  P SPALLATION  CROSS SECTION FOR MASS  7 ;    E=21.7 MEV
   ---------------------------------------------------------------

 N= 431392  P=2.21CM HG  Q=.510E 01  H=23.1CM  R=24.7CM  B=.109CM

                         CONTRIB.
  LAB       DIFF.       TO TOTAL    ASSIGNED          LOW E   MONITOR
 ANGLE   CROSS SECT.  CROSS SECT.    ERROR     YIELD  CORR.    COUNTS

  15.0    .113E 02     .479E 01    .462E 00    6099   1447     50768
  30.0    .846E 01     .694E 01    .552E 00    3226    598     63776
  45.0    .643E 01     .745E 01    .811E 00    1652    450     64291
  60.0    .463E 01     .658E 01    .743E 00    1042    295     68914
  75.0    .304E 01     .481E 01    .652E 00     537    192     63497
  90.0    .210E 01     .344E 01    .508E 00     352    141     63962
 105.0    .186E 01     .294E 01    .690E 00     214    185     56184
   FOR                 .607E 00    .585E-01
  BACK                 .360E 01    .845E 00
                       --------    --------
                       .412E 02    .532E 01

 TOTAL CROSS SECTION = 41.2 MB± 7.2 MB (TOTAL ERROR=18 % )
```

```
   14 N  P SPALLATION  CROSS SECTION FOR MASS 10 ;    E=21.7 MEV
   ---------------------------------------------------------------

 N= 431392  P=2.21CM HG  Q=.510E 01  H=23.1CM  R=24.7CM  B=.109CM

                         CONTRIB.
  LAB       DIFF.       TO TOTAL    ASSIGNED          LOW E   MONITOR
 ANGLE   CROSS SECT.  CROSS SECT.    ERROR     YIELD  CORR.    COUNTS

  15.0    .306E 02     .130E 02    .233E 01   13125   7323     50768
  30.0    .219E 02     .179E 02    .334E 01    6205   3677     63776
  45.0    .152E 02     .177E 02    .423E 01    2599   2383     64291
  60.0    .745E 01     .106E 02    .297E 01     944   1206     68914
  75.0    .458E-01     .726E-01    .198E-01      11      0     63497
  90.0    .102E 00     .168E 00    .279E-01      24      0     63962
 105.0    .466E-02     .738E-02    .738E-02       1      0     56184
   FOR                 .164E 01    .295E 00
  BACK                 .903E-02    .903E-02
                       --------    --------
                       .611E 02    .132E 02

 TOTAL CROSS SECTION = 61.1 MB±13.6 MB (TOTAL ERROR=22 % )
```

Table 8. (continued)

```
   14 N  P SPALLATION  CROSS SECTION FOR MASS 11 ;    E=21.7 MEV
   ------------------------------------------------------------------

 N= 431392  P=2.21CM HG   Q=.510E 01   H=23.1CM  R=24.7CM  B=.109CM

                          CONTRIB.
   LAB       DIFF.       TO TOTAL     ASSIGNED              LOW E   MONITOR
  ANGLE   CROSS SECT.  CROSS SECT.     ERROR       YIELD    CORR.    COUNTS

   15.0    .485E 01     .206E 01     .386E-01      3197       47      50768
   30.0    .411E 01     .337E 01     .829E-01      1821       36      63776
   45.0    .322E 01     .373E 01     .122E 00      1022       30      64291
   60.0    .275E 01     .390E 01     .142E 00       772       21      68914
   75.0    .302E 01     .479E 01     .180E 00       709       16      63497
   90.0    .268E 01     .440E 01     .173E 00       618       12      63962
  105.0    .941E 00     .149E 01     .107E 00       189       13      56184
   FOR                  .261E 00     .488E-02
   BACK                 .155E 02     .263E 00
                        --------     --------
                        .395E 02     .111E 01

 TOTAL CROSS SECTION = 39.5 MB± 9.0 MB (TOTAL ERROR=23 % )
```

```
   14 N  P SPALLATION  CROSS SECTION FOR MASS  6 ;   E=25.8 MEV
   ------------------------------------------------------------------

 N= 760607  P=4.27CM HG   Q=.503E 01   H=26.9CM  R=27.5CM  B=.075CM

                          CONTRIB.
   LAB       DIFF.       TO TOTAL     ASSIGNED              LOW E   MONITOR
  ANGLE   CROSS SECT.  CROSS SECT.     ERROR       YIELD    CORR.    COUNTS

   15.0    .631E 01     .268E 01     .492E 00       917      527      30315
   30.0    .448E 01     .368E 01     .589E 00       758      351      60967
   45.0    .351E 01     .406E 01     .952E 00       322      280      59020
   60.0    .156E 01     .221E 01     .452E 00       296      200     133142
   75.0    .945E 00     .150E 01     .397E 00       177      196     182690
   90.0    .580E 00     .111E 01     .328E 00        88      124     174110
  110.0    .207E 00     .424E 00     .116E 00        33       37     150363
   FOR                  .339E 00     .623E-01
   BACK                 .325E 00     .890E-01
                        --------     --------
                        .163E 02     .348E 01

 TOTAL CROSS SECTION = 16.3 MB± 3.7 MB (TOTAL ERROR=23 % )
```

Table 8. (continued)

```
  14 N   P SPALLATION  CROSS SECTION FOR MASS  7 ;   E=25.8 MEV
  ------------------------------------------------------------

N= 760607  P=4.27CM HG  Q=.503E 01  H=26.9CM  R=27.5CM  B=.075CM

                        CONTRIB.
 LAB        DIFF.      TO TOTAL    ASSIGNED            LOW E   MONITOR
ANGLE    CROSS SECT.  CROSS SECT.    ERROR     YIELD   CORR.    COUNTS

 15.0     .559E 01    .237E 01    .186E 00     1089     189     30315
 30.0     .482E 01    .396E 01    .486E 00      906     287     60967
 45.0     .376E 01    .435E 01    .390E 00      539     106     59020
 60.0     .305E 01    .434E 01    .472E 00      769     205    133142
 75.0     .225E 01    .357E 01    .498E 00      646     243    182690
 90.0     .160E 01    .305E 01    .522E 00      388     196    174110
110.0     .104E 01    .213E 01    .430E 00      212     139    150363
  FOR                 .300E 00    .235E-01
 BACK                 .163E 01    .329E 00
                      --------    --------
                      .257E 02    .334E 01

TOTAL CROSS SECTION = 25.7 MB± 4.2 MB (TOTAL ERROR=16 % )
```

```
  14 N   P SPALLATION  CROSS SECTION FOR MASS 10 ;   E=25.8 MEV
  ------------------------------------------------------------

N= 760607  P=4.27CM HG  Q=.503E 01  H=26.9CM  R=27.5CM  B=.075CM

                        CONTRIB.
 LAB        DIFF.      TO TOTAL    ASSIGNED            LOW E   MONITOR
ANGLE    CROSS SECT.  CROSS SECT.    ERROR     YIELD   CORR.    COUNTS

 15.0     .237E 02    .101E 02    .126E 01     4069    1351     30315
 30.0     .186E 02    .153E 02    .236E 01     3189    1417     60967
 45.0     .126E 02    .146E 02    .278E 01     1347     820     59020
 60.0     .730E 01    .104E 02    .250E 01     1208    1122    133142
 75.0     .355E 01    .562E 01    .167E 01      571     831    182690
 90.0     .160E 01    .306E 01    .111E 01      160     426    174110
110.0     .591E-01    .121E 00    .412E-01        7      13    150363
  FOR                 .127E 01    .159E 00
 BACK                 .928E-01    .316E-01
                      --------    --------
                      .605E 02    .119E 02

TOTAL CROSS SECTION = 60.5 MB±12.2 MB (TOTAL ERROR=20 % )
```

Table 8. (continued)

```
  14 N  P SPALLATION  CROSS SECTION FOR MASS 11 ;   E=25.8 MEV
  --------------------------------------------------------------

N= 760607  P=4.27CM HG  Q=.503E 01  H=26.9CM  R=27.5CM  B=.075CM

                        CONTRIB.
 LAB       DIFF.        TO TOTAL    ASSIGNED               LOW E   MONITOR
ANGLE   CROSS SECT.  CROSS SECT.     ERROR        YIELD   CORR.    COUNTS

 15.0    .404E 01     .171E 01     .198E 00       716     207      30315
 30.0    .318E 01     .261E 01     .421E 00       537     250      60967
 45.0    .272E 01     .315E 01     .536E 00       312     155      59020
 60.0    .206E 01     .292E 01     .344E 00       508     148     133142
 75.0    .166E 01     .263E 01     .247E 00       542     114     182690
 90.0    .199E 01     .380E 01     .663E 00       476     250     174110
110.0    .110E 01     .226E 01     .569E 00       187     186     150363
  FOR                 .217E 00     .251E-01
 BACK                 .346E 01     .872E 00
                      --------     --------
                      .228E 02     .387E 01

TOTAL CROSS SECTION = 22.8 MB± 5.6 MB (TOTAL ERROR=25 % )
```

```
  14 N  P SPALLATION  CROSS SECTION FOR MASS  6 ;   E=28.6 MEV
  --------------------------------------------------------------

N=1026222  P=4.11CM HG  Q=.748E 01  H=26.2CM  R=27.6CM  B=.076CM

                        CONTRIB.
 LAB       DIFF.        TO TOTAL    ASSIGNED               LOW E   MONITOR
ANGLE   CROSS SECT.  CROSS SECT.     ERROR        YIELD   CORR.    COUNTS

 20.0    .647E 01     .248E 01     .639E-01      1479      12      32621
 25.0    .649E 01     .150E 01     .955E-01      1278     170      39030
 30.0    .639E 01     .376E 01     .236E 00      1638     219      62753
 45.0    .407E 01     .472E 01     .415E 00      1153     235     103480
 60.0    .265E 01     .376E 01     .420E 00       738     203     132042
 75.0    .116E 01     .184E 01     .892E-01       454      18     168217
 90.0    .777E 00     .127E 01     .116E 00       340      64     223078
105.0    .508E 00     .805E 00     .913E-01       223      57     228391
120.0    .480E 00     .682E 00     .141E 00       132      89     171014
  FOR                 .618E 00     .159E-01
 BACK                 .590E 00     .122E 00
                      --------     --------
                      .220E 02     .181E 01

TOTAL CROSS SECTION = 22.0 MB± 2.2 MB (TOTAL ERROR=10 % )
```

Table 8. (continued)

```
   14 N  P SPALLATION  CROSS SECTION FOR MASS  7 ;   E=28.6 MEV
   ----------------------------------------------------------------

  N=1026222  P=4.11CM HG  Q=.748E 01  H=26.2CM  R=27.6CM  B=.076CM

                          CONTRIB.
   LAB       DIFF.       TO TOTAL    ASSIGNED            LOW E   MONITOR
  ANGLE   CROSS SECT.  CROSS SECT.    ERROR      YIELD   CORR.    COUNTS

   20.0   .350E 01     .134E 01    .569E-01      765      42     32621
   25.0   .340E 01     .787E 00    .445E-01      690      68     39030
   30.0   .316E 01     .186E 01    .103E 00      833      85     62753
   45.0   .255E 01     .296E 01    .186E 00      775      95    103480
   60.0   .204E 01     .290E 01    .242E 00      615     111    132042
   75.0   .150E 01     .237E 01    .148E 00      547      60    168217
   90.0   .118E 01     .194E 01    .158E 00      523      90    223078
  105.0   .908E 00     .144E 01    .203E 00      364     136    228391
  120.0   .600E 00     .852E 00    .914E-01      225      51    171014
    FOR                .334E 00    .142E-01
   BACK                .737E 00    .790E-01
                       --------    --------
                       .175E 02    .133E 01

  TOTAL CROSS SECTION = 17.5 MB± 1.8 MB (TOTAL ERROR=10 % )
```

```
   14 N  P SPALLATION  CROSS SECTION FOR MASS 10 ;   E=28.6 MEV
   ----------------------------------------------------------------

  N=1026222  P=4.11CM HG  Q=.748E 01  H=26.2CM  R=27.6CM  B=.076CM

                          CONTRIB.
   LAB       DIFF.       TO TOTAL    ASSIGNED            LOW E   MONITOR
  ANGLE   CROSS SECT.  CROSS SECT.    ERROR      YIELD   CORR.    COUNTS

   20.0   .182E 02     .695E 01    .364E 00     3761     421     32621
   25.0   .175E 02     .405E 01    .372E 00     3196     707     39030
   30.0   .159E 02     .935E 01    .687E 00     3954     667     62753
   45.0   .101E 02     .117E 02    .103E 01     2833     597    103480
   60.0   .691E 01     .982E 01    .138E 01     1768     687    132042
   75.0   .391E 01     .620E 01    .119E 01      980     607    168217
   90.0   .197E 01     .323E 01    .758E 00      547     478    223078
  105.0   .120E 01     .190E 01    .588E 00      251     408    228391
  120.0   .878E 00     .125E 01    .476E 00       96     308    171014
    FOR                .173E 01    .908E-01
   BACK                .108E 01    .412E 00
                       --------    --------
                       .572E 02    .735E 01

  TOTAL CROSS SECTION = 57.2 MB± 8.2 MB (TOTAL ERROR=14 % )
```

Table 8. (continued)

```
   14 N  P SPALLATION  CROSS SECTION FOR MASS 11 ;   E=28.6 MEV
   --------------------------------------------------------------

 N=1026222  P=4.11CM HG  Q=.748E 01  H=26.2CM  R=27.6CM  B=.076CM

                          CONTRIB.
  LAB       DIFF.         TO TOTAL    ASSIGNED           LOW E  MONITOR
 ANGLE   CROSS SECT.  CROSS SECT.      ERROR     YIELD   CORR.   COUNTS

  20.0    .412E 01     .158E 01     .180E 00     740     210     32621
  25.0    .712E 01     .165E 01     .360E 00     895     693     39030
  30.0    .406E 01     .239E 01     .552E 00     637     543     62753
  45.0    .195E 01     .227E 01     .395E 00     437     229    103480
  60.0    .156E 01     .222E 01     .299E 00     411     144    132042
  75.0    .128E 01     .203E 01     .119E 00     476      44    168217
  90.0    .893E 00     .146E 01     .938E-01     420      44    223078
 105.0    .109E 01     .173E 01     .317E 00     384     217    228391
 120.0    .970E 00     .138E 01     .344E 00     225     221    171014
   FOR                 .394E 00     .449E-01
  BACK                 .238E 01     .596E 00
                       --------     --------
                       .195E 02     .330E 01

 TOTAL CROSS SECTION = 19.5 MB± 4.6 MB (TOTAL ERROR=23 % )
```

```
   14 N  P SPALLATION  CROSS SECTION FOR MASS  6 ;   E=31.9 MEV
   --------------------------------------------------------------

 N=  15704  P=5.36CM HG  Q=.100E 00  H=25.7CM  R=26.3CM  B=.076CM

                          CONTRIB.
  LAB       DIFF.         TO TOTAL    ASSIGNED           LOW E  MONITOR
 ANGLE   CROSS SECT.  CROSS SECT.      ERROR     YIELD   CORR.   COUNTS

  15.0    .715E 01     .303E 01     .758E-01    2307      70     28419
  30.0    .576E 01     .472E 01     .336E 00    1075     164     35519
  45.0    .401E 01     .465E 01     .271E 00    2206     274     73288
  60.0    .257E 01     .365E 01     .321E 00     504      96     71363
  75.0    .180E 01     .285E 01     .231E 00     382      61     83930
  90.0    .104E 01     .171E 01     .128E 00     282      35    107217
 105.0    .585E 00     .927E 00     .824E-01     164      23    108880
 120.0    .435E 00     .618E 00     .673E-01     123      23    102567
   FOR                 .384E 00     .960E-02
  BACK                 .534E 00     .583E-01
                       --------     --------
                       .231E 02     .158E 01

 TOTAL CROSS SECTION = 23.1 MB± 1.9 MB (TOTAL ERROR= 8 % )
```

Table 8. (continued)

```
  14 N  P SPALLATION  CROSS SECTION FOR MASS  7 ;    E=31.9 MEV
  --------------------------------------------------------------

N=  15704  P=5.36CM HG  Q=.100E 00  H=25.7CM  R=26.3CM  B=.076CM

                        CONTRIB.
 LAB       DIFF.       TO TOTAL    ASSIGNED           LOW E   MONITOR
ANGLE   CROSS SECT.  CROSS SECT.    ERROR     YIELD   CORR.    COUNTS

 15.0    .263E 01     .112E 01    .557E-01     808      67     28419
 30.0    .214E 01     .175E 01    .121E 00     411      49     35519
 45.0    .178E 01     .207E 01    .163E 00     941     163     73288
 60.0    .212E 01     .301E 01    .445E 00     353     142     71363
 75.0    .144E 01     .228E 01    .271E 00     276      78     83930
 90.0    .822E 00     .135E 01    .104E 00     226      24    107217
105.0    .720E 00     .114E 01    .102E 00     200      30    108880
120.0    .581E 00     .825E 00    .915E-01     159      36    102567
  FOR                 .141E 00    .706E-02
 BACK                 .714E 00    .792E-01
                      --------    --------
                      .144E 02    .144E 01

TOTAL CROSS SECTION = 14.4 MB± 1.8 MB (TOTAL ERROR=13 % )
```

```
  14 N  P SPALLATION  CROSS SECTION FOR MASS 10 ;    E=31.9 MEV
  --------------------------------------------------------------

N=  15704  P=5.36CM HG  Q=.100E 00  H=25.7CM  R=26.3CM  B=.076CM

                        CONTRIB.
 LAB       DIFF.       TO TOTAL    ASSIGNED           LOW E   MONITOR
ANGLE   CROSS SECT.  CROSS SECT.    ERROR     YIELD   CORR.    COUNTS

 15.0    .146E 02     .621E 01    .263E 00    4477     390     28419
 30.0    .114E 02     .938E 01    .578E 00    2171     289     35519
 45.0    .746E 01     .866E 01    .310E 00    4311     304     73288
 60.0    .574E 01     .815E 01    .104E 01    1006     335     71363
 75.0    .380E 01     .603E 01    .111E 01     594     343     83930
 90.0    .214E 01     .351E 01    .789E 00     361     290    107217
105.0    .107E 01     .170E 01    .280E 00     234     109    108880
120.0    .554E 00     .787E 00    .154E 00     116      70    102567
  FOR                 .787E 00    .333E-01
 BACK                 .681E 00    .133E 00
                      --------    --------
                      .459E 02    .469E 01

TOTAL CROSS SECTION = 45.9 MB± 5.2 MB (TOTAL ERROR=11 % )
```

Table 8. (continued)

```
   14 N  P SPALLATION  CROSS SECTION FOR MASS 11 ;   E=31.9 MEV
   ----------------------------------------------------------------

  N=  15704  P=5.36CM HG  Q=.100E 00  H=25.7CM  R=26.3CM  B=.076CM

                         CONTRIB.
   LAB       DIFF.      TO TOTAL     ASSIGNED            LOW E   MONITOR
  ANGLE   CROSS SECT.  CROSS SECT.    ERROR       YIELD  CORR.    COUNTS

   15.0    .572E 01     .243E 01    .405E 00      1271     631     28419
   30.0    .648E 01     .532E 01    .124E 01       746     649     35519
   45.0    .350E 01     .406E 01    .101E 01      1091    1074     73288
   60.0    .178E 01     .252E 01    .422E 00       280     135     71363
   75.0    .913E 00     .145E 01    .181E 00       175      50     83930
   90.0    .697E 00     .114E 01    .107E 00       182      30    107217
  105.0    .748E 00     .119E 01    .825E-01       221      18    108880
  120.0    .101E 01     .143E 01    .309E 00       194     144    102567
    FOR                 .307E 00    .513E-01
   BACK                 .247E 01    .536E 00
                        --------    --------
                        .223E 02    .434E 01

  TOTAL CROSS SECTION = 22.3 MB± 5.6 MB (TOTAL ERROR=25 % )
```

```
   14 N  P SPALLATION  CROSS SECTION FOR MASS  6 ;   E=35.1 MEV
   ----------------------------------------------------------------

  N=  78775  P=4.50CM HG  Q=.588E 00  H=24.3CM  R=26.3CM  B=.076CM

                         CONTRIB.
   LAB       DIFF.      TO TOTAL     ASSIGNED            LOW E   MONITOR
  ANGLE   CROSS SECT.  CROSS SECT.    ERROR       YIELD  CORR.    COUNTS

   15.0    .813E 01     .345E 01    .185E 00      6514     763     78775
   30.0    .696E 01     .571E 01    .556E 00      1835     434     55436
   45.0    .482E 01     .559E 01    .565E 00      1153     283     71679
   60.0    .300E 01     .427E 01    .359E 00       988     188    115309
   75.0    .203E 01     .321E 01    .364E 00       594     165    122957
   90.0    .149E 01     .245E 01    .419E 00       335     168    114468
  105.0    .903E 00     .143E 01    .232E 00       208      94    109794
  120.0    .106E 01     .151E 01    .271E 00       119      62     50231
    FOR                 .437E 00    .234E-01
   BACK                 .130E 01    .235E 00
                        --------    --------
                        .294E 02    .321E 01

  TOTAL CROSS SECTION = 29.4 MB± 3.9 MB (TOTAL ERROR=13 % )
```

Table 8. (continued)

```
   14 N   P SPALLATION  CROSS SECTION FOR MASS  7 ;   E=35.1 MEV
   ---------------------------------------------------------------

N=   78775   P=4.50CM HG   Q=.588E 00   H=24.3CM   R=26.3CM   B=.076CM

                              CONTRIB.
 LAB          DIFF.        TO TOTAL    ASSIGNED              LOW E   MONITOR
ANGLE     CROSS SECT.  CROSS SECT.     ERROR        YIELD    CORR.   COUNTS

 15.0      .265E 01      .112E 01     .120E 00      1875      498     78775
 30.0      .172E 01      .141E 01     .987E-01       495       65     55436
 45.0      .181E 01      .210E 01     .231E 00       427      112     71679
 60.0      .170E 01      .242E 01     .299E 00       508      159    115309
 75.0      .124E 01      .196E 01     .231E 00       360      103    122957
 90.0      .125E 01      .205E 01     .440E 00       243      178    114468
105.0      .924E 00      .146E 01     .253E 00       206      103    109794
120.0      .545E 00      .774E 00     .198E 00        47       46     50231
  FOR                    .142E 00     .152E-01
 BACK                    .670E 00     .171E 00
                         --------     --------
                         .141E 02     .206E 01

TOTAL CROSS SECTION = 14.1 MB± 2.4 MB (TOTAL ERROR=17 % )
```

```
   14 N   P SPALLATION  CROSS SECTION FOR MASS 10 ;   E=35.1 MEV
   ---------------------------------------------------------------

N=   78775   P=4.50CM HG   Q=.588E 00   H=24.3CM   R=26.3CM   B=.076CM

                              CONTRIB.
 LAB          DIFF.        TO TOTAL    ASSIGNED              LOW E   MONITOR
ANGLE     CROSS SECT.  CROSS SECT.     ERROR        YIELD    CORR.   COUNTS

 15.0      .144E 02      .614E 01     .390E 00     11306     1632     78775
 30.0      .127E 02      .104E 02     .138E 01      3038     1090     55436
 45.0      .948E 01      .110E 02     .198E 01      1813     1013     71679
 60.0      .528E 01      .749E 01     .891E 00      1581      485    115309
 75.0      .274E 01      .434E 01     .610E 00       742      283    122957
 90.0      .195E 01      .320E 01     .784E 00       337      320    114468
105.0      .239E 01      .379E 01     .104E 01       363      436    109794
120.0      .826E 00      .117E 01     .395E 00        47       94     50231
  FOR                    .777E 00     .494E-01
 BACK                    .102E 01     .341E 00
                         --------     --------
                         .493E 02     .785E 01

TOTAL CROSS SECTION = 49.3 MB± 8.5 MB (TOTAL ERROR=17 % )
```

Table 8. (continued)

```
  14 N  P SPALLATION  CROSS SECTION FOR MASS 11 ;   E=35.1 MEV
  ------------------------------------------------------------

 N=  78775  P=4.50CM HG  Q=.588E 00  H=24.3CM  R=26.3CM  B=.076CM

                          CONTRIB.
  LAB       DIFF.        TO TOTAL    ASSIGNED            LOW E   MONITOR
 ANGLE  CROSS SECT.  CROSS SECT.      ERROR      YIELD   CORR.    COUNTS

  15.0   .612E 01     .260E 01    .322E 00      4124    1353     78775
  30.0   .465E 01     .381E 01    .589E 00      1052     464     55436
  45.0   .329E 01     .381E 01    .676E 00       636     344     71679
  60.0   .233E 01     .331E 01    .868E 00       436     477    115309
  75.0   .143E 01     .227E 01    .482E 00       312     225    122957
  90.0   .737E 00     .121E 01    .931E-01       222      26    114468
 105.0   .314E 00     .498E 00    .723E-01        79      26    109794
 120.0   .131E 01     .186E 01    .555E 00        92     132     50231
   FOR                .329E 00    .408E-01
  BACK                .323E 01    .960E 00
                      --------    --------
                      .229E 02    .466E 01

 TOTAL CROSS SECTION = 22.9 MB± 6.3 MB (TOTAL ERROR=28 % )
```

```
  14 N  P SPALLATION  CROSS SECTION FOR MASS  6 ;   E=37.9 MEV
  ------------------------------------------------------------

 N= 126329  P=2.11CM HG  Q=.274E 01  H=24.2CM  R=24.8CM  B=.108CM

                          CONTRIB.
  LAB       DIFF.        TO TOTAL    ASSIGNED            LOW E   MONITOR
 ANGLE  CROSS SECT.  CROSS SECT.      ERROR      YIELD   CORR.    COUNTS

  15.0   .851E 01     .361E 01    .263E 00      2885     478     18191
  30.0   .575E 01     .471E 01    .345E 00      1206     193     20822
  45.0   .454E 01     .627E 01    .530E 00       707     132     22031
  65.0   .302E 01     .598E 01    .569E 00       389      81     23491
  85.0   .261E 01     .568E 01    .882E 00       234      99     21020
 105.0   .186E 01     .393E 01    .727E 00       157      87     20774
   FOR                .458E 00    .333E-01
  BACK                .338E 01    .625E 00
                      --------    --------
                      .340E 02    .397E 01

 TOTAL CROSS SECTION = 34.0 MB± 5.8 MB (TOTAL ERROR=17 % )
```

Table 8. (continued)

```
   14 N  P SPALLATION  CROSS SECTION FOR MASS  7 ;   E=37.9 MEV
   ---------------------------------------------------------------

 N= 126329  P=2.11CM HG  Q=.274E 01  H=24.2CM  R=24.8CM  B=.108CM

                          CONTRIB.
  LAB       DIFF.         TO TOTAL    ASSIGNED             LOW E   MONITOR
 ANGLE  CROSS SECT.  CROSS SECT.       ERROR       YIELD   CORR.    COUNTS

  15.0    .377E 01      .160E 01     .157E 00      1203     285     18191
  30.0    .283E 01      .232E 01     .272E 00       533     155     20822
  45.0    .220E 01      .304E 01     .381E 00       311      96     22031
  65.0    .238E 01      .471E 01     .855E 00       239     131     23491
  85.0    .211E 01      .459E 01     .848E 00       173      96     21020
 105.0    .115E 01      .242E 01     .367E 00       109      41     20774
   FOR                  .202E 00     .199E-01
  BACK                  .208E 01     .316E 00
                        --------     --------
                        .210E 02     .322E 01

 TOTAL CROSS SECTION = 21.0 MB± 4.3 MB (TOTAL ERROR=21 % )
```

```
   14 N  P SPALLATION  CROSS SECTION FOR MASS 10 ;   E=37.9 MEV
   ---------------------------------------------------------------

 N= 126329  P=2.11CM HG  Q=.274E 01  H=24.2CM  R=24.8CM  B=.108CM

                          CONTRIB.
  LAB       DIFF.         TO TOTAL    ASSIGNED             LOW E   MONITOR
 ANGLE  CROSS SECT.  CROSS SECT.       ERROR       YIELD   CORR.    COUNTS

  15.0    .125E 02      .530E 01     .691E 00      3649    1281     18191
  30.0    .980E 01      .804E 01     .102E 01      1787     598     20822
  45.0    .717E 01      .990E 01     .127E 01       992     333     22031
  65.0    .466E 01      .922E 01     .134E 01       518     206     23491
  85.0    .268E 01      .583E 01     .980E 00       231     111     21020
 105.0    .118E 01      .250E 01     .434E 00       105      50     20774
   FOR                  .671E 00     .875E-01
  BACK                  .215E 01     .373E 00
                        --------     --------
                        .436E 02     .619E 01

 TOTAL CROSS SECTION = 43.6 MB± 7.4 MB (TOTAL ERROR=17 % )
```

Table 8. (continued)

```
 14 N   P SPALLATION  CROSS SECTION FOR MASS 11 ;    E=37.9 MEV
 ---------------------------------------------------------------

N= 126329  P=2.11CM HG  Q=.274E 01  H=24.2CM  R=24.8CM  B=.108CM

                      CONTRIB.
LAB        DIFF.      TO TOTAL    ASSIGNED            LOW E   MONITOR
ANGLE  CROSS SECT.  CROSS SECT.    ERROR       YIELD   CORR.   COUNTS

 15.0   .902E 01    .383E 01    .581E 00      2487    1077    18191
 30.0   .678E 01    .556E 01    .103E 01      1044     606    20822
 45.0   .378E 01    .522E 01    .929E 00       453     245    22031
 65.0   .248E 01    .490E 01    .113E 01       210     175    23491
 85.0   .737E 00    .160E 01    .212E 00        75      19    21020
105.0   .810E 00    .171E 01    .184E 00        92      14    20774
  FOR                .485E 00    .736E-01
 BACK                .294E 01    .316E 00
                     --------    --------
                     .262E 02    .445E 01

TOTAL CROSS SECTION = 26.2 MB± 6.0 MB (TOTAL ERROR=23 % )
```

```
  VAC   P SPALLATION  CROSS SECTION FOR MASS  6 ;    E=37.9 MEV
 ---------------------------------------------------------------

N=  10000  P=2.11CM HG  Q=.300E 00  H=24.2CM  R=24.8CM  B=.108CM

                      CONTRIB.
LAB        DIFF.      TO TOTAL    ASSIGNED            LOW E   MONITOR
ANGLE  CROSS SECT.  CROSS SECT.    ERROR       YIELD   CORR.   COUNTS

 15.0   .295E 01    .125E 01    .549E-01      2038     172    25004
 30.0   .114E 01    .933E 00    .612E-01       414      45    25006
 45.0   .973E 00    .113E 01    .144E 00       258      80    30003
 60.0   .102E 01    .144E 01    .930E-01       330      29    37027
  FOR                .158E 00    .696E-02
 BACK                .442E 01    .284E 00
                     --------    --------
                     .933E 01    .644E 00

TOTAL CROSS SECTION =  9.3 MB± 2.9 MB (TOTAL ERROR=31 % )
```

Table 8. (continued)

```
    VAC  P SPALLATION  CROSS SECTION FOR MASS  7 ;    E=37.9 MEV
   ------------------------------------------------------------------

N=   10000  P=2.11CM HG  Q=.300E 00  H=24.2CM  R=24.8CM  B=.108CM

                           CONTRIB.
 LAB        DIFF.        TO TOTAL    ASSIGNED              LOW E   MONITOR
ANGLE   CROSS SECT.  CROSS SECT.      ERROR       YIELD   CORR.    COUNTS

 15.0    .189E 01      .802E 00    .349E-01      1316     100      25004
 30.0    .994E 00      .815E 00    .968E-01       312      89      25006
 45.0    .774E 00      .898E 00    .129E 00       197      72      30003
 60.0    .725E 00      .103E 01    .855E-01       224      32      37027
  FOR                  .102E 00    .442E-02
 BACK                  .315E 01    .262E 00
                       --------    --------
                       .679E 01    .612E 00

TOTAL CROSS SECTION =  6.8 MB± 2.2 MB (TOTAL ERROR=32 % )


    VAC  P SPALLATION  CROSS SECTION FOR MASS 10 ;    E=37.9 MEV
   ------------------------------------------------------------------

N=   10000  P=2.11CM HG  Q=.300E 00  H=24.2CM  R=24.8CM  B=.108CM

                           CONTRIB.
 LAB        DIFF.        TO TOTAL    ASSIGNED              LOW E   MONITOR
ANGLE   CROSS SECT.  CROSS SECT.      ERROR       YIELD   CORR.    COUNTS

 15.0    .102E 01      .431E 00    .639E-01       540     221      25004
 30.0    .421E 00      .345E 00    .257E-01       162       8      25006
 45.0    .553E 00      .641E 00    .459E-01       183       9      30003
 60.0    .371E 00      .527E 00    .443E-01       131       0      37027
  FOR                  .546E-01    .809E-02
 BACK                  .161E 01    .135E 00
                       --------    --------
                       .361E 01    .323E 00

TOTAL CROSS SECTION =  3.6 MB± 1.1 MB (TOTAL ERROR=32 % )
```

Table 8. (continued)

```
   VAC  P SPALLATION  CROSS SECTION FOR MASS 11 ;   E=37.9 MEV
  -------------------------------------------------------------

 N=   10000   P=2.11CM HG   Q=.300E 00   H=24.2CM   R=24.8CM   B=.108CM

                         CONTRIB.
  LAB       DIFF.       TO TOTAL     ASSIGNED              LOW E    MONITOR
 ANGLE   CROSS SECT.  CROSS SECT.     ERROR        YIELD   CORR.    COUNTS

  15.0    .590E 00     .250E 00     .117E-01        431      11      25004
  30.0    .396E 00     .325E 00     .295E-01        141      19      25006
  45.0    .357E 00     .414E 00     .449E-01        106      18      30003
  60.0    .430E 00     .611E 00     .828E-01        116      36      37027
   FOR                 .317E-01     .149E-02
  BACK                 .187E 01     .253E 00
                       --------     --------
                       .350E 01     .424E 00

 TOTAL CROSS SECTION =  3.5 MB± 1.4 MB (TOTAL ERROR=39 % )
```

```
  14 N  P SPALLATION  CROSS SECTION FOR MASS  6 ;   E=40.0 MEV
  -------------------------------------------------------------

 N=   80353   P=1.37CM HG   Q=.284E 01   H=26.1CM   R=27.2CM   B=.076CM

                         CONTRIB.
  LAB       DIFF.       TO TOTAL     ASSIGNED              LOW E    MONITOR
 ANGLE   CROSS SECT.  CROSS SECT.     ERROR        YIELD   CORR.    COUNTS

  15.0    .486E 01     .206E 01     .191E 00       1600     352      29916
  30.0    .435E 01     .356E 01     .387E 00       1099     296      44452
  45.0    .339E 01     .394E 01     .448E 00        911     260      66624
  60.0    .249E 01     .354E 01     .418E 00        886     266     108429
  75.0    .155E 01     .245E 01     .351E 00        534     208     124779
  90.0    .103E 01     .168E 01     .283E 00        305     149     118344
 105.0    .827E 00     .131E 01     .277E 00        232     165     123380
 120.0    .607E 00     .727E 00     .140E 00        233     141     141192
 130.0    .884E 00     .742E 00     .142E 00        106      61      37085
   FOR                 .261E 00     .242E-01
  BACK                 .163E 01     .313E 00
                       --------     --------
                       .219E 02     .298E 01

 TOTAL CROSS SECTION = 21.9 MB± 3.8 MB (TOTAL ERROR=18 % )
```

Table 8. (continued)

```
   14 N  P SPALLATION  CROSS SECTION FOR MASS  7 ;    E=40•0 MEV
   --------------------------------------------------------------

N=  80353  P=1•37CM HG  Q=•284E 01  H=26•1CM  R=27•2CM  B=•076CM

                        CONTRIB•
 LAB        DIFF•      TO TOTAL    ASSIGNED               LOW E   MONITOR
ANGLE    CROSS SECT•  CROSS SECT•    ERROR       YIELD    CORR•    COUNTS

 15•0     •223E 01     •947E 00    •111E 00       691      204     29916
 30•0     •147E 01     •121E 01    •106E 00       398       74     44452
 45•0     •159E 01     •185E 01    •224E 00       422      127     66624
 60•0     •107E 01     •152E 01    •174E 00       389      107    108429
 75•0     •952E 00     •151E 01    •211E 00       334      123    124779
 90•0     •832E 00     •136E 01    •203E 00       263      105    118344
105•0     •521E 00     •825E 00    •122E 00       181       69    123380
120•0     •602E 00     •722E 00    •126E 00       245      126    141192
130•0     •635E 00     •533E 00    •954E-01        81       39     37085
  FOR                  •120E 00    •141E-01
 BACK                  •117E 01    •209E 00
                       --------    --------
                       •118E 02    •160E 01

TOTAL CROSS SECTION = 11•8 MB± 2•2 MB (TOTAL ERROR=19 % )
```

```
   14 N  P SPALLATION  CROSS SECTION FOR MASS 10 ;    E=40•0 MEV
   --------------------------------------------------------------

N=  80353  P=1•37CM HG  Q=•284E 01  H=26•1CM  R=27•2CM  B=•076CM

                        CONTRIB•
 LAB        DIFF•      TO TOTAL    ASSIGNED               LOW E   MONITOR
ANGLE    CROSS SECT•  CROSS SECT•    ERROR       YIELD    CORR•    COUNTS

 15•0     •788E 01     •334E 01    •485E 00      2250      912     29916
 30•0     •752E 01     •616E 01    •888E 00      1722      690     44452
 45•0     •559E 01     •649E 01    •939E 00      1376      554     66624
 60•0     •394E 01     •560E 01    •978E 00      1191      633    108429
 75•0     •216E 01     •343E 01    •707E 00       613      426    124779
 90•0     •138E 01     •226E 01    •479E 00       354      256    118344
105•0     •969E 00     •153E 01    •349E 00       256      209    123380
120•0     •866E 00     •104E 01    •292E 00       235      299    141192
130•0     •693E 00     •582E 00    •169E 00        56       75     37085
  FOR                  •423E 00    •614E-01
 BACK                  •638E 00    •186E 00
                       --------    --------
                       •315E 02    •553E 01

TOTAL CROSS SECTION = 31•5 MB± 5•9 MB (TOTAL ERROR=19 % )
```

Table 8. (continued)

```
   14 N  P SPALLATIØN  CRØSS SECTIØN FØR MASS 11 ;   E=40.0 MEV
   ----------------------------------------------------------------

 N=  80353  P=1.37CM HG  Q=.284E 01  H=26.1CM  R=27.2CM  B=.076CM

                      CØNTRIB.
 LAB      DIFF.      TØ TØTAL    ASSIGNED             LØW E   MØNITØR
 ANGLE  CRØSS SECT.  CRØSS SECT.   ERRØR      YIELD   CØRR.    CØUNTS

 15.0    .106E 02    .452E 01    .102E 01     2351     1924     29916
 30.0    .696E 01    .571E 01    .127E 01     1243      992     44452
 45.0    .327E 01    .379E 01    .774E 00      669      458     66624
 60.0    .152E 01    .215E 01    .516E 00      367      334    108429
 75.0    .107E 01    .170E 01    .494E 00      216      298    124779
 90.0    .509E 00    .834E 00    .823E-01      189       36    118344
105.0    .542E 00    .858E 00    .806E-01      220       40    123380
120.0    .563E 00    .675E 00    .474E-01      312       35    141192
130.0    .789E 00    .662E 00    .707E-01      126       23     37085
  FØR                .572E 00    .129E 00
 BACK                .145E 01    .155E 00
                     --------    --------
                     .229E 02    .464E 01

TØTAL CRØSS SECTIØN = 22.9 MB± 5.5 MB (TØTAL ERRØR=24 % )
```

```
   14 N  P SPALLATIØN  CRØSS SECTIØN FØR MASS  6 ;   E=41.9 MEV
   ----------------------------------------------------------------

 N=  81252  P=2.16CM HG  Q=.260E 01  H=24.4CM  R=24.7CM  B=.108CM

                      CØNTRIB.
 LAB      DIFF.      TØ TØTAL    ASSIGNED             LØW E   MØNITØR
 ANGLE  CRØSS SECT.  CRØSS SECT.   ERRØR      YIELD   CØRR.    CØUNTS

 15.0    .606E 01    .257E 01    .145E 00     5663      699     32758
 30.0    .523E 01    .429E 01    .393E 00     2550      561     34451
 45.0    .391E 01    .540E 01    .541E 00     1260      306     32341
 65.0    .232E 01    .521E 01    .416E 00      557       93     28185
 90.0    .155E 01    .380E 01    .441E 00      252       68     22688
110.0    .108E 01    .221E 01    .395E 00      212      113     30979
  FØR                .326E 00    .183E-01
 BACK                .169E 01    .303E 00
                     --------    --------
                     .255E 02    .265E 01

TØTAL CRØSS SECTIØN = 25.5 MB± 3.6 MB (TØTAL ERRØR=14 % )
```

Table 8. (continued)

```
   14 N  P SPALLATION  CROSS SECTION FOR MASS  7 ;    E=41.9 MEV
   ------------------------------------------------------------

N=  81252  P=2.16CM HG  Q=.260E 01  H=24.4CM  R=24.7CM  B=.108CM

                        CONTRIB.
 LAB        DIFF.      TO TOTAL    ASSIGNED             LOW E   MONITOR
ANGLE   CROSS SECT.  CROSS SECT.    ERROR       YIELD   CORR.    COUNTS

 15.0    .303E 01     .129E 01    .932E-01      2736     449     32758
 30.0    .260E 01     .213E 01    .209E 00      1251     295     34451
 45.0    .224E 01     .309E 01    .380E 00       681     214     32341
 65.0    .154E 01     .346E 01    .362E 00       349      83     28185
 90.0    .125E 01     .305E 01    .399E 00       196      61     22688
110.0    .831E 00     .170E 01    .273E 00       175      76     30979
  FOR                 .163E 00    .118E-01
 BACK                 .131E 01    .209E 00
                      --------    --------
                      .162E 02    .194E 01

TOTAL CROSS SECTION = 16.2 MB± 2.6 MB (TOTAL ERROR=16 % )
```

```
   14 N  P SPALLATION  CROSS SECTION FOR MASS 10 ;    E=41.9 MEV
   ------------------------------------------------------------

N=  81252  P=2.16CM HG  Q=.260E 01  H=24.4CM  R=24.7CM  B=.108CM

                        CONTRIB.
 LAB        DIFF.      TO TOTAL    ASSIGNED             LOW E   MONITOR
ANGLE   CROSS SECT.  CROSS SECT.    ERROR       YIELD   CORR.    COUNTS

 15.0    .885E 01     .376E 01    .431E 00      7167    2123     32758
 30.0    .717E 01     .588E 01    .421E 00      3661     598     34451
 45.0    .554E 01     .765E 01    .104E 01      1618     600     32341
 65.0    .321E 01     .720E 01    .839E 00       696     203     28185
 90.0    .140E 01     .343E 01    .560E 00       199      90     22688
110.0    .804E 00     .165E 01    .253E 00       173      70     30979
  FOR                 .476E 00    .545E-01
 BACK                 .126E 01    .194E 00
                      --------    --------
                      .313E 02    .380E 01

TOTAL CROSS SECTION = 31.3 MB± 4.5 MB (TOTAL ERROR=14 % )
```

Table 8. (continued)

```
   14 N  P SPALLATION  CROSS SECTION FOR MASS 11 ;    E=41.9 MEV
   ----------------------------------------------------------------

N=  81252  P=2.16CM HG  Q=.260E 01  H=24.4CM  R=24.7CM  B=.108CM

                          CONTRIB.
  LAB         DIFF.       TO TOTAL    ASSIGNED               LOW E   MONITOR
 ANGLE    CROSS SECT.  CROSS SECT.     ERROR        YIELD    CORR.    COUNTS

  15.0     .973E 01     .413E 01     .452E 00      7984     2229     32758
  30.0     .649E 01     .532E 01     .743E 00      2787     1072     34451
  45.0     .417E 01     .575E 01     .100E 01      1090      578     32341
  65.0     .155E 01     .348E 01     .716E 00       259      176     28185
  90.0     .606E 00     .148E 01     .168E 00       105       20     22688
 110.0     .642E 00     .132E 01     .109E 00       175       19     30979
   FOR                  .523E 00     .572E-01
  BACK                  .202E 01     .167E 00
                        --------     --------
                        .240E 02     .342E 01

TOTAL CROSS SECTION = 24.0 MB± 4.5 MB (TOTAL ERROR=19 % )


   14 N  P SPALLATION  CROSS SECTION FOR MASS  9 ;    E=25.8 MEV
   ----------------------------------------------------------------

N= 760607  P=4.27CM HG  Q=.503E 01  H=26.9CM  R=27.5CM  B=.075CM

                          CONTRIB.
  LAB         DIFF.       TO TOTAL    ASSIGNED               LOW E   MONITOR
 ANGLE    CROSS SECT.  CROSS SECT.     ERROR        YIELD    CORR.    COUNTS

  15.0     .988E 00     .420E 00     .101E 00       119      107     30315
  30.0     .740E 00     .607E 00     .181E 00        75      108     60967
  45.0     .629E 00     .729E 00     .262E 00        31       77     59020
  60.0     .132E 00     .187E 00     .638E-01        14       28    133142
  75.0     .278E-01     .441E-01     .120E-01        11        0    182690
  90.0     .246E-01     .471E-01     .157E-01         9        0    174110
 110.0     .591E-02     .121E-01     .606E-02         2        0    150363
   FOR                  .531E-01     .128E-01
  BACK                  .928E-02     .464E-02
                        --------     --------
                        .211E 01     .659E 00

TOTAL CROSS SECTION =  2.1 MB±  .7 MB (TOTAL ERROR=32 % )
```

Table 8. (continued)

```
   14 N   P SPALLATION  CROSS SECTION FOR MASS  9 ;   E=28.6 MEV
   -----------------------------------------------------------------

 N=1026222  P=4.11CM HG  Q=.748E 01  H=26.2CM  R=27.6CM  B=.076CM

                           CONTRIB.
  LAB       DIFF.         TO TOTAL    ASSIGNED           LOW E  MONITOR
 ANGLE   CROSS SECT.  CROSS SECT.     ERROR      YIELD   CORR.   COUNTS

  20.0    .235E 01      .901E 00    .123E 00      399     143     32621
  25.0    .223E 01      .516E 00    .746E-01      358     139     39030
  30.0    .191E 01      .112E 01    .195E 00      366     189     62753
  45.0    .134E 01      .155E 01    .376E 00      237     219    103480
  60.0    .597E 00      .848E 00    .183E 00      123      89    132042
  75.0    .416E 00      .660E 00    .234E 00       50     119    168217
  90.0    .227E 00      .372E 00    .100E 00       56      62    223078
 105.0    .763E-01      .121E 00    .391E-01       16      26    228391
 120.0    .124E 00      .176E 00    .615E-01       18      39    171014
   FOR                  .225E 00    .307E-01
  BACK                  .152E 00    .532E-01
                        --------    --------
                        .665E 01    .147E 01

 TOTAL CROSS SECTION =  6.6 MB± 1.6 MB (TOTAL ERROR=24 % )
```

```
   14 N   P SPALLATION  CROSS SECTION FOR MASS  9 ;   E=31.9 MEV
   -----------------------------------------------------------------

 N=  15704  P=5.36CM HG  Q=.100E 00  H=25.7CM  R=26.3CM  B=.076CM

                           CONTRIB.
  LAB       DIFF.         TO TOTAL    ASSIGNED           LOW E  MONITOR
 ANGLE   CROSS SECT.  CROSS SECT.     ERROR      YIELD   CORR.   COUNTS

  15.0    .291E 01      .124E 01    .100E 00      822     147     28419
  30.0    .184E 01      .151E 01    .108E 00      351      44     35519
  45.0    .109E 01      .126E 01    .657E-01      622      51     73288
  60.0    .809E 00      .115E 01    .152E 00      145      44     71363
  75.0    .296E 00      .470E 00    .892E-01       48      25     83930
  90.0    .240E 00      .394E 00    .102E 00       37      36    107217
 105.0    .206E 00      .327E 00    .111E 00       22      44    108880
 120.0    .864E-01      .123E 00    .305E-01       17      12    102567
   FOR                  .157E 00    .127E-01
  BACK                  .106E 00    .264E-01
                        --------    --------
                        .673E 01    .799E 00

 TOTAL CROSS SECTION =  6.7 MB±  .9 MB (TOTAL ERROR=13 % )
```

Table 8. (continued)

```
 14 N  P SPALLATION  CROSS SECTION FOR MASS  9 ;   E=35.1 MEV
 --------------------------------------------------------------

N=  78775  P=4.50CM HG  Q=.588E 00  H=24.3CM  R=26.3CM  B=.076CM

                        CONTRIB.
 LAB        DIFF.      TO TOTAL    ASSIGNED             LOW E   MONITOR
ANGLE    CROSS SECT.  CROSS SECT.   ERROR       YIELD   CORR.    COUNTS

 15.0    .368E 01     .156E 01    .169E 00      2589     708     78775
 30.0    .317E 01     .260E 01    .415E 00       707     326     55436
 45.0    .203E 01     .235E 01    .368E 00       420     185     71679
 60.0    .117E 01     .166E 01    .360E 00       263     196    115309
 75.0    .975E 00     .155E 01    .462E 00       148     217    122957
 90.0    .493E 00     .809E 00    .242E 00        68      98    114468
105.0    .272E 00     .431E 00    .131E 00        37      54    109794
120.0    .117E-01     .166E-01    .833E-02         2       0     50231
  FOR                 .198E 00    .215E-01
 BACK                 .144E-01    .720E-02
                      --------    --------
                      .112E 02    .218E 01

TOTAL CROSS SECTION = 11.2 MB± 2.2 MB (TOTAL ERROR=20 % )
```

```
 14 N  P SPALLATION  CROSS SECTION FOR MASS  9 ;   E=37.9 MEV
 --------------------------------------------------------------

N= 126329  P=2.11CM HG  Q=.274E 01  H=24.2CM  R=24.8CM  B=.108CM

                        CONTRIB.
 LAB        DIFF.      TO TOTAL    ASSIGNED             LOW E   MONITOR
ANGLE    CROSS SECT.  CROSS SECT.   ERROR       YIELD   CORR.    COUNTS

 15.0    .403E 01     .171E 01    .225E 00      1178     413     18191
 30.0    .243E 01     .199E 01    .200E 00       480     111     20822
 45.0    .175E 01     .241E 01    .305E 00       247      76     22031
 65.0    .121E 01     .239E 01    .443E 00       122      66     23491
 85.0    .635E 00     .138E 01    .237E 00        57      24     21020
105.0    .344E 00     .725E 00    .166E 00        27      18     20774
  FOR                 .216E 00    .285E-01
 BACK                 .624E 00    .143E 00
                      --------    --------
                      .115E 02    .175E 01

TOTAL CROSS SECTION = 11.5 MB± 2.1 MB (TOTAL ERROR=18 % )
```

Table 8. (continued)

```
     VAC  P SPALLATIØN  CRØSS SECTIØN FØR MASS  9 ;    E=37.9 MEV
   ---------------------------------------------------------------

 N=  10000  P=2.11CM HG  Q=.300E 00  H=24.2CM  R=24.8CM  B=.108CM

                        CØNTRIB.
  LAB       DIFF.      TØ TØTAL   ASSIGNED              LØW E  MØNITØR
 ANGLE  CRØSS SECT. CRØSS SECT.    ERRØR       YIELD   CØRR.   CØUNTS

  15.0   .843E 00    .358E 00    .362E-01      512     120     25004
  30.0   .394E 00    .323E 00    .260E-01      150       9     25006
  45.0   .492E 00    .571E 00    .417E-01      164       7     30003
  60.0   .292E 00    .414E 00    .402E-01      103       0     37027
   FØR               .453E-01    .458E-02
  BACK               .127E 01    .123E 00
                     --------    --------
                     .298E 01    .272E 00

 TØTAL CRØSS SECTIØN =  3.0 MB±  .9 MB (TØTAL ERRØR=31 % )
```

```
    14 N  P SPALLATIØN  CRØSS SECTIØN FØR MASS  9 ;   E=40.0 MEV
   ---------------------------------------------------------------

 N=  80353  P=1.37CM HG  Q=.284E 01  H=26.1CM  R=27.2CM  B=.076CM

                        CØNTRIB.
  LAB       DIFF.      TØ TØTAL   ASSIGNED              LØW E  MØNITØR
 ANGLE  CRØSS SECT. CRØSS SECT.    ERRØR       YIELD   CØRR.   CØUNTS

  15.0   .268E 01    .114E 01    .188E 00      725     351     29916
  30.0   .210E 01    .172E 01    .267E 00      468     205     44452
  45.0   .172E 01    .199E 01    .342E 00      392     200     66624
  60.0   .962E 00    .137E 01    .275E 00      269     176    108429
  75.0   .458E 00    .726E 00    .143E 00      136      84    124779
  90.0   .362E 00    .593E 00    .145E 00       84      76    118344
 105.0   .340E 00    .538E 00    .161E 00       67      96    123380
 120.0   .177E 00    .212E 00    .419E-01       69      40    141192
 130.0   .349E 00    .293E 00    .787E-01       32      34     37085
   FØR               .144E 00    .238E-01
  BACK               .643E 00    .173E 00
                     --------    --------
                     .936E 01    .184E 01

 TØTAL CRØSS SECTIØN =  9.4 MB± 2.2 MB (TØTAL ERRØR=23 % )
```

Table 8. (continued)

```
   14 N   P SPALLATION  CROSS SECTION FOR MASS  9 ;   E=41.9 MEV
   -----------------------------------------------------------------

N=  81252  P=2.16CM HG  Q=.260E 01  H=24.4CM  R=24.7CM  B=.108CM

                            CONTRIB.
 LAB        DIFF.          TO TOTAL    ASSIGNED            LOW E   MONITOR
ANGLE    CROSS SECT.  CROSS SECT.       ERROR       YIELD   CORR.    COUNTS

 15.0     .321E 01       .136E 01     .140E 00       2687     686     32758
 30.0     .248E 01       .203E 01     .209E 00       1178     295     34451
 45.0     .156E 01       .216E 01     .307E 00        453     173     32341
 65.0     .127E 01       .285E 01     .591E 00        211     145     28185
 90.0     .528E 00       .130E 01     .278E 00         65      44     22688
110.0     .298E 00       .611E 00     .951E-01         67      23     30979
  FOR                    .173E 00     .178E-01
 BACK                    .468E 00     .728E-01
                         --------     --------
                         .110E 02     .171E 01

TOTAL CROSS SECTION =  11.0 MB± 2.0 MB (TOTAL ERROR=18 % )
```

```
    VAC   P SPALLATION  CROSS SECTION FOR MASS  9 ;   E=41.9 MEV
   -----------------------------------------------------------------

N= 242535  P=2.16CM HG  Q=.713E 01  H=24.4CM  R=24.7CM  B=.108CM

                            CONTRIB.
 LAB        DIFF.          TO TOTAL    ASSIGNED            LOW E   MONITOR
ANGLE    CROSS SECT.  CROSS SECT.       ERROR       YIELD   CORR.    COUNTS

 15.0     .411E 00       .175E 00     .127E-01        165       0     13384
 30.0     .452E 00       .371E 00     .375E-01        115      18     18256
 45.0     .750E 00       .869E 00     .148E 00        103      47     17289
 60.0     .535E 00       .760E 00     .943E-01        102      24     24702
 75.0     .733E 00       .116E 01     .226E 00         69      39     17147
 90.0     .593E 00       .973E 00     .144E 00         65      19     16961
  FOR                    .221E-01     .161E-02
 BACK                    .162E 01     .239E 00
                         --------     --------
                         .595E 01     .904E 00

TOTAL CROSS SECTION =   5.9 MB± 1.7 MB (TOTAL ERROR=29 % )
```

Table 8. (continued)

```
 16 O  P SPALLATION  CROSS SECTION FOR MASS  6 ;   E=30.0 MEV
 --------------------------------------------------------------

N=  27783  P=2.27CM HG  Q=.307E 00  H=24.1CM  R=24.5CM  B=.109CM

                        CONTRIB.
 LAB        DIFF.       TO TOTAL    ASSIGNED              LOW E   MONITOR
ANGLE    CROSS SECT.  CROSS SECT.    ERROR       YIELD   CORR.    COUNTS

 15.0     .306E 00     .130E 00    .172E-01       52       7      15872
 30.0     .257E 00     .211E 00    .270E-01       47       0      27783
 45.0     .161E 00     .187E 00    .356E-01       21       0      27613
 60.0     .199E 00     .283E 00    .590E-01       18       6      30965
 75.0     .499E 00     .791E 00    .128E 00       36       7      24525
  FOR                  .164E-01    .218E-02
 BACK                  .177E 01    .286E 00
                       --------    --------
                       .339E 01    .555E 00

TOTAL CROSS SECTION =  3.4 MB± 1.4 MB (TOTAL ERROR=43 % )
```

```
 16 O  P SPALLATION  CROSS SECTION FOR MASS 11 ;   E=30.0 MEV
 --------------------------------------------------------------

N=  27783  P=2.27CM HG  Q=.307E 00  H=24.1CM  R=24.5CM  B=.109CM

                        CONTRIB.
 LAB        DIFF.       TO TOTAL    ASSIGNED              LOW E   MONITOR
ANGLE    CROSS SECT.  CROSS SECT.    ERROR       YIELD   CORR.    COUNTS

 15.0     .133E 01     .565E 00    .760E-01      193      64      15872
 30.0     .105E 01     .863E 00    .812E-01      165      27      27783
 45.0     .261E 00     .303E 00    .605E-01       23      11      27613
 60.0     .332E-01     .472E-01    .236E-01        4       0      30965
 75.0     .813E-01     .129E 00    .368E-01        7       0      24525
  FOR                  .716E-01    .962E-02
 BACK                  .289E 00    .825E-01
                       --------    --------
                       .227E 01    .370E 00

TOTAL CROSS SECTION =  2.3 MB±  .5 MB (TOTAL ERROR=23 % )
```

Table 8. (continued)

```
 16 Ø  P SPALLATIØN  CRØSS SECTIØN FØR MASS  6 ;   E=33•7 MEV
 ------------------------------------------------------------

N=  79459  P=2•14CM HG  Q=•141E 01  H=26•6CM  R=27•2CM  B=•075CM

                        CØNTRIB•
 LAB       DIFF•       TØ TØTAL    ASSIGNED          LØW E   MØNITØR
ANGLE   CRØSS SECT•  CRØSS SECT•    ERRØR     YIELD  CØRR•    CØUNTS

 15•0    •401E 00     •170E 00    •203E-01     163     43     48848
 30•0    •253E 00     •208E 00    •210E-01     120     20     97606
 45•0    •620E 00     •719E 00    •796E-01      89     14     41575
 60•0    •473E 00     •672E 00    •918E-01      51      8     37884
 75•0    •176E 00     •279E 00    •928E-01       9      0     17240
  FØR                 •216E-01    •258E-02
 BACK                 •624E 00    •208E 00
                      --------    --------
                      •269E 01    •516E 00

TØTAL CRØSS SECTIØN =  2•7 MB±  •8 MB (TØTAL ERRØR=31 % )



 16 Ø  P SPALLATIØN  CRØSS SECTIØN FØR MASS  7 ;   E=33•7 MEV
 ------------------------------------------------------------

N=  79459  P=2•14CM HG  Q=•141E 01  H=26•6CM  R=27•2CM  B=•075CM

                        CØNTRIB•
 LAB       DIFF•       TØ TØTAL    ASSIGNED          LØW E   MØNITØR
ANGLE   CRØSS SECT•  CRØSS SECT•    ERRØR     YIELD  CØRR•    CØUNTS

 15•0    •378E 00     •160E 00    •203E-01     151     43     48848
 30•0    •210E 00     •172E 00    •205E-01      95     21     97606
 45•0    •403E 00     •467E 00    •691E-01      53     14     41575
 60•0    •305E 00     •433E 00    •766E-01      29      9     37884
 75•0    •976E-01     •155E 00    •619E-01       5      0     17240
  FØR                 •203E-01    •258E-02
 BACK                 •347E 00    •139E 00
                      --------    --------
                      •175E 01    •390E 00

TØTAL CRØSS SECTIØN =  1•8 MB±  •6 MB (TØTAL ERRØR=32 % )
```

Table 8. (continued)

```
 16 O  P SPALLATION  CROSS SECTION FOR MASS 10 ;   E=33.7 MEV
 ------------------------------------------------------------

N=  79459  P=2.14CM HG  Q=.141E 01  H=26.6CM  R=27.2CM  B=.075CM

                         CONTRIB.
 LAB        DIFF.       TO TOTAL    ASSIGNED            LOW E   MONITOR
ANGLE   CROSS SECT.  CROSS SECT.     ERROR      YIELD   CORR.    COUNTS

 15.0    .790E 00     .336E 00     .371E-01      323      83     48848
 30.0    .413E 00     .339E 00     .514E-01      163      65     97606
 45.0    .343E 00     .398E 00     .726E-01       40      17     41575
 60.0    .281E 00     .399E 00     .117E 00       16      19     37884
 75.0    .976E-01     .155E 00     .619E-01        5       0     17240
  FOR                 .425E-01     .469E-02
 BACK                 .347E 00     .139E 00
                      --------     --------
                      .201E 01     .484E 00

TOTAL CROSS SECTION =  2.0 MB±  .7 MB (TOTAL ERROR=33 % )
```

```
 16 O  P SPALLATION  CROSS SECTION FOR MASS 11 ;   E=33.7 MEV
 ------------------------------------------------------------

N=  79459  P=2.14CM HG  Q=.141E 01  H=26.6CM  R=27.2CM  B=.075CM

                         CONTRIB.
 LAB        DIFF.       TO TOTAL    ASSIGNED            LOW E   MONITOR
ANGLE   CROSS SECT.  CROSS SECT.     ERROR      YIELD   CORR.    COUNTS

 15.0    .804E 01     .341E 01     .711E 00     2413    1718     48848
 30.0    .477E 01     .391E 01     .805E 00     1555    1081     97606
 45.0    .356E 01     .412E 01     .104E 01      295     296     41575
 60.0    .108E 01     .154E 01     .250E 00       95      40     37884
 75.0    .703E 00     .111E 01     .319E 00       17      19     17240
  FOR                 .432E 00     .900E-01
 BACK                 .250E 01     .715E 00
                      --------     --------
                      .170E 02     .393E 01

TOTAL CROSS SECTION = 17.0 MB± 5.3 MB (TOTAL ERROR=31 % )
```

Table 8. (continued)

```
  16 O  P SPALLATION  CROSS SECTION FOR MASS  6 ;   E=37.9 MEV
  ---------------------------------------------------------------

N= 257351  P=2.06CM HG  Q=.508E 01  H=24.2CM  R=24.8CM  B=.108CM

                          CONTRIB.
 LAB       DIFF.        TO TOTAL    ASSIGNED            LOW E   MONITOR
ANGLE  CROSS SECT.  CROSS SECT.     ERROR      YIELD   CORR.   COUNTS

 15.0   .101E 01     .428E 00     .997E-01     282     242     26977
 30.0   .525E 00     .431E 00     .116E 00      97     110     37997
 45.0   .479E 00     .556E 00     .143E 00      81      82     45689
 60.0   .468E 00     .665E 00     .175E 00      78      84     56450
 75.0   .471E 00     .746E 00     .175E 00      90      76     63796
 90.0   .355E 00     .583E 00     .183E 00      39      63     53419
  FOR                .542E-01     .126E-01
 BACK                .971E 00     .305E 00
                     --------     --------
                     .443E 01     .121E 01

TOTAL CROSS SECTION =  4.4 MB± 1.7 MB (TOTAL ERROR=39 % )
```

```
  16 O  P SPALLATION  CROSS SECTION FOR MASS  7 ;   E=37.9 MEV
  ---------------------------------------------------------------

N= 257351  P=2.06CM HG  Q=.508E 01  H=24.2CM  R=24.8CM  B=.108CM

                          CONTRIB.
 LAB       DIFF.        TO TOTAL    ASSIGNED            LOW E   MONITOR
ANGLE  CROSS SECT.  CROSS SECT.     ERROR      YIELD   CORR.   COUNTS

 15.0   .766E 00     .325E 00     .578E-01     260     138     26977
 30.0   .624E 00     .512E 00     .122E 00     131     115     37997
 45.0   .682E 00     .791E 00     .253E 00      85     147     45689
 60.0   .408E 00     .579E 00     .129E 00      80      61     56450
 75.0   .459E 00     .728E 00     .194E 00      77      85     63796
 90.0   .265E 00     .434E 00     .123E 00      34      42     53419
  FOR                .412E-01     .732E-02
 BACK                .724E 00     .206E 00
                     --------     --------
                     .413E 01     .109E 01

TOTAL CROSS SECTION =  4.1 MB± 1.5 MB (TOTAL ERROR=35 % )
```

Table 8. (continued)

```
  16 O  P SPALLATION  CROSS SECTION FOR MASS 10 ;   E=37.9 MEV
  ----------------------------------------------------------------

N= 257351  P=2.06CM HG  Q=.508E 01  H=24.2CM  R=24.8CM  B=.108CM

                         CONTRIB.
 LAB       DIFF.        TO TOTAL   ASSIGNED             LOW E   MONITOR
ANGLE  CROSS SECT.  CROSS SECT.     ERROR       YIELD   CORR.    COUNTS

 15.0    .221E 01     .937E 00    .148E 00      788     359     26977
 30.0    .159E 01     .130E 01    .190E 00      448     178     37997
 45.0    .429E 00     .498E 00    .165E 00       50      96     45689
 60.0    .442E 00     .628E 00    .221E 00       46     107     56450
 75.0    .343E 00     .543E 00    .175E 00       44      77     63796
 90.0    .282E 00     .463E 00    .143E 00       32      49     53419
  FOR                 .119E 00    .188E-01
 BACK                 .771E 00    .238E 00
                      --------    --------
                      .526E 01    .130E 01

TOTAL CROSS SECTION =  5.3 MB± 1.7 MB (TOTAL ERROR=32 % )
```

```
  16 O  P SPALLATION  CROSS SECTION FOR MASS 11 ;   E=37.9 MEV
  ----------------------------------------------------------------

N= 257351  P=2.06CM HG  Q=.508E 01  H=24.2CM  R=24.8CM  B=.108CM

                         CONTRIB.
 LAB       DIFF.        TO TOTAL   ASSIGNED             LOW E   MONITOR
ANGLE  CROSS SECT.  CROSS SECT.     ERROR       YIELD   CORR.    COUNTS

 15.0    .156E 02     .664E 01    .909E 00     5913    2220     26977
 30.0    .107E 02     .881E 01    .141E 01     2875    1356     37997
 45.0    .655E 01     .759E 01    .144E 01     1385     841     45689
 60.0    .336E 01     .478E 01    .100E 01      678     486     56450
 75.0    .442E 00     .701E 00    .225E 00       57      99     63796
 90.0    .331E 00     .543E 00    .144E 00       46      49     53419
  FOR                 .841E 00    .115E 00
 BACK                 .904E 00    .240E 00
                      --------    --------
                      .308E 02    .549E 01

TOTAL CROSS SECTION = 30.8 MB± 6.1 MB (TOTAL ERROR=20 % )
```

Table 8. (continued)

```
   16 O   P SPALLATION   CROSS SECTION FOR MASS   6 ;    E=41.9 MEV
   ----------------------------------------------------------------

 N= 242535   P=2.16CM HG   Q=.713E 01   H=24.4CM   R=24.7CM   B=.108CM

                            CONTRIB.
 LAB        DIFF.          TO TOTAL     ASSIGNED              LOW E    MONITOR
 ANGLE   CROSS SECT.    CROSS SECT.      ERROR       YIELD    CORR.     COUNTS

 15.0     .222E 01       .942E 00      .134E 00      1599      630      33546
 30.0     .182E 01       .149E 01      .201E 00       730      262      33823
 45.0     .165E 01       .191E 01      .275E 00       469      183      34187
 60.0     .214E 01       .304E 01      .493E 00       721      340      52009
 75.0     .151E 01       .239E 01      .424E 00       433      233      51379
 90.0     .112E 01       .183E 01      .373E 00       211      140      37591
  FOR                    .119E 00      .170E-01
 BACK                    .305E 01      .621E 00
                         --------      --------
                         .148E 02      .254E 01

 TOTAL CROSS SECTION = 14.8 MB± 4.1 MB (TOTAL ERROR=28 % )
```

```
   16 O   P SPALLATION   CROSS SECTION FOR MASS   7 ;    E=41.9 MEV
   ----------------------------------------------------------------

 N= 242535   P=2.16CM HG   Q=.713E 01   H=24.4CM   R=24.7CM   B=.108CM

                            CONTRIB.
 LAB        DIFF.          TO TOTAL     ASSIGNED              LOW E    MONITOR
 ANGLE   CROSS SECT.    CROSS SECT.      ERROR       YIELD    CORR.     COUNTS

 15.0     .258E 01       .110E 01      .154E 00      1870      726      33546
 30.0     .181E 01       .148E 01      .197E 00       729      257      33823
 45.0     .168E 01       .195E 01      .263E 00       490      174      34187
 60.0     .156E 01       .222E 01      .416E 00       488      287      52009
 75.0     .136E 01       .216E 01      .429E 00       366      236      51379
 90.0     .117E 01       .191E 01      .381E 00       223      143      37591
  FOR                    .139E 00      .195E-01
 BACK                    .318E 01      .634E 00
                         --------      --------
                         .141E 02      .249E 01

 TOTAL CROSS SECTION = 14.1 MB± 4.1 MB (TOTAL ERROR=29 % )
```

Table 8. (continued)

```
  16 O  P SPALLATION  CROSS SECTION FOR MASS 10 ;   E=41.9 MEV
  ------------------------------------------------------------

N= 242535  P=2.16CM HG  Q=.713E 01  H=24.4CM  R=24.7CM  B=.108CM

                         CONTRIB.
 LAB      DIFF.        TO TOTAL    ASSIGNED            LOW E   MONITOR
ANGLE  CROSS SECT.  CROSS SECT.     ERROR      YIELD   CORR.    COUNTS

 15.0   .429E 01     .182E 01    .427E 00     2293    2020     33546
 30.0   .229E 01     .188E 01    .325E 00      818     429     33823
 45.0   .151E 01     .175E 01    .270E 00      416     180     34187
 60.0   .137E 01     .195E 01    .391E 00      411     270     52009
 75.0   .185E 01     .294E 01    .706E 00      427     392     51379
 90.0   .685E 00     .112E 01    .242E 00      125      90     37591
  FOR                .231E 00    .541E-01
 BACK                .187E 01    .403E 00
                     --------    --------
                     .136E 02    .282E 01

TOTAL CROSS SECTION = 13.6 MB± 3.8 MB (TOTAL ERROR=28 % )
```

```
  16 O  P SPALLATION  CROSS SECTION FOR MASS 11 ;   E=41.9 MEV
  ------------------------------------------------------------

N= 242535  P=2.16CM HG  Q=.713E 01  H=24.4CM  R=24.7CM  B=.108CM

                         CONTRIB.
 LAB      DIFF.        TO TOTAL    ASSIGNED            LOW E   MONITOR
ANGLE  CROSS SECT.  CROSS SECT.     ERROR      YIELD   CORR.    COUNTS

 15.0   .210E 02     .890E 01    .155E 01    13722    7351     33546
 30.0   .124E 02     .102E 02    .162E 01     4639    2153     33823
 45.0   .787E 01     .913E 01    .157E 01     2043    1071     34187
 60.0   .474E 01     .674E 01    .148E 01     1322    1030     52009
 75.0   .289E 01     .457E 01    .125E 01      581     694     51379
 90.0   .138E 01     .226E 01    .672E 00      177     256     37591
  FOR                .113E 01    .197E 00
 BACK                .377E 01    .112E 01
                     --------    --------
                     .467E 02    .947E 01

TOTAL CROSS SECTION = 46.7 MB±11.6 MB (TOTAL ERROR=25 % )
```

Table 8. (continued)

```
    VAC  P SPALLATION  CROSS SECTION FOR MASS 10 ;   E=41.9 MEV
   -------------------------------------------------------------

N= 242535  P=2.16CM HG  Q=.713E 01  H=24.4CM  R=24.7CM  B=.108CM

                         CONTRIB.
 LAB        DIFF.       TO TOTAL    ASSIGNED            LOW E   MONITOR
ANGLE    CROSS SECT.  CROSS SECT.    ERROR       YIELD  CORR.    COUNTS

 15.0     .364E 00     .155E 00    .178E-01      119     27      13384
 30.0     .350E 00     .287E 00    .385E-01       82     21      18256
 45.0     .550E 00     .638E 00    .648E-01      100     10      17289
 60.0     .616E 00     .875E 00    .180E 00       88     57      24702
 75.0     .814E 00     .129E 01    .262E 00       74     46      17147
 90.0     .536E 00     .880E 00    .220E 00       40     36      16961
  FOR                  .196E-01    .225E-02
 BACK                  .147E 01    .366E 00
                       --------    --------
                       .561E 01    .115E 01

TOTAL CROSS SECTION =   5.6 MB± 1.9 MB (TOTAL ERROR=34 % )
```

```
    VAC  P SPALLATION  CROSS SECTION FOR MASS 11 ;   E=41.9 MEV
   -------------------------------------------------------------

N= 242535  P=2.16CM HG  Q=.713E 01  H=24.4CM  R=24.7CM  B=.108CM

                         CONTRIB.
 LAB        DIFF.       TO TOTAL    ASSIGNED            LOW E   MONITOR
ANGLE    CROSS SECT.  CROSS SECT.    ERROR       YIELD  CORR.    COUNTS

 15.0     .232E 00     .985E-01    .953E-02       93      0      13384
 30.0     .431E 00     .354E 00    .435E-01      103     24      18256
 45.0     .545E 00     .632E 00    .106E 00       76     33      17289
 60.0     .607E 00     .863E 00    .143E 00      100     43      24702
 75.0     .427E 00     .677E 00    .924E-01       53     10      17147
 90.0     .438E 00     .718E 00    .135E 00       42     20      16961
  FOR                  .125E-01    .121E-02
 BACK                  .120E 01    .225E 00
                       --------    --------
                       .455E 01    .756E 00

TOTAL CROSS SECTION =   4.5 MB± 1.4 MB (TOTAL ERROR=30 % )
```

Table 8. (continued)

```
  VAC  P SPALLATION  CROSS SECTION FOR MASS  6 ;   E=41.9 MEV
 ---------------------------------------------------------------

N= 242535  P=2.16CM HG  Q=.713E 01  H=24.4CM  R=24.7CM  B=.108CM

                        CONTRIB.
 LAB       DIFF.       TO TOTAL    ASSIGNED            LOW E   MONITOR
ANGLE   CROSS SECT.  CROSS SECT.    ERROR      YIELD   CORR.    COUNTS

 15.0    .120E 01     .508E 00    .740E-01      345     135     13384
 30.0    .103E 01     .847E 00    .168E 00      186     118     18256
 45.0    .119E 01     .139E 01    .197E 00      176      63     17289
 60.0    .133E 01     .190E 01    .452E 00      166     148     24702
 75.0    .977E 00     .155E 01    .336E 00       84      60     17147
 90.0    .109E 01     .180E 01    .352E 00       97      58     16961
  FOR                 .643E-01    .936E-02
 BACK                 .299E 01    .585E 00
                      --------    --------
                      .110E 02    .218E 01

TOTAL CROSS SECTION =  11.0 MB± 3.7 MB (TOTAL ERROR=33 % )
```

```
  VAC  P SPALLATION  CROSS SECTION FOR MASS  7 ;   E=41.9 MEV
 ---------------------------------------------------------------

N= 242535  P=2.16CM HG  Q=.713E 01  H=24.4CM  R=24.7CM  B=.108CM

                        CONTRIB.
 LAB       DIFF.       TO TOTAL    ASSIGNED            LOW E   MONITOR
ANGLE   CROSS SECT.  CROSS SECT.    ERROR      YIELD   CORR.    COUNTS

 15.0    .122E 01     .520E 00    .102E 00      301     190     13384
 30.0    .104E 01     .852E 00    .198E 00      166     140     18256
 45.0    .985E 00     .114E 01    .172E 00      142      55     17289
 60.0    .841E 00     .119E 01    .224E 00      127      71     24702
 75.0    .807E 00     .128E 01    .247E 00       76      43     17147
 90.0    .104E 01     .170E 01    .363E 00       87      60     16961
  FOR                 .658E-01    .129E-01
 BACK                 .283E 01    .604E 00
                      --------    --------
                      .959E 01    .192E 01

TOTAL CROSS SECTION =  9.6 MB± 3.4 MB (TOTAL ERROR=35 % )
```

Table 9. Summary of Measured Cross-Sections for Proton Spallation of ^{14}N and ^{16}O.

TOTAL CROSS SECTIONS FROM PROTON SPALLATION OF 14 N

E_p (MEV)	MASS 6	MASS 7	MASS 9	MASS10	MASS11
17.0	.0± .0	36.6±14.1	.0+ .0	26.4±11.2	67.9±16.4
21.7	3.1± .7	41.2± 7.2	.0+ .0	61.1±13.6	39.5±10.1
25.8	16.3± 3.7	25.7± 4.2	2.1± .7	60.5±12.2	22.8± 5.6
28.6	22.0± 2.2	17.5± 1.8	6.6± 1.6	57.2± 8.2	19.5± 4.6
31.9	23.1± 1.9	14.4± 1.8	6.7± .9	45.9± 5.2	22.3± 5.6
35.1	29.4± 3.9	14.1± 2.4	11.2± 2.2	49.3± 8.5	22.9± 6.3
37.9	28.8± 5.8	16.9± 4.3	9.5± 2.1	41.4± 7.4	23.8± 6.0
40.0	21.9± 3.8	11.8± 2.2	9.4± 2.2	31.5± 5.9	22.9± 5.5
41.9	17.7± 2.5	9.3± 1.5	6.8± 1.5	27.4± 3.5	20.8± 3.5

TOTAL CROSS SECTIONS FROM PROTON SPALLATION OF 16 O

E_p (MEV)	MASS 6	MASS 7	MASS10	MASS11
30.0	1.5± .5	.0+ .0	.0+ .0	2.3± .5
33.7	2.7± .8	1.8± .6	2.0± .7	17.0± 5.3
37.9	4.4± 1.7	4.1± 1.5	5.3± 1.7	30.8± 6.1
41.9	3.8± 1.5	4.5± 1.5	8.0± 2.5	42.2±10.2

TOTAL CROSS SECTIONS FROM PROTON SPALLATION OF 12 C

E_P (MEV)	MASS 6	MASS 7	MASS 8	MASS 9	MASS10	MASS11
21•7	•0+ •0	•0+ •0	•0+ •0	•0+ •0	•0+ •0	45•± 7•
24•6	•0+ •0	•0+ •0	•0+ •0	•0+ •0	3•7± •6	64•± 17•
28•0	3•9± •8	3•2± •6	•0+ •0	•0+ •0	7•0± 1•1	96•± 22•
29•5	4•0± •8	8•7± 2•1	•0+ •0	•0+ •0	10•0± 1•8	113•± 20•
32•0	6•3± 1•0	15•2± 3•0	•6± •2	•7± •2	9•7± 1•7	121•± 28•
34•0	8•6± 1•4	23•2± 3•7	•9± •2	1•3± •3	10•2± 1•8	116•± 25•
36•0	7•2± 1•1	24•1± 4•2	1•8± •4	1•7± •4	11•1± 2•1	95•± 21•
39•8	9•9± 1•5	33•1± 5•4	1•9± •5	2•4± •5	16•3± 3•3	91•± 18•
44•0	11•2± 2•2	34•4± 6•6	2•4± •6	2•5± •6	18•4± 4•1	87•± 20•

Table 10. Summary of Cross-Sections for Proton Spallation of ^{12}C (DLA 70).

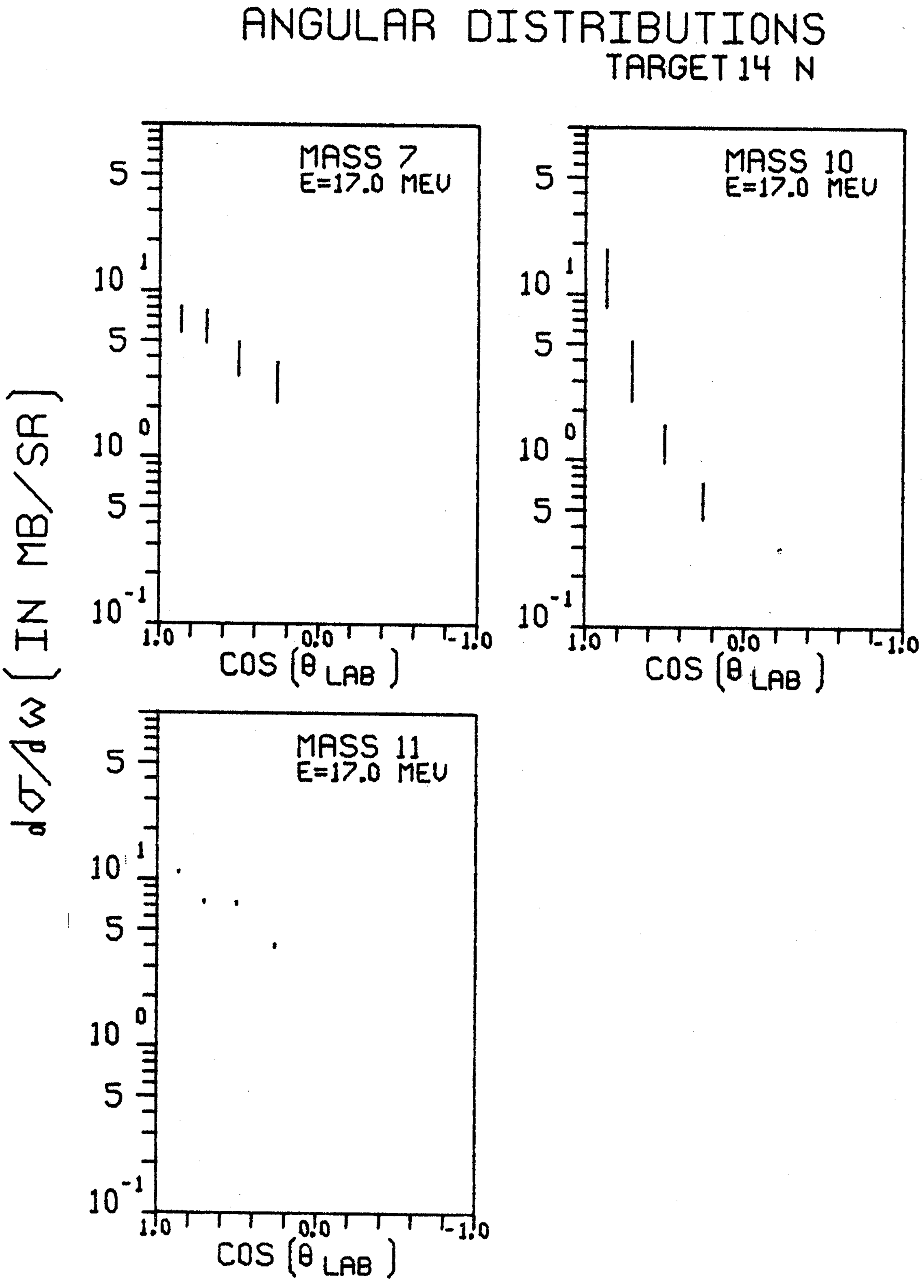

Figure 12. Angular Distribution for Masses 6 to 11 from Proton Spallation of ^{14}N and ^{16}O.

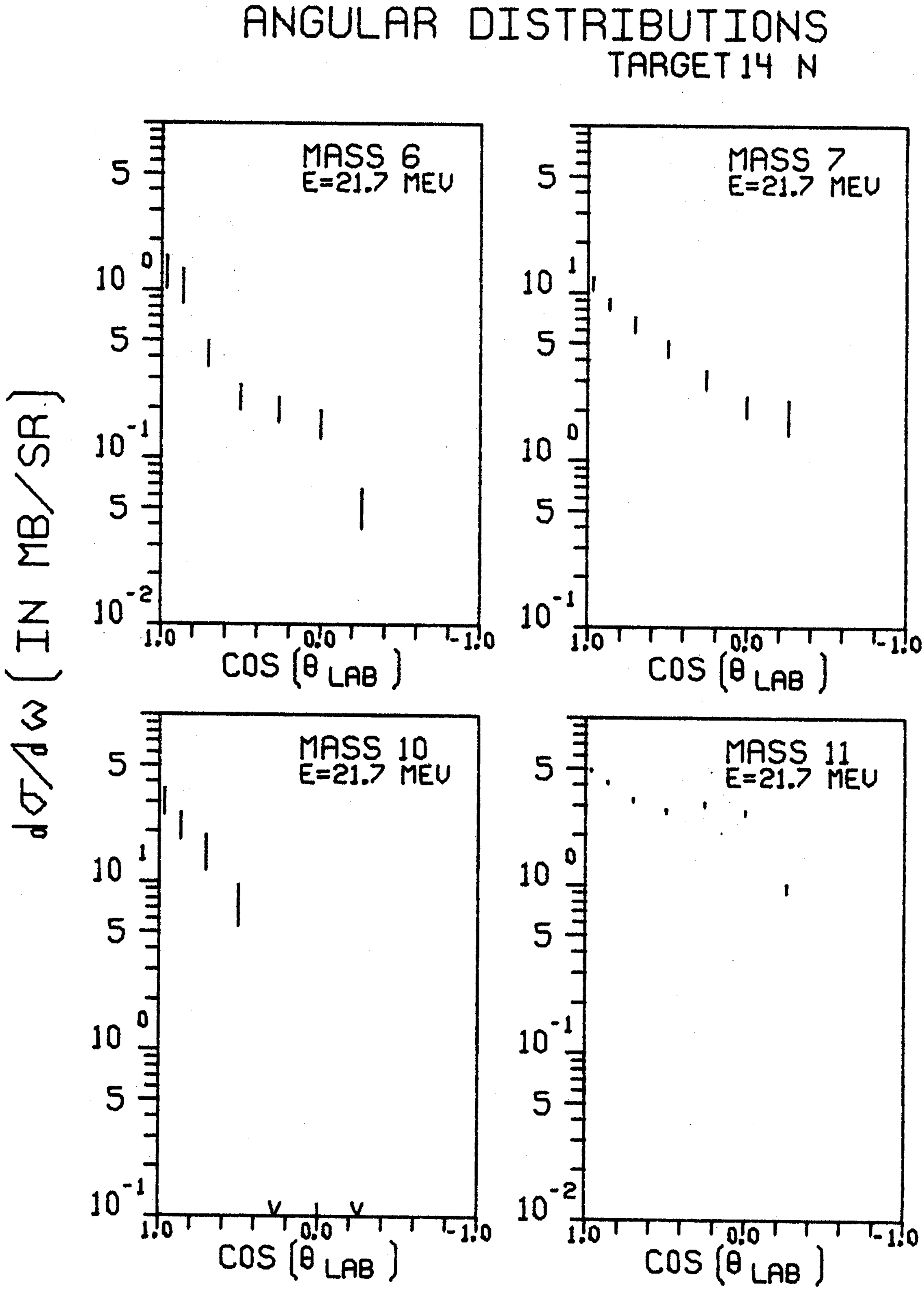

Figure 12. (continued)

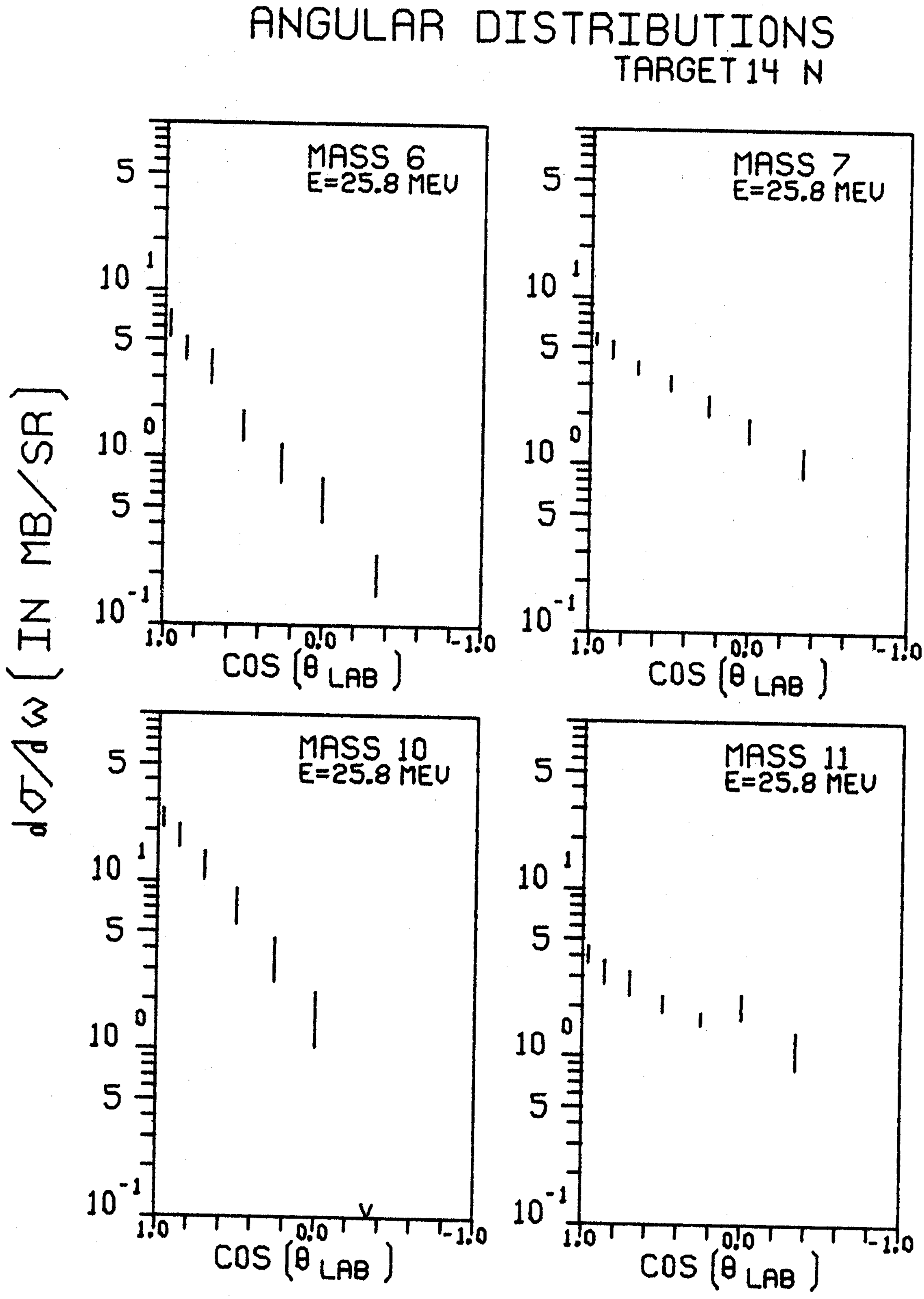

Figure 12. (continued)

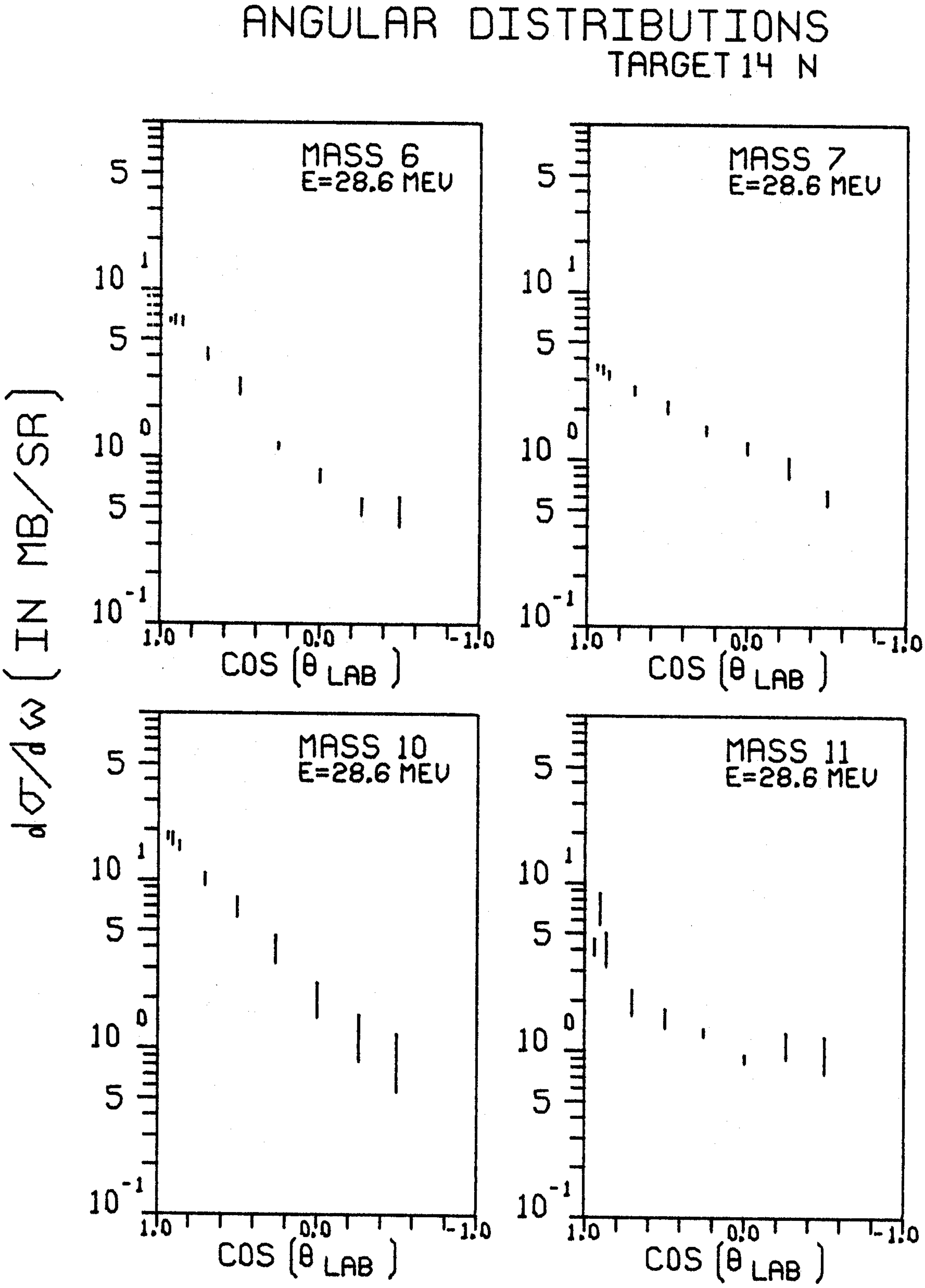

Figure 12. (continued)

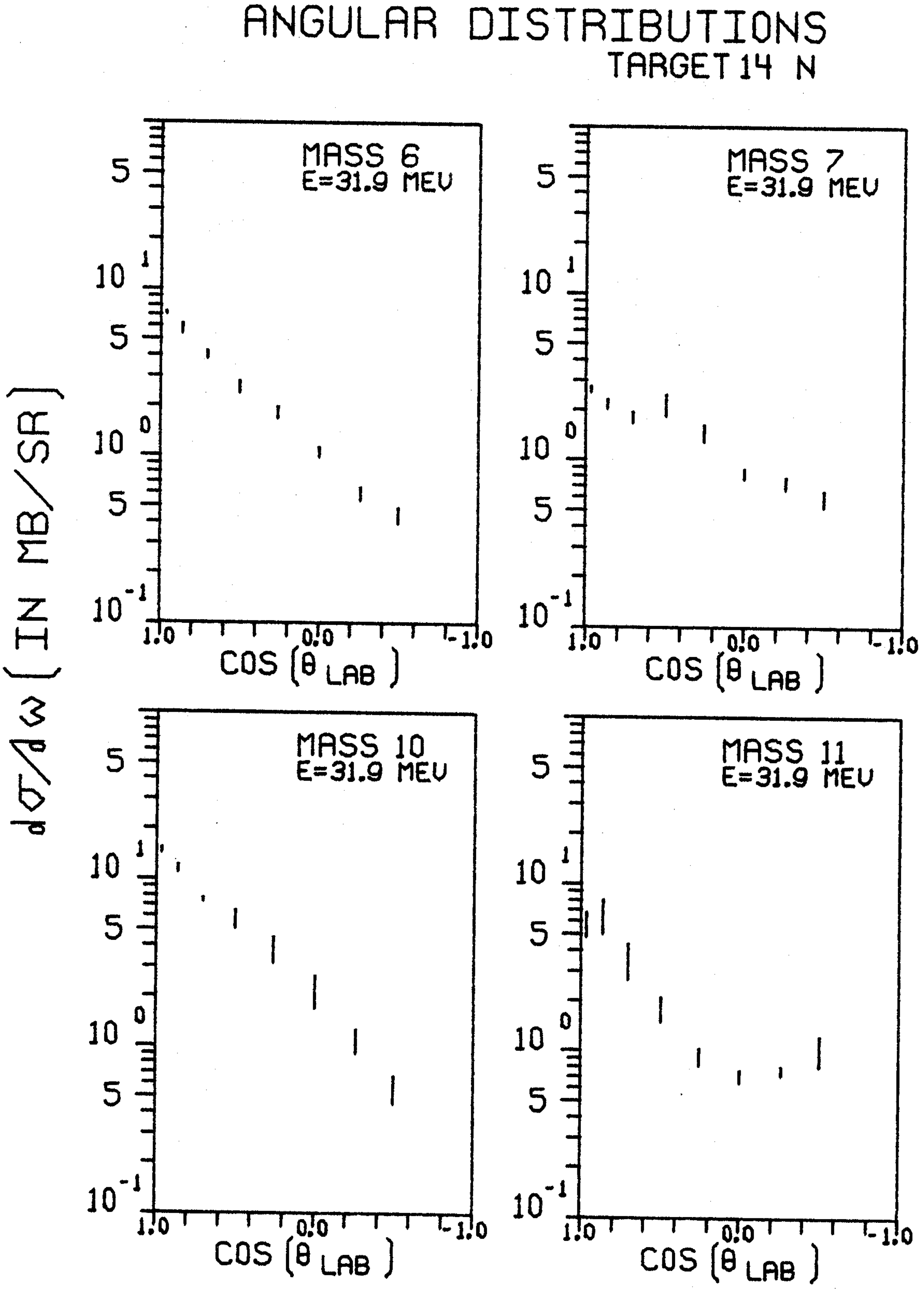

Figure 12. (continued)

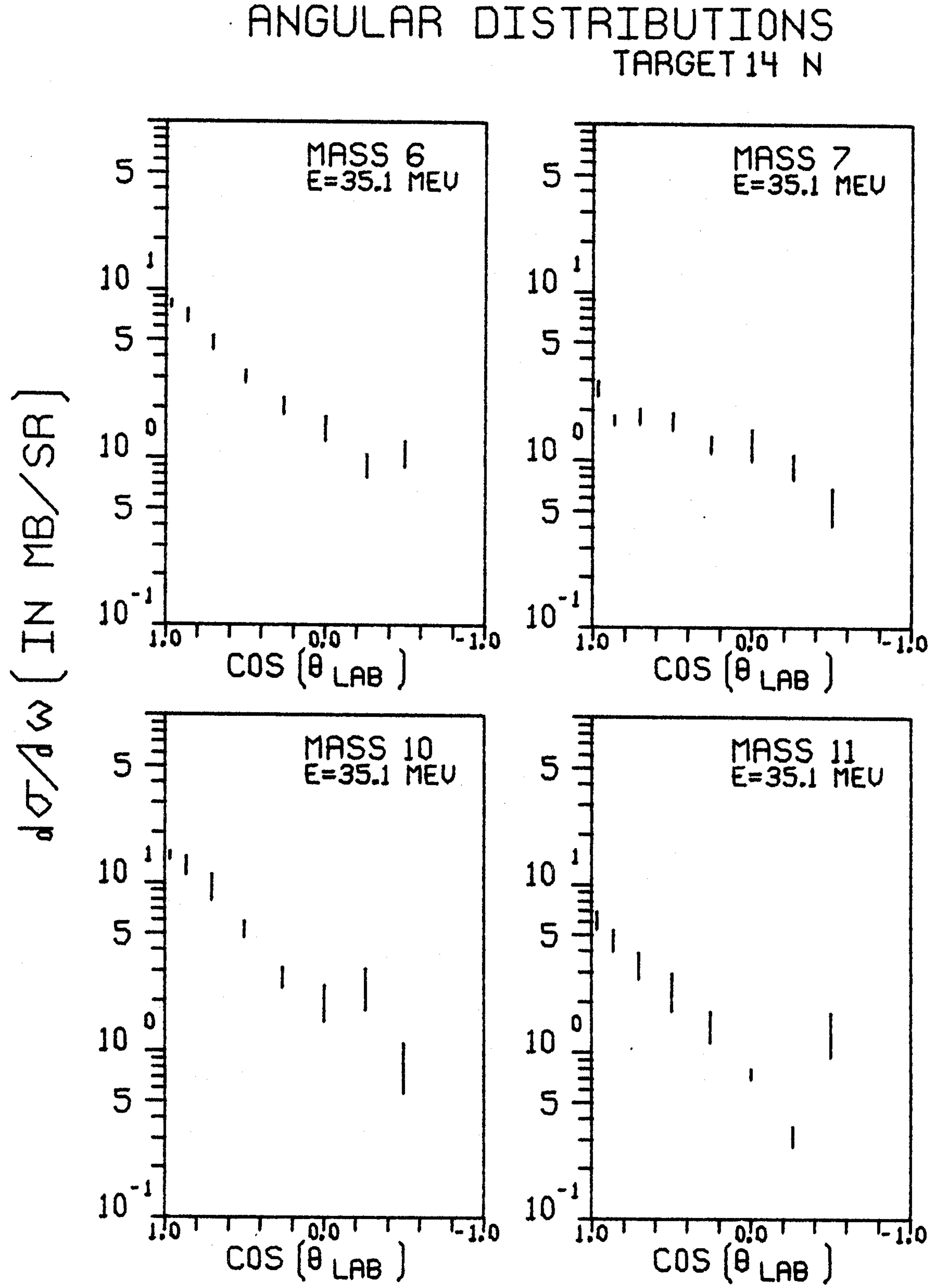

Figure 12. (continued)

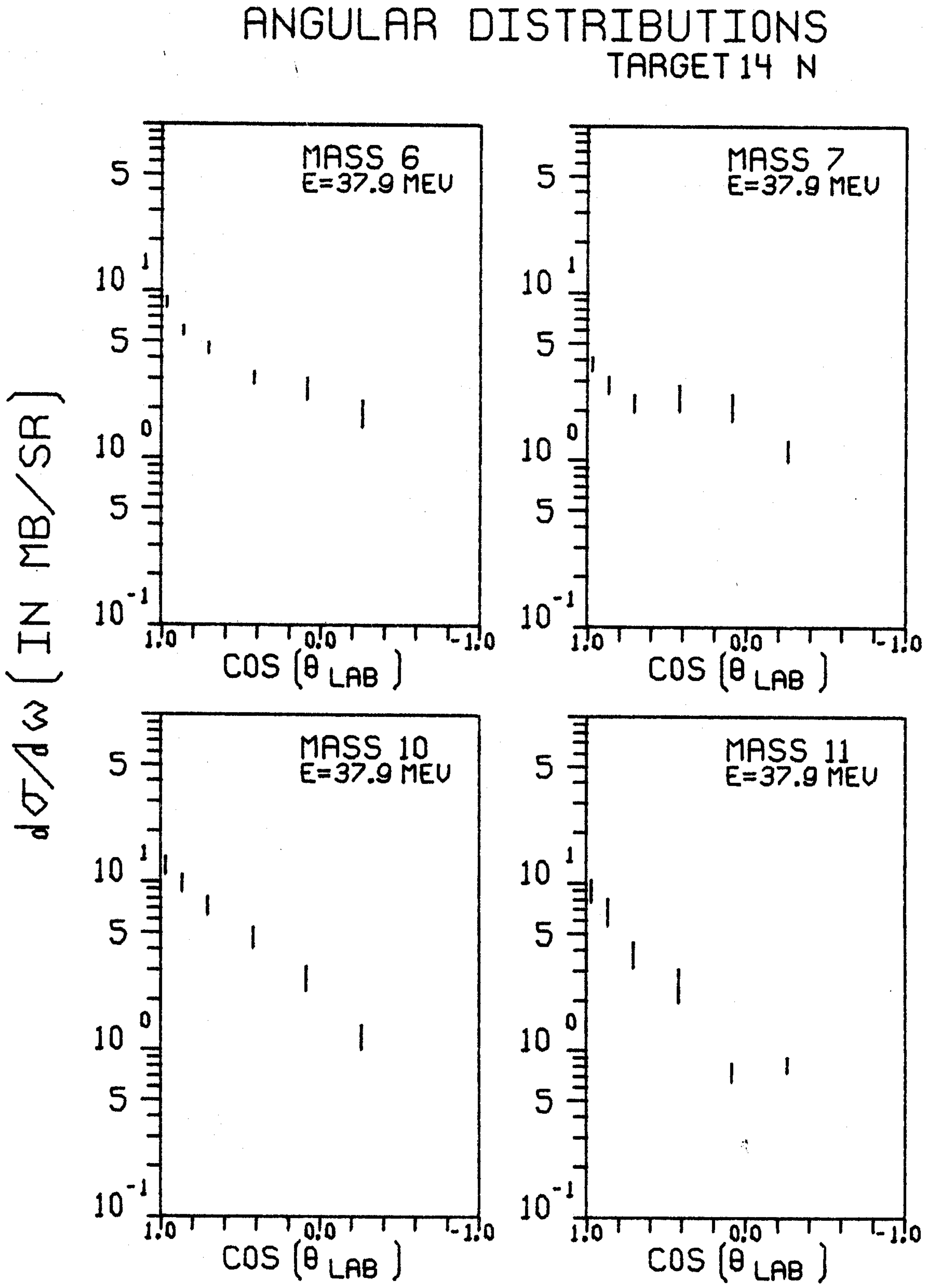

Figure 12. (continued)

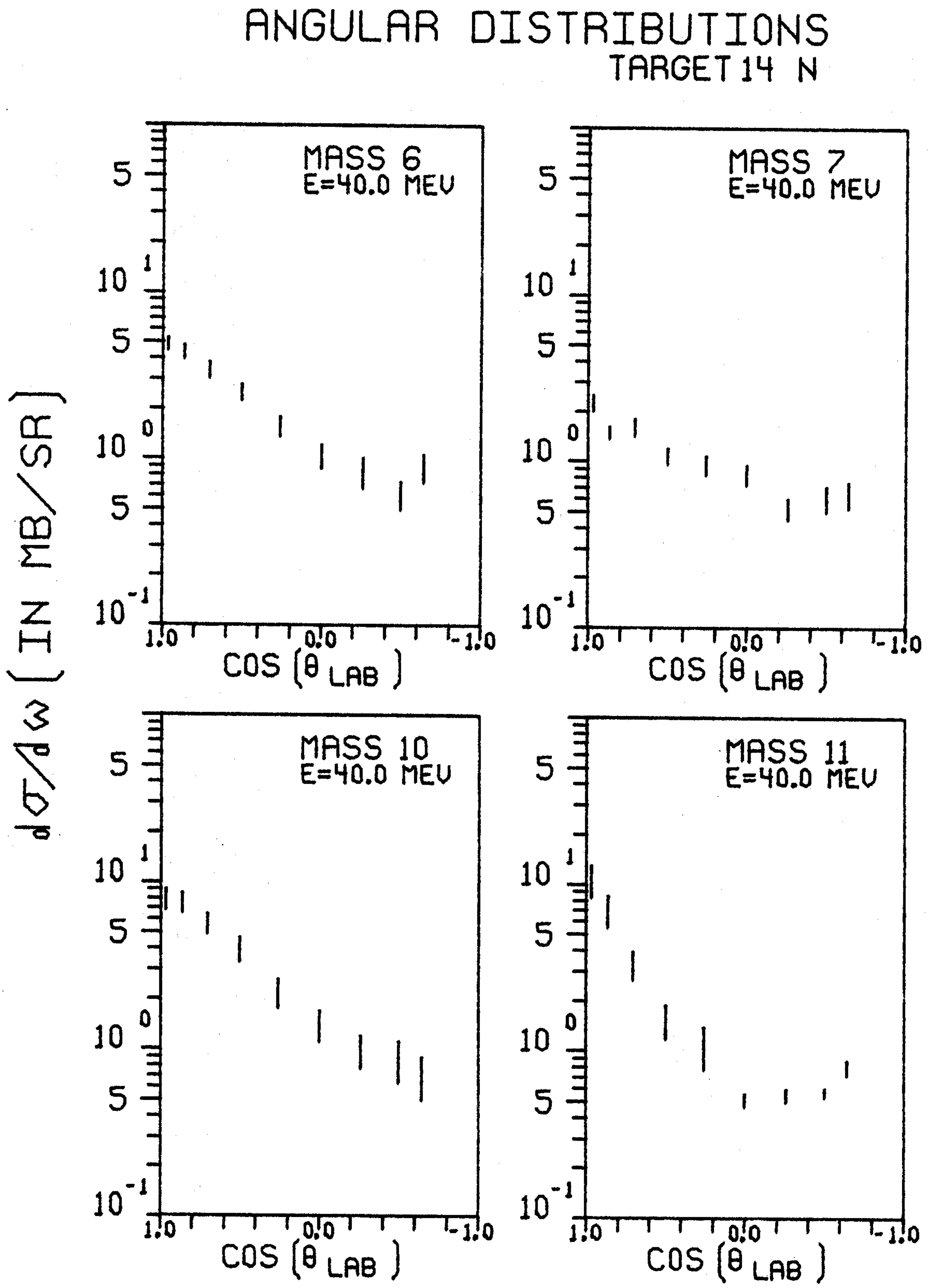

Figure 12. (continued)

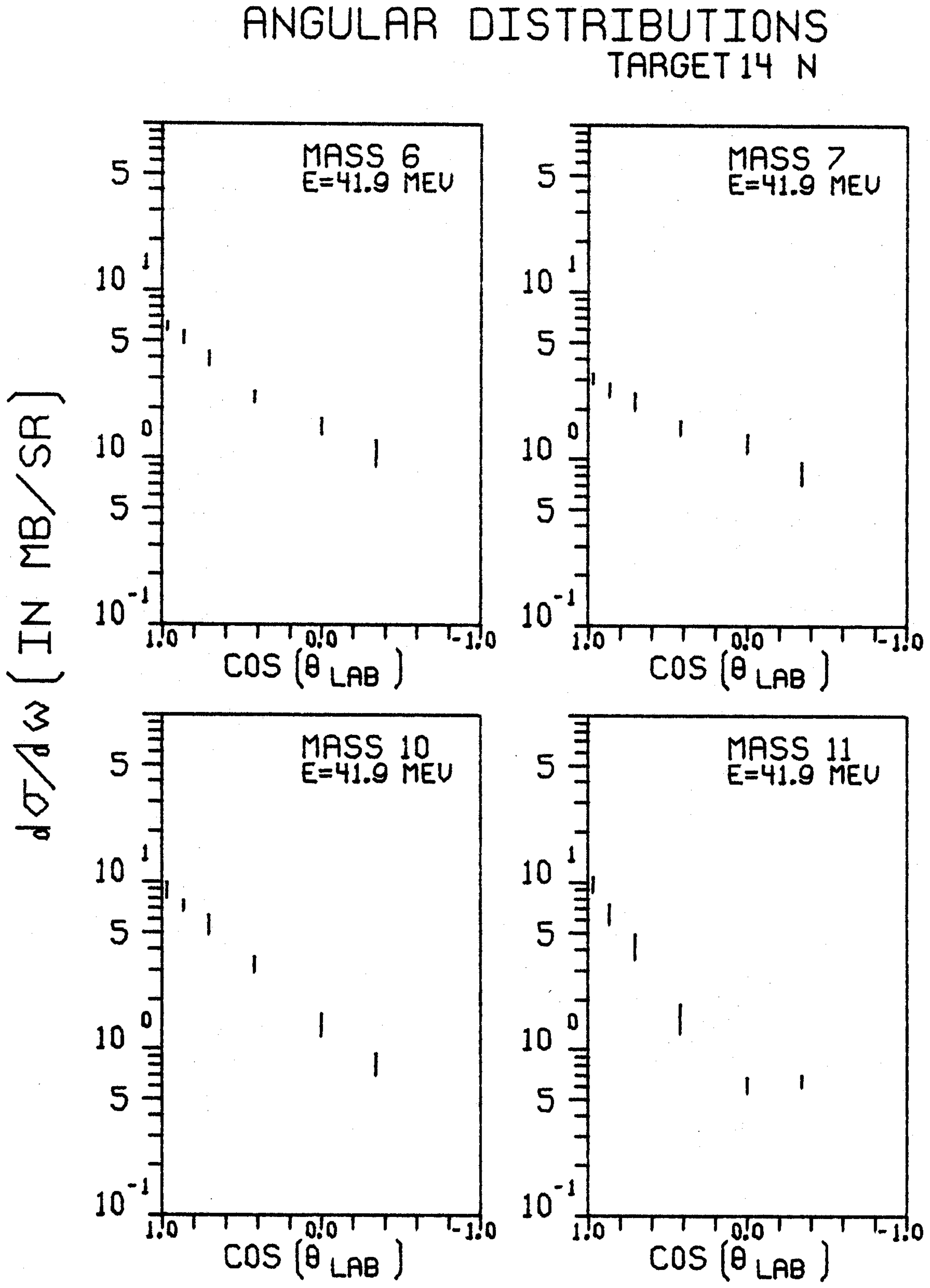

Figure 12. (continued)

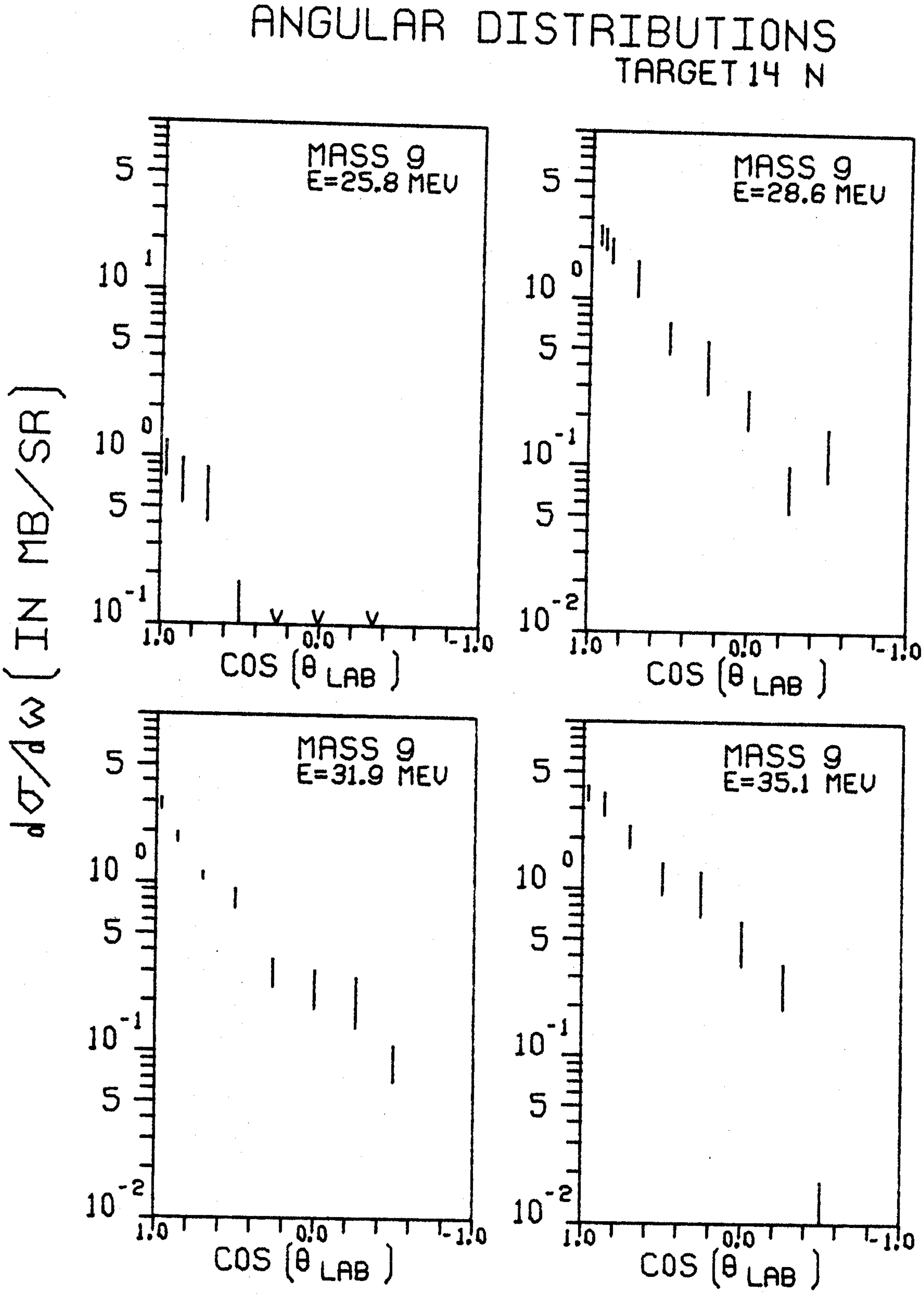

Figure 12. (continued)

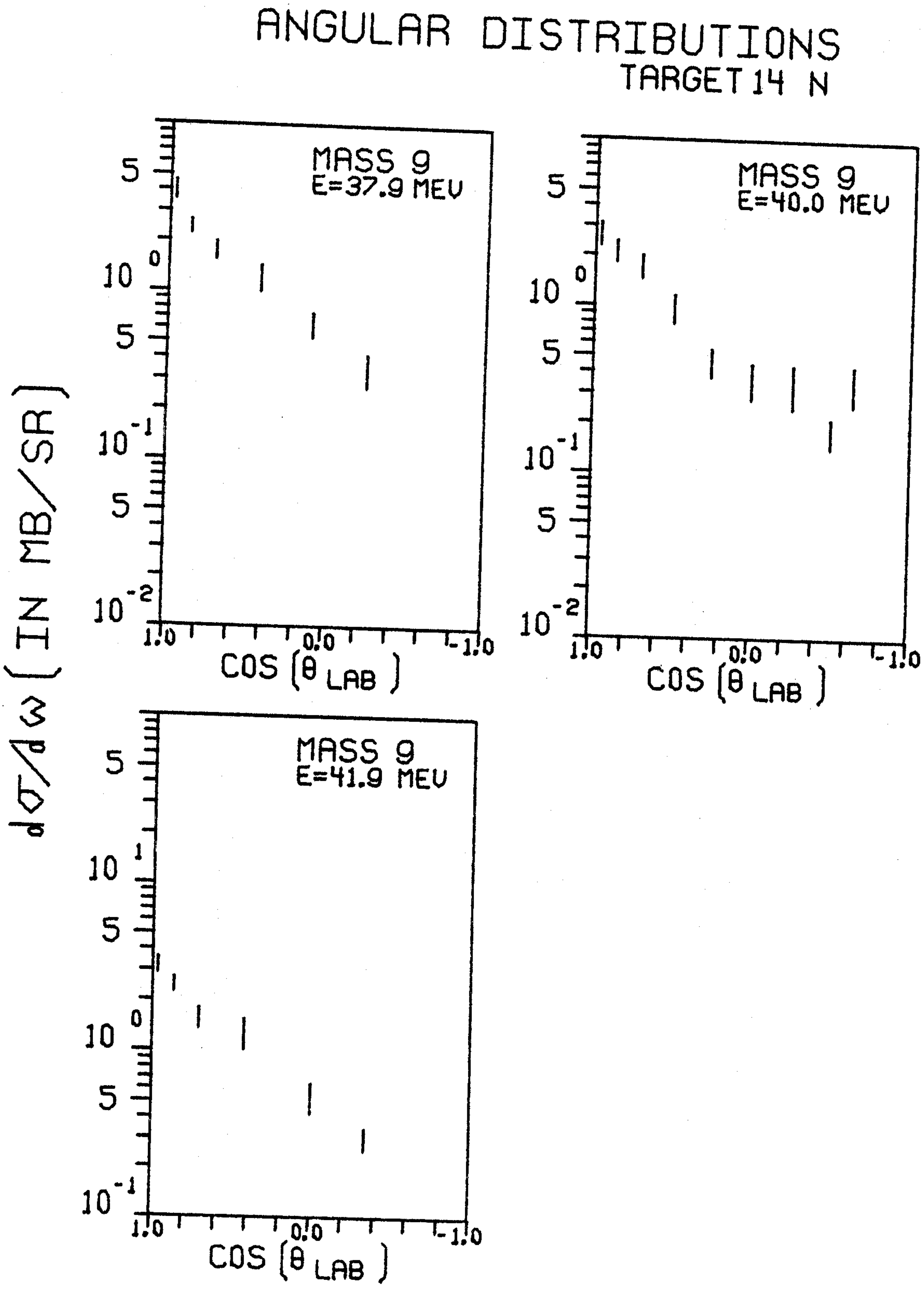

Figure 12. (continued)

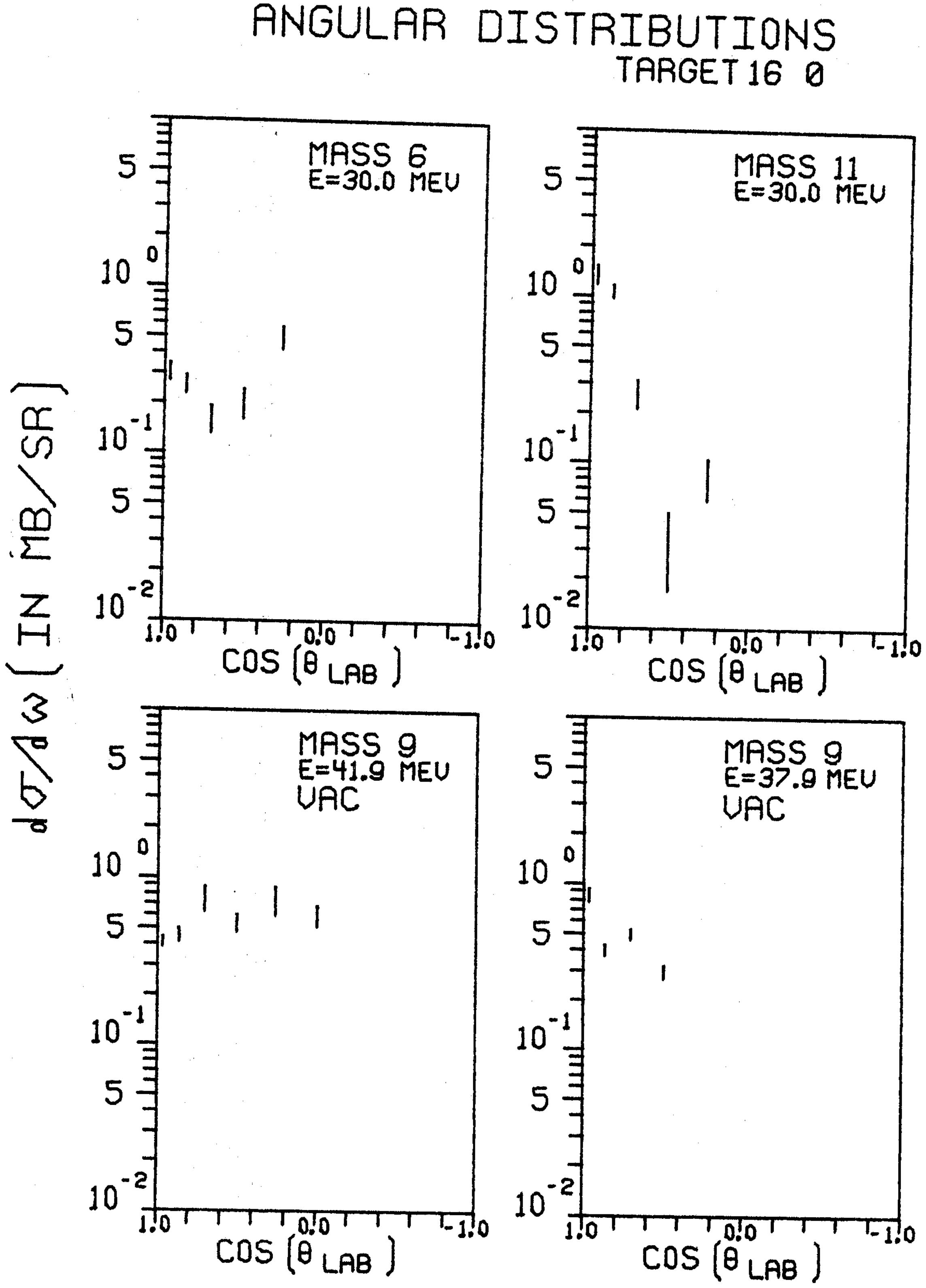

Figure 12. (continued)

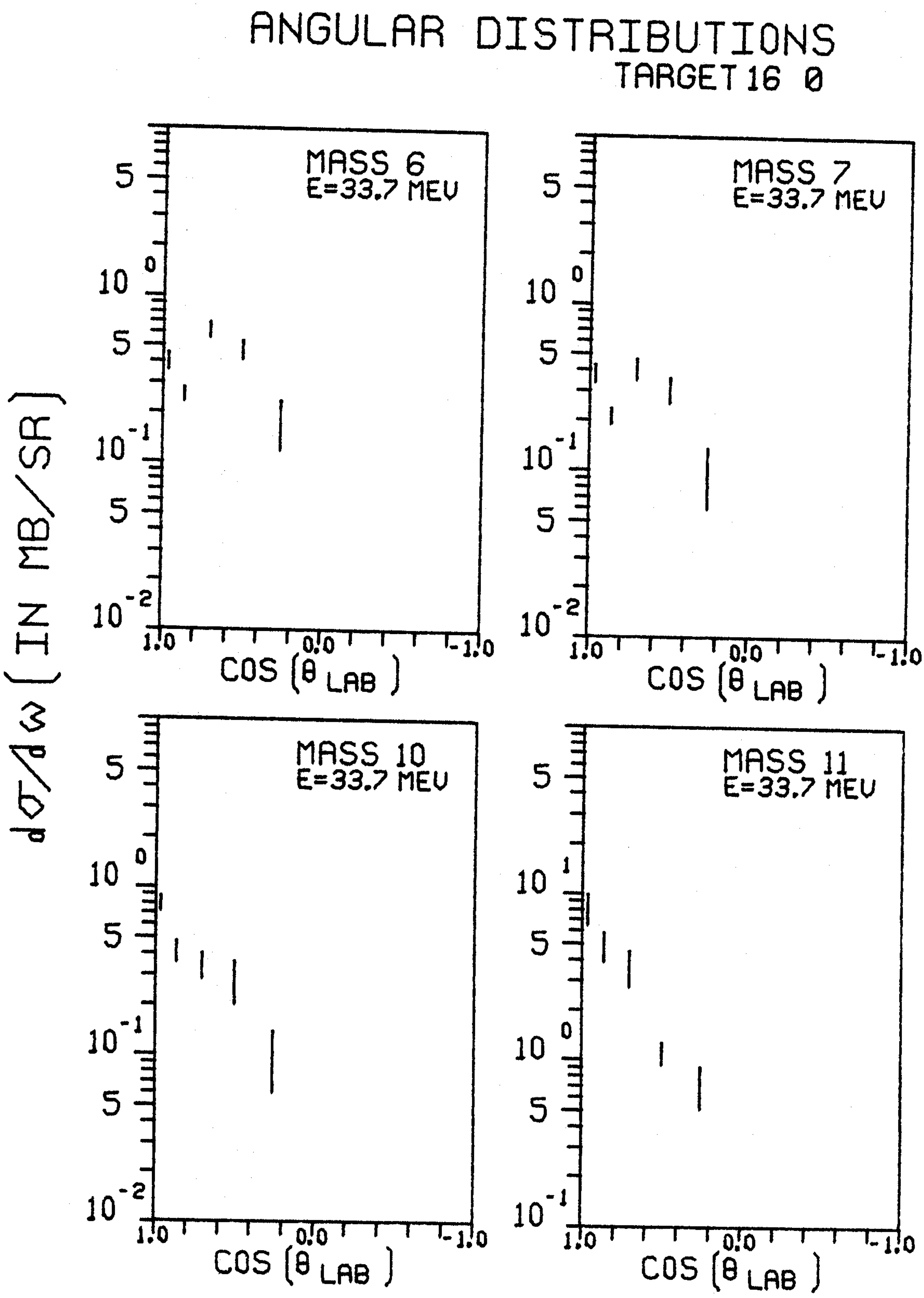

Figure 12. (continued)

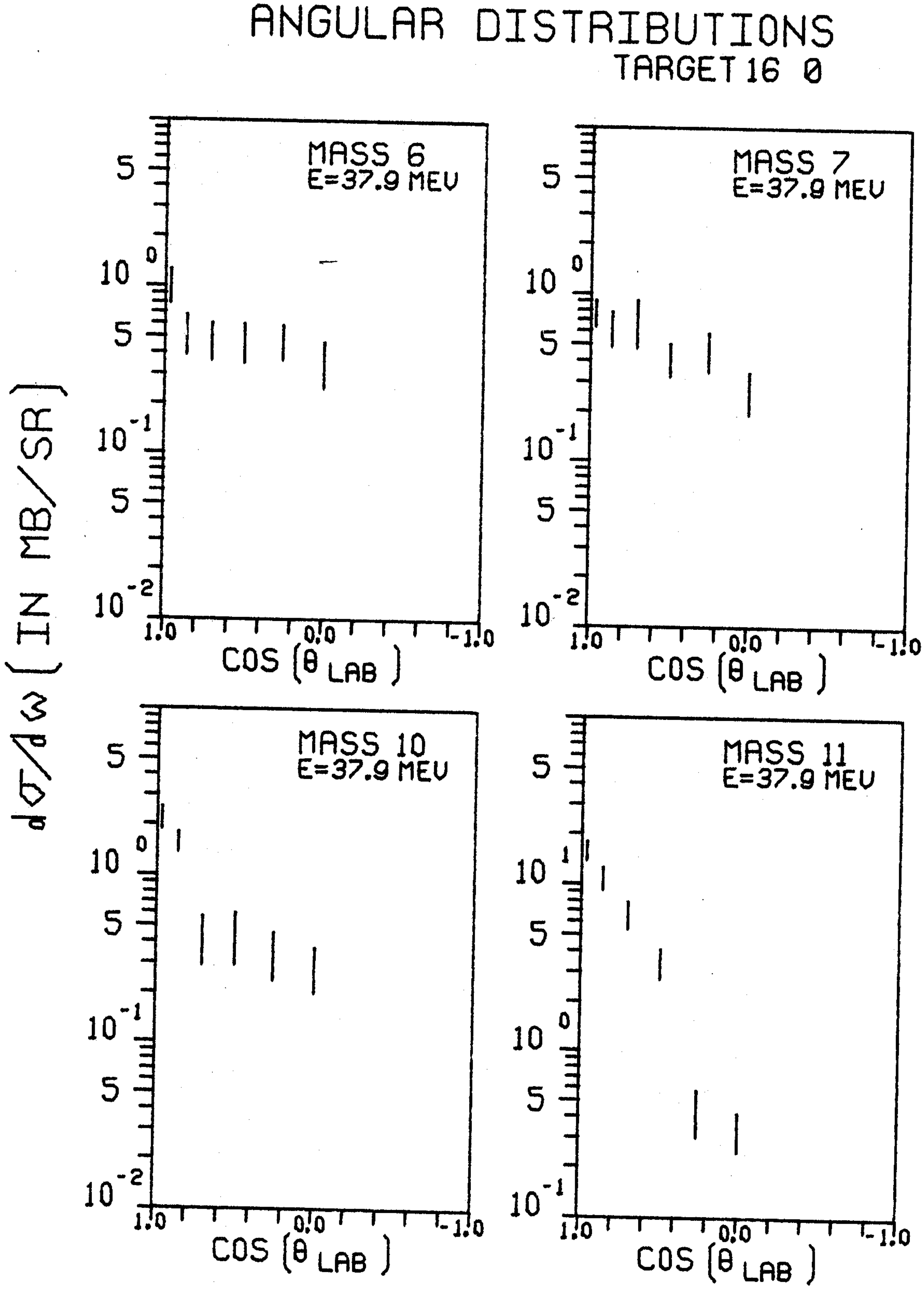

Figure 12. (continued)

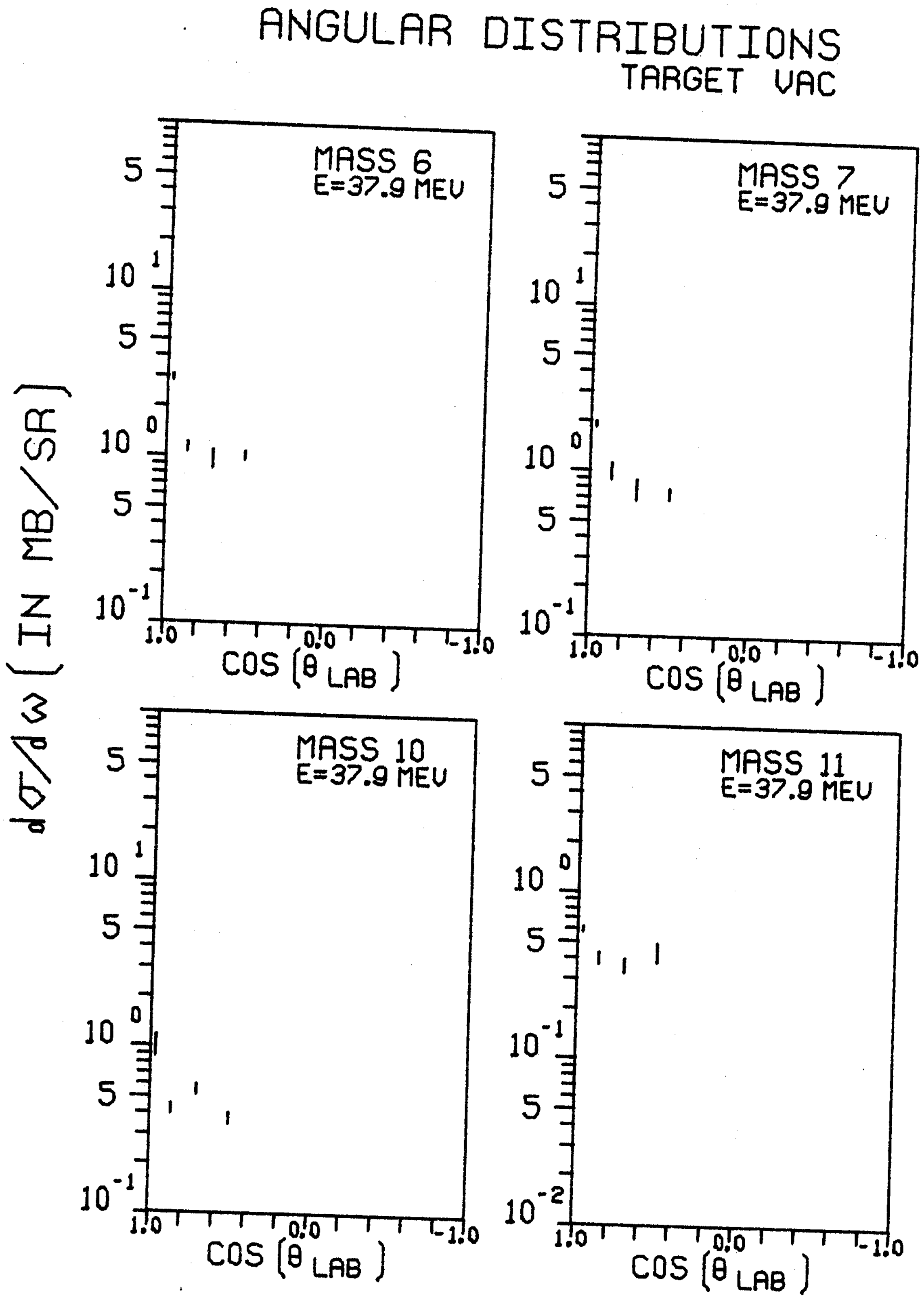

Figure 12. (continued)

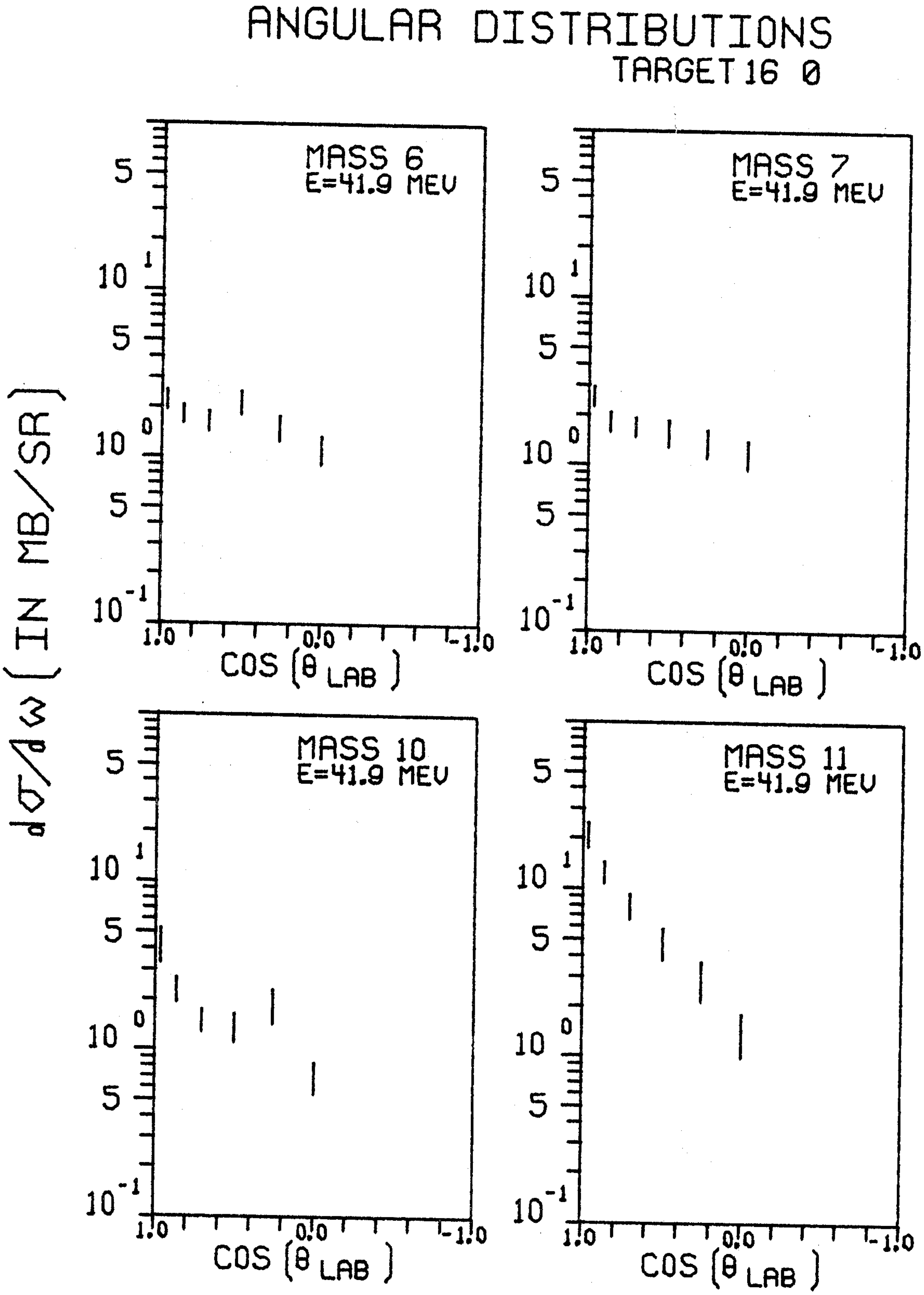

Figure 12. (continued)

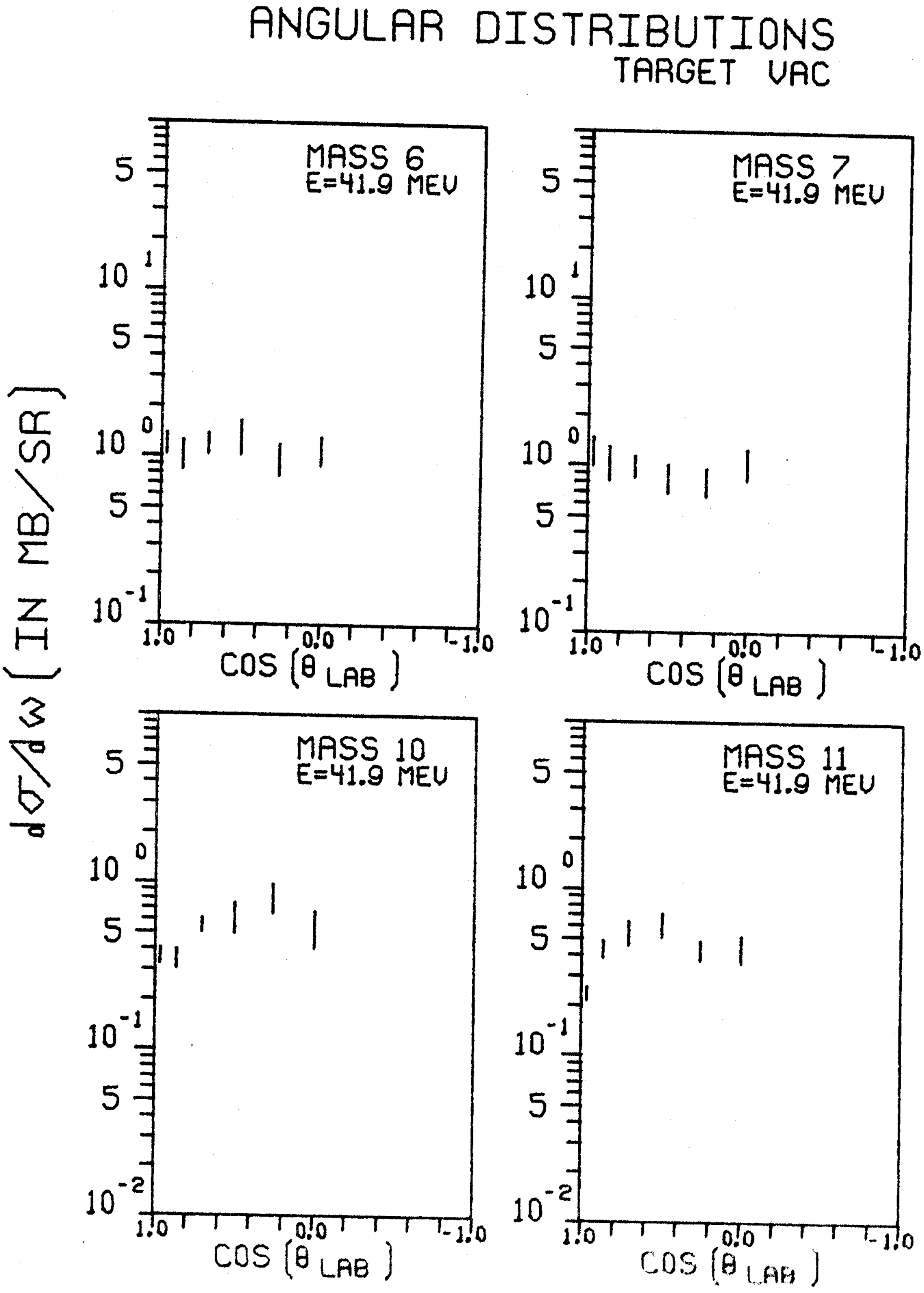

Figure 12. (continued)

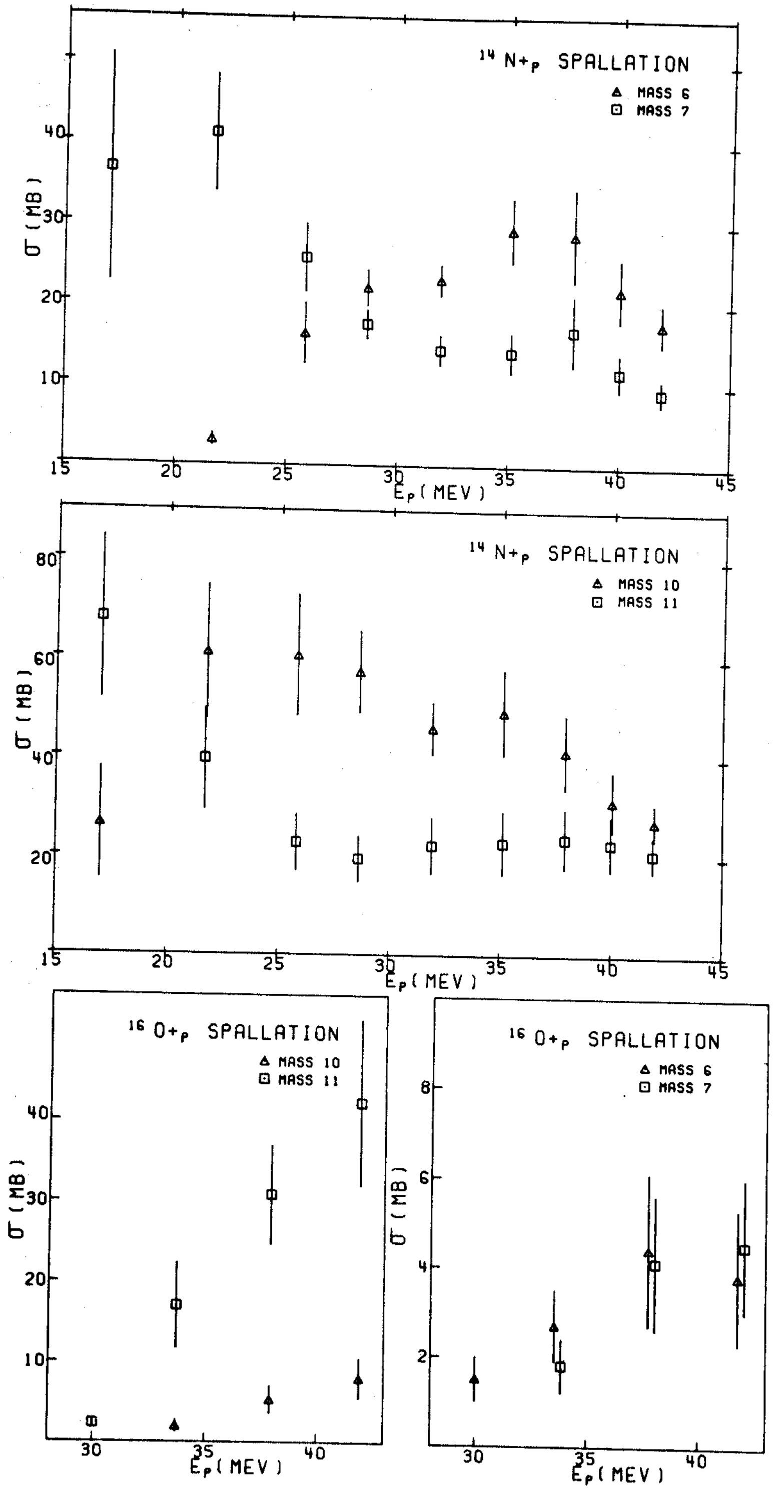

Figure 13. Cross-Sections for Masses 6,7,10,11 from Proton Spallation of Targets ^{14}N and ^{16}O in the Energy Range E_p = 17 to 42 MeV.

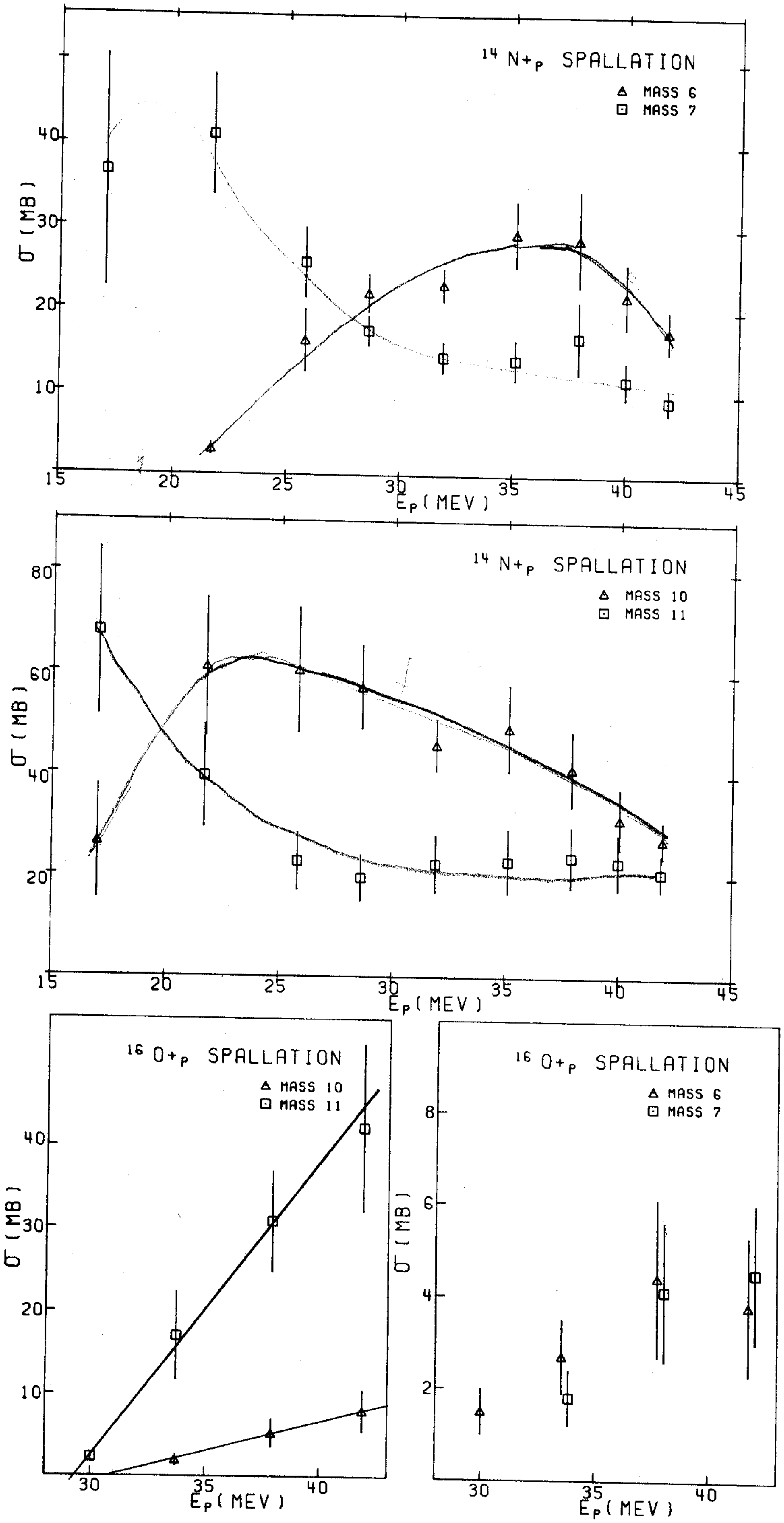

$^{16}_{8}O_{8} + ^{1}_{1}p_{0} \rightarrow ^{11}_{5}B_{6} + ^{6}_{4}Be_{2}$

23 Na

Figure 13. Cross-Sections for Masses 6,7,10,11 from Proton Spallation of Targets ^{14}N and ^{16}O in the Energy Range E_p = 17 to 42 MeV.

5. RADIOACTIVATION AND DECAY MEASUREMENTS

5.1 Introduction

Since the time-of-flight technique is limited by the low energy cutoff, it is desirable to have an alternate technique which could be used to check cross-sections at one energy. A 22 MeV proton colliding with a ^{14}N nucleus at rest makes 20.5 MeV available in the center of mass. This is just below the 20.7 MeV threshold for ^{11}B production. Thus the only mass 11 isobar produced at this proton beam energy is ^{11}C; similarly the only mass 7 isobar made is ^{7}Be. The decay of ^{11}C is by β^+ emission with a half-life of 20.5 min, so its cross-section can be measured by counting 0.511 annihilation γ-rays. The decay of ^{7}Be is by electron capture with a half-life of 52.6 days, and 10.3±0.16% (TM 62) of the time it decays to the 0.477 state in ^{7}Li; so finding the intensity of this γ-ray yields the ^{7}Be cross-section.

5.2 Cell Construction

Finding a suitable nitrogen target is again an important consideration. A small gas cell with Kapton windows to hold the ^{14}N target gas was designed for γ-ray counting with a lithium-drifted-Ge detector. Figure 14 shows a diagram of the cell assembly. The Kapton windows are pressed against O-rings by the 1/16" thick aluminum disks. The ports, open during irradiation, are plugged with 1/16" aluminum disks when the γ-ray counting is done. The aluminum stops even the most energetic positrons from ^{11}C decay. Hence all γ-rays originate within the cell volume or on the inner

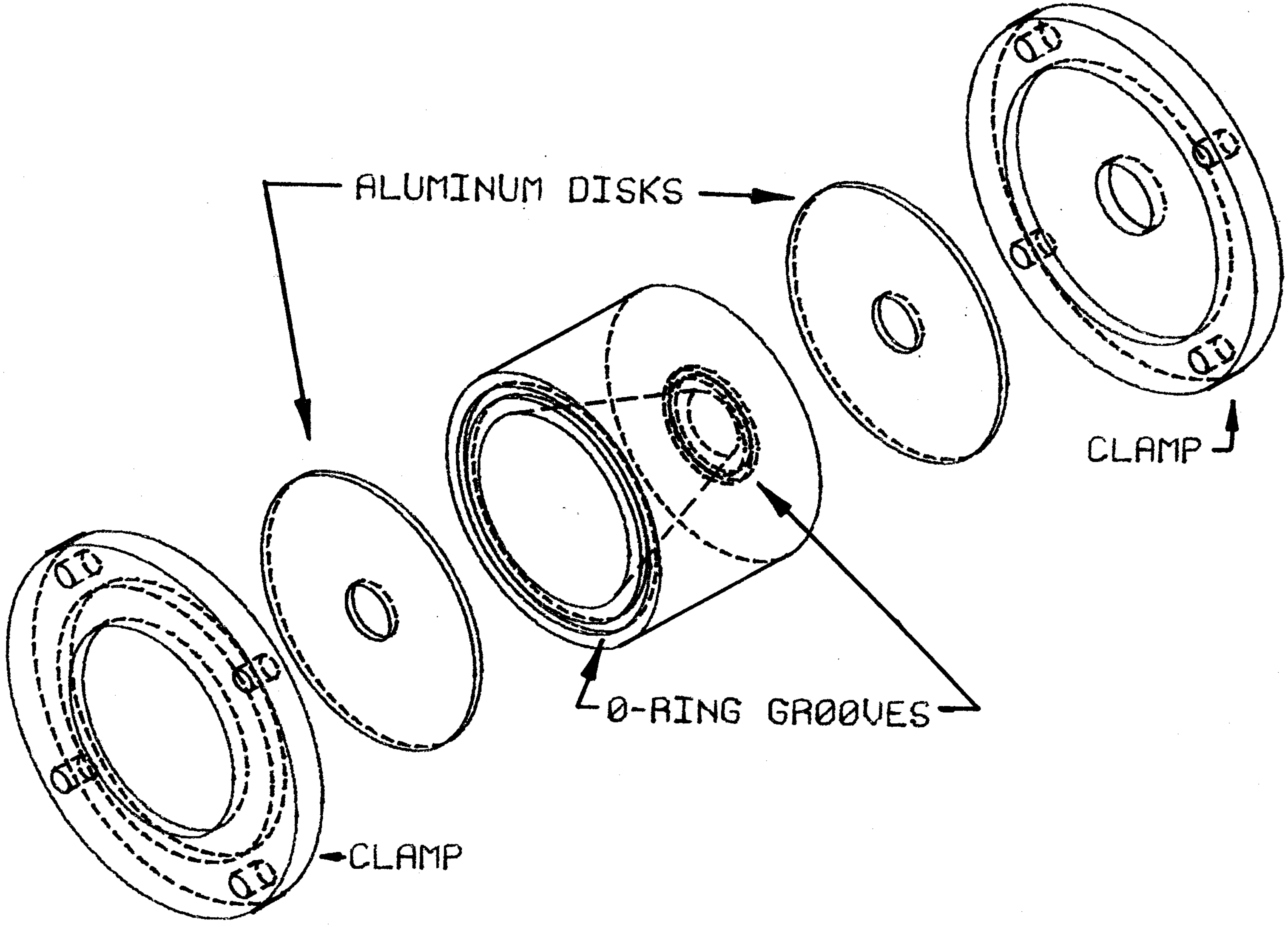

Figure 14. Partial Assembly Drawing of Gas Cell for Activation and γ-ray Counting.

walls. The frustum design was chosen so no γ-ray has to go through more than 1/16" of aluminum plus 1/16" of brass (^{11}C positrons penetrate up to 0.5 mm of brass before annihilation) to get to the detector. A γ-ray intensity attenuation correction can thus be made with confidence. Assuming the average ^{11}C γ-ray traverses 1.5 mm of aluminum and 0.75 mm of brass (one-half the maximum possible) the attenuation correction factor is 1.091. In the absence of a proper averaging procedure I assign an error of ±3% to this number. For the ^{7}Be γ-ray which only traverses 1.5 mm aluminum the correction factor is 1.036 with better than 1% accuracy.

A 9559B-1MM Circle Seal valve with a 1/4" Eastman Poly Flow fitting was soldered directly into the cylinder of the cell body (not shown in Figure 14). The volume of gas in the closed valve is less than 1% of the total cell volume. Hence the resulting counting error due to asymmetry of the volume holding the radioactive gas is quite negligible.

The Kapton windows are the main source of 0.511 MeV and 0.477 MeV background γ-rays. However a minimum thickness of Kapton is needed to stop ^{11}C and ^{7}Be from escaping the cell. For ^{11}C, 0.0005" Kapton windows are sufficient to stop even the forward scattered nuclei. For the ^{7}Be measurement 0.001" Kapton had to be used as exit window to accomplish the same purpose (Appendix A).

5.3 Irradiation Technique

For each cross-section measurement two irradiations were performed. Two identical gas cells were prepared. One cell was filled with ^{14}N, its twin with ^{4}He. The pressure was chosen to be 1 atmosphere so that no stress was exerted on the cell windows before and after irradiation. The chance that leaks would develop was minimized in this way. With the ^{4}He filled cell the contribution to the total yield by the Kapton was determined. A Helium filled cell rather than an empty one was used to ensure that any changes in the Kapton are similar for both irradiations. The most important effect is due to heating. Kapton in vacuum and in contact with a gas should have different equilibrium temperatures. Also the stress of 1 atmosphere pressure on the heated Kapton may deform it.

5.4 Counting Method for ^{7}Be and ^{11}C Decays

The γ-rays were counted with a lithium drifted Ge[1] detector. An electronics block diagram is shown in Figure 15. For good counting geometry the gas cell was placed at 10 inches from the detector. The detector efficiency at this distance was established for the 0.511 γ-ray using a standard ^{22}Na source (from the Bureau of Standards, 5% accuracy quoted). The relative efficiency of the 0.477 MeV γ-ray with respect to the 0.511 MeV γ-ray was found by assuming log (γ-energy) vs. log (relative efficiency) is a

---

[1] Manufactured by Nuclear Diodes, Prairie View, Ill.; Relative peak efficiency 10.4%.

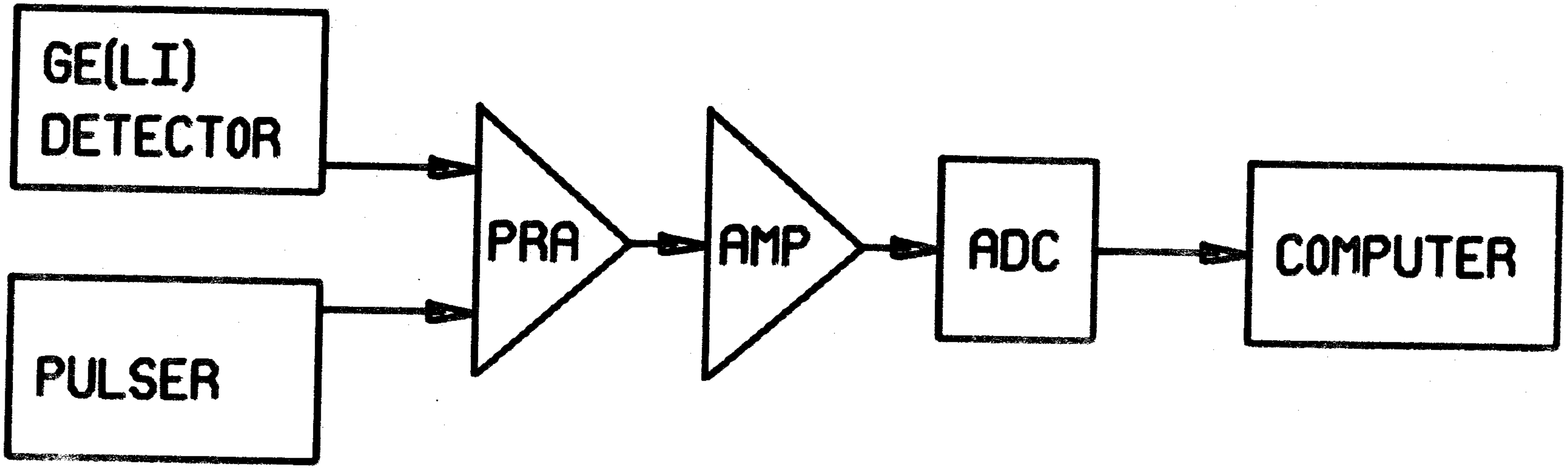

Figure 15. γ-Ray Counting Electronics Block Diagram.

straight line, determined by the 0.511 MeV γ-ray and the 1.274 MeV γ-ray of ^{22}Na. A Ge(Li) detector for which a more complete efficiency curve is available (DO 70) exhibits this relationship in the range from 200 keV to 5 MeV.

The β^+ decay γ-ray origin, and the frustum geometry of the cell make precise positioning difficult. Consider case 1, γ-rays originate from all inner cell surfaces with equal likelihood or, case 2, γ-rays originate from the gas volume only. To effectively place the cell at 10" from the detector I find the cell position for the first case is 0.024" closer to the detector than for the second case. This still represents a negligible error of 0.24% in distance or ≃0.5% in cross-section.

In the case of ^{7}Be the irradiation time is short compared to the half-life. For a cross-section calculation one then needs the gas pressure, the total charge traversing the cell and the distance traveled by the beam in ^{14}N. In section 5.7 these measurements are combined with the measured γ-decay rate, detector efficiency and branching ratio to yield the ^{7}Be total cross-section. The 0.477 MeV γ-rate was measured by counting for 4 hours each on the ^{14}N filled and ^{4}He filled gas cells. The counting was done at least 24 hrs after irradiation so that the background due to annihilation 0.511 γ's was low. The γ-ray was identified by its energy and by its 53 day half-life.

^{11}C has a half-life of 20.5 min. An adequate irradiation consisted of 500 namp of proton beam for a duration of

10 minutes. Beam intensity fluctuations can therefore not be neglected. A chart recorder running at 3 in/min was used to record the instantaneous beam intensity.

The ^{11}C counting was started 3 minutes after irradiation. Counting was continued for 3 hrs.; intervals were chosen to be a 5 min. step followed by 10 min. steps. A pulser with the frequency of 19.1 counts/sec was injected into the detector preamplifier and was used to correct for deadtime losses.

5.5 Data Reduction

The 0.511 MeV γ-decay curves for (Kapton + ^{4}He) and (Kapton + ^{14}N) show that besides the 20.5 minute component there are shorter and longer half-lifes involved (see Figure 16). Care had been taken during irradiation and counting that both gas cells had received the same treatment. Hence the decay curve for the ^{4}He filled cell could be subtracted point for point from the one for the ^{14}N filled cell. Since protons bombarding ^{4}He do not lead to products which β^{+} decay, the difference curve for the two cells then represents the contribution of ^{14}N proton spallation products to β^{+} decay.

At 22 MeV bombarding energy the only relatively long lived radioactive isotopes from $^{14}N+p$ which contribute to the 0.511 MeV annihilation radiation are ^{13}N with a half-life of 9.96 min and ^{11}C with a half-life of 20.5 minutes. $^{15}O(124s)$, $^{14}O(71s)$, $^{10}C(14s)$ are also produced but have much shorter half-lifes. The decay curves and their

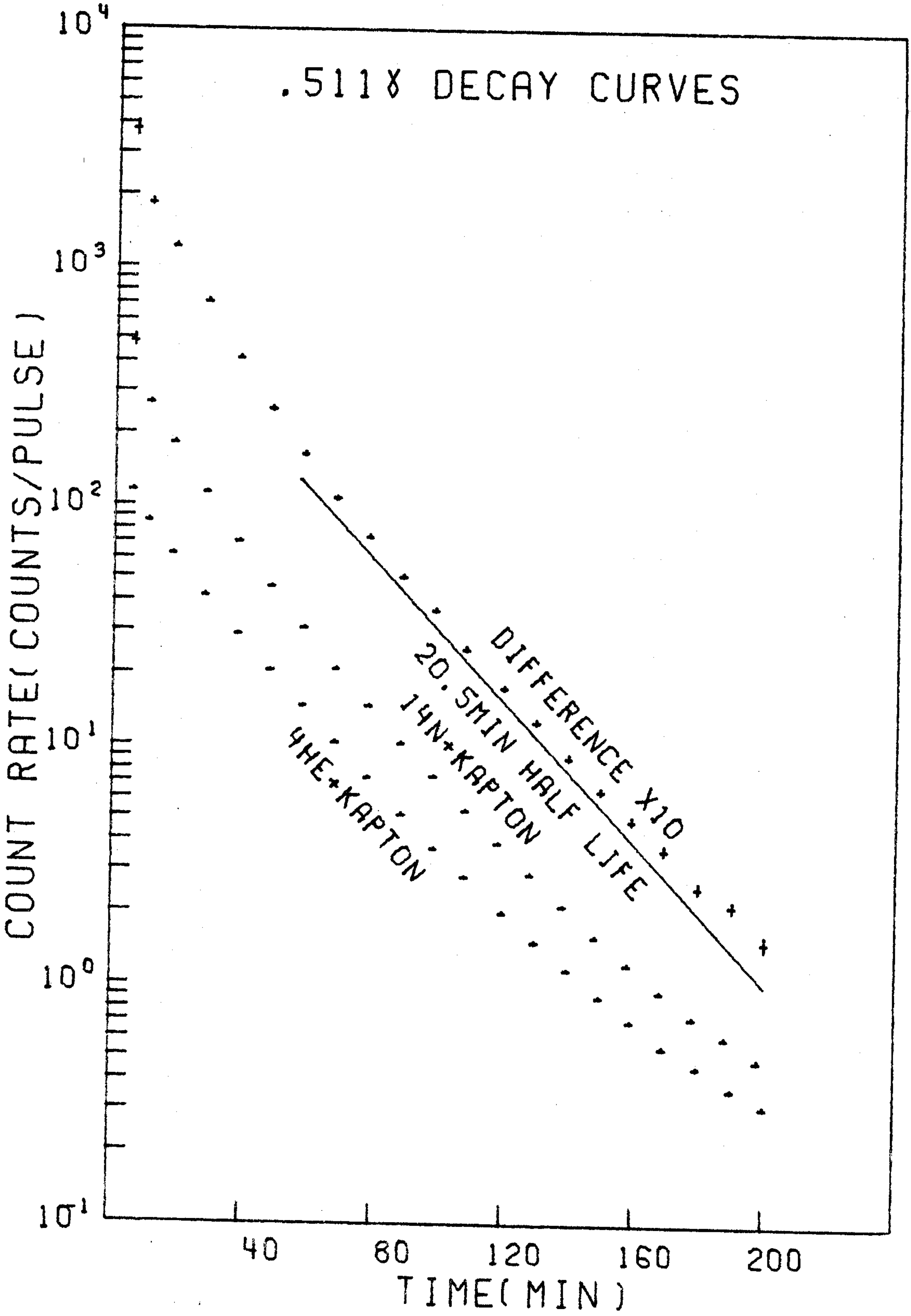

Figure 16. Data Points of 0.511γ Decay Curves for Nitrogen and Helium Filled Gas Cells and the Curve Resulting from Taking their Difference.

difference is shown in Figure 16. The line shown represents a 20.5 min half-life and is only included as a reference. It can be seen that shorter and longer half-lifes are present. The shorter half-lifes can be understood since they may be present as pointed out above. The longer half-life must represent a difference in irradiation between the cells and is not understood at present. The error introduced in determining the 20.5 min half-life intensity is 10%. In Figure 17 a number of fits to the difference curve are shown with the fit parameters given for each curve. The time scale is only valid for the left most data set. Other curves were displaced to the right for display purposes. The crosses in Figure 17 represent the data. We consider half-lifes 10 min, 20.5 min and also a longer half-life, either 41 min or 324 min. For a fit using two half-lifes we select two data points; for three half-lifes we need three data points. The selected points, boxed in Figure 61, determine counting rate contributions of the different half-life components. The solid line represents the calculated counting rate. The contributions by the 20.5 min component at 41 min after the end of irradiation to the fits shown in Figure 61 are from left to right, 487, 460, 394, 430, and 435 counts/sec. We use the value 438±45 counts/sec in our cross-section calculations.

5.6 Cross-Section Calculations for ^{11}C

To calculate the ^{11}C production cross-section from the observed rate after irradiation, the decay of ^{11}C during

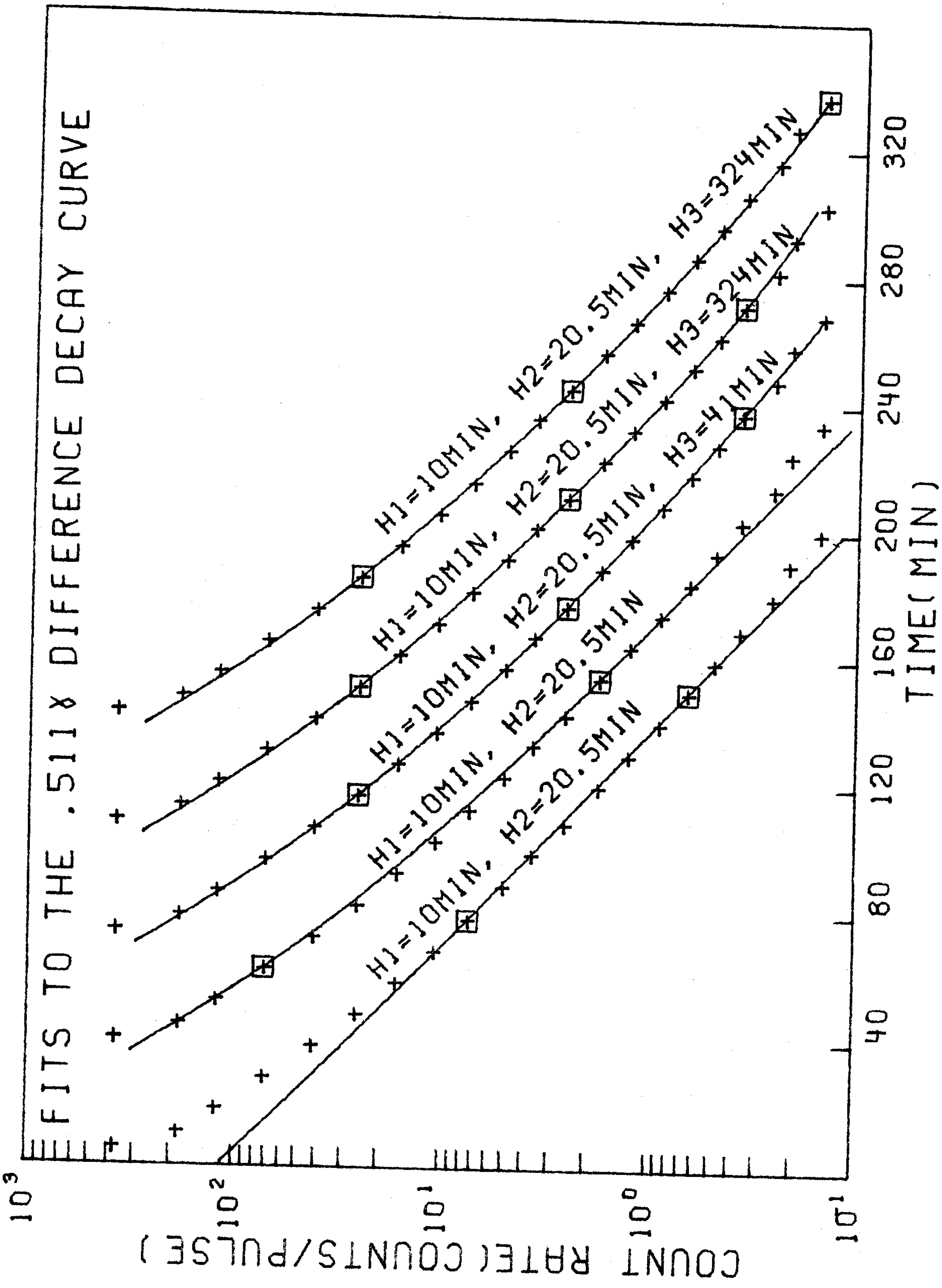

Figure 17. Sample Fits to the 0.511 γ Difference Decay Curve.

irradiation has to be taken into account. A numerical integration fortran program was written based on the equation:

$$dN = \frac{-N \log 2}{H} 2^{-\Delta t/H} \Delta t + \sigma n_t \Delta n_i$$

dN represents the net change in the number of ^{11}C nuclei during the time interval Δt.

N is the number of ^{11}C nuclei present at the beginning of Δt.

H is the half-life;

σ is the total cross-section for spallation production of ^{11}C.

n_t is the number of target nuclei per cm^2.

Δn_i is the total number of incident protons during the time interval Δt.

The program is given an arbitrary value for σ such as 1 mb, and it starts by calculating dN for the first second of irradiation. This becomes the value of N during the next second after which the new dN is added to N. This is done in one second time steps to the end of irradiation. The γ counting rate at 2 half-lifes after the end of irradiation is then calculated. The correct value for the cross-section is then given by:

$$\sigma = 1 \text{ mb} \frac{\text{observed rate}}{\text{calculated rate}}$$

The irradiation histories for the ^{14}N and the ^{4}He activations yield cross-sections which differ by only 0.37% justifying the direct subtraction technique explained in section 5.5.

5.7 Cross-Section Calculations for ^{7}Be.

The decay of a radioactive nucleus is governed by the well known equation :

$$N = N_o 2^{-t/H}$$

N_o is the number of radioactive nuclei present at time $t = 0$.

H is the half-life of the nucleus considered.

The decay rate is then given by

$$\frac{dN}{dt} = -\frac{\log 2}{H}(N_o 2^{-t/H})$$

The initial number of nuclei $N_o = \sigma n_t n_i$.

In our case σ is the total cross-section for ^{7}Be production from ^{14}N. The total number of incident protons, n_i, is related to the collected charge Q(coulombs) by

$$n_i = Q/(1.6021 \times 10^{-19} \text{ coulombs})$$

and n_t, the total number of target nuclei/cm^2, for ^{14}N gas is given by

$$n_t = \ell P \frac{273.1}{T} (2)(2.687) \times 10^{+19} \text{cm}^{-2}$$

The quantity P is the gas cell pressure in atmospheres,

T is the gas temperature in °K,

ℓ(cm) is the total length of gas traversed by the beam.

We measured ℓ by pressurizing the cell to 1 atmosphere above atmospheric pressure and measuring the distance between Kapton windows with a micrometer. P was the pressure of the atmosphere at the time of filling the gas cell. This was corrected for billowing of the windows when the cell is placed in vacuum.

The rate measured by the counter for a γ-ray from one source is:

$$R = \frac{\log 2}{H} (N_o 2^{-t/H}) X\varepsilon G = \frac{dN}{dt} X\varepsilon G$$

X is the number of γ's per decay. For ^{7}Be this is equal to the branching ratio to the 0.477 MeV level in ^{7}Li; X = 0.103. ε is the photopeak efficiency of the detector for a point source at 25.6 cm, G is a geometric factor taking account of the finite extent of the gas cell, N_o is the number of radioactive nuclei present at time t=0 and H is the half-life of the nucleus considered.

ε was found by counting γ-rays from a N.B.S. calibrated ^{22}Na source rated at 1.62 μcuries ±5% on 11-11-70. The efficiency measurement was performed on 3-21-71. The center of the source was placed 25.6 cm from the Ge detector. 653500±2500 counts were accumulated in the 0.511 γ-ray peak. 162500±700 counts were accumulated in the 1.274 γ-ray peak. 194200 counts were accumulated in a peak due to a pulser running at 5 pulses/sec.

The error assignments are obtained from $\sqrt{\text{counts in Peak+2Background}}$ G=1 can be assumed for the source since it is quite small. X=1.8 for the 0.511 γ-ray and X=1.0 for the 1.274 γ-ray.

From this data and the assumption that the logarithm of the γ-ray energy vs. the logarithm of the relative efficiency traces out a straight line, ε=1.818x10^{-4} is obtained for the absolute efficiency of the 0.477 γ-ray from ^{7}Be.

The constants for the equation used to relate decay rate to ^{11}C cross-section are mostly the same as those for ^{7}Be. The photopeak efficiency for the 0.511 γ-ray is 1.714×10^{-4}. The half-life for ^{11}C decay was taken to be 20.5 min. X, the number of γ's per decay, is equal to 2.0.

5.8 Error Analysis

Table 11 summarizes error contributions to the cross-section determination by radioactivation-decay measurements.

5.9 Cross-section Comparison

Table 12 compares our 21.7 MeV ^{11}C and ^{7}Be cross-section measurements by the time-of-flight and γ-counting methods, as well as the recently published values (ES 71), (BCJR 71). There is agreement within the quoted errors. From the Epherre data it is also apparent that the ^{11}C cross-section falls rapidly with increasing proton beam energy near 21 MeV; hence, the marginal agreement for ^{11}C is not unexpected. Our 17 MeV ^{11}C time-of-flight data does not agree with the Epherre data, but error bars almost meet at 87 mb.

Table 11. Error Contributions to the Radioactivation-Decay Measurements.

Error Source	Error in %	Comments
ε efficiency	6.0	
P pressure	0.5	From Lansing Weather Bureau Station
T temperature	1.5	
d distance of detector from cell	0.24	Explained in Section 5.4
ℓ distance beam travels in ^{14}N	0.5	Micrometer measurement
Q integrated charge	3.0	
$R_{^{11}C}$ decay rate after irradiation	10.3	
$R_{^{7}Be}$ decay rate after irradiation	3.0	
$X_{^{7}Be}$ branching ratio	1.6	(TM 62)
γ attenuation for ^{11}C	3.0	
γ attenuation for ^{7}Be	1.0	

Added in quadrature the error for the ^{11}C cross-section is then 13% and the error for the ^{7}Be cross-section is 8%.

Table 12. ^{11}C and ^{7}Be Cross-section Measurement Comparison.

	Radioactivation γ counting	Time-of-Flight	Epherre et al. (ES 71) Read from a graph	Bodansky et al. (BCJR 71) 20 MeV
	Cross-sections at 21.7 MeV in mb			
^{11}C	36.2±4.5	39.5±10.1	50±12	
^{7}Be	49.0±3.8	41.2±7.2	45±8	46±5
	Cross-sections at 17 MeV in mb			
^{11}C		69±16	110±27	
^{7}Be		36.6±14	30±5	

6. REVIEW OF PAPERS ON ASTROPHYSICAL THEORIES OF LiBeB PRODUCTION

6.1 Introduction

A complete theory of LiBeB production has to explain abundances and isotopic ratios encountered in nature. Table 13 is a short compilation of the presently available data of importance to the theories on L(LiBeB) nuclei production. The following pages give a short history of light element synthesis theories by reviewing excerpts of papers on the subject. The values used often vary somewhat from those in Table 13, but the conclusions drawn in the various papers are not sensitive to changes of that magnitude.

6.2 Early Theories of Nucleosynthesis of LiBeB

The early theories of nucleosynthesis recognized that there was difficulty in producing the light elements even in their comparatively low abundances. In 1955 Hayakawa (Ha 55) and Fowler _et al_. (FBB 55) proposed stellar surfaces as a creation site with high energy protons causing spallation of the heavier constituents of the stellar atmosphere. Fowler _et al_. considered two possibilities. They envisioned hot spots in magnetic spots where $\rho = 10^{-8} - 10^{-7}$ g/cm^3 and $kT \simeq 5$MeV and claimed under these conditions (Li, Be, B)/(C,N,O)=1, the observed galactic cosmic ray ratio. They then weakened this hypothesis by observing that in Apm stars, the proposed site for the magnetic activity, the low Be abundance speaks against this mechanism. The second possibility considered was proton spallation of C,N,O at energies > 100 MeV in regions

Table 13. Abundances of Interest in LiBeB Production.

	Abundances ($H = \log \varepsilon_H = 12$)		
Element or Isotope	Solar System (CA 67)	Sun (MU 68)	Sun
H	12.00	12	
He	10.91		
^{6}Li	2.11		.29 (PE 68)
^{7}Li	3.21	< .9	
^{9}Be	1.42	2.34	
^{10}B	1.67	<3.6	
^{11}B	2.28		
C	8.72	8.51	
N	7.97	8.06	
O	8.96	8.83	
Ne	7.96		
Si	7.59	7.70,7.24	

Ratios

In Cosmic Rays

$\text{LiBeB}/n_{\text{CNO}} = .24$ (GMS 70)

Li:Be:B = .5:.45:1 (FGS 68)

In Sun (MU 68)

	Photosphere	Corona UV	Solar Cosmic Rays
C/N	2.8	10	3.1
O/N	5.9	7.7	5.3

$^6\text{Li}/^7\text{Li} \leq 0.05$

Table 13. (continued)

In Rocks (Earth) and Meteorites

$^{7}Li/^{6}Li = 12.5$

$^{11}B/^{10}B = 4.0$

of $\rho < 10^{-9}$ g/cm^3. For either of these, Apm stars were found to be too few in number to account for the cosmic abundance.

They then considered the possibility of this spallation mechanism in M dwarfs being the source of the light elements. They assumed M dwarfs contributed all of the LiBeB and 5×10^{-5} of the total cosmic abundance of matter in a time span of 10^9 years. To produce the observed abundance of LiBeB, the ratio of (Li,Be,B)/(C,N,O) in the ejected material must be in the range 10^{-3} - 10^{-2}. This represents 0.1 to 1 percent efficiency assuming a ratio of one is the maximum possible attainable by spallation of C,N,O in the gas. However since the magnetic activity of M dwarfs is much less than that of Apm stars the authors did not feel it was evident that this ratio could be achieved in the ejected material.

In the classic paper on the synthesis of elements in stars Burbidge, Burbidge, Fowler, and Hoyle (BBFH 57) still found stellar atmospheres a possible synthesis site, but they also considered gaseous nebulae and supernovae as possible candidates. No calculation for the latter two were attempted. In this paper there was also speculation that ^{7}Li may be synthesized in helium burning cores of late-type stars by $^3\text{He}(\alpha,\gamma)\ ^7\text{Be} \xrightarrow{\text{K captures}} {}^7\text{Li}$. The ^{7}Li can be brought to the surface provided the hydrogen envelopes only extend to depths where the temperature is less than $\approx 10^6$ degrees.

In 1960 a paper by W. K. Bonsack and J. L. Greenstein (BG 60) on the abundance of lithium in T-Tauri stars gave new impetus to spallation-at-the-surface-of-stars theories.

They found that the Li abundance in T-Tauri stars is about 100 times the solar value or about the same as observed terrestially. They also observed that the surrounding nebulae have at least ten times less lithium per gram than the T-Tauri atmosphere, which strongly suggests that Li is made in the star. A number of calculations were performed in this paper.

To check whether cosmic ray Li could be the source of stellar Li they started with the cosmic ray number ratio $(\frac{Li}{H})_{cr} = 10^{-3}$, a cosmic ray energy density $U_{cr} = 1$ ev/cm^3 and a mean cosmic ray energy of $\bar{E} = 10^9$ev, and the particle density of hydrogen $n_H = 1/\text{cm}^3$. After condensation the Li/H ratio due to cosmic ray Li abundance is then

$$\frac{Li}{H} \leq 10^{-3} \frac{U_{cr}}{\bar{E}n_H} \leq 10^{-12}$$

which is compared to the approximate solar abundance ratio 10^{-11} and hence is found to be too low even for normal stars.

The authors also attempted to calculate the energy required of each star to produce the observed high-abundance of $\frac{Li}{H} = 10^{-9}$. They assume 100 MeV is needed per Li atom synthesis. Assuming an efficiency factor β, the ratio of E_{Li}, the total energy needed for Li synthesis, to L_t, the total stellar energy from hydrogen burning, is given by

$$\frac{E_{Li}}{L_t} = \frac{1.6 \times 10^{-7}}{\beta} ,$$

which appears quite possible, but the authors do not postulate a mechanism for actually bringing about the nucleosynthesis.

They also make a calculation for a spallation origin of Li due to cosmic rays striking stationary heavy nuclei in the atmosphere of a proto-star. The assumptions are: the cosmic ray spectrum for protons is a delta function in proton energy with $E_p = 1$ BeV; a target nucleus of atomic weight A, abundance N_A, will have a spallation cross-section of $A^{2/3}$ in millibarns; the efficiency α_A for producing Li per interaction is linear between A=12 and A=20 with $\alpha_A=0.1$ for A=12 and $\alpha_A=1$ for $A \geq 20$. The authors obtain the ratio

$$\frac{Li}{H} = \frac{U_{cr}}{E_p} \left[\frac{\sum_{A=12}^{56} N_A \alpha_A A^{2/3}}{N_H^2} \right] ,$$

where U_{cr} is the cosmic ray energy density at the surface of the star as it condenses. The term in brackets is estimated to be 4×10^{-3}. For $U_{cr} = 1$ ev/cm^2 and $E_p = 10^9$ ev they then obtain $Li/H = 4 \times 10^{-12}$. This is low compared to 10^{-9}.

The authors then point out that the observed Li abundance in a star can be up to $M/\Delta M$ of the net abundance in the star, where ΔM is the optically accessible mass of the star and M is its total mass. This enrichment factor would imply that the spallation process is due to a surface phenomenon, concentrating cosmic ray or magnetic field energy at the surface of a forming star. The authors claim trapped magnetic field could supply the energy to produce the observed Li abundance in T-Tauri stars, provided the energy is dissipated near the stars' surface so $\Delta M/M$ is sufficiently small, where ΔM now stands for the mass in the active region of the star. In a volume of space containing one solar mass of gas and initial magnetic field H the total magnetic energy stored is estimated at 5×10^{55} H^2 ergs. Assuming 250 BeV are needed to create one Li nucleus (from the cosmic ray result cited above) the observed abundance ratio becomes $Li/H = .1H^2M/\Delta M$. Thus for an interstellar magnetic field of $H = 1 \times 10^{-5}$ gauss and $\Delta M/M = 10^{-2}$; $Li/H = 10^{-9}$ can be achieved.

Following the paper by Bonsack and Greenstein (BG 60), T. Gold (G 60) pointed out that the surrounding nebulae of T-Tauri stars could be gas remaining after star formation. Spallation reactions in the surface at an early age of the star (during strong magnetic activity) could then create Li in a surface shell of the star. This could then be tied in with a theory of the origin of the solar system in which the shell is thrown off and most of the angular momentum of the sun is transferred to it possibly by magnetic coupling. The high lithium abundance in the earth and meteorites could thus be explained.

In S. Bashkin and D. C. Peaslee (BP 61) the authors come to the following conclusion with regard to light element production: "L nuclei (Li,Be, and B) are produced by spallation, most abundantly during the contraction stages of a forming star. This qualitatively accounts for L abundances in the solar system and T-Tauri stars. For the present sun it is uncertain whether the L nuclei observed are currently produced by flares or are the remains of an original stock."

The paper attempts an abundance calculation:

Consider $p(F)dF = aVe^{-aF}dF$

where $p(F)dF$ is the number of flares per second containing between F and F+dF fast protons ($E_p \gtrsim 70$ MeV), V is the total rate of flare occurrence in the sun, and a is a parameter specifying the distribution of sizes.

$V \simeq 0.8 \times 10^{-4}$/sec,

The rate of flares of size F_o or larger is $P(F_o) = Ve^{-aF_o}$. For $F_o \simeq 10^{33}$, $P(F_o) \approx 0.5$/year; hence, $a \simeq 8.5 \times 10^{-33}$. The authors then point out that half of the protons in a flare will go into the sun's surface where they will cause spallation reactions or, more likely, will be stopped by protons. From the p-p cross-section for $E_p = 0.1 - 0.3$ BeV they obtain a mean free path of 6×10^{25} protons/cm^2. Given a target nucleus, of abundance f relative to hydrogen which has a cross-section for producing particle x of $\sigma(x)$mb for fast protons, its probability of yielding a particle x per fast proton is $0.06\ f\sigma(x)$. The production rate for a particular spallation product is then $Y(x) = 6 \times 10^{26}\ f\sigma(x)$/sec where the total proton flux per second is given by

$$\int_{F=0}^{\infty} P(F)FdF = \int aVe^{-aF}FdF = \frac{V}{a} .$$

For the more numerous protons in the range 10-70 MeV the corresponding rate is $Y'(x) = 2 \times 10^{28}\ f\sigma'(x)$ where account has been taken of the shorter mean free path of protons in this energy range. The authors then present a more or less quantitative technique which results in an estimate of 80 mb for light-isotope (L) production for the (C,N,O,Ne) targets; with $f = 0.002$ this leads to $Y(L) \simeq 10^{26}$/sec. The authors then show that this production rate is too low to account for even solar abundances:

$$f(L) = \frac{Y(L)T}{N_H} \approx 3 \times 10^{-13}$$

where f(L) is the abundance with respect to hydrogen in the convective envelope of the sun; $T = 1.5 \times 10^{17}$ sec is the age of the sun, and $N_H = 5 \times 10^{55}$ is the number of H atoms in the convective zone. They claim the observed L abundance in the sun is about 10^3 greater than this.

It is also pointed out that the ratio $\frac{Be}{Li} \approx 30$ as observed in the sun is difficult to understand, claiming preferential loss of Li in photosphere or convective zone is not expected.

The series of papers: Fowler, Greenstein, and Hoyle (FGH 61); Fowler, Greenstein, and Hoyle (FGH 62); Burnett, Fowler, and Hoyle (BFH 65); concerns itself specifically with an elaborate theory on the production of the light elements in the spirit of the suggestion by Gold (1960). Mitler (1964) also made detailed calculations based on this model.

The assumptions of the model are: planetary formation has progressed to the point where solid bodies appear in the gaseous disk surrounding the sun. Their composition is $\approx$ 3/4 ice, $\approx$ 1/4 silicates and perhaps 5% carbon. A proton flux with $\bar{E} \approx 500$ MeV impinges on the material in the disk. In the absence of experimental production cross-sections of the light elements from spallation of O, and Si, the authors assumed production ratios $^7Li/^6Li = 1$ and inferred from the model that $^{11}B/^{10}B = .3$. The proton flux, besides causing spallation of the target elements to form Li, Be, B, also gives rise to a neutron flux which is thermalized by the hydrogen present. The thermalized neutrons then deplete ^{6}Li and ^{10}B to yield the observed terrestial isotopic ratios ^{7}Li/^{6}Li = 12.5 and ^{11}B/^{10}B = 4. To estimate the energy needed to form the L nuclei in terrestial planets, the authors assume one L nucleus is formed in nine proton reactions. Assuming $\bar{E}_p$ = 500 MeV they require [4.5GeV/L nucleus produced]. Assuming [50 L nuclei/10^{6}Si] were produced by spallation, and taking 4.6 x 10^{49}Si nuclei present in terrestial planets, implies 1.7 x 10^{43} ergs is required. They then consider an estimate by Hoyle according to which 5 x 10^{45} ergs have to be dissipated in the transfer of the angular momentum of the sun to the planets. If 4% of the energy appears as high energy particles, they find only 10% of the protons need to interact to produce the L nuclei. At present the weakest point of the theory is the ^{11}B/^{10}B ratio. Based on the presently known cross-sections for ^{11}B and ^{10}B production from ^{12}C and ^{16}O, and assuming the contribution of Si spallation does not greatly affect the net production, the ^{11}B/^{10}B spallation ratio is 2 for 500 MeV protons. If lower energy protons are considered this ratio can be greater than 4. Hence the depletion of ^{10}B by neutrons only increases this ratio above the terrestially observed value.

6.3 Current Theories of Nucleosynthesis of LiBeB

Ideas present in the early theories combined with new data resulted in a number of elaborate papers. The theories proposed for light element production are quite distinct.

R. Bernas, E. Gradsztajn, H. Reeves, and E. Schatzman (BGRS 67) attempt to identify the Li,Be,B production site and mechanism as proton spallation of C,N,O,Ne in the solar atmosphere before the Hayashi (fully convective) phase of the sun. The $^7Li/^6Li$ ratio is then changed by $^6Li(p,\alpha)$ reactions at temperatures between 2 and 4 million degrees at the bottom of the surface convective zone during the Hayashi phase. The material forming the planetary system would still later have separated from the sun.

A number of spallation production cross-sections with 150-MeV protons on ^{12}C and ^{16}O had been measured by these authors. They supplemented these with estimates based on isospin formalism or with calculations based on the Serber statistical method. Thus starting with a complete set of cross-section values and a probable target mixture they could calculate the formation rate of the light isotopes from

$$\frac{dn_L}{dt} = \sum_M n_M \int_{Q_{M,L}} \sigma(M,L)\Phi(E_p)dE_p \qquad 6.31$$

where n_L is the density of isotope L produced (nuclei/cm^3),

n_M is the density of target isotope M (nuclei/cm^3),

$\sigma(M,L)$ is the cross-section for producing L from M by protons of energy E_p,

$Q_{M,L}$ is the threshold proton energy for producing nucleus L from target M,

and $\Phi(E_p)$ is the proton flux.

The authors use $n_C/n_H = 3 \times 10^{-3}$, $n_N/n_H = 10^{-4}$, $n_O/n_H = 10^{-3}$, $n_{Ne}/n_H = 3 \times 10^{-3}$ for the isotopic target composition. They consider a probable average proton energy spectrum as observed in solar flares and calculate isotopic spallation ratios $^7Li/^6Li = 2.5 \pm 1.0$ and $^{11}B/^{10}B = 5 \pm 2.5$. They compare these with the terrestial-meteoritic values and find that the $^{11}B/^{10}B$ ratio requires no depletion mechanism while the $^7Li/^6Li$ spallation ratio must be modified by the mechanism outlined above. Of the light elements the energy requirement for Be production is largest.

For stellar production the time integral of equation 6.31 yields for the production of the light nucleus L

$$\frac{n_L}{n_H} \leq \int \phi_p(t)\,\sigma(L)\,(n_{CNONe}/n_H)\,X(t)\,dt \qquad 6.32$$

where $X(t) = M_i/M_c$ is a dilution factor; M_i is the mass in which the spallation process occurs; M_c is the total mass of the convective zone on which M_i can be mixed. The possibility of burn up at the bottom of the convective zone is allowed for by the < sign. From the estimated average spallation cross-sections leading to Be of 2 mb and the abundance of Be in the sun the integral equation becomes

$$\int \phi_p(E>40 \text{ MeV})\,X(t)\,dt \simeq 10^{20}/\text{cm}^2 .$$

For the present sun the authors estimate $X(t) \simeq 10^{-8}$ and the proton flux capable of spallation is $\phi_p(t) = 10^7/\text{cm}^2$ sec. Assuming the age of the sun is 5×10^9 years, the integral yields 1.6×10^{16}. The authors place the limits 7×10^{15}

$< \int \phi_p X dt < 7 \times 10^{16}$, and find the activity is too low by about 10^3. In the case of T-Tauri stars the authors estimate the convective mass is 0.1 of the total mass hence $X(t) = 10^{-11}$; the period of the phase $\simeq 10^{6.5}$ years, so to yield $\int \phi_p X dt = 10^{20}$ the particle flux must be $\simeq 10^{16}$ protons/cm^2/sec or 10^{42} erg/year. For a star the size of the sun, this is a very large energy requirement. The authors then point out that the Herbig-Haro phase of a star, before it becomes luminous, might also be the production site.

To estimate the production of light elements in galactic cosmic rays the authors considered a proton flux above 100 MeV of about 2 particles/cm^2/sec. The ratio $n_{CNONe}/n_H = 3 \times 10^{-4}$ is taken as a time average over the age of the galaxy (10^{10} years).

$$\frac{n_L}{n_H} = \int \phi_p (n_{CNONe}/n_H) \sigma_L dt$$

for $\sigma_L \simeq 30$ mb this yields $n_{LiBeB}/n_H \simeq 1.6 \times 10^{-11}$, while 10^{-9} is found in several stars, the meteorites, and the earth.

H. E. Mitler (MI 67) wrote a critical review of theories on the origin of the rare light nuclides. In particular he made calculations on the energy requirement for producing cosmic abundances by proton spallation of CNONe on the surface of stars and compared the total energy to the energy available from gravitational contraction. This is of interest for the T-Tauri phase and the Herbig-Haro phase as considered in the Bernas et al. model. The ratio is $\simeq 300$ for the Herbig-Haro phase hence eliminating it from consideration. For the T-Tauri phase the ratio is 2 for the Bernas et al. model.

These calculations are based on the Be abundance in the sun, which represents the most severe energy requirement. Similar calculations based on our measured cross-sections yield almost identical results.

Mitler considers that the accelerating distance for a proton may be $\approx$ 4 times its stopping distance, hence the irradiated material could be about 5 times as great as considered by Bernas, yielding a ratio of $E_{spal}/E_{grav} = 0.4$; this puts the T-Tauri phase in the energetically just possible range. Mitler then proposes an alternate theory where most of the lithium (^{7}Li) is made in a big bang and the remaining light isotopes are produced by spallation during the T-Tauri phase. No burn up of ^{6}Li and hence no mixing in a convective zone before ejection is required in this model. The energy requirement then decreases by over a factor of 100, making the process energetically quite possible.

The difficulties encountered in theories of autogenetic origin of light elements in stars led H. Reeves, W. A. Fowler, and F. Hoyle (RFH 70) to a theory which attempted to show that the light elements were produced by galactic cosmic rays. They divided the energy range of galactic cosmic rays into three regions; $E < 5$ MeV/nucleon, $5<E<30$ MeV/nucleon, and $E > 30$ MeV/nucleon. They then considered the contribution of p+C, N, O; α+C, N, O; p, α+Mg, Si, Fe; and $\alpha+\alpha$ in the middle and high energy region, where they assigned likely mean cross-sections for the various production mechanisms.

For the case of spallation of heavy fast particles on residual gas the escape form the galactic disk and the nuclear destruction of the light elements produced were taken into consideration. The generation rate of lithium per H atom was found to be $\frac{d}{dt}\left(\frac{Li}{H}\right) \approx 7 \times 10^{-28}\ \mathrm{sec}^{-1}$. To achieve a lithium abundance of $\frac{Li}{H} \sim 10^{-9}$ a total time integrated flux of 5×10^{18} particles/cm^2 is needed. For a galactic age of 1.2×10^{10} years this represents an average flux of 12 particles/cm^2 sec instead of the present flux of 3.6 particles/cm^2 sec.

It is instructive to compare this calculation with the estimate in the paper by Bernas et al. (BGRS 67), which found the discrepancy to be a factor of 170.

Bernas et al.		Reeves et al.
protons>100MeV$\approx$2/cm^{2}sec		protons>30MeV$\approx$3.6/cm^{2}sec
$n_{CNONe}/n_H = 3\mathrm{x}10^{-4}$		$n_{CNO}/n_H = 15 \times 10^{-4}$
time $\approx 10^{10}$years		time $\approx 1.2 \times 10^{10}$years
$\sigma_{Li} \approx 30$ mb	4.5 enhancement factor	$\sigma_{Li} \approx 30$ mb
		+ equal production from heavy cosmic ray spallation.
		+ 1/2 production from α spallation.
		+ 2x production from α-α.

All together this yields a factor of 50. Thus some new data, a new production mechanism plus some bias on either side can make a significant change in the evaluation of a theory.

Better data especially in the low energy region of cosmic rays and solar flares, as well as for abundance measurements of light and medium heavy nuclei may very well lead to revised theories.

From the low threshold of $^{14}N+p \rightarrow {}^{11}C \rightarrow {}^{11}B$ and the solar system ratio of $^{11}B/^{10}B$, the authors find that the contribution to ^{11}B from the flux in the medium energy region is low, and imply the flux at protons in the $5<E<30$ MeV range is $\leq 5/cm^2$sec. The observed terrestial abundance of deuterium cannot be accounted for by galactic cosmic rays. The authors suggested big bang nucleosynthesis or neutron capture in the atmosphere of neutron stars.

H. E. Mitler (MI 70) gave a detailed calculation of light element production in galactic cosmic rays, using then available cross-sections for ^{12}C and ^{16}O and estimates for $\alpha+\alpha$ reactions. He made a more or less arbitrary extrapolation of the cosmic ray flux below 100 MeV/nucleon for his calculations. The abundances obtained by Mitler, assuming the galaxy is unchanged since its birth, were extremely close to those observed in meteorites (Be and B especially). It should be pointed out that absolute abundances are very uncertain, values obtained for the crust of the earth, for example, are about ten times higher than those obtained for chondritic meteorites. Mitler then allowed for higher production in the primitive galaxy as well as processing of galactic material and found that at the time of solar genesis the abundances of the first calculation would be increased by a factor of 2.5. He concluded that he could not make sufficient ^{7}Li in galactic cosmic rays and suggests cosmological production as in Mitler (MI 67). There is also difficulty with the ^{11}B/^{10}B ratio (too low) as well as with low isotopic ratios ^{7}Li/^{6}Li observed in stars. Mitler lists the usual palliatives plus the possibility of a neighborhood supernova supplying thermonuclear lithium.

One additional observational aspect should be mentioned because it has bearing on the question of light element production in stars. Herbig (HE 65) pointed out an interesting correlation of Li abundance and stellar age. Young stars seem to have more lithium than older stars; the usual explanation is that a slow destruction mechanism such as (p,α) reactions at the bottom of a convective zone is operative. ^{7}Li/^{6}Li ratios are known for many stars and vary from 2 to greater than 20. The lower ratio is assumed to be the spallation ratio which will tend to increase during depletion since the ^{6}Li(p,α) rate is faster than the ^{7}Li(p,α) rate at the temperatures estimated. However at present there is no correlation between high ^{7}Li/^{6}Li ratios and stellar age. A good summary of light element observations in stars is given by I.J. Danziger (DA 67).

Cosmological production of the light elements has also been investigated and may possibly account for ^{7}Li production as calculated by R. V. Wagoner, W. A. Fowler, and F. Hoyle (WFH 67). In a calculation for nucleosynthesis in exploding objects (little bangs) R. Wagoner (WA 69) finds that ^{7}Li and ^{9}Be production would exceed and dominate the spallation contributions as estimated in (BGRS 67), while ^{6}Li and B would be due to spallation production.

7. IMPACT OF NEW CROSS-SECTIONS

7.1 Introduction

Our cross-section measurements are particularly valuable for model calculations of the type proposed in (BGRS 67). The most significant calculations are based on the precise isotopic ratios $^7Li/^6Li$ and $^{11}B/^{10}B$. Net abundances are much more difficult to measure since chemical weathering does separate elements but has no effect on the isotopic composition of a particular element. It was found that the ratio $^7Li/^6Li = 12.5$ holds for chondritic meteorites and for rock samples of the earth (KM 64). Similarly the ratio $^{11}B/^{10}B = 4.0$ holds for meteorite (SH 63) and earth rock samples (RA 63).

7.2 Isotopic Ratio Calculations

To calculate these ratios we consider the following model for proton spallation in stellar atmosphere type environments:

1) target mixture: $^{12}C:^{14}N:^{16}O = 3:1:5$ [This holds for solar cosmic rays according to E.A. Muller (Mu 68).]
2) proton flux with spectrum $E^{-\gamma}$ [Solar flares usually fit this (FW 65).]

The relative production of a particular isotope is then given by:

$$I_i = \sum_j \int_{E_o}^{\infty} \sigma_{ji}(E) E^{-\gamma} X_j dE \ , \qquad 7.21$$

σ_{ji} is the cross-section for producing isotope i from target j,

X_j is the weighing factor for target j as given above,

E_o is the threshold energy of $\sigma_{ji} \neq 0$.

To perform the integration we supplement the cross-section measurements performed at this lab with other available data summarized in Table 14. A linear interpolation between data points is used. This is the cause of the kinked curved lines in the logarithmic graphs of Figure 18 where all the $\sigma_{ji}(E)$ used in the integration are shown. Cases of conflicting data were resolved as follows: the last published values by the same authors were preferred over earlier data; emulsion data was given least credence; final data were preferred over preliminary data. The high energy region (>200 MeV) of mass 10 from ^{12}C was based on the cross-section for ^{10}C at 1 GeV, which was doubled to account for ^{10}B. The high energy region (>42 MeV) for mass 11 from ^{14}N is based on ^{11}C cross-sections only; no correction was attempted since the cross-section for mass 11 measured at 42 MeV was comparable to ^{11}C cross-sections at higher proton energy and other spallation cross-section curves tend to slowly decrease towards higher energy. Where data were available at closely spaced points (ES 71), representative points were plotted.

We then calculated the ratios I_7/I_6 and I_{11}/I_{10} for $1.25 \leq \gamma \leq 5.25$. For $\gamma \leq 2$ there must be an energy cutoff $E_{max} < \infty$ since otherwise the average proton energy is not finite. In the calculation for I_j this is not critical however; the value E_{max}=30 GeV is taken for all integrations. For a constant cross-section of σ, $\gamma = 1.25$, and $E_o = 10$ MeV,

Table 14. Spallation Data for ^{12}C, ^{14}N and ^{16}O Targets.

			Cross-Sections in mb.				
Source	E_p	Target	Mass 6	Mass 7	Mass 9	Mass 10	Mass 11
GR 65	50	^{12}C	9.2	32.7			
GR 65	155	^{12}C	9.8	19.9			
GR 65	550	^{12}C	7.4	16.6			
AER 67	50	^{12}C					^{11}C 86.4
AER 67	150	^{12}C				>8.6	61
JU 70	125	^{12}C	8.3				
AER 67	980	^{12}C				^{10}C 3.3	
AER 69	3 GeV	^{12}C	8.3	18.7			
FPLYB 71	150	^{12}C			3.2		
FPLYB 71	600	^{12}C			5.3		
JU 70	125	^{14}N	12.7	11.1			
AER 69	3000	^{14}N		^{7}Be 12			
AER 67	156	^{14}N					^{11}C 15
AER 67	522	^{14}N					^{11}C 22
AER 67	980	^{14}N					^{11}C 25.5
AER 67	5700	^{14}N		^{7}Be8.6			^{11}C 11
ES 71	4.5	^{14}N					10
ES 71	5.5	^{14}N					56
ES 71	6.5	^{14}N					190
ES 71	8.5	^{14}N					220
ES 71	10.5	^{14}N		0.3			180
ES 71	14.5	^{14}N		5.6			140
BCJR 71	14	^{14}N					190

Table 14. (continued)

Source	E_p	Target	Mass 6	Mass 7	Mass 9	Mass 10	Mass 11
YBDFGB 68	135	^{16}O	10.	13.4	1.7	11	25
GR 65	155	^{16}O	9.8	19	1.7		
AER 67	155	^{16}O		13		11	25
YI 68	600	^{16}O	12.4	19.3	2.6	12	25
YI 68	19000	^{16}O	14.4	25.0	3.6	15	<45

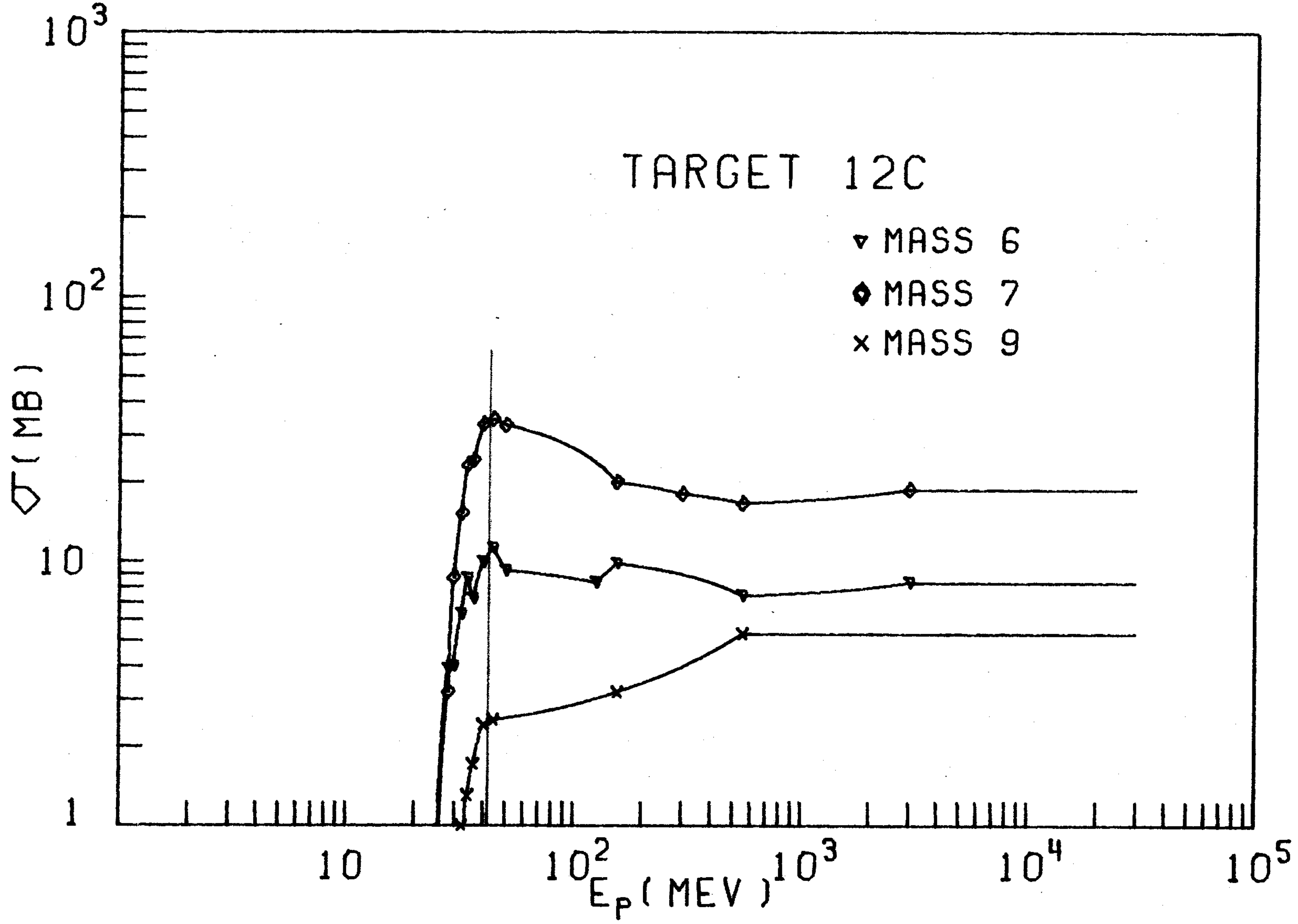

Figure 18. Total Cross-Sections as a Function of Proton Energy for Spallation Products Mass 6 to Mass 11 from Targets ^{12}C, ^{14}N and ^{16}O.

Figure 18. (continued)

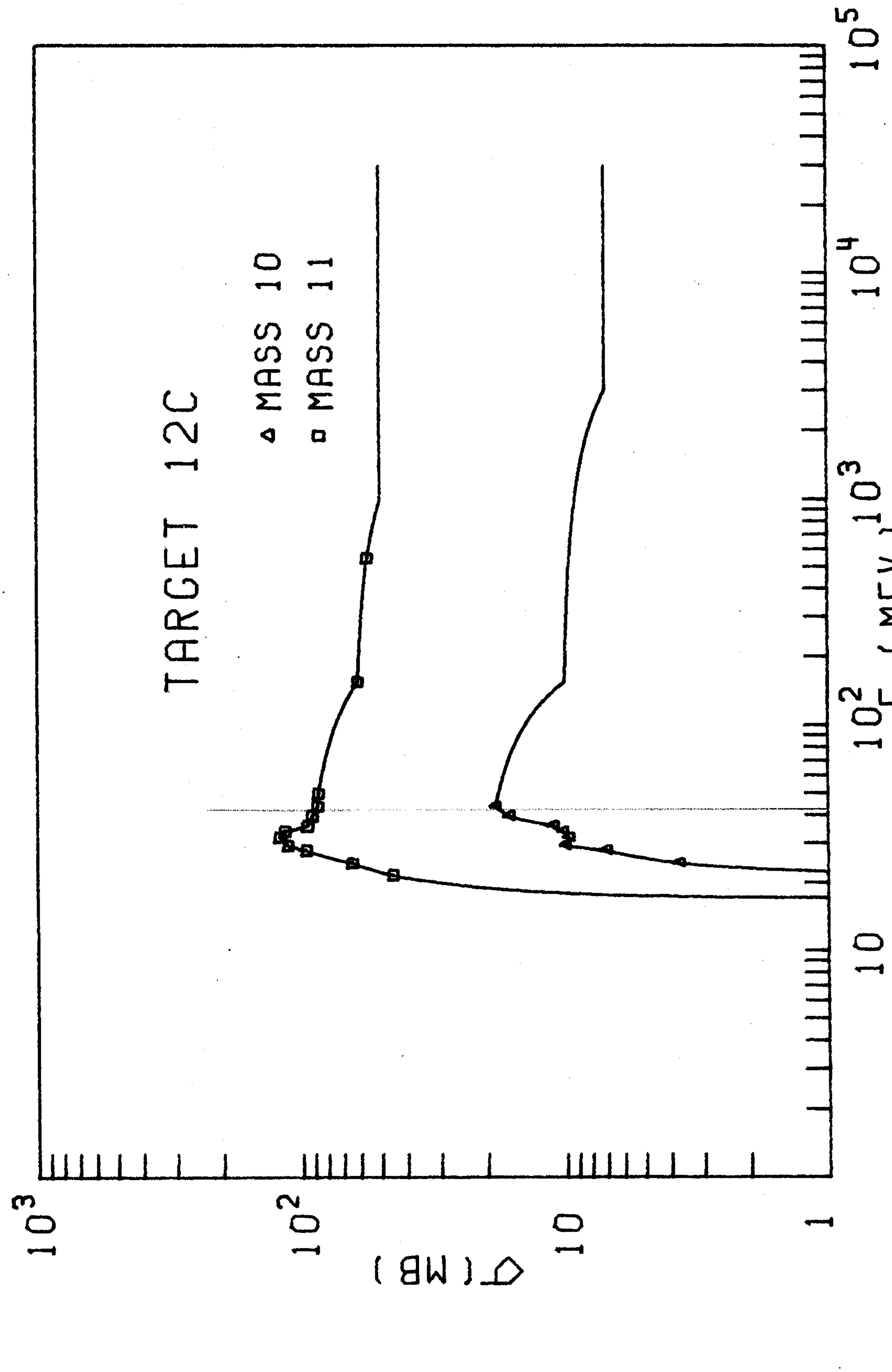

Figure 18. (continued)

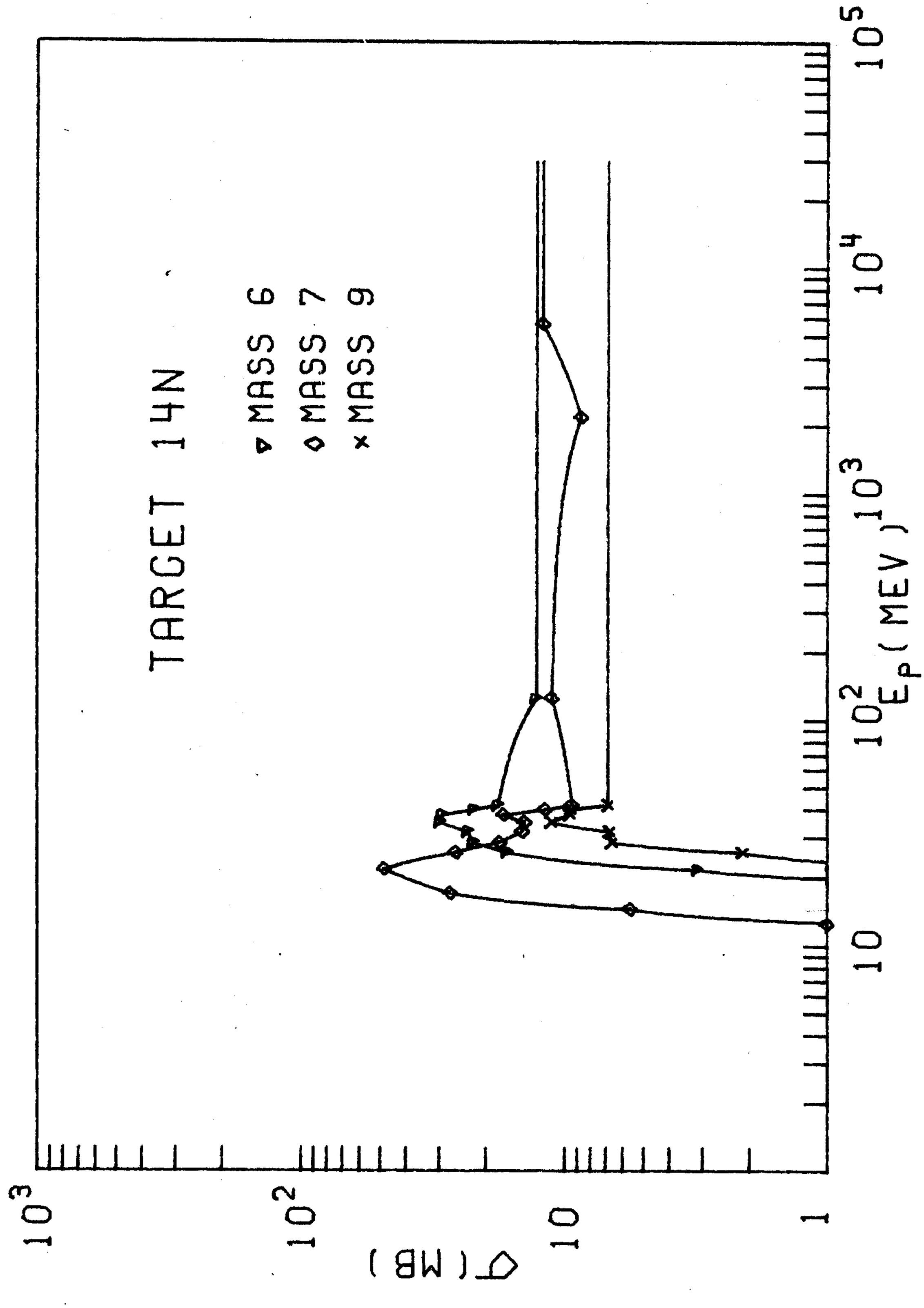

Figure 18. (continued)

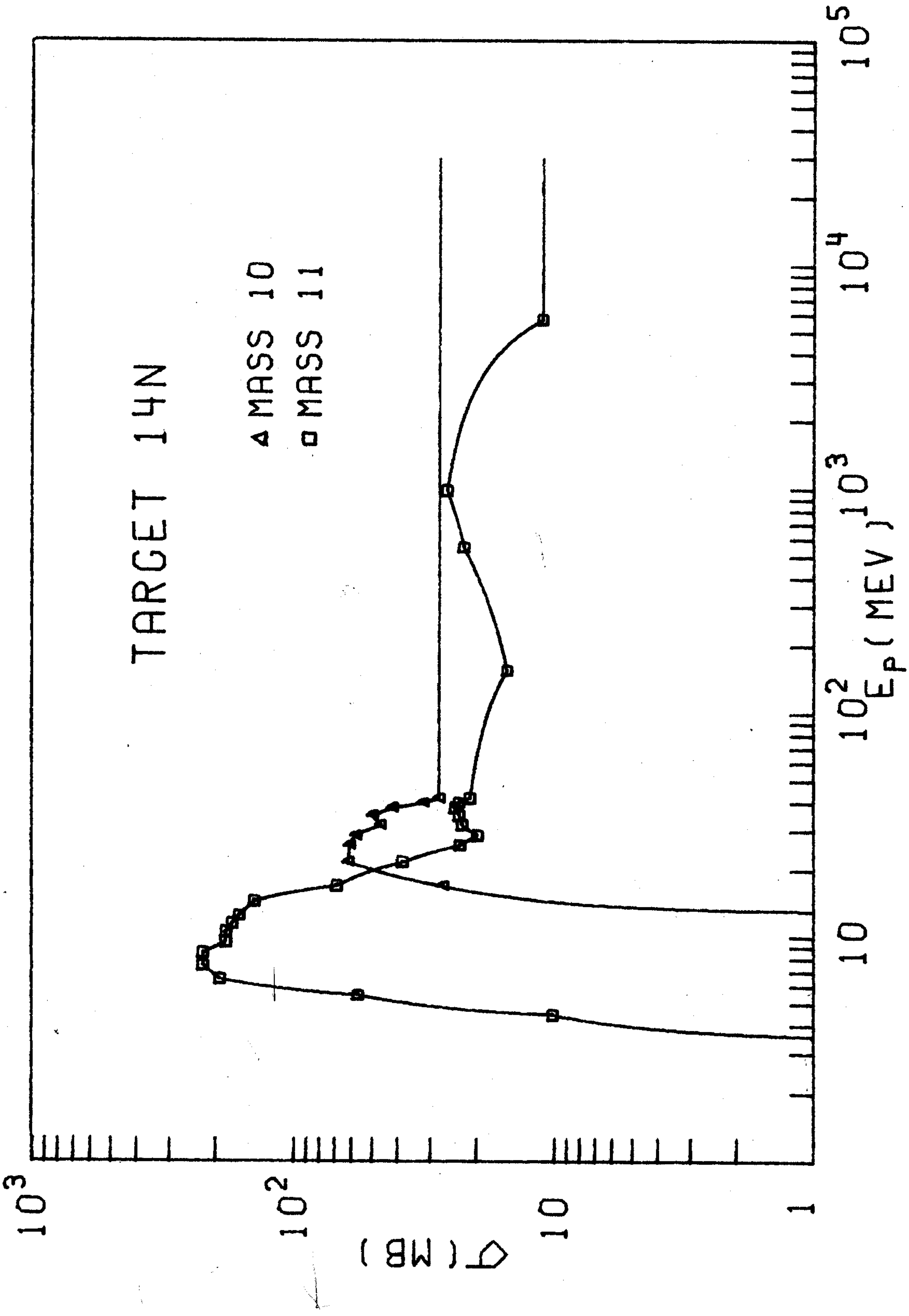

Figure 18. (continued)

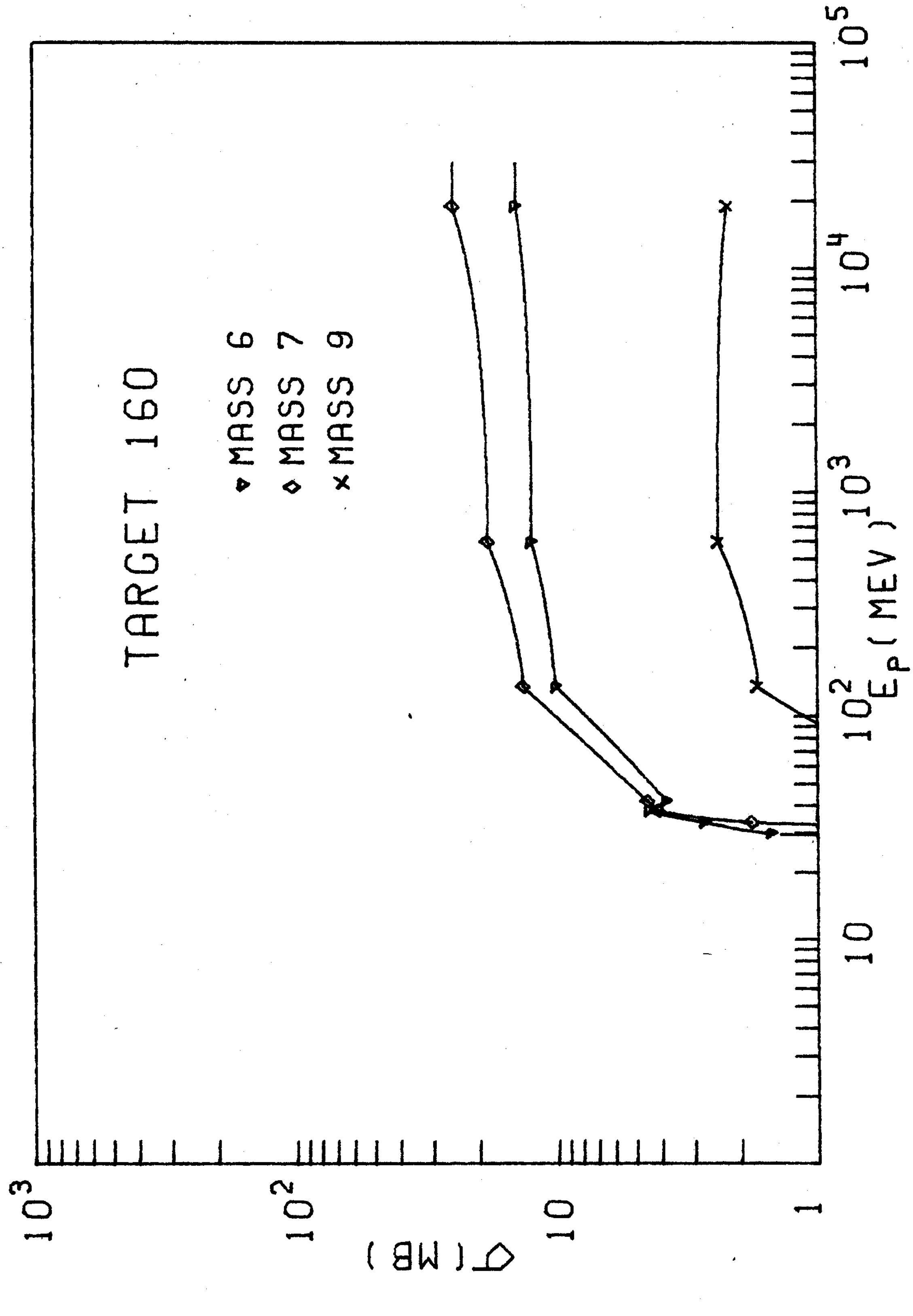

Figure 18. (continued)

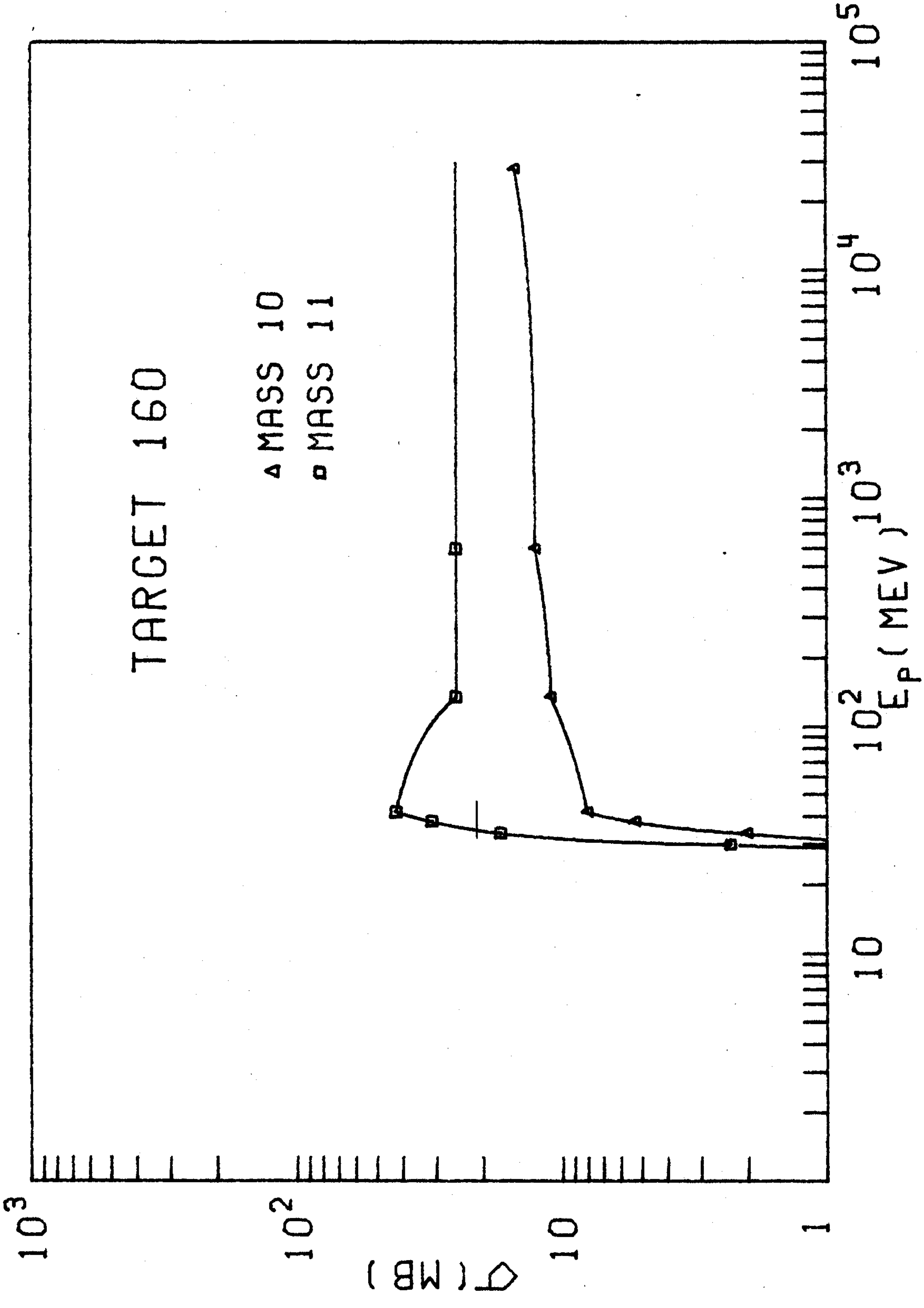

$I_j(E_{max}=30\text{ GeV})/I_j(E_{max}=\infty) = 0.96$; for $\gamma = 1.50$ the ratio is already 0.998. When no cross-section measurements are available at this energy, the cross-section at the nearest lower energy is assumed to be constant out to E_{max}. Figure 19 shows a bar graph which exhibits the net contribution to isotope j by the different targets for two values of γ. It is evident that ^{14}N is the most important target in this model in spite of its lower abundance.

Figure 20 and Table 15 summarize the calculated ratios. Comparing the observed isotopic ratios $^{7}Li/^{6}Li = 12.5$ and $^{11}B/^{10}B = 4.0$ to these values, one finds that the boron ratio is matched only for γ close to 1.25 and then increases rapidly with increasing γ, while the Li ratio is near 2 for low values of γ and even for $\gamma = 5.25$ it only reaches the value 6. There is hence no hope of attaining both observed ratios with a proton spectrum of the proposed form and a specific γ. From Figure 10 for ^{14}N cross-sections it is evident that a special proton spectrum, peaked below 30 MeV but not rising as a high power of E to 10 MeV, can reproduce the observed ratios (this type of argument was already proposed in Bernas et al. (BGRS 67).). That this represents a physical situation is not at all clear however. More likely is some type of preferential depletion mechanism for ^{6}Li or also cosmological ^{7}Li production. Even the boron ratio is not really satisfactory. Solar flares with $\gamma \simeq 3$ are what is actually observed. We get a ratio of

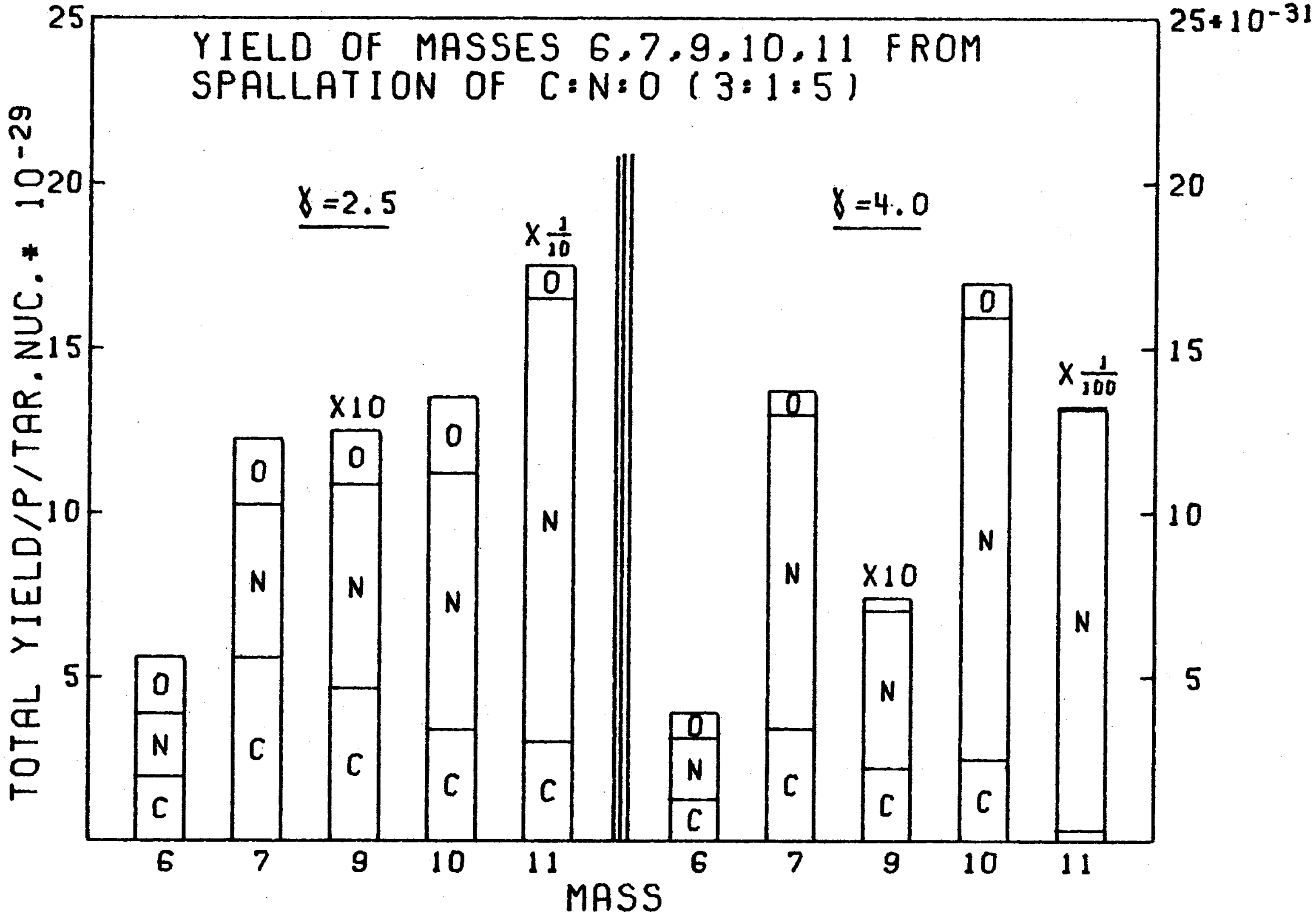

Figure 19. The Net Contribution from the Targets C:N:O (3:1:5) to the Yield of Masses 6,7,9,10 and 11 by Proton Spectra of the Form $E^{-2.5}$ and $E^{-4.0}$.

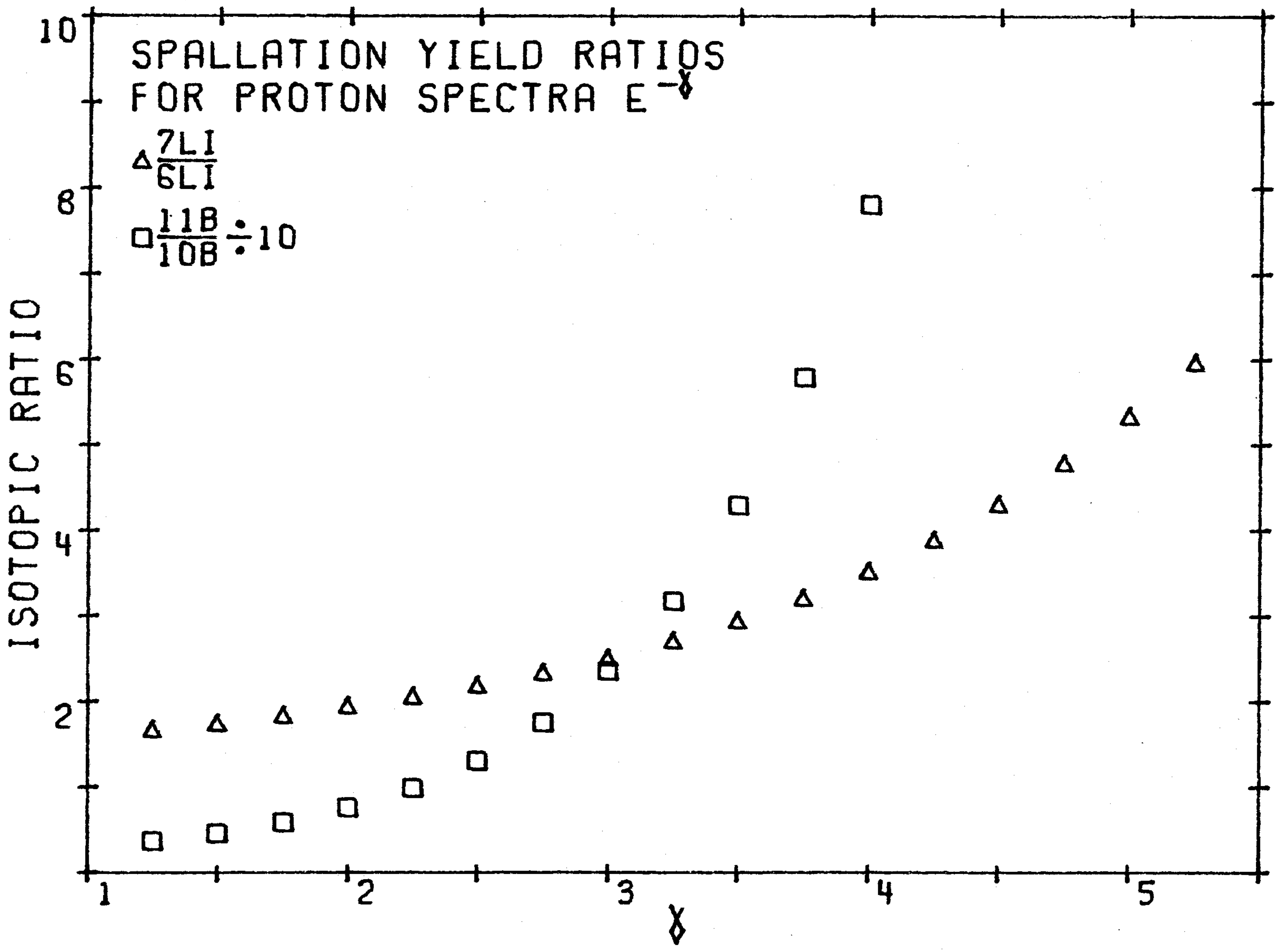

Figure 20. Isotopic Spallation Ratios as a Function of Proton Spectra.

Table 15. Isotopic and Elemental Spallation Production Ratios From a Target Mixture C:N:O (3:1:5) by Proton Spectra $E^{-\gamma}$.

γ	7LI/6LI	11B/10B	LI/BE	B/BE	B/LI
1.25	1.7	3.7	9.2	22.8	2.5
1.50	1.8	4.6	10.0	32.4	3.2
1.75	1.8	5.8	11.0	47.2	4.3
2.00	1.9	7.5	12.1	69.1	5.7
2.25	2.1	9.8	13.2	101.7	7.7
2.50	2.2	13.0	14.3	150.9	10.6
2.75	2.3	17.3	15.4	225.6	14.6
3.00	2.5	23.3	16.7	339.6	20.3
3.25	2.7	31.5	18.2	513.8	28.3
3.50	2.9	42.6	19.8	779.9	39.4
3.75	3.2	57.6	21.6	1186.4	54.8
4.00	3.5	77.8	23.8	1807.2	76.0
4.25	3.9	104.9	26.3	2754.4	104.9
4.50	4.3	141.2	29.1	4199.5	144.2
4.75	4.8	189.8	32.4	6403.6	197.4
5.00	5.3	254.8	36.3	9765.1	269.2
5.25	6.0	341.5	40.7	14893.5	365.8

$^{11}B/^{10}B \simeq 20$ in that case. Thermal neutrons would increase this ratio (they deplete ^{10}B preferentially), thermal protons decrease it only at a temperature which would lead to complete destruction of Li. Hence a mechanism to alter this ratio is difficult to come by.

Thus far we may draw the following conclusions: While ^{14}N dominates the light element production (especially for $\gamma \geq 3$), we have not obtained results that differ greatly from calculations based on guesses for the ^{14}N cross-sections, indicating these early results were rather fortuitously correct. The $^{11}B/^{10}B$ ratio suggests that the proton spectrum causing spallation is rather flatter than what is observed in solar flares.

7.3 Energy Requirement of (BGRS 67) Model

The energy requirement in the (BGRS 67) theory is critical to its validity, we calculate it for the most severe case, the ^9Be abundance in the sun. Starting from equation 6.31 we find after integrating with respect to energy and time that for a time integrated proton flux $\int \phi_p(t)dt \propto E^{-\gamma}$, the minimum areal energy density

$$W(\mathrm{MeV/cm^2}) \equiv \int_{E_C}^{\infty} \phi(E)EdE$$

required to produce all the ^9Be in the sun is given by (provided $\gamma > 2$):

$$-W = \frac{n_{^9Be} \quad E_C^{-\gamma+2} \qquad M_C}{n_{CNO} \quad (-\gamma+2)(I_9) \quad M_i}$$

E_C is the low energy cutoff of the proton spectrum and to obtain a lower limit on W this is chosen close to the ^{9}Be production threshold. The other variables are defined in section 6.3 and 7. For solar abundances from Table 13 and for $\frac{M_i}{M_C} = 2 \times 10^{-8}$ (MI 67):

$$W \simeq \frac{10\ E_C^{-\gamma+2}}{(\gamma-2)I_9} \quad .$$

For $E_C = 30$ MeV, $\gamma = 3$, equation 7.21 yields $I_9 = \frac{0.11 \times 10^{-29}}{\mathrm{MeV}^2}\ \mathrm{cm}^2$; we obtain

$$W = 3 \times 10^{29}\ \mathrm{MeV/cm}^2.$$

For the surface of the sun the total energy required is then 3×10^{46} erg. For $\gamma = 4$, $E_C = 30$ MeV, equation 7.21 yields $I_9 = \frac{0.249 \times 10^{-31}}{\mathrm{MeV}^3}\ \mathrm{cm}^2$ so that

$$W = 2.2 \times 10^{29}\ \mathrm{MeV/cm}^2 \ .$$

Both values are close to the estimates in (MI 67) and (BGRS 67).

7.4 Observations

A reliable calculation of the net contribution of various light element production mechanisms is at present not possible. To repeat the calculations by H.E. Mitler (MI 70) without measurements of (α+α) cross-sections or better knowledge of the low energy cosmic ray flux would be premature. The calculations for stellar production depend critically on stellar models since mixing and burnup in convective zones can cause large changes in relative abundances. Cosmological contributions are the most difficult to estimate since very little observational evidence can be found which is directly related to this mechanism. To all this is added the large uncertainty in the actual net abundance measurements, so even if a calculation is attempted, one does not really know with what one should compare. It would be very interesting to have boron isotopic ratios available from stars. Unlike the range of lithium isotopic ratios observed, from 2 (close to the spallation ratio for low γ) to over 20, which is usually explained by cosmological production or differential depletion, the boron isotopic ratio, apparently not changed by either of these mechanisms, should be the production ratio. Large fluctuation in the ratio are not expected and any such fluctuations would provide better insight into the production mechanism.

APPENDICES

APPENDIX A

IONS TRAVERSING KAPTON

The manufacturer of Kapton does not reveal its exact formula. However from the 21.65 MeV γ-counting experiment it is easily inferred that it is mostly carbon.

By weighing several pieces of 1 mil Kapton an average areal density 3.8±0.1 mg/cm^2 was found. The stopping powers for protons on ^{12}C as shown in Table 16 are taken from (WBP 66).

Table 16. Proton energy loss in Kapton.

Proton Energy (MeV)	Stopping Power (MeV cm^2/g)	Proton energy loss (MeV) in 0.0005" Kapton
22 MeV	21.4	.081
42 MeV	12.7	.048

For the 21.65 MeV γ-counting experiment it is important to know whether ^{7}Be and ^{11}C are stopped by the Kapton. The relations

$$R = R_o \frac{m}{m_o} \left(\frac{Z_o}{Z}\right)^2$$

and

$$E = E_o \left(\frac{m}{m_o}\right)$$

make it possible to use (WBP 66) to find the approximate ranges for ^{7}Be and ^{11}C.

R_o is the range of the tabulated nucleus;

Z_o is its charge;

m_o is its mass;

E_o is its energy.

R,Z,m, and E are the corresponding variables for the nucleus of interest. In the energy range 1 MeV/nucleon and using ^{4}He data, these formulas underestimate by a factor of 2 the ^{12}C range in water and aluminum (see SE 68, Figures 25 and 26).

At 21.65 MeV the maximum energy for ^{7}Be is 9.56 MeV; the maximum energy for ^{11}C is 10.13 MeV. The lab angle is of course 0° with respect to the beam for these cases. To find the range for these particles one first calculates the energy of the α particle given by the energy relation

$$E_o^{^{7}Be} = (9.56 \text{ MeV})(4/7) = 5.46 \text{ MeV for } {}^{7}Be$$

$$E_o^{^{11}C} = (10.13 \text{ MeV})(4/11) = 3.48 \text{ MeV for } {}^{11}C$$

The range of the α particle in ^{12}C at a calculated energy can now be looked up in (WBP 66).

$$R_o^{^{7}Be} = 4.7 \times 10^{-3} \text{ g/cm}^2$$

$$R_o^{^{11}C} = 2.4 \times 10^{-3} \text{ g/cm}^2$$

The range can now be calculated using the first equation

$$R^{^{7}Be} = (4.7 \times 10^{-3} \text{ g/cm}^2)(7/4)(2/4)^2 = 2.05 \times 10^{-3} \text{g/cm}^2$$

$$R^{^{11}C} = (2.4 \times 10^{-3} \text{ g/cm}^2)(11/4)(2/6)^2 = 0.73 \times 10^{-3} \text{g/cm}^2$$

Since these are underestimates by a factor of 2, it is evident that while 0.0005" Kapton is thick enough to stop the ^{11}C; 0.001" Kapton is needed to stop all ^{7}Be.

APPENDIX B

SLIT SYSTEM DESIGN CALCULATIONS

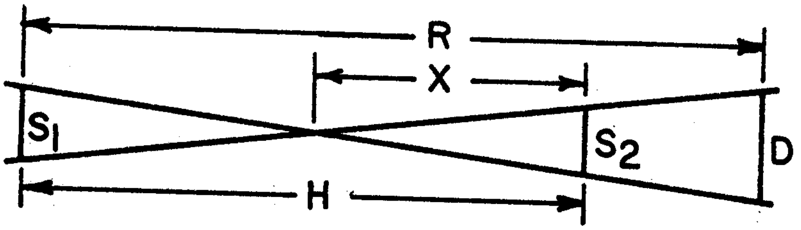

Figure 21. Geometry of Slit System with Beam at 90°.

In Figure 21 S_1 and S_2 represent the back and front slit respectively. D represents the part of the beam trajectory visible to the detector for the beam at 90° to the slit axis. The yield $Y \propto S_1S_2$ should be maximized for a given D. From Figure 21 the geometrical relationships are evident:

$$\frac{\frac{S_2}{2} + \frac{S_1}{2}}{H} = \frac{\frac{S_2}{2}}{X} = \frac{\frac{D}{2}}{X+R-H}$$

These results then follow:

$$X = H \frac{S_2}{S_2+S_1}$$

$$D = \left(H \frac{S_2}{S_2+S_1} + R - H\right)\left(\frac{S_2+S_1}{H}\right) = \frac{R}{H} S_2 + \frac{(R-H)S_1}{H}$$

To maximize Y set $dY = 0 = S_2dS_1 + S_1dS_2$ subject to D = constant

$$\frac{R}{H} + \frac{R-H}{H} \frac{dS_1}{dS_2} = 0$$

$$-dS_2 = \frac{R-H}{R} dS_1$$

$$S_2dS_1 + S_1\left(\frac{H-R}{R} dS_1\right) = 0$$

$$S_2 = S_1\left(\frac{R-H}{R} \right)$$

The last formula has the following meaning. If $H \approx R$, that is if the front slit is very close to the beam, then the size of the back slit is only limited by the detector size. The choice of the front slit opening is critical for beam trajectories other than 90°. Then the range of possible flight paths depends strongly on both beam width W and front slit width S_2. This is shown in Figure 22.

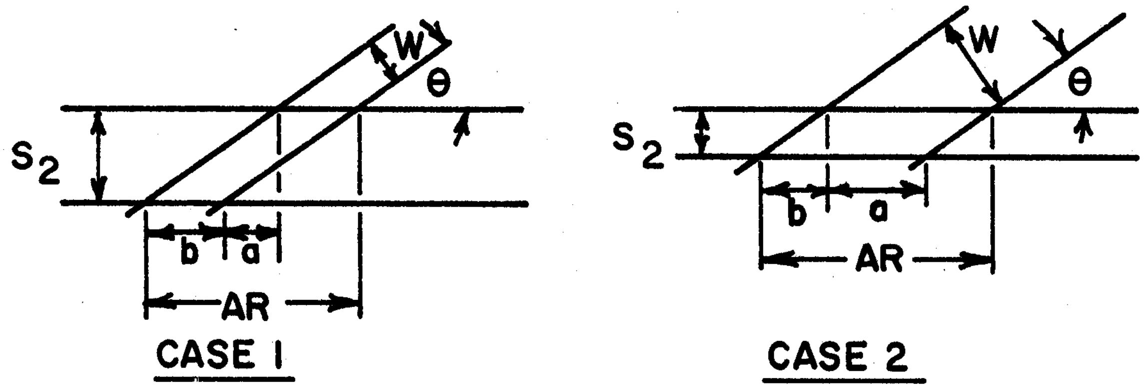

Figure 22. Approximate Range of Path Length Differences.

AR is the approximate range of path lengths. From Figure 22 it is seen that AR = a + 2b.

$$\text{case 1:} \quad a+b = \frac{S_2}{\tan\theta} \qquad b = \frac{W}{\sin\theta} \qquad (S_2 > W)$$

$$\text{case 2:} \quad a+b = \frac{W}{\sin\theta} \qquad b = \frac{S_2}{\tan\theta} \qquad (W > S_2)$$

$$AR = \frac{W}{\sin\theta} + \frac{S_2}{\tan\theta} \quad \text{for both cases.}$$

This shows that for small angles θ, the beam spot size and front slit width are equally critical as far as timing resolution is concerned. Yield $Y \propto WS_2$. This is so because in making the beam spot small, the beam intensity is cut down proportionally. It is thus of advantage to have $W \approx S_2$. This maximizes yield for constant timing resolution for small θ. Near $\theta = 90°$, $AP \approx W$ and the front slit width is not critical.

APPENDIX C

FORMVAR FILM THICKNESS MEASUREMENT

The stopping power for a compound can be calculated from the stopping power of constituent elements using the formula.

$$\text{STOPPING POWER} = \frac{dE}{d(\rho_C x)} = \sum_E \frac{dE}{d(\rho_E x)} \frac{\rho_C}{(\rho_E)} \qquad (1)$$

ρ_C is the density of the compound

ρ_E is the density of an element

ρx is the areal density.

The formula of formvar is $H_{16}C_8O_4$ so

$$\frac{dE}{d(\rho_F x)} = \frac{dE}{d(\rho_H x)} \frac{\rho_H}{\rho_F} + \frac{dE}{d(\rho_C x)} \frac{\rho_C}{\rho_F} + \frac{dE}{d(\rho_O x)} \frac{\rho_O}{\rho_F} \qquad (2)$$

F = formvar, H = hydrogen, C = carbon, O = oxygen.

The stopping powers for 5.48 MeV α's were taken from (WBP 66). One obtains from Eq. (2):

$$\frac{dE}{d(\rho_F x)} = [(21.82)\frac{16}{176} + 7.463(\frac{96}{176}) + 6.892(\frac{64}{176})] \times 10^2 \frac{\text{MeV cm}^2}{\text{g}}$$

$$= 8.565 \times 10^2 \frac{\text{MeV cm}^2}{\text{g}} \qquad (3)$$

It was found that 5.48 MeV particles lost 0.089±.009 MeV in traversing 44 double layers of formvar.

$$\frac{dE}{d\rho_F x} = 8.565 \times 10^2 \text{ MeV cm}^2/\text{g}$$

$$dE = 0.089 \text{ MeV}$$

$$d({}_{F}x) = \frac{0.089}{8.565\text{x}10^{2}}\ \text{g/cm}^{2} = 1.04 \times 10^{-4}\ \text{g/cm}^{2}\ .$$

1 double layer = $2.36\ \mu\text{g/cm}^{2} \approx 2.4 \pm 0.2\ \mu\text{g/cm}^{2}$.

APPENDIX D

GAS HEATING MODEL

To estimate the instantaneous heating of the gas a calculation with the model given below is carried out.

When an object of cross-section A moves with uniform velocity v through a gas, it will displace a volume Avt in time t. The minimum velocity that must be imparted to the volume Avt is v. This way the gas in front of the object is transported just behind the object in time t. The work done in moving this amount of gas must be supplied by the object.

Suppose the proton beam traversing the gas heats a volume element of height h, width w and length ℓ to a temperature T_f. Due to buoyancy the volume element will rise, its terminal velocity should satisfy the equation

$$vt\left(\rho V - \rho\frac{VT_i}{T_f}\right)g = \rho(vt\ell w)\frac{v^2}{2} .$$

V is the volume element = ℓhw;

T_i is the temperature of the surrounding gas;

T_f is the temperature of the heated gas;

v is the terminal velocity;

ρ is the surrounding gas density;

g is the acceleration due to gravity.

The left side represents the change in potential energy when the heated volume rises the distance vt. The right side represents the energy needed to move the gas of volume $vt\ell w$ out of the way.

One obtains for the terminal velocity:

$$v = \left[\frac{2(T_f - T_i)}{T_f} hg \right]^{\frac{1}{2}}$$

Assume the total amount of energy E deposited in volume V is equal to the energy deposited in the gas during time $t = h/v$;

so $E = t\ell\rho SI$

S is the stopping power of the gas for protons of the energy under consideration. I is the proton current.

The temperature rise of volume element V is then given by

$$E/(\rho VK) = T_f - T_i,$$

where K is the specific heat of the bombarded gas. Substituting for E, V, and t one obtains:

$$T_f - T_i = (h\rho\ell SI)/(v\rho\ell hwK) = SI/(vwK)$$

$$(T_f - T_i)^2 v^2 = (T_f - T_i)^3 2hg/T_f = S^2 I^2/(K^2 w^2)$$

$$(T_f - T_i)^3 = T_f S^2 I^2/(2hw^2 gK^2)$$

This last equation can be easily solved by iteration. Chosen units are:

S in $(\mathrm{MeV\ cm^2})/\mathrm{g}$

I in μ coulombs/sec

K in cal/(g C°)

$$\left(\frac{SI}{K}\right)^2 = \left[\frac{\mathrm{MeV\ cm^2}}{\mathrm{g}} \; \frac{1.60\text{x}10^{-6}\,\mathrm{erg}}{\mathrm{MeV}} \; \frac{\mathrm{cal}}{4.184\text{x}10^{7}\,\mathrm{erg}} \; \frac{10^{-6}\,\mathrm{coul/sec}}{1.60\text{x}10^{-19}\,\mathrm{coul/proton}} \right.$$

$$\left. \text{x} \; \frac{\mathrm{g\ C°}}{\mathrm{cal}} \right]$$

$$= \left(\frac{1}{4.184} \right)^2 (\mathrm{C°})^2 \; \frac{\mathrm{cm^4}}{\mathrm{sec^2}}$$

$$(T_f - T_i)^3 = \frac{T_f (C^\circ)^2 cm^4}{(4.184)^2 sec^2} \frac{S^2 I^2}{K^2} \frac{1}{2hw^2 g}$$

For the experiment on ^{20}Ne gas the values are I =0.5 and 0.1 respectively.

$w = 0.063$ cm, $h = 0.114$ cm

$S = 13.9$

$K = 0.246$

For these values I find $T_f(I{=}.5) = 321°K$ and $T_f(I{=}.1) = 304°K$.

A 22 MeV proton loses .081 MeV in a 1 mil Kapton window. The stopping power of 22 MeV protons in nitrogen is 20.88 MeV cm^2/g. When the gas pressure is 30 cm (oil) the energy deposited in the cell per proton is then:

$$\Delta E = (4.75)(2.54cm) \frac{28g}{22.4x10^3 cm^3} \frac{30\ cm}{13.8x76cm} \frac{20.88cm^2}{g}\ MeV$$
$$= 0.9 \times 10^{-2}\ MeV$$

So the total energy loss in gas and Kapton is 0.09 MeV per proton. The usual beam intensity was 0.5μamp.

$$Power = (0.09MeV)(0.5x10^{-6} coul/sec)(1/1.6x10^{-19} coul)$$
$$= 2.8 \times 10^{11} MeV/sec \approx 0.01\ calories/sec.$$

The gas cell body is made of brass and weighs 1450 g. Take the specific heat of brass at 0.09 cal/g, then the rate of temperature rise of the cell is

$$\frac{0.01}{(1450)(.09)} \frac{C^\circ}{sec} = 0.8 \times 10^{-4}\ C^\circ/sec$$

Since the gas cell is in metal contact with the scattering chamber, no long term heating of the cell is expected to result. The above assumes efficient cooling of the gas by the brass body of the cell.

APPENDIX E

CALCULATIONS FOR BEAM DEGRADER

Energy straggling for a beam of particles with nuclear charge z passing through a target of nuclear charge Z, atomic number A and density ρ is given by (EV 55):

$$\overline{(\Delta E)^2} = 4\pi z^2 e^4 (Z/A)(\rho X) N \qquad (1)$$

where X is the distance of target traversed, N is Avagadro's number.

Suppose a proton beam with energy 21.65 MeV is to be degraded to 17 MeV. In (WBP 66) one finds the range of 21.65 MeV protons and 17 MeV protons in Al. The difference in range is the desired aluminum thickness; 0.2307 g/cm^2. For lead one obtains 0.414 g/cm^2.

To compare the energy spread from formula (1) above, consider

$$\frac{Z}{A}\,(\rho X) = (13/17)(0.2307\,\frac{g}{cm^2}) = 0.111\ g/cm^2 \text{ for aluminum,}$$

$$\frac{Z}{A}\,(\rho X) = (82/207)(0.414\,\frac{g}{cm^2}) = 0.164\ g/cm^2 \text{ for lead.}$$

Hence, aluminum is the better degrader. The actual energy spread for aluminum is:

$$\overline{\Delta E}^2 = 1.565 \times 10^{-1}\,\frac{Z}{A}\,(\rho X)\ \text{MeV}^2$$

$$\overline{\overline{\Delta E}^2} = 0.132\ \text{MeV}\ .$$

A 0.035" thick aluminum plate was used as degrader. The 6061 aluminum alloy has the composition:

98.0 %	Al
1.0 %	Mg
0.6 %	Si
0.20%	Cr
0.25%	Cu
0.05%	impurities.

It is thus safe to use the ranges for protons in pure aluminum to calculate the expected energy loss using (WBP 66). 0.035" aluminum represents an areal density ρX:

$$\rho X = (2.7 \text{g/cm}^3)(.035)(2.54) = 0.240 \text{ g/cm}^3.$$

From (WBP 66) a 21.65 MeV proton has a range 0.6610 g/cm^2 in aluminum. The range 0.421 g/cm^2 corresponds to a proton beam of 16.8 MeV.

The angular beam spread is given by

$$\theta = \frac{21 (\text{MeV})}{2E (\text{MeV})} \sqrt{\frac{L}{L(\text{rad})}}$$

L = length in scatterer =0.035"

E = proton energy

$L_{(\text{rad})}$ = radiation length of aluminum = 8.9 cm

$\therefore \theta = 3.3°.$

APPENDIX F

BAND RESOLUTION CALCULATIONS

TOOTSIE plots a number proportional to Et^2 against a number proportional to E where E is the energy of the particle and t is the flight time. One may rewrite:

$$Et^2 = \left(\frac{1}{2} mv^2 \right) (d/v)^2 = \frac{1}{2} md^2 \qquad (1)$$

where d is the flight path. Hence the plot by TOOTSIE should be a set of straight bands, parallel to the x-axis, each band representing a mass. The width of the bands depends on energy resolution of the detector, time resolution of the beam pulse, flight path range, and time resolution of the electronics. The last can be ignored except for very low energy pulses, where it is extremely difficult to estimate.

$$\Delta Et^2 = \frac{\delta}{\delta E} (Et^2) \Delta E + \frac{\delta}{\delta t} (Et^2) \Delta t = t^2 \Delta E + 2Et\Delta t \qquad (2)$$

$$\frac{\Delta Et^2}{Et^2} = \frac{\Delta E}{E} + 2 \frac{\Delta t}{t} \qquad (3)$$

Δt has two contributing sources, δt the beam pulse width, and $\Delta d/v$ from the range of flight paths. Since $t = d/v$, Eq. (3) can be written

$$\frac{\Delta Et^2}{Et^2} = \frac{\Delta E}{E} + 2 \left(\frac{\delta t}{t} + \frac{\Delta d}{d} \right) \qquad (4)$$

The three contributions limiting the mass resolution are independent of each other, so for a comparison with data the square root of the sum of their squares is appropriate.

ΔE was always 40 keV or better as measured from the FWHM of the 5.48 MeV alpha peak from an americium source. The percent error then varies inversely with E.

The average beam pulse width was 0.5nsec. The percentage error varies inversely with flight time, hence with energy:

$$t = d/v = \frac{d}{c\sqrt{2}}\sqrt{\frac{mc^2}{E}}$$

maximum E $\simeq$ 20 MeV, minimum mc^2 of interest is 6 x 938 MeV;

$d \simeq 30$ cm.

$\therefore t_{min} \approx 12$ nsec.

$t_{max} = 12$ nsec + RF $\simeq$ 65 to 84.

Hence the percent error contribution to $\frac{\Delta(Et^2)}{Et^2}$ varies from 8% to 1.2%.

The error due to path length variation is largest at small forward angles. The following calculation is for a 0.040" beam width (horizontal dimension) and a 0.040" wide front slit with the detector at 15° to the beam. The range of flight path distance is calculated for 90% of the particles reaching the detector.

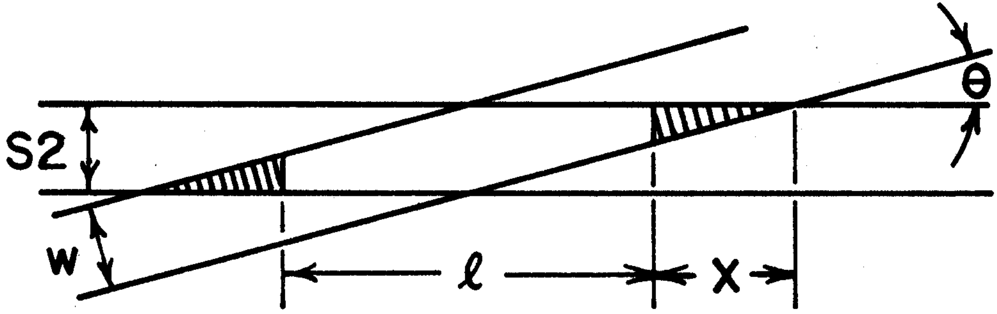

Figure 23. Range of Flight-Distance for 90% of Particles Reaching the Detector.

$$\text{Total area} = \frac{S2^*w}{\sin\theta}$$

$$\text{Shaded area} = x^2\tan\theta$$

For shaded area to be 10% of total area requires:

$$\frac{S2^*w}{\sin\theta}\,\frac{1}{10} = x^2\tan\theta$$

$$x = \frac{S2^*w\cos\theta}{10\,\sin^2\theta}$$

$$\ell = \frac{w}{\sin\theta} + \frac{S2}{\tan\theta} - 2x$$

where ℓ is the range of path lengths desired. For $\theta = 15°$, $S = 0.040"$, $w = 0.040"$, I find $\ell = 0.0256" = .65\text{cm}$.

For a flight distance of 26 cm, the percent contribution to $\frac{\Delta Et^2}{Et^2}$ is then 2(0.65/26.0)100% = 5%.

APPENDIX G

TIME-OF-FLIGHT CROSS-SECTION INTEGRATION RELATED FORMULAS

Some details for calculating cross-sections from angular distributions.

Below are tabulated a few fortran statements representing equations used in the cross-section calculations.

The equation to calculate the number of channels corresponding to energy loss in gas and window:

```
ECHC=((RA(L)-H)*P*2./7.6/.2241+2.0)*2.335/10.**2*Z1(M3)**
     1.207*Z2/(Z1(M3)**.6667+Z2**.6667)**1.5*ECAL
```

(RA(L)-H)	is the average distance the reaction product travels in the gas; this varies with angle.
P	is the gas pressure in cm Hg.
Z1(M3)	is the charge of the reaction product, the average for the expected products for a particular mass band is used.
Z2	is the charge of the target gas.
ECAL	is the number of channels per MeV of particle energy from the energy calibration curve.

An integration factor :

```
F(L) = (COSD((A(L-1)+A(L))/2.)-COSD((A(L)+A(L+1))/2.))/NM(L)
```

A(I) are angles at which data was taken.

NM(L) is the number of monitor counts for data taken at angle A(L).

The factor combining most constants and geometric variables:

```
G(L)=(CNM/Q)*(H/B1)((R/P)*(SIND(BA)/Z)*(.2241/.17854)
     *(.76/.6452)*(.1602/.15625)*(.6283/.6025)*((T+273.1)
    /273.1)
```

CNM	is the number of monitor counts for the calibration run.
Q	is the total collected charge for the calibration run in 10^{-8} coulombs.
P	is the pressure in inches Hg for the calibration run.
T	is the gas temperature in °C assumed to be equal to room temperature.
H	is the distance from S_1 to S_2 (see Figure 70) in inches.
R	is the mean flight path length to S_1 in inches.
B1	is the width of S_2 in inches.
BA	is the angle at which data is taken, hence this is A(L).
Z	is the number of atoms per target molecule.

The number (.15625)(.17854)(6.452) represents the area of S_1 in cm^2.

The quantity F(L)*G(L)*NSY is then the contribution to the total cross-section for data taken at angle A(L). NSY is the number of counts in a specific energy spectrum corrected for the low energy cutoff.

APPENDIX H

SETUP PROCEDURE

To set up the electronics systems a pulser is used to simulate detector pulses at the preamplifier input. First the time-pickoff control logic pulse output is monitored with a cathode ray oscilloscope; and its sensitivity is set so that it just does not free run and triggers only occasionally on random noise. After this adjustment the pulser is turned on and the fast timing logic is checked out. The fast discriminators are checked for multiple triggering. The delays for the RF stop pulse and the start pulse to the TAC are adjusted so that pulses which arrive simultaneously at the fast anticoincidence circuit also would arrive simultaneously at the TAC (if the 25 nsec anticoincidence requirement would not be in effect). The TAC pulses generated by the pulser are monitored with a ND 160 multichannel analyzer. A flat, continuous random time spectrum should be observed. The single channel analyzer pulses to the slow coincidence module have to arrive at the same time. This is done by turning the delay knob on a SCA module while monitoring with the scope. The veto pulse is similarly adjusted, choosing pulse length and delay on the gate and delay generator module. The output of the Universal Coincidence is checked next. It should give logic pulses if the veto is disabled, and should have no output if the pulser is also connected to the veto preamplifier. The logic pulse from the slow coincidence gates the energy and TAC pulses. The linear signals have to have the correct delay to be passed by the linear gate and stretchers. The amplifier provides a properly delayed unipolar linear signal. The TAC pulse is delayed with a 427A delay amplifier (not shown in the electronics diagram). The linear gate and stretcher controls are adjusted so linear signals are 3 μsec long and arrive at the same time at the ADC's.

BIBLIOGRAPHY

BIBLIOGRAPHY

AC 60 L. H. Aller and S. Chapman, Astrophys. J. 132, 461 (1960).

AC 70 W. David Arnett, Donald D. Clayton, Nature 227, 780 (1970).

AER 67 J. Audouze, M. Epherre, and H. Reeves in "High-Energy Nuclear Reactions in Astrophysics" edited by B.S.P. Shen (W.A. Benjamin, Inc., 1967), pp.256.

AER 69 Complement to AER 67.

BA 71 D. L. Bayer, MSUCL-34, (Michigan State University, East Lansing, Michigan), 1971.

BBFH 57 E. M. Burbidge, G. R. Burbidge, W. A. Fowler, and F. Hoyle, Rev. Mod. Phys. 29, 547 (1957).

BCJR 71 D. Bodansky, J. Cameron, W. Jacobs, and P.A. Russo, Nucl. Phys. Lab., U. of Wash. Annual Report (1971).

BFH 65 D. S. Burnett, W. A. Fowler, and F. Hoyle, Geochim. et Cosmochim. Acta 29, 1209 (1965).

BG 60 W. K. Bonsack and J. L. Greenstein, Astrophys. J. 131, 83 (1960).

BGRS 67 R. Bernas, E. Gradsztajn, H. Reeves, and E. Schatzman, Ann. Phys. 44, 426 (1967).

BP 61 S. Bashkin and D. C. Penslee, Astrophys. J. 134, 981 (1961).

CA 67 A. G. W. Cameron, in "Origin and Distribution of the Elements", edited by L. H. Ahrens (Pergamon Press, Oxford, 1968), p. 130.

CL 68 D. D. Clayton, "Principles of Stellar Evolution and Nucleosynthesis", (McGraw-Hill, Inc., 1968).

DA 67 I. J. Danziger in "High-Energy Nuclear Reactions in Astrophysics", edited by B.S.P. Shen (W. A. Benjamin, Inc., 1967), pp.81.

DLA 70 Cary N. Davids, Helmut Laumer, and Sam M. Austin, Phys. Rev. C1, 270 (1970).

DO 70 Raymond E. Doebler, Ph.D. Thesis, Michigan State University (1970).

ES 71 M. Epherre and C. Seide, Phys. Rev. C3, 2167 (1971).

EV 55 R. Evans, in "The Atomic Nucleus", McGraw-Hill, 661 (1965).

FBB 55 W. A. Fowler, G. R. Burbidge, and E. M. Burbidge, Astrophys. J., suppl. 2, 167 (1955).

FGH 61 W. A. Fowler, J. L. Greenstein, and F. Hoyle, Am. J. Phys. 29, 393 (1961).

FGH 62 W. A. Fowler, J. L. Greenstein, and F. Hoyle, Geophys. J. Roy. Astron. Soc. 6, 148 (1962).

FGS 68 C. Y. Fan, G. Gloechler, and J. A. Simpson, Tenth International Conf. Cosmic Rays, Calgary; Canadian J. Phys. 46, S548 (1968).

FPLYB 71 P. Fontes, C. Perron, J. Lestringuez, F. Yiou and R. Bernas, Nuc. Phys. A165, 405 (1971).

FW 63 P. S. Freier and W. R. Webber, J. Geophys. Res. 68, 1605 (1963).

GO 60 T. Gold, Astrophys. J. 132, 274 (1960).

GR 65	Élie Gradsztajn, Ann. de Phys. 10, 804 (1965).
GMS 69	M. Garcia-Munoz, J. A. Simpson, "Proceedings of the 11th International Conference on Cosmic Rays", Budapest 1, 325 (1970).
HA 55	S. Hayakawa, Prog. Theor. Phys. 13, 464 (1955).
HE 65	G. H. Herbig, Astrophys. J. 141, 588 (1965).
IB 66	Iben, Astrophys. J. 143, 516 (1966).
JU 70	M. Jung, C. Jacquot, C. Baixeras-Aiguabella, R. Schmitt, and H. Braun, Phys. Rev. C1, 435 (1970).
KM 64	Krankowsky and Müller, Geo. Cosmo. Acta 28, 1625 (1964).
LS 61	J. Lindhard and M. Scharff, Phys. Rev. 124, 128 (1961).
MI 64	H. E. Mitler, Phys. Rev. 136B, 298 (1964).
MI 67	H. E. Mitler in "High-Energy Nuclear Reactions in Astrophysics", edited by B.S.P. Shen (W. A. Benjamin, Inc., 1967), pp. 59.
MI 70	H. E. Mitler, "Cosmic-Ray Production of Light Elements in the Galaxy", Smithsonian Astrophysical Observatory Special Report 330, (1970).
MU	E. A. Muller, in "Origin and Distribution of the Elements", edited by L. H. Ahrens (Pergamon Press, Oxford, 1968), p. 155.
NO 63	Lee C. Northcliffe, Annual Review of Nuclear Science 13, 67 (1963).
PE 68	J. V. Peach, Mon. Nat. Roy. Astron. Soc. 139, 403 (1968).
RA 63	K. Rankama, in "Progress in Isotope Geology", Wiley, New York, (1963).

RFH 70	H. Reeves, W. A. Fowler, and F. Hoyle, Nat. 226, 727 (1970).
SE 68	P. G. Steward, UCRL-18127, (University of California, Berkeley, Calif.), 1968.
SH 63	Shima and Honda, J. Geophys. Res. 68, 2849 (1963).
SI 59	E. Silverstein, Nucl. Inst. Methods 4, 53 (1959).
ST 63	R. M. Sternheimer, in "Methods of Experimental Physics" 5-Part B, Appendix 2, edited by C. Marton (Academic Press, 1963).
TM 62	Taylor and Merritt, Can. J. Phys. 40, 926 (1962).
WA 69	R. V. Wagoner, Ast. Journal Supp. 18, 247 (1969).
WBP 66	C. F. Williamson, J. P. Boujot, J. Picard, Rapport CEA-R3042 (Centre D'Etudes Nucleaires De Saclay), 1966.
WFH 67	R. V. Wagoner, W. A. Fowler, and F. Hoyle, Ap. J. 148, 3 (1967).
YBDFGB 68	F. Yiou, M. Baril, J. Dufaure dé Citres, P. Fontes, E. Gradsztajn, and R. Bernas, Phys. Rev. 166, 968 (1968).
YI 68	F. Yiou, Ann. Physique 3, 169 (1968).